Spatial Variations of the **P**hase shift between **O**cean Surface Warming, **E**vaporation and Changes of Continental Ice Volume at **T**ermination I

(Code Name: P.O.E.T)

DISSERTATION

zur Erlangung des Doktorgrades

an der Mathematisch-Naturwissenschaftlichen Fakultät

der Christian-Albrechts-Universität zu Kiel

vorgelegt von

Christian Horn

Kiel, 2011

Referent: Prof. Dr. rer. nat. Anton Eisenhauer

Koreferent: Prof. Dr. rer. nat. Martin Frank

Tag der mundlichen Prufung: 29.09.2011

Zum Druck genehmigt: 10.11.2011

gez. Prof. Dr. rer. nat. Lutz Kipp, Dekan

Hiermit erkläre ich, dass ich die vorliegende Doktorarbeit selbständig und ohne Zuhilfenahme unerlaubter Hilfsmittel erstellt habe. Weder diese noch eine ähnliche Arbeit wurde an einer anderen Abteilung oder Hochschule im Rahmen eines Prüfungsverfahrens vorgelegt, veröffentlicht oder zur Veröffentlichung vorgelegt. Ferner versichere ich, dass die Arbeit unter Einhaltung der Regeln guter wissenschaftlicher Praxis der Deutschen Forschungsgemeinschaft entstanden ist.

Christian Horn

Abstract

Previous studies of coupled Mg/Ca_{foram} and $\delta^{18}O_{foram}$ measurements across the transition from the last glacial period to the Holocene, Termination 1, in tropical settings have shown that the planktonic Mg/Ca signal leads the $\delta^{18}O$ signal by several thousand years (e.g. *Lea et al.,* [2000]; *Nürnberg et al*., [2000]; *Visser et al*., [2003]). This leads to the conclusion that the tropical ocean warmed before the melting of Northern Hemisphere ice sheets challenging the role of the North Atlantic as the pacemaker of glacial/interglacial transitions and emphasizing the tropical ocean as an important area for triggering global climate change.

This thesis tests this hypothesis by applying a multi-proxy approach of coupled $\delta^{18}O$, Mg/Ca ratios and $\delta^{44/40}Ca$ measurements on planktonic foraminifera in order to decouple the influence of sea surface temperatures (SST) and sea surface salinity (SSS) during the Termination on the individual proxy. The sediment cores selected for this study cover a transect of the ocean from the tropics to high northern latitudes.

Our results show a phase shift of ~4000 years in the timing of the glacial / interglacial temperature transition between Mg/Ca_{foram} and $\delta^{18}O_{foram}$ signals for *G.sacculifer* in the Central Caribbean Sea in accordance with previous observations.

However, in contrast to earlier interpretations this proxy data can be reconciled by taking dynamic local Caribbean variations of the evaporation/precipitation ratio into account which were calculated employing $\delta^{44/40}Ca$ generated SST values. Latter SSS dynamic most likely reflects temporal variations of the ITCZ triggered by the glacial / interglacial transitions and is not in support of an early warming of the tropical ocean. Furthermore, no trace of a phase shift between the Mg/Ca and $\delta^{18}O$ ratios in foraminifera could be observed in the Atlantic or Arctic Ocean, thus this phenomenon is limited to the tropics and the presence of dynamic salinity changes as the additional modeled results imply.

Our results underline the importance of understanding the reaction of a proxy signal to different environmental changes, even on shorter time scales of a few thousand years, to help to interpret the changes in tropical and other ocean regions during glacial/interglacial transitions and strengthen the selective use of the $\delta^{44/40}Ca$ isotope system in foraminifera to decipher SSS variations.

Kurzzusammenfassung

Die Bearbeitungen von kombinierten Mg/Ca- und $\delta^{18}O$- Messungen an planktonischen Foraminiferen-Schalen aus Sedimentkernen haben für tropische Ozeane ergeben, dass Änderungen des Mg/Ca-Verhältnisses während der Übergangsphase vom letzten Glazial zum Holozän (Termination 1) bereits einige tausend Jahre vor einem entsprechenden Wechsel des $\delta^{18}O$-Signals eingetreten sind (z.B. *Lea et al.,* [2000]; *Nürnberg et al.* [2000]; *Visser et al.* [2003]). Als Schlussfolgerung aus diesen Beobachtungen wurde die Hypothese aufgestellt, dass sich der tropische Ozean vor dem Abschmelzen der polaren Eiskappe der nördlichen Hemisphäre erwärmte und damit als Schrittmacher von glazialen zu interglazialen Übergängen angesehen werden kann. Der tropische Ozean wäre damit ein entscheidender Auslöser von globalen Klimaänderungen.

In der vorliegenden Dissertation wird die genannte Hypothese durch kombinierte Messungen sowohl der $\delta^{44/40}Ca$ als auch der $\delta^{18}O$ und Mg/Ca-Verhältnisse an Schalen von planktonischen Foraminiferen (´multi-proxy-approach´) untersucht mit dem Ziel, die Einflüsse von Oberflächen-Temperaturen (SST) und der Oberflächen-Salinität (SSS) des Meerwassers während der Übergangsphase Glazial / Interglazial von den indirekten Temperatur-Indikatoren (´climate proxies´) zu entkoppeln. Die für die Untersuchungen ausgewählten Sedimentkerne überdecken eine Traverse vom tropischen Ozean zu hohen Breiten des Nordatlantiks.

In Übereinstimmung mit früheren Beobachtungen zeigen die Ergebnisse der Bearbeitung eine Verzögerung von ~4000 Jahren des Temperatur-Wechsels vom glazialen zum interglazialen Übergang zwischen den Mg/Ca und $\delta^{18}O$ Messwerten für die Foraminiferen-Schalen von *G. sacculifer* in der zentralen Karibik.

Im Gegensatz zu früheren Interpretationen können diese Phasenverschiebungen der Temperatur-Proxy-Daten jedoch durch dynamische lokale Änderungen der Verdunstung / Niederschlags-Verhältnisse im tropischen Ozean erklärt werden, die sich aus den errechneten $\delta^{44/40}Ca$-Oberflächenwasser-Temperaturen (SST) ergeben. Die sich daraus ableitende Dynamik der Änderungen der Oberflächen-Salinität (SSS) reflektiert vermutlich temporäre Verschiebungen der Inner-Tropischen-Konvergenz-Zone (ITCZ), die durch glaziale / interglaziale Übergänge ausgelöst werden, und

damit nicht im Zusammenhang mit einer frühen Erwärmung der tropischen Ozeane stehen. Eine weitere Bestätigung dieser Interpretation ist das Fehlen von Phasenverschiebungen im Atlantischen und Arktischen Ozean. Zusammenfassend zeigt sich, dass die genannten Phasenverschiebungen auf die tropischen Ozeane beschränkt sind und damit dynamische Salinitäts-Änderungen widerspiegeln, wie auch zusätzliche Modellierungen bestätigt haben.

Die in der vorliegenden Bearbeitung niedergelegten Ergebnisse unterstreichen die Bedeutung, die Abhängigkeit der verschiedenen Temperatur-Proxy-Messungen von Änderungen der Umweltbedingungen zu erkennen und zu berücksichtigen, selbst für kürzere Zeiträume von wenigen tausend Jahren, wie z.B. während der Übergangsphasen von glazialen zu interglazialen Klimaänderungen. Als weiterer Aspekt wird in der Bearbeitung auf die Ergebnisse einer selektiven Anwendung von $\delta^{44/40}$Ca-Temperatur-Messungen an planktonischen Foraminiferen-Schalen hingewiesen, die die Bestimmung von Salinitäts-Änderungen (SSS) in Kombination mit herkömmlichen Mg/Ca und δ^{18}O-Messungen ermöglichen.

1 INTRODUCTION

Paleo-climate research of the last 25 years has focussed on the North Atlantic Ocean and in particular on the potential of processes for glacial timescale climate variability in high northern latitudes [e.g., *deMenocal et al*., 2000; *Kiefer et al*., 2001; *Sarnthein and Tiedemann*, 1990; *Sarnthein et al*., 2000; *Stuiver et al*., 1997; *Voelker et al*., 1998]. Less emphasis was directed to the role of the tropical oceans as a result of the "Climate/Long Range Investigation, Mapping, and Prediction Project" (CLIMAP) which predicted only minor temperature variations in the order of 1-2°C in sea surface temperatures (SST) in the low latitudes, although a decade ago, *Bacastow* [1996] already stated that even small changes in tropical sea surface temperatures (SST) of ~1°C may have led to an increase in atmospheric pCO_2 concentrations by ~11 to 16 ppm. Today, the CLIMAP reconstructions still serve as a base for paleoclimate research, but many of its results remain controversial because a new range of methods, like Mg/Ca and U^k37, for reconstructing SSTs have been developed in the past years with partly different results to the earlier findings of CLIMAP.

A very accurate and reliable method to reconstruct ocean water temperature and its timing is the combined measurement of $\delta^{18}O_{foram}$ and Mg/Ca_{foram} signals from the same foraminiferal species [*Nürnberg et al*., 1996; *Nürnberg et al*., 2000; *Lea et al.,* 2000]. This so called multi-proxy approach is thought to produce more accurate SST reconstructions and may also allow a better control on the timings of the warming of the oceans and changes of the salinity with respect to the melting of the continental ice volume during deglaciations. In this regard *Nürnberg et al*. [2000] and *Lea et al.* [2000] observed larger temperature variations in the tropical ocean of up to ~5°C. In addition, time lags between the $\delta^{18}O_{foram}$ and Mg/Ca_{foram} signals were found in samples from tropical oceans during deglaciation phases. These observations led to a better understanding of the causal chains that trigger climate changes, because leads and lags between different ocean and climate parameters could be defined more accurately.

An additional temperature proxy, although rarely applied method for determinations in tropical oceans is the use of Calcium isotope ratios measured in foraminifera. The $\delta^{44/40}Ca$ isotope system has been successfully employed by *Zhu* and *McDougall* [1998] and *N. Gussone et al.* [2004] compared the results with the measurements of

the Mg/Ca ratios of the same samples. Their approach allowed for the divided reconstruction of salinity and temperature since the Ca isotope ratio proxies seem to be independent to salinity variations. Regrettably only two species of foraminifera, *G. sacculifer* and *N. pachyderma*, are so far known to have a temperature slope sensitive enough for measurements. The slopes of these two species are by a factor of ten larger when compared with other species of foraminifera.

Furthermore *Hippler et al.* [2006] were able to measure $\delta^{44/40}$Ca ratios and successfully compared the results to their corresponding Mg/Ca ratios [*Nürnberg et al.* 2000] for *G. sacculifer* from the South Atlantic Ocean from the GeoB 1112 core in the Gulf of Guinea. Both evaluations showed comparable results over Termination 1 and 2, i.e. an increase in the ocean surface temperature of ~3.5℃; distinctly more than the 1-2℃ predicted by CLIMAP. It was emphasiz ed in both publications that the good correlation of both temperature proxies, Mg/Ca and $\delta^{44/40}$Ca ratios, is an excellent criterion in order to verify the robustness of temperature reconstructions by foraminifera.

Measurements of temperature proxies at high northern latitudes suffer from the fact that the planktonic foraminiferal assemblages are almost monospecific with *N. pachyderma sinistral* often being the only available species in sediment cores. This species is well suited for $\delta^{44/40}$Ca ratio measurements [*Hippler et al*, 2006; *R. Kozdon* et al., 2009]. Similar to the observations from *G. sacculifer,* the $\delta^{44/40}$Ca based temperature reconstructions are in accord with the reconstructions based on Mg/Ca measurements [*Nürnberg*, 1995] and δ^{18}O ratios [*Jones and Keigwin*, 1988; *Vogelsang*, 1990]. One major finding in this regard is that the use of *N. pachyderma* as an archive for temperature reconstructions may be restricted to the fact that this species tends to stay in the same water masses with a distinct salinity. Hence, *N. pachyderma* based temperature reconstructions show small glacial / interglacial variations reflecting sea surface temperature only to a minor extent [*Kozdon et al.*, 2006].

In 2002 *Visser et al.* explained the timing of glacial / interglacial climate changes on a global scale in order to verify the impact of the earth's tropical areas on the high southern latitudes. Their samples were taken in the Makassar Strait, in the centre of the Indo-Pacific warm pool. The combined $\delta^{18}O_{foram}$ and Mg/Ca_{foram} measurements resulted in the observation that the Mg/Ca_{foram} signal is not synchronous with the change in $\delta^{18}O_{foram}$, but leads the $\delta^{18}O_{foram}$ signal by two to three thousand years

across glacial / interglacial Terminations 1 and 2, respectively. In contrast the Mg/Ca signals correlated with the atmospheric records, e.g. the deuterium isotope ratios (δD) in the Vostok ice core [*Petit et al*., 1999], which reflect atmospheric warming and cooling over Antarctica. Previously it was suggested that changes in the concentrations of carbon dioxide (CO_2) in the atmosphere and temperature changes in the Southern Hemisphere are synchronous and lead variations in the Northern Hemisphere ice sheets by several thousand years [*Broecker et al.,* 1998; *Shackelton et al*., 2000]. As a consequence these measurements would indicate that the tropics are the driving force behind the onset of the glacial/interglacial cycles [*Visser et al.,* 2003].

On the other hand it has also been shown by *Lea et al.* [1999] that the onset of the deglaciation, more accurately the onset of the warming, was synchronous at both poles. The discrepancy between these observations and in particular the origin of the phase shift, however, remained unresolved.

A major challenge would be to evaluate the unresolved problem whether the tropical oceans or the Northern North Atlantic are the pacemaker of the onset of the last deglaciation. In particular, it is important to test the influence of salinity variations on the Mg/Ca- and $\delta^{18}O$ records because regional glacial / interglacial salinity variations have the potential to obscure the original temperature signal. Hence, the topic of this study is a detailed analysis of the observed phase shift between the $\delta^{18}O_{foram}$ and Mg/Ca_{foram} ratios at Termination 1. In order to fulfil these objectives a hitherto unique approach was applied, namely not only the application of the well established combined measurement of Mg/Ca and $\delta^{18}O$ ratios but in addition the integration of the $\delta^{44/40}Ca$ stable isotope ratios, measured in the same planktonic foraminiferal species.

With these combined Mg/Ca, $\delta^{18}O$ and $\delta^{44/40}Ca$ measurements, it is anticipated to decipher variations in the evaporation to precipitation ratios in tropical and high northern latitude oceans and to extract the pure temperature signal from the salinity variations. Following this approach the timing and phase shift of events, e.g. salinity and temperature variations can be unravelled in a greater detail.

2 APPROACH and BACKGROUND

2.1 The dependency of oxygen isotope fractionation ($\delta^{18}O$) from temperature and salinity changes

The oxygen isotope system consists of three stable isotopes: ^{16}O, ^{17}O and ^{18}O of which the ^{16}O isotope is the most abundant one (99.76%), while the occurrence of the other two is only 0.04% and 0.2% respectively. The variation of the $^{18}O/^{16}O$-ratio of seawater is a consequence of natural isotope fractionation, reported in the usual δ-notation as $\delta^{18}O_{seawater}$ (equation 1), which is one of the most important tools in paleoclimatology [c.f. *Shakelton and Opdyke*, 1973].

Equation 1:

$$\delta^{18}O[‰] = \left[\frac{\left[\frac{^{18}O}{^{16}O}\right]_{sample} - \left[\frac{^{18}O}{^{16}O}\right]_{standard}}{\left[\frac{^{18}O}{^{16}O}\right]_{standard}} - 1 \right] \times 1000$$

The $\delta^{18}O_{seawater}$ ratios are mostly measured relative to the Standard Mean Ocean Water (V-SMOW). The basic principles of mass spectrometry and the necessary preparations of the samples were first established by *McCrea* [1950] and *Epstein and Mayeda* [1953].

It has been found that $\delta^{18}O_{seawater}$ was not constant over time but changed within certain limits due to various fractionation control mechanisms. In particular kinetic and Raleigh type isotope fractionations [*Zeebe*, 2001] related to evaporation/precipitation processes summarized below tend to alter $\delta^{18}O$-values values on all time scales:

1. Due to kinetic isotope effects during the evaporation of sea water, the water vapor is depleted in the heavy ^{18}O-isotope resulting in a value of 9.8 ‰ whereas the remaining sea water is enriched in the heavy isotope in the same order of magnitude [*Majoube*, 1971].
2. During the formation of sea ice, the newly formed ice is enriched in ^{18}O in the order of 2.5 ‰ [*Craig and Gordon*, 1965; *Mac Donald et. al*., 1995]. Latter effect is of major interest only at the sea ice margin.
3. During precipitation, the incremental rain water becomes enriched in the heavy isotope resulting in more positive $\delta^{18}O$-values by up to 1.5 ‰ [*Craig and Gordon*, 1965] depending on the reservoir size of the clouds..
4. The $\delta^{18}O$ ratio of the sea water can change due to the mixing of water masses of different isotopic compositions, e.g. melt water influxes and rainwater.
5. Alterations of the global ice volume as a consequence of glacial/interglacial variations have an impact on the $\delta^{18}O$ ratio [*Waelbroeck et al.*, 2003]. The differences between the $\delta^{18}O$ ratios of seawater during the last glacial maximum and present day conditions are more than 1 to 1.5 ‰. The main signal variations occur during glacial / interglacial Terminations (e.g. Termination 1 and 2 during the Late Quaternary). For a more detailed description refer to section 2.3.1.

   The Fig. 2.1 shows qualitatively, how variations of ocean water parameters influence the $\delta^{18}O$ ratios in planktonic foraminifera. Note, that the processes one to four in the list above are relatively short term processes whereas process five is a long term process. Hence, processes one to four would be superimposed on temporary and spatial variations of the general $\delta^{18}O_{seawater}$-signal.

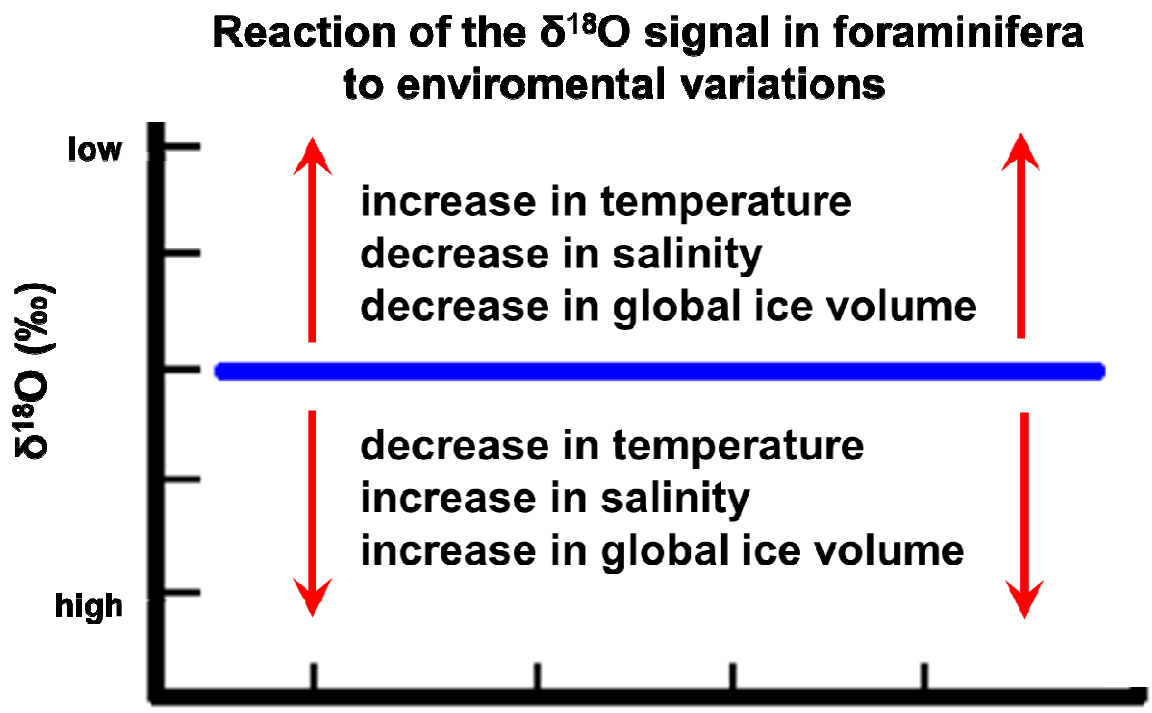

Figure 2.1: Schematic illustration of the influence of variations in ocean parameters like seawater temperature, global ice volume and salinity on the measured $\delta^{18}O$ signal in planktonic foraminifera. Note, that the increase in global ice volume is a long term process which is superimposed by the other effects being short term processes. Latter short term processes cause regional and spatial differences in the $\delta^{18}O$ records as seen in marine sediments.

Complications for paleo-reconstructions may arise from the fact that a rise in water temperature and a simultaneous decrease in the global ice volume both tend to shift the $\delta^{18}O$ signal in planktonic foraminifera to lower values (Fig. 2.1). The two effects superimpose each other and can shift the signal by more than 4 ‰ as calculations suggest.

On the contrary, an increase in sea surface salinity (SSS) will push the $\delta^{18}O$ values to more positive values. Hence, it is possible to outweigh the influence of one or more effects on the $\delta^{18}O_{seawater}$ record. At glacial / interglacial transitions a possible scenario would be that during a period of major deglaciations and / or SST change the $\delta^{18}O_{seawater}$ should change to lower ratios. However, if at the same time the salinity of the surrounding water rises, the $\delta^{18}O_{seawater}$-signals will be shifted to relatively higher values, possibly outweighing the temperature and sea-ice volume effect to a certain degree.

2.2 The Mg/Ca system

An additional independent approach to gain information about past ocean water temperatures from planktonic foraminifera is the measurement of the Mg/Ca ratio in their calcium carbonate shells [*Nürnberg et al*.,1996; *Nürnberg et al*., 2000; *Lea et al.,* 2000]. The ratio of the Mg/Ca uptake into the foraminiferal calcite lattice of the shell is not constant but influenced by factors of which the temperature is considered to be the most important one. This relationship is the basis of the Mg/Ca paleothermometry [e.g., *Nürnberg*, 2000]. Recent studies [*Kisakürek et al.*, 2008; *Regenberg et al*., 2009], however, have shown that also a salinity component in *G. ruber* and *G. sacculifer* plays an important role in this relationship.

As a result, the exact equation for *G. ruber* is:

Equation 2:

$$\mathbf{Mg/Ca}\left[\frac{\mathbf{mmol}}{\mathbf{mol}}\right] = \mathbf{exp}[\mathbf{0.06}(\pm\mathbf{0.02}) \times \mathbf{S}\,[\mathbf{psu}] + \mathbf{0.08}(\pm\mathbf{0.02}) \times \mathbf{T}\,[℃] - \mathbf{2.8}(\pm\mathbf{1.0})]$$

S=Salinity, T=Temperature, [*Kisakürek et al.*, 2009]

The change of the Mg/Ca ratio is about 6 % per unit psu [Practical Salinity Unit] and 8 % per ℃ for *G. ruber.* Note that the relationship between salinity and temperature for the Mg/Ca ratios for foraminiferal species is still not understood. There is a significant species dependency on the Mg/Ca-temperature relationship. Furthermore, Mg/Ca ratios in foraminifera are in general significantly different than the Mg/Ca ratios of inorganic calcite. This indicates that there is a strong physiological control on the uptake of Mg from seawater by foraminifera [*Erez*, 2003].

Culturing experiments, net catches and core top samples suggest an exponential relationship between the Mg/Ca ratio in a foraminiferal sample and the surrounding seawater [*Nürnberg et al*., 1996; *Mashiotta et al*., 1999; *Lea et al*., 2000; *Elderfield and Ganssen*, 2000; *Dekens et al*., 2002; *Anand et al*., 2003; *McKenna and Prell*, 2004]. Several different studies, however, have also shown a linear relationship [*Hastings et al*., 1998; *Rosenthal and Lohmann*, 2000]. A possible explanation for these species dependent variations in the salinity/temperature-relationships could be a kinetic effect introduced by a growth-rate-dependency of the Mg discrimination that

influences the uptake of Mg into the $CaCO_3$ shell of the foraminifera [*Kisakürek et al.,* 2008].

Furthermore, additional studies have discussed the impact of calcite dissolution processes the effects of the shells of various foraminifera species in core top samples, in particular by salinity variations and pH-changes on the Mg/Ca ratios [e.g., *Brown and Elderfield*, 1996; *Rosenthal et al*., 2000; *Dekens et al*. 2002; *Rosenthal and Lohmann,* 2002]. Recently *Regenberg et al.* [2006] provided dissolution correction factors for Mg/Ca ratio calibration equations. The dissolution of the foraminiferal shells commences in water depths of about 3500m below the CCD (Carbonate Compensation Depth).

2.3 Combined $\delta^{18}O_{foram}$ and Mg/Ca_{foram} studies

2.3.1 Phase Shift between $\delta^{18}O$ and Mg/Ca

Studies applying combined $\delta^{18}O_{foram}$ and Mg/Ca_{foram} measurements in foraminifera showed that the Mg/Ca_{foram} signal is not always synchronous with the change in the planktonic $\delta^{18}O_{foram}$, Mg/Ca_{foram} can lead the $\delta^{18}O_{foram}$ signal by several thousand years across glacial / interglacial transition [e.g. *Nürnberg et al.,* 2000, *Lea et al.,* 2000, *Visser et al.,* 2003].

This discrepancy in the timing between the two proxy records was referred to in the literature as the ´Phase Shift´ which is defined as the time difference between the Terminations of the individual signal variations. The Terminations are defined as the point in time when 50% of the transition between the glacial to interglacial has occurred. This point in time can differ depending on the type of proxy measured.

During glacial / interglacial transitions the Mg/Ca ratios change on short time scale: A jump of about 1 mmol/mol in the Mg/Ca ratios, which corresponds to a temperature increase of ~1.5℃, from lower values in sediment c ore sections, corresponding to glacial periods relative to interglacial core sections has been observed [see e.g. *Hippler et al*., 2006]. The $\delta^{18}O$ ratios also show a significant variation of about 1 to 2 ‰, although the onset of this variation can differ by a phase shift of several thousand years in comparison to the Mg/Ca data.

2.3.1.1 Possible scenarios / patterns of the Phase Shift

A set of three schematic diagrams (Figs. 2.3.1 to 2.3.3) illustrates different scenarios for a possible phase shift between the Mg/Ca ratios and their corresponding $\delta^{18}O$ signals. Note, that for a matter of convenience all $\delta^{18}O$ values are plotted inversely relative to the Mg/Ca ratios to allow better comparisons.

The figure 2.3.1 shows the possible signal pattern of the Mg/Ca and $\delta^{18}O$ ratios across a glacial / interglacial transition at which only a gradual increase of the sea surface temperature occurred. No significant phase shift between the two proxies would be expected due to their similar signal patterns.

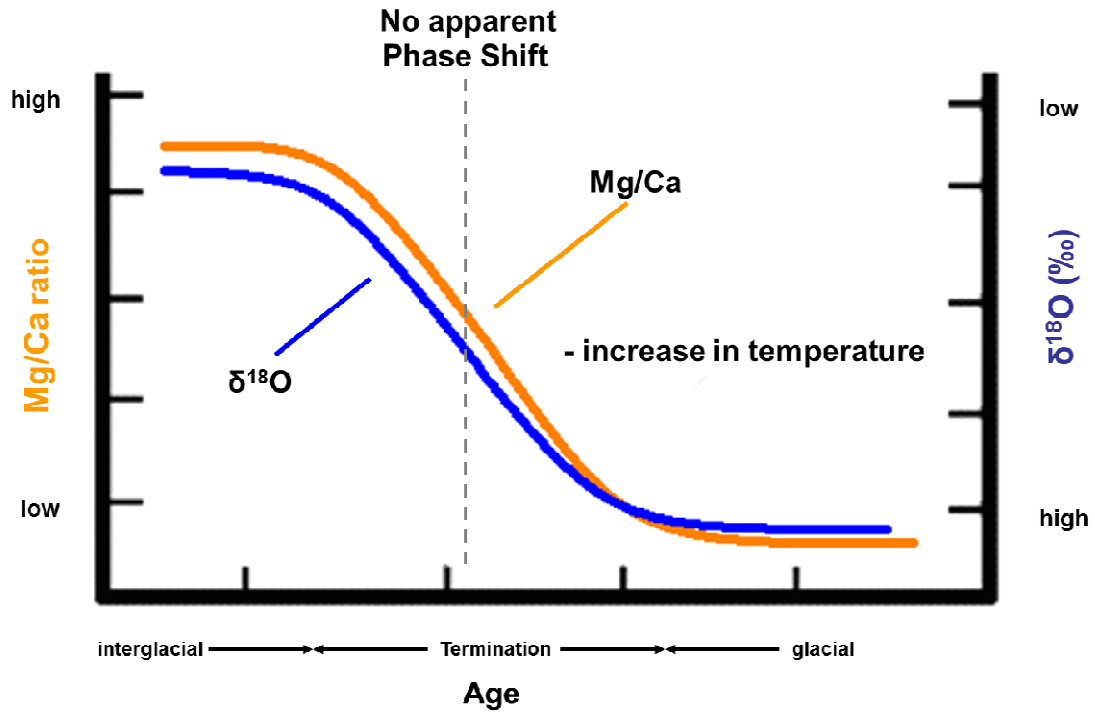

Figure 2.3.1: Schematic presentation of a possible signal pattern without a significant phase shift between the Mg/Ca and $\delta^{18}O$ ratios during the transition from a glacial maximum to an interglacial warm period. The vertical dotted line marks the estimated position of the Termination. The X-axis represents time and the Y-axis shows the Mg/Ca and $\delta^{18}O$ ratios.

In figure 2.3.2 a scenario with a possible phase shift between Mg/Ca and $\delta^{18}O$ ratios over a glacial to interglacial transition is schematically presented with an increase in SST and simultaneous decrease of SSS and ice coverage. The Termination of the $\delta^{18}O$ signal would probably lead the Mg/Ca ratio signal by a measureable time, most likely a few thousand years.

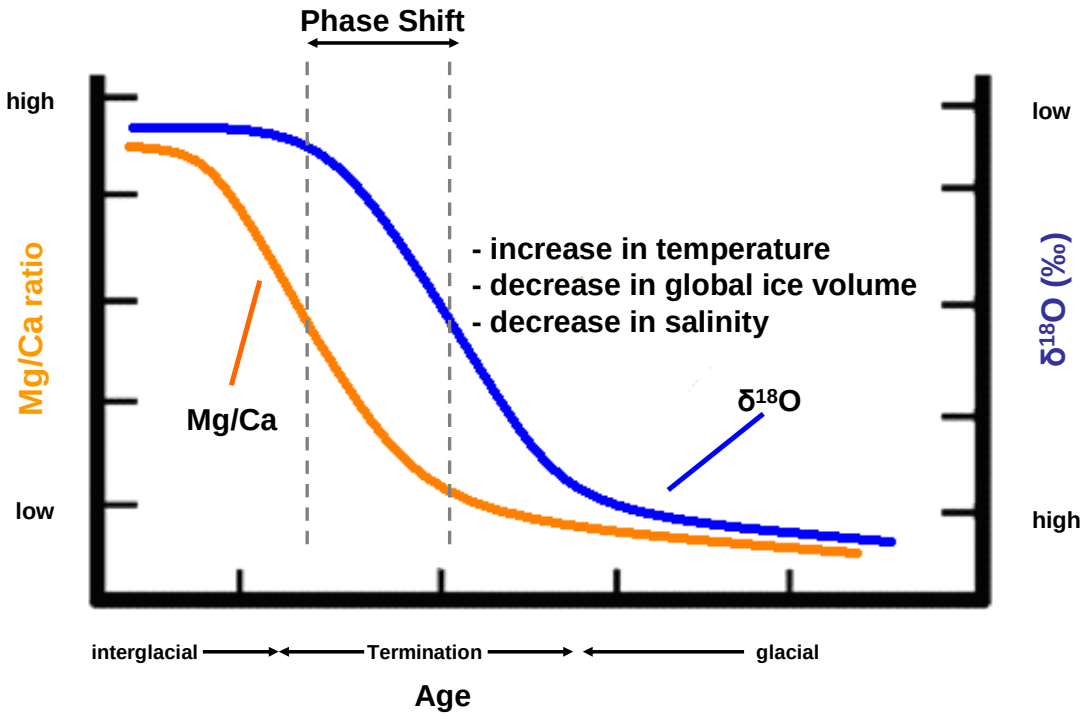

Figure 2.3.2: Schematic presentation of a possible phase phift between Mg/Ca and $\delta^{18}O$ ratios during the transition from a glacial to an interglacial period. The signal pattern represents an increase in temperature with a simultaneous decrease in sea surface salinity and ice coverage. The X-axis represents time and the Y-axis shows the Mg/Ca and $\delta^{18}O$ ratios, respectively. Note that the Termination for the Mg/Ca record lags behind the one for $\delta^{18}O$ record.

The diagram (figure 2.3.3) shows the possible signal pattern over a glacial to interglacial transition period at which the Mg/Ca and $\delta^{18}O$ ratios are exposed to a strong and simultaneous increase in SST (>1.5℃) and SSS (+1 / +2 psu). These differences in SST and SSS have been previously observed and discussed [e.g. *Nürnberg et al.,* 2000, *Lea et al.,* 2000, *Visser et al.,* 2003] and thus are considered to be a realistic scenario for this approach.

These abrupt changes in surface ocean waters should cause a phase shift between the two proxy signals. The increase in SSS compensates the influence of the rising water temperatures and causes the $\delta^{18}O$ to remain unchanged during the Transition.

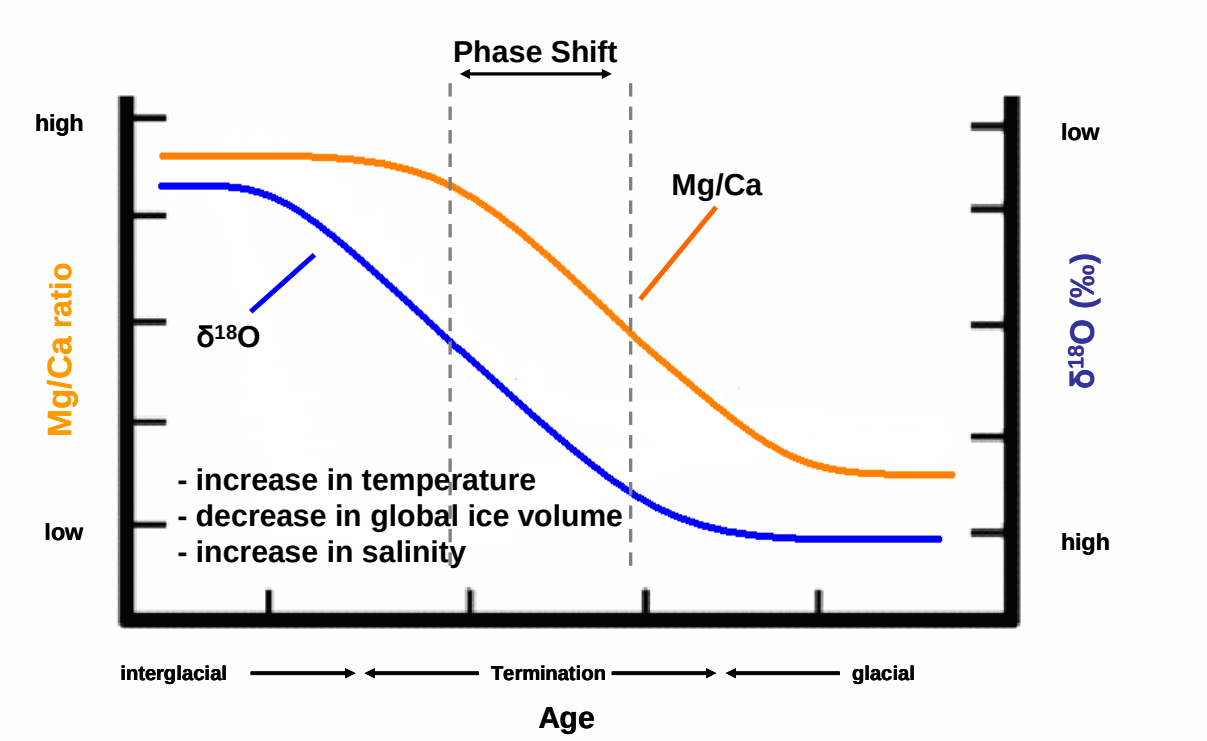

Figure 2.3.3: Schematic presentation of the most likely scenario of a possible phase shift between Mg/Ca and $\delta^{18}O$ ratios during the transition from a glacial to an interglacial period. The signal pattern represents an increase in SST and an increase in sea surface salinity with a simultaneous decrease in global ice coverage. The X-axis represents time and the Y-axis shows the Mg/Ca and $\delta^{18}O$ ratios.

The latter is the most likely scenario which we consider for our core site SO 164-03-4 in the Central Caribbean Sea. Similarly, a phase shift of this type has previously already been observed in tropical oceans (for more details refer to the end of section 2.3) [*Visser et al.,* 2003].

Finally in figure 2.3.4 a hypothetical scenario is presented in which the influence of a gradual temperature increase and a strong jump in SSS on the Mg/Ca and $\delta^{18}O$ ratios is outlined. These unusual ocean conditions would cause the two proxies to totally loose correspondence and most likely form an unusual signal pattern. This behaviour of the Mg/Ca and $\delta^{18}O$ ratios has not been observed for the last Transition from the glacial to interglacial period.

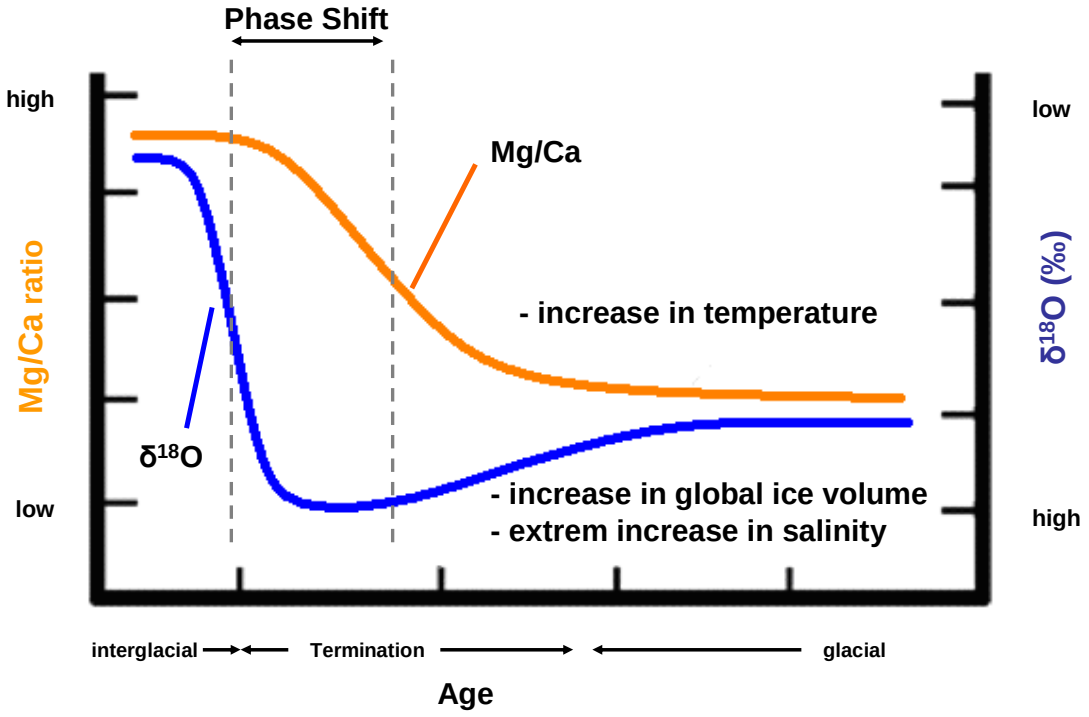

Figure 2.3.4: Schematic presentation of a hypothetical phase shift between Mg/Ca and $\delta^{18}O$ ratios during the transition from a glacial maximum to a warm period. The signal pattern represents an extreme environment with increase in SST and a very large jump in SSS. The X-axis represents time and the Y-axis shows the Mg/Ca and $\delta^{18}O$ ratios.

2.3.1.2 Observation of the Phase Shift

The ´Phase Shift´ was observed in tropical oceans by *Hippler et al*. [2006], *Lea et al*. [2000] and *Nürnberg et al*. [2000]. Further, *Visser et al*. [2003] demonstrated in a high-resolution study across Termination 1 and 2 in sediment cores from the tropical West Pacific (Makassar Strait) that the change in the Mg/Ca ratios measured in *G. ruber* leads the $\delta^{18}O_{foram}$ signal by ~2.000 to ~3.000 years. In contrast, the Mg/Ca signals correlate very well with atmospheric records [*Visser et al*., 2003], e.g. the deuterium isotope record in the Vostok ice core [*Petit et al*., 1999]. This result was interpreted that the onset of the warming of the tropical ocean and the atmosphere over Antarctica took place simultaneously. A later melting of the polar ice volumes of two to three thousand years was considered responsible for the phase shift of the $\delta^{18}O_{foram}$ signals.

It has to be noted that the phase shift has so far been observed in different glacial / interglacial transition periods but only in tropical environments and only if the sample density and the time resolution is significantly higher than the actual phase shift.

2.3.2 The Possible Impact of Salinity

In general the $\delta^{18}O_{foram}$ and Mg/Ca_{foram} values measured in foraminifera do not solely reflect temperatures but are also controlled by their dependency on sea water salinity (see equations 2 and 3). From our understanding (see section 2.3 above), leads and lags may not only be triggered by a delay of temperature exchanges between the North Atlantic and the tropical oceans but also by differential changes in salinity triggered by dynamic variations of the precipitation / evaporation ratios (e.g. in tropical oceans) and the local influences of melt water inputs (e.g. in high northern latitude and southern oceans). In order to resolve the problem, a multi-proxy approach using a combined method of analysing $\delta^{18}O_{foram}$, Mg/Ca_{foram} and $\delta^{44/40}Ca_{foram}$ as SST proxies can theoretically be applied. This thesis will examine the validity of such an approach.

2.3.3 A model of the expected variation during transition periods

In view of the importance of the patterns of the signal variations in $\delta^{18}O$ and Mg/Ca ratios over the Transition a simple model will be employed, using the Mg/Ca temperature and salinity relationship for *G. ruber* (see section 2.2) [*Kisakürek et al.*, 2009].

The exact salinity relationship for $\delta^{18}O$ over time in planktonic foraminifera is not known thus a simplified estimation will be applied. The influence of temperature variations on carbonates by *Shakleton* [1974] will be combined with the salinity variation by *Schmidt et al.* [1999]. The influence of the global ice volume will be neglected in this basic model. The full equations are presented in the appendix section 4.

The following schematic diagram highlights the modelled time interval. The focus will only be on the transition period which contains the expected Termination point.

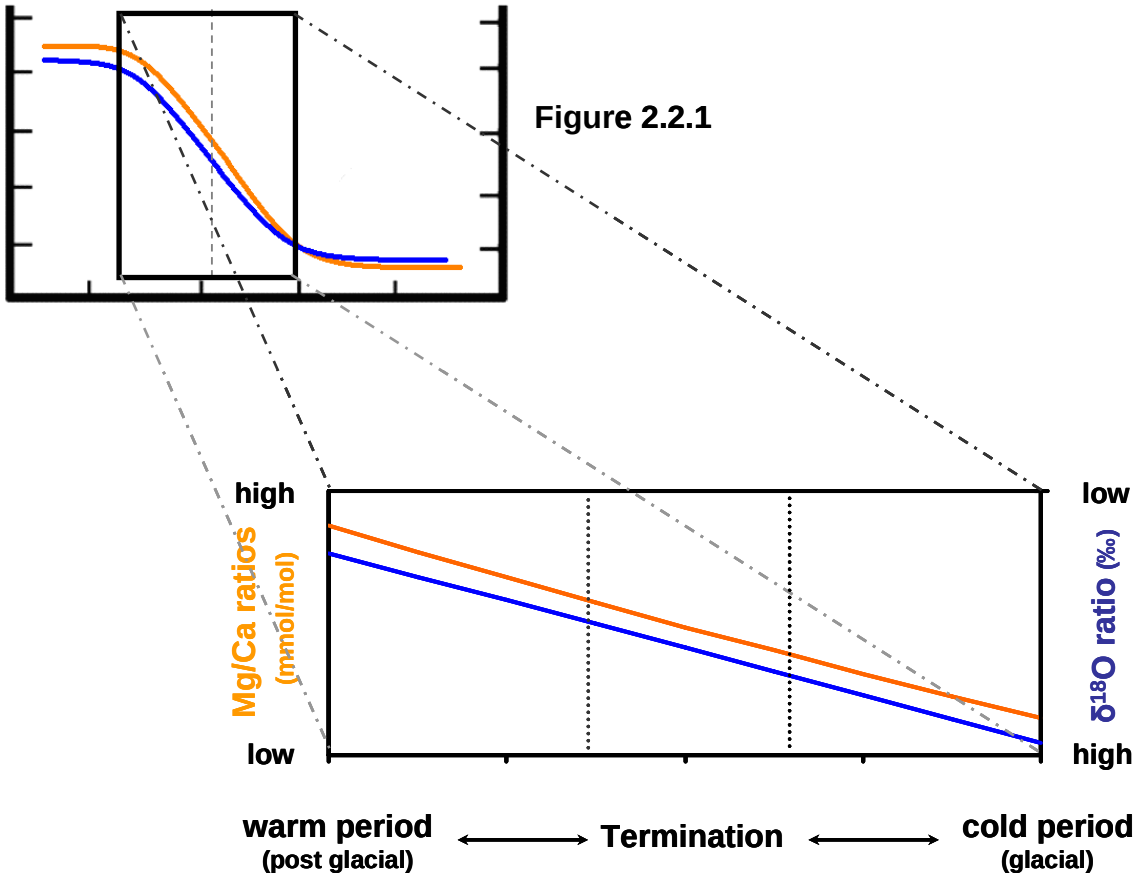

Figure 2.3.5: Schematic presentation of the modelled time interval. In the model all other parameters will be left unchanged outside of this time window.

A temperature increase of 2℃ over a time span of 2 000 years with a variation of different changes in salinity will be modelled. A linear temperature increase is

assumed at all times in order to observe the influence of salinity variations and the occurrence of a phase shift between the two proxies. The starting conditions will be 25℃ and a salinity of 33 psu.

Five different scenarios were modelled for *G. ruber* for transition periods as follows: The $\delta^{18}O$ [‰] ratios are always presented in blue whereas the Mg/Ca [mmol/mol] ratios are presented in orange. The X-axis represents the time span of a transition period: 2000 years being the oldest point in time (glacial period) and 0 years the youngest (postglacial period). As a matter of convenience, the $\delta^{18}O$ ratios are illustrated with an inverse second Y-axis in all figures.

As a reference in figure 2.3.6 the effect of a variation in salinity [ΔS=1 (psu)] over the modelled time interval with no variation in temperature [ΔT=0 (℃)] is presented; the calculated values in table 2.3.3.1. The different reactions of the two proxies to this simple change in environmental conditions are observable.

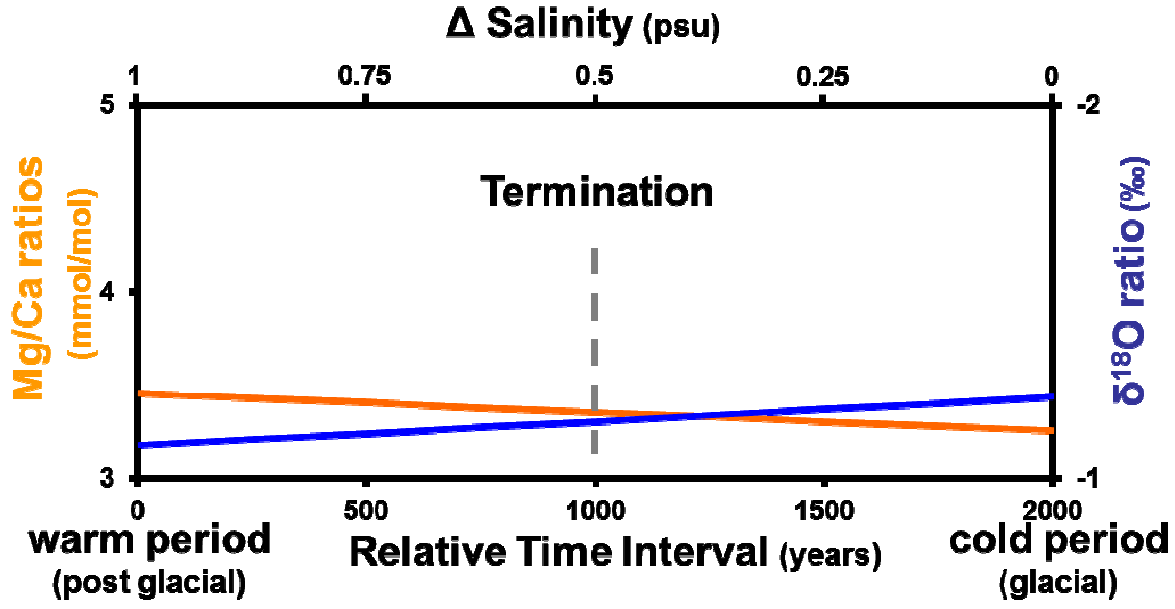

Figure 2.3.6: Model calculations show a salinity increase of 1 psu over 2000 years. Both signals show no phase shift but different signal patterns.

A variation in the signal patterns of the two proxies is observed but this is due to the presentation method.

Table 2.3.3.1:

1	2	3	4	5
Age	**T (°C)**	**S (psu)**	**Mg/Ca [mmol/mol]**	**$\delta^{18}O$ [‰]**
2000	25	33	3.25	-1.22
1750	25	33.125	3.28	-1.20
1500	25	33.25	3.30	-1.18
1250	25	33.375	3.33	-1.17
1000	25	33.5	3.35	-1.15
750	25	33.625	3.38	-1.14
500	25	33.75	3.40	-1.12
250	25	33.875	3.43	-1.10
0	25	34	3.46	-1.09

4: Mg/Ca ratios calculated with equation 2 employing the values from **2** and **3**

5: $\delta^{18}O$ values calculated with equation A (see appendix) employing the values from **2** and **3**

The salinity variation of 1 psu increases the values of both proxies by ~ 0.1 and due to the linear nature of the modelled variation the Termination for both proxies is identical, thus no phase shift is observed.

The two figures 2.3.7 and 2.3.8, table 2.3.3.2 contains the calculated values, represent a temperature variation of 2℃ over a tra nsition period of 2000 years with different increases in salinity.

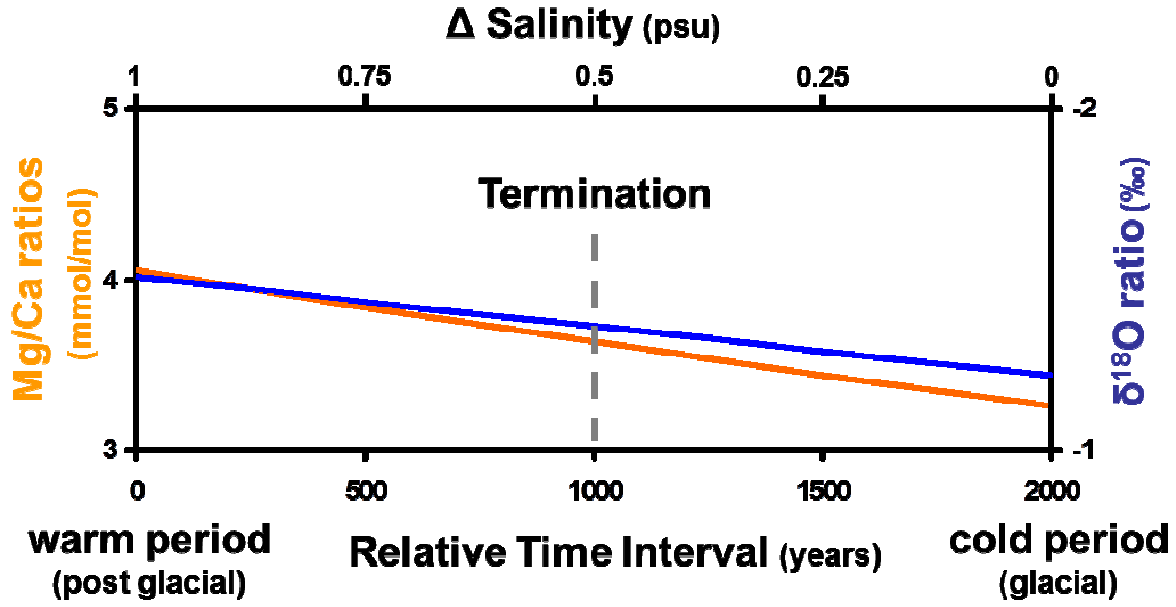

Figure 2.3.7: Model calculations show a temperature increase of 2℃ and a salinity increase of 1 psu over 2000 years. Both signals show no significant phase shift and a similar pattern.

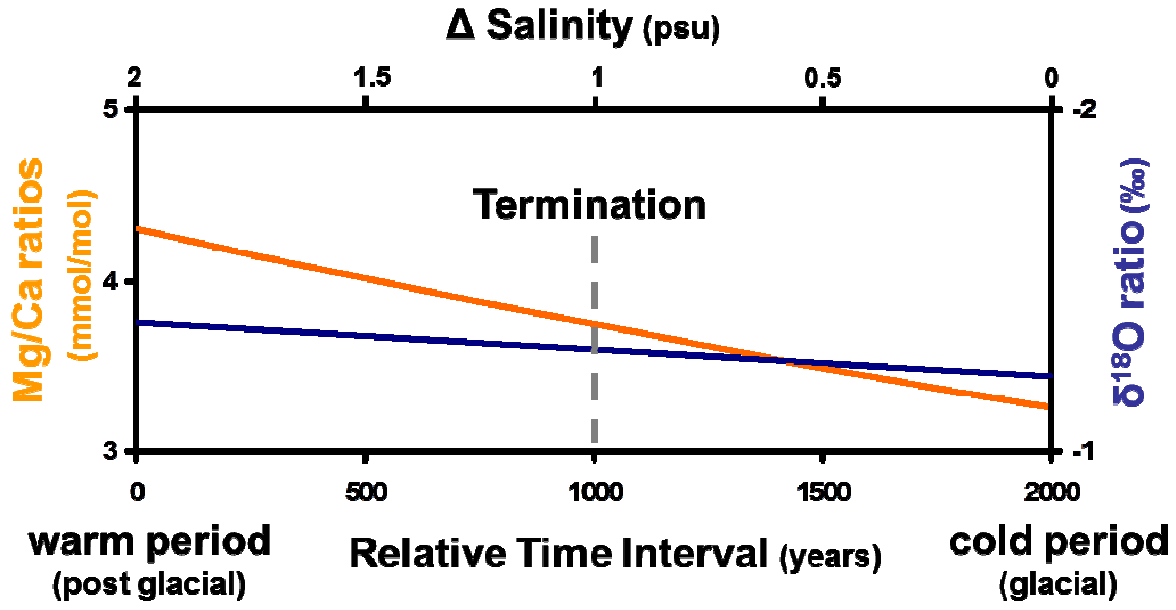

Figure 2.3.8: This diagram shows the model results for an increase of 2℃ and 2 psu over 2000 years. The signals show no phase shift, the $\delta^{18}O$ ratios show only minor variations.

For both modelled scenarios the signal variations of the proxies are linear and the Terminations are all around the 1000 year position in the model. In comparison to

figure 2.3.6 the combined influence of salinity and temperature variations are clearly visible.

Table 2.3.3.2:

1	2	3	4	5	6	7	8
Age	**T (°C)**	**S (psu)**	**S (psu)**	**Mg/Ca [mmol/mol]**	**$\delta^{18}O$ [‰]**	**Mg/Ca [mmol/mol]**	**$\delta^{18}O$ [‰]**
2000	25	33	33	3.25	-1.22	3.25	-1.22
1750	25.25	33.125	33.25	3.35	-1.25	3.37	-1.24
1500	25.5	33.25	33.5	3.44	-1.29	3.49	-1.26
1250	25.75	33.375	33.75	3.53	-1.33	3.61	-1.28
1000	26	33.5	34	3.63	-1.36	3.74	-1.30
750	26.25	33.625	34.25	3.73	-1.40	3.88	-1.32
500	26.5	33.75	34.5	3.84	-1.43	4.01	-1.34
250	26.75	33.875	34.75	3.95	-1.47	4.16	-1.36
0	27	34	35	4.06	-1.51	4.31	-1.38

5: Mg/Ca ratios calculated with equation 2 employing the values from **2** and **3 (figure 2.3.3.1)**

6: $\delta^{18}O$ values calculated with equation A (see appendix) employing the values from **2** and **3 (figure 2.3.3.1)**

7: Mg/Ca ratios calculated with equation 2 employing the values from **2** and **4 (figure 2.3.3.2)**

8: $\delta^{18}O$ values calculated with equation A (see appendix) employing the values from **2** and **4 (figure 2.3.3.2)**

The effect of the differences in salinity is observed in figure 2.3.8 compared to figure 2.3.7: The calculated model shows a small variation in the order of ~0.15 ‰ for the $\delta^{18}O$ record compared to the ~0.3 ‰ in figure 2.3.3.1. Furthermore the addition of a temperature component has led to a decrease in the overall $\delta^{18}O$ values.

For comparison note that a linear increase of 2℃ over the same time frame with no salinity variation will result in a change of ~0.45 ‰ for the $\delta^{18}O$ record.

The Mg/Ca ratios react differently to the combined temperature and salinity increase. The Mg/Ca ratios are higher by about 0.3 mmol/mol relative to the scenario as seen in figure 2.3.7. Both salinity and temperature variations influence the Mg/Ca ratios similarly.

As a consequence this means that the influence of salinity on the $\delta^{18}O$ record cannot be neglected, thus the combination of temperature and salinity increase has a great influence on the $\delta^{18}O$ signal pattern.

The conclusion of these simple modelled conditions is that a variation of salinity has a significant influence on the $\delta^{18}O$ ratios in the shells of *G. ruber* during a glacial / interglacial transition period.

The modelled results change if a decrease in salinity is assumed. This can be caused during the transition from a glacial to an interglacial period by large amounts of fresh water, resulting in a local salinity decrease, as they enter the ocean. A decrease of 1 psu is modelled in figure 2.3.9; the values are presented in table 2.3.3.3.

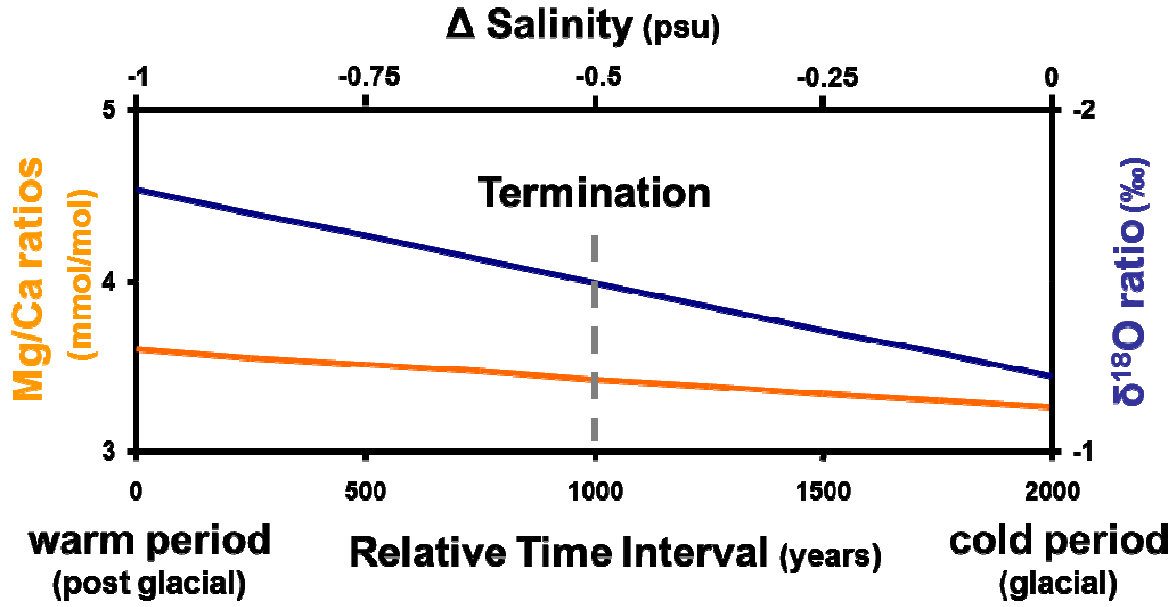

Figure 2.3.9: Increase of 2℃ and a decrease of 1 psu over 2000 years. The Mg/Ca ratios show only minor signal variations, whereas the $\delta^{18}O$ ratios show a strong reaction.

Table 2.3.3.3:

1	2	3	4	5
Age	T (°C)	S (psu)	Mg/Ca [mmol/mol]	$\delta^{18}O$ [‰]
2000	25	33	3.25	-1.22
1750	25.25	32.875	3.30	-1.29
1500	25.5	32.75	3.34	-1.36
1250	25.75	32.625	3.38	-1.42
1000	26	32.5	3.42	-1.49
750	26.25	32.375	3.46	-1.56
500	26.5	32.25	3.51	-1.63
250	26.75	32.125	3.55	-1.70
0	27	32	3.60	-1.77

4 Mg/Ca ratios calculated with equation 2 employing the values from **2** and **3**

5 $\delta^{18}O$ values calculated with equation A (see appendix) employing the values from **2** and **3**

The Mg/Ca ratios increase only by ~0.35 ‰, since the lower salinity compensates most of the temperature induced effects, whereas the $\delta^{18}O$ ratios change by more than 0.5 ‰. A scenario like this could create a phase shift similar to figure 2.3.2 but the modelled linear changes cannot recreate or reflect this signal pattern.

The final two figures (2.3.10 and 2.3.11) model a possible signal pattern with a fluctuating salinity; the modelled values are presented in table 2.3.3.4. The other parameters are the same as in the three models above. Variations in SSS are known throughout the past and thus this scenario has to be considered a very likely one.

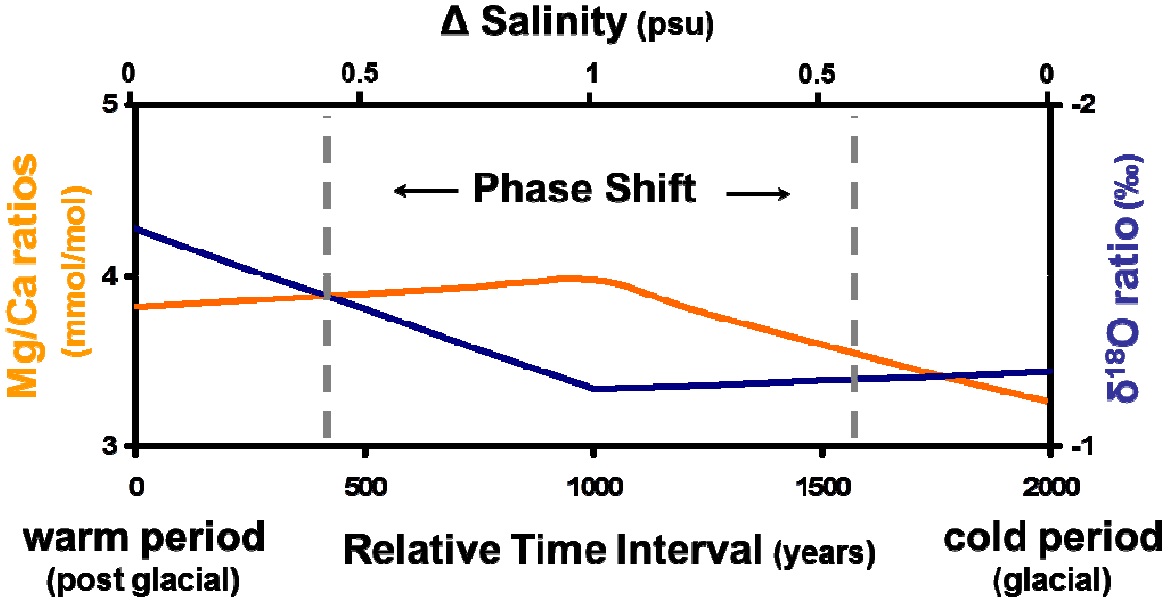

Figure 2.3.10: Increase of 2℃ over 2000 years with a salinity max imum of +1 psu at 1000 years in the middle of the transition period. The start and end variation in salinity is zero.

A salinity maximum during the transition phase creates a phase shift between the Mg/Ca and $\delta^{18}O$ ratios.

Table 2.3.3.4:

1	2	3	4	5
Age	T (°C)	S (psu)	Mg/Ca [mmol/mol]	$\delta^{18}O$ [‰]
2000	25	33	3.25	-1.22
1750	25.25	33.5	3.42	-1.20
1500	25.5	34	3.60	-1.19
1250	25.75	34.5	3.78	-1.18
1000	26	35	3.97	-1.17
750	26.25	34.5	3.94	-1.28
500	26.5	34	3.90	-1.40
250	26.75	33.5	3.86	-1.52
0	27	33	3.82	-1.64

4 Mg/Ca ratios calculated with equation 2 employing the values from **2** and **3**

5 $\delta^{18}O$ values calculated with equation A (see appendix) employing the values from **2** and **3**

The signal patterns of the two proxies in figure 2.3.10 are interesting: An increase in the modelled Mg/Ca values by about 0.7 mmol/mol and $\delta^{18}O$ ratios by 0.05 ‰ at the beginning of the transition period (from 2000 to 1000 years) is followed by a decrease of about 0.15 mmol/mol and 0.5 ‰, during the final 1000 years. The Termination for the Mg/Ca proxy is at ~1600 years, whereas the Termination for the $\delta^{18}O$ values is at ~400 year mark. This underlines the strong influence of a fluctuation in sea surface salinity during a glacial/interglacial Termination phase.

The final modelled situation is an increase of salinity over the 2000 year transition period by 1 psu but with a salinity maximum of +2 psu at the 1000 year mark.

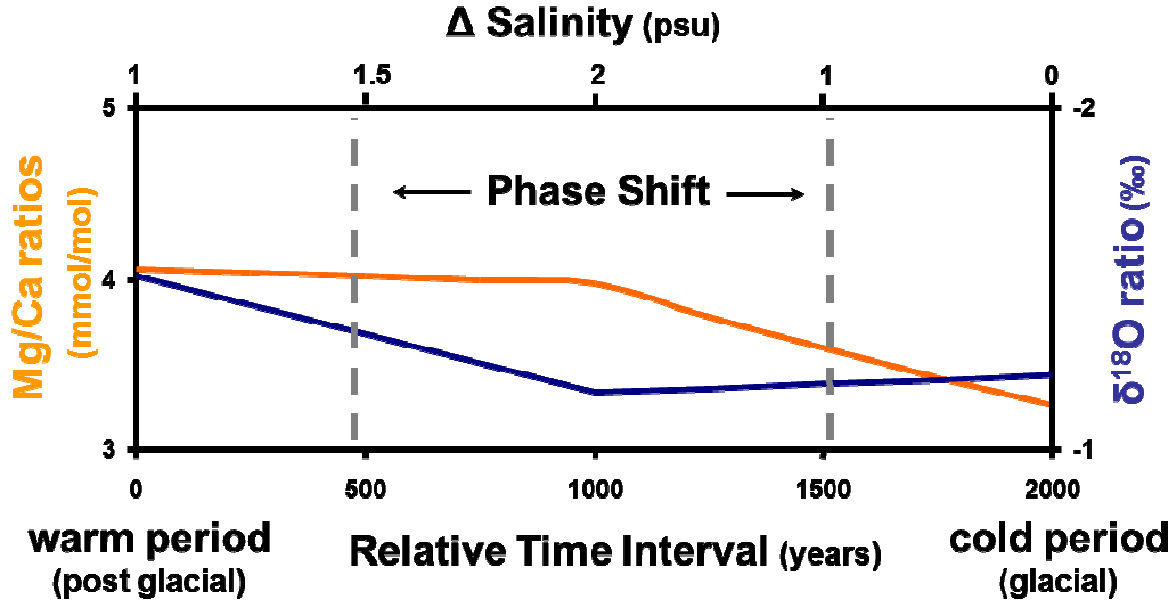

Figure 2.3.11: Increase of 2℃ over 2000 years with a salinity inc rease of 2 psu at 1000 years. The end increase in salinity is 1 psu. Between 0 and 1000 year mark the Mg/Ca ratios are stable and $\delta^{18}O$ ratios increase, different signal reactions are observed.

This alternative model presented in figure 2.3.11; see table 2.3.3.5 for values; produces a signal pattern similar to figure 2.3.10 but there are significant differences: The Mg/Ca ratios hardly vary, only by +0.09 mmol/mol, between the 0 to 1000 year marks. An expected temperature induced increase in the Mg/Ca ratios is not observed because the decrease in salinity almost fully compensates this effect under these conditions.

Table 2.3.3.5:

1	2	3	4	5
Age	**T (°C)**	**S (psu)**	**Mg/Ca [mmol/mol]**	**$\delta^{18}O$ [‰]**
2000	25	33	3.25	-1.22
1750	25.25	33.5	3.42	-1.20
1500	25.5	34	3.60	-1.19
1250	25.75	34.5	3.78	-1.18
1000	26	35	3.97	-1.17
750	26.25	34.75	3.99	-1.25
500	26.5	34.5	4.01	-1.34
250	26.75	34.25	4.03	-1.42
0	27	34	4.06	-1.51

4 Mg/Ca ratios calculated with equation 2 employing the values from **2** and **3**

5 $\delta^{18}O$ values calculated with equation A (see appendix) employing the values from **2** and **3**

On the other hand the $\delta^{18}O$ ratios show a considerable jump of ~0.4 ‰ for the same time interval from 0 to 1000 years. The drop in salinity and the coinciding increase in temperature both influence the $\delta^{18}O$ signal in the same way, pushing the values to more negative ratios. Furthermore, during the 1000 to 2000 year interval the strong increase in salinity (+2 psu) has a larger impact on the signal variations than the increase in temperature (+1℃ per 1000 years). This different behaviour of the proxies to these environmental changes creates the phase shift in this scenario.

An observed phase shift with a signal pattern between the Mg/Ca and $\delta^{18}O$ ratios similar to figure 2.3.11 is an indication for salinity maximum during the transition from a cold to warm period.

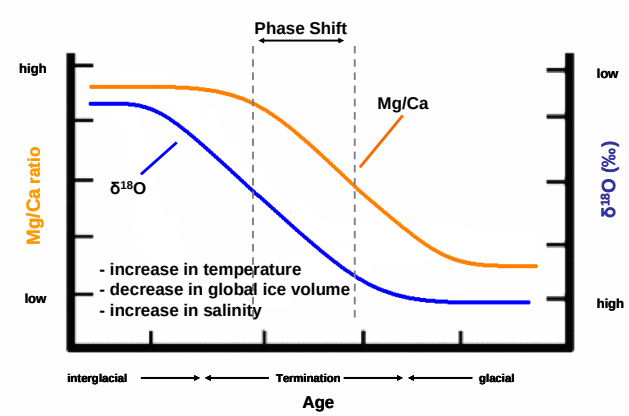

This would indicate that non-linear variations in salinity are the cause for the occurrence of a Phase Shift between the Mg/Ca and $\delta^{18}O$ ratios in foraminifera during glacial to interglacial transitions.

Figure 2.3.3 is presented as an example of this phase shift pattern.

2.4 The $\delta^{44/40}$Ca system

The $\delta^{44/40}$Ca-isotope system is a relatively new isotope tool applied in paleo oceanography for the reconstruction of ocean temperatures from foraminifera shells [*Nägler et al.,* 2000]. Nevertheless, the $\delta^{44/40}$Ca-isotope system has already proved to be applicable among others for independent temperature reconstructions [*Gussone et al.*, 2003; *Heuser at al.,* 2002; *Heuser et al*., 2005; *Hippler et al*., 2003; *Hippler et al*., 2005].

The $\delta^{44/40}$Ca proxy has been tested in particular for the planktonic foraminiferal species *G. sacculifer* and *N. pachyderma* [*Gussone et al*., 2003; *Hippler et al.*, 2006; *Nägler et al*., 2000] because these archives have been proven to show the most temperature sensitive relationship in their $\delta^{44/40}$Ca records [Gussone et al., 2003]. The best valuable attribute of the $\delta^{44/40}$Ca proxy is that it is presumably less affected neither by diagenetic alterations nor by foraminiferal ecology [*Gussone et al*., 2003]. Furthermore the quality of temperature reconstructions can be verified by the positive correlation of $\delta^{44/40}$Ca and Mg/Ca ratios which has recently successfully been proven by *Kozdon et al.* [2006].

2.5 Sea Surface Salinity reconstructions

As previously shown, the $\delta^{18}O$ values are influenced by variations in ocean temperature, sea water salinity and by fluctuations in the global ice volume [e.g. *Epstein et al.*, 1953; *Shackleton*, 1974, *Waelbroeck et al.*, 2002]. Since the composition of the $\delta^{18}O_{seawater}$ signal is known [*Shackleton,* 1974] or approximated by Mg/Ca-temperature reconstructions ($T_{Mg/Ca}$) it is possible to estimate the individual values of the SST and SSS components by employing the following equation [*Thunnel et al.*, 1999]:

Equation 3:

$$\boldsymbol{\delta^{18}O_{seawater}\,[‰] = \frac{[T_{Mg/Ca}\,(°C) - 14.9]}{4.8} + (\delta^{18}O_{foram}\,[‰] + 0.27)}$$

The $T_{Mg/Ca}$ are converted into their corresponding $\delta^{18}O$ values and subtracted from the measured $\delta^{18}O$ value of the same sample. This generates temperature independent $\delta^{18}O_{seawater}$ values. The influence of the global ice volume is still included and has to be corrected for the dynamic changes of the global ice volume. The mean-ocean $\delta^{18}O$ time series correction factor for variations in regional sea level (RSL) of *Waelbroeck et al.,* [2002] can be applied as an approximation for variations in the global ice volume as follows:

Equation 4:

$$\boldsymbol{\Delta\delta^{18}O_{ivf-seawater}\,[‰] = \delta^{18}O_{seawater}\,[‰] - \delta^{18}O_{ice-volume}\,[‰]}$$

ivf = ice volume free

For convenience and comparison purposes the resulting local $\Delta\delta^{18}O_{ivf\text{-}seawater}$ can then be normalized to their mean Holocene values [*Nürnberg and Groeneveld*, 2006]. This normalization is necessary because it allows for easier recognition of major deviations in a time series of the $\Delta\delta^{18}O_{ivf\text{-}seawater}$ values which reflect changes in the sea surface evaporation to precipitation ratio.

As a final note it is important to mention that the reconstruction of absolute salinity values is not possible since the $\delta^{18}O_{seawater}$-salinity relationship is a local factor reflecting the balance between precipitation and evaporation which is not constant over time and varies regionally.

2.6 The Inner Tropical Convergence Zone (ITCZ)

The Inner Tropical Convergence Zone (ITCZ) originates from the increased solar radiance in the tropics and is defined as the region near the equator, where the trade winds of the Northern and Southern Hemispheres converge [*Barry, Roger Graham; Chorley, Richard J.*, 1992]. The intense sun and warm water of the equator heat up the air, increase its humidity and make it buoyant. As a consequence of the convergence of the trade winds, the buoyant air rises and creates a stable low pressure zone at ground level. As the air rises it expands and cools, releasing the accumulated moisture in an almost perpetual series of heavy rainfalls and thunderstorms. Warm and moist air from the north and south is drawn into this low pressure zone which results in a high precipitation (P) to evaporation (E) ratio directly at the current position of the ITCZ (P>E) and a reversed P < E ratio in the vicinity to the north and south. A short schematic for the overall pattern of the ITCZ is presented below.

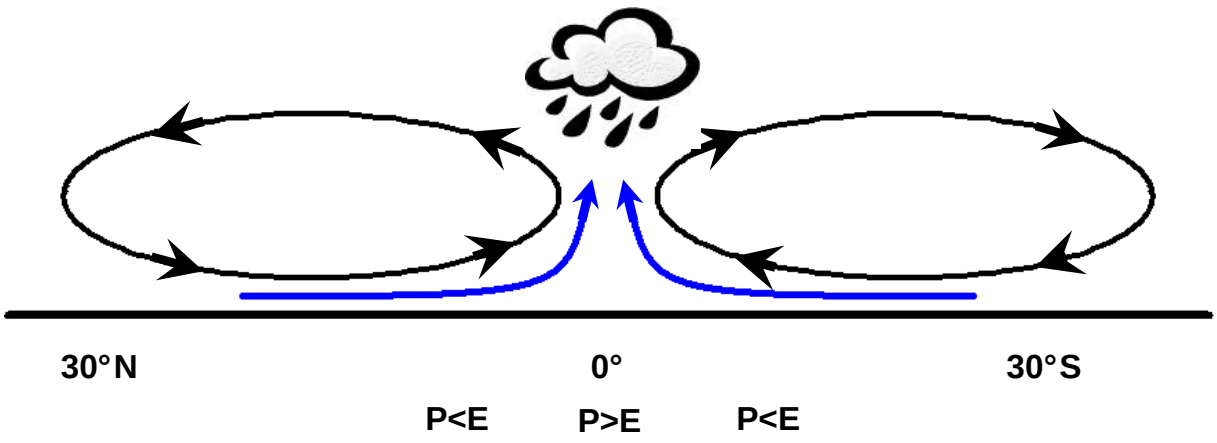

Figure 2.6.1: Simplified sketch of the structure of the Inner Tropical Convergence Zone (ITCZ). Blue arrows mark the main path of water moisture; P: precipitation; E: Evaporation.

The ITCZ is meteorically characterized by a visible band of clouds where precipitation of rainwater exceeds evaporation of seawater (P>E zone). Latter zone may extend for many hundreds of miles, sometimes broken into smaller line segments (figure 2.6.2).

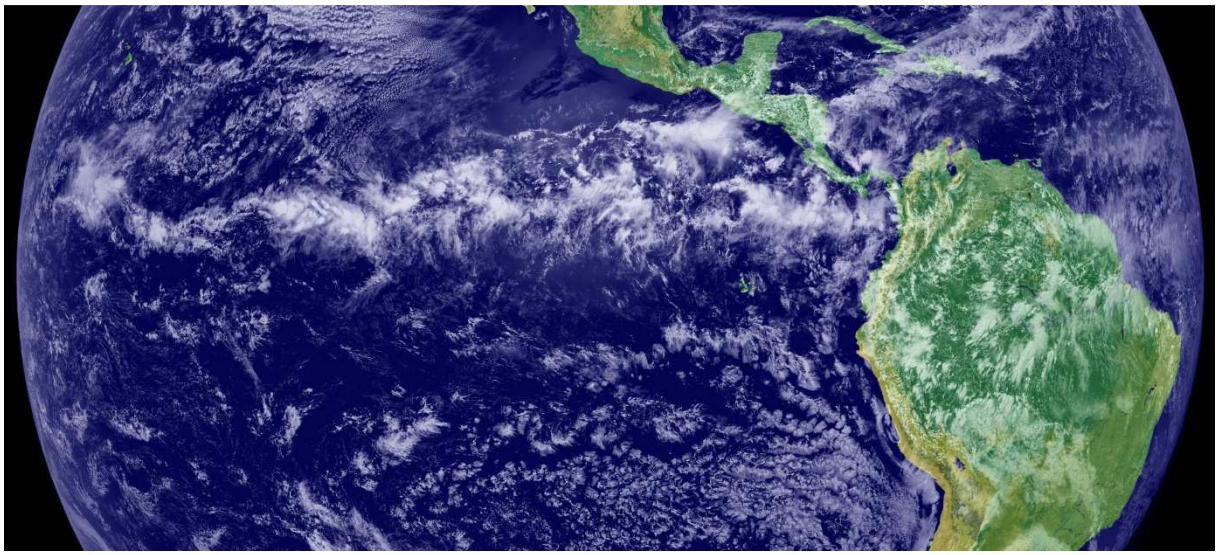

Figure 2.6.2: The Inner Tropical Convergence Zone (ITCZ) is the band of bright white clouds in the center of the image. [Image from Nasa.org]

The position of the ITCZ is not fixed but varies as a function of the seasons. In figure 2.6.3 below the seasonal migration of the ITCZ is displayed.

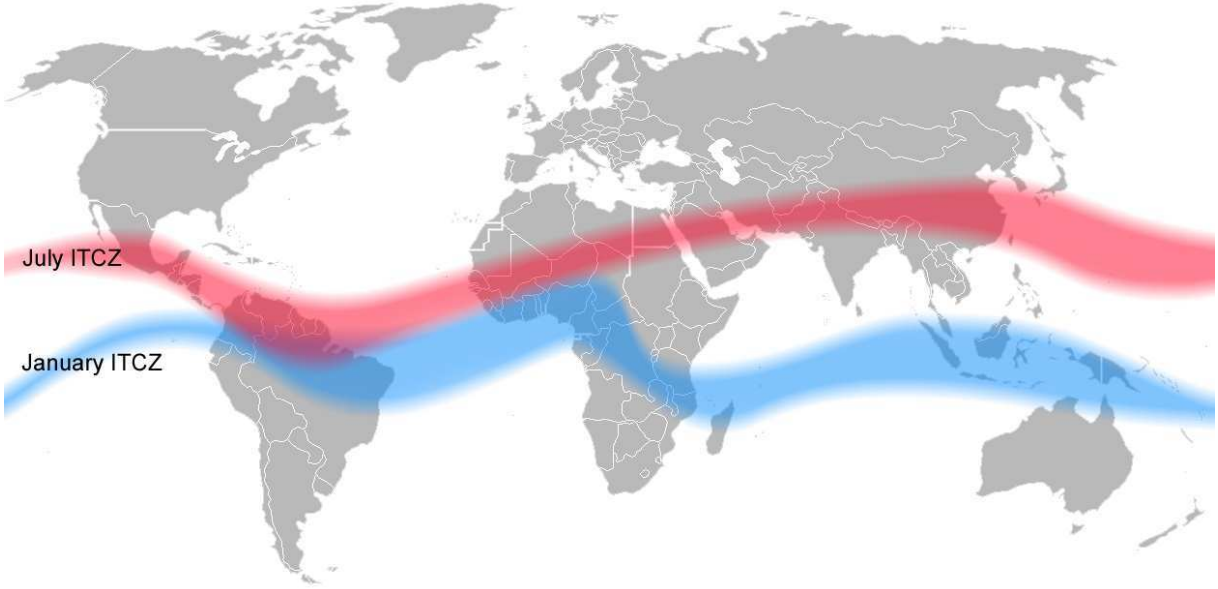

Figure 2.6.3: Seasonal variation of the position of the Inner Tropical Convergence Zone (ITCZ). [image from Wikipedia]

The migration of the ITCZ has a strong influence on the annual hydrologic cycle of Central and South America and in particular on the South Caribbean Sea. This results in two seasons in the Caribbean Sea today: A warm and wet season in late summer and early fall when the ITCZ is located farthest to the north which is also the hurricane season in this part of the world and a cooler and drier season during winter when the ITCZ migrates southwards [*Stidd*, 1967].

Movements of the ITCZ-system as a whole are known from the past. Cooling in the North Atlantic has been linked to a southward migration of the average position of the Atlantic ITCZ on centennial, millennial, and orbital timescales [*Black et al.*, 1999; *Hughen et al.*, 1996; *Lin et al.*, 1997; *Haug et al.,* 2001; *Peterson and Haug*, 2006; *Schmidt et al.*, 2004].

3 SELECTED ARCHIVES and SAMPLE LOCATIONS

3.1 Selected Marine Archive (foraminifera)

Foraminifera are a large group of amoeboids that typically produce calcite shells and are distributed throughout the entire water column (planktonic foraminifera). Certain species also inhabit the sea floor (benthic foraminifera).

Foraminifera are normally smaller than 1 mm in diameter but larger specimens are also known. Some species of foraminifera living in the photic zone have symbiotic algae, which have an influence on the size and composition of the shell. Foraminifera are a diverse group of amoeboids with more than 250.000 recognized species which have survived many different ocean environments and seawater compositions since Cambrian time [see e.g. *Bé*, 1977; *Fairbanks et al*., 1982; *Deuser*, 1987; *Bijma et al.,* 1994; *Kroon and Darling*, 1995; *Schmuker and Schiebel*, 2002].

Furthermore foraminifera directly employ seawater in order to calcify their shells. They vaculize seawater and use this enclosed water as their source of calcite [*Erez et al.,* 2003]. Ideally, in thermodynamic equilibrium the chemical composition of the shell of the foraminifera enables the reconstruction of the chemical properties of the ambient seawater in which the shell was originally formed such as temperature, carbonate ion concentration and sea water salinity. Due to the differences in habitats of the individual species, e.g. in near surface waters or embedded in the upper centimetres of the sea floor it is possible to generate cross sections for the above chemical properties through the water column. However, the chemical and isotopic composition of the shell is often not reflecting chemical equilibrium with the seawater because foraminifera tend to manipulate the chemical composition of the shell. The biogenic carbonate is different from inorganic carbonate precipitation. In particular, the Mg/Ca ratio in foraminifera is much lower than in inorganic calcite. The deviation of the physiological controlled signal in foraminifera from the inorganically expected signal is termed the “vital effect”.

Although large efforts have been made in recent years, most of the physiological control mechanisms remain still to be solved. The foraminifera follow a seasonal cycle. Some species are most active in summer time and the gathered proxy data will represent July / August conditions in the northern hemisphere but January / February in the southern hemisphere. On the other hand benthic foraminifera are usually not influenced by changes in the surface ocean waters like seasons and sea surface temperature fluctuations.

Other important parameters which have an influence on the composition of the shells, and thus have to be taken into account, are:

- The size of the shells; larger shells grow faster and thus have a different composition, e.g. trace minerals are depleted in the shells.
- The time of death of the individual, before or after the reproductive cycle; some species form an additional layer of calcite on their outer shell, which has a distinctively different composition than the inner shell.
- The water depth of the core; if the core is drawn from below the calcium carbonate compensation depth (CCD), dissolution will occur.

Even though the compositions of the shells of the foraminifera are influenced by many different factors, they are a very useful archive because it is possible to correct for some of the parameters which influence the precipitation of the foraminiferal shells.

All foraminifera in this study were picked by the author with the support of A. Bahr and N. Gehricke for the core ODP 999 and D. Nürnberg and J. Schönfeld for the core SO 164-03-4.

3.2 Species of foraminifera examined in this study

3.2.1 *Globigerinoides ruber* (d´Orbigny, 1839)

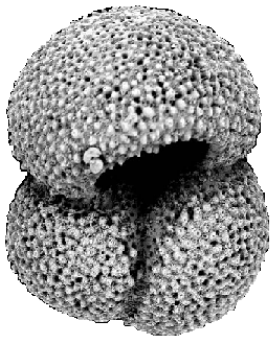

Picture 3.2.1: Shell with a diameter of ~300 µm

G. ruber is a spinose, shallow living and symbiotic-bearing foraminifera. It reaches its highest abundances in the upper 50 m of the water column; some subspecies prefer to inhabit the very near surface. An almost uniform occurrence throughout the year makes this species ideal to reflect annual surface hydrological conditions. This is further underlined by the very shallow calcifying depth which results in higher Mg/Ca ratios in comparison to other species of foraminifera. The Mg/Ca versus temperature calibration for *G. ruber* by *Lea et al.* [2000] was employed as follows:

$$Mg/Ca = 0.30 * \exp(0.089 * T)$$

3.2.2 *Globigerinoides sacculifer* (Brady, 1877)

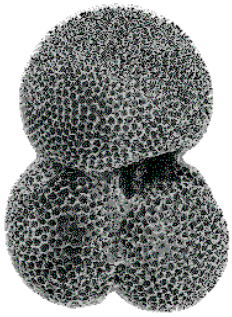

Picture 3.2.2: Shell with a diameter of ~200 µm

Like *G. ruber* the species *G. sacculifer* is a spinose and symbiotic-bearing species. It occurs in the top layer of the water column around 50 m. The main occurrence is during the high summer season. Recently it has been discovered that the sizes of very large shells (>400 µm) directly correlate with the water depth in which the organisms live: The larger the shell the shallower it´s habitat, because the increased activity and growth of the symbionts near the surface is transferred to the foraminifera [*Spero et al.*, 2009].

G .sacculifer normally calcifies deeper than *G. ruber*; this means that *G. sacculifer* has a generally lower Mg/Ca ratio. For *G. sacculifer* the temperature calibration for Mg/Ca versus temperature was established by *Nürnberg et al.* [1996] and *Nürnberg et al*. [2000] and for the $\delta^{44/40}$Ca ratio the temperature calibration was established by *Nägler et al*., [2000] and *Hippler et al.,* [2006] as follows:

$$Mg/Ca = 0.49 * \exp(0.076 * T)$$

$$\delta^{44/40}Ca[‰] = 0.22\ (\pm 0.05)*T\ [℃] - 4.88$$

3.2.3 *Globorotalia truncatulinoides* (d´Orbigny, 1839)

Picture 3.2.3: Shell with a diameter of ~250 µm

G. truncatulinoides is a typical subtropical species which occurs over a broad range of sea surface temperatures and salinities. It´s main habitat is at a water depth of about 200 m below sea level which means it calcifies at a greater depth than e.g. *G. ruber*. The shell will reflect intermediate ocean conditions at about 200 m. It prefers areas with little seasonality in salinity in contrast to broad tolerances for seasonal change in sea surface temperatures. Due to its deep habitat, the Mg/Ca ratios of *G. truncatulinoides* are significantly lower than shallower living species. The Mg/Ca temperature calibration by *McKenna & Prell* [2005] was employed as follows:

$$Mg/Ca = 0.355 * \exp(0.098 * T)$$

3.2.4 *Cibicides wuellerstorfi* (Schwager, 1866)

Picture 3.2.4: Shell with a diameter of ~300 µm

Cibicides wuellerstorfi is a widely used benthic foraminifera which can be found in most major ocean seabeds. It lives in the top centimeters of the sea floor and can migrate in this area. Their shells will reflect the bottom water conditions at the sample site. The individual specimens are usually quite large in contrast to planktonic foraminifera and easy to extract from an individual sediment samples.

Since the habitat of this species is not influenced by changes in the surface water conditions of oceans, like temperature and salinity, it is possible to track long term variations in the $\delta^{18}O$ ratio of seawater. This makes it an ideal stratification tool with the shallower dwelling foraminifera for defining stratifications of water columns through time.

3.2.5 *Neogloboquadrina pachyderma sinistral* (Ehrenberg, 1861)

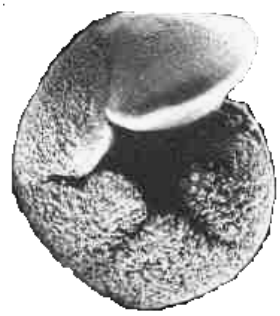

Picture 3.2.5: Shell with a diameter of ~250 µm

The planktonic foraminifera *N. pachyderma* has a very large habitat and lives in high latitudes. It is found at water temperatures as low as -1.4℃. In addition, *N. pachyderma* can tolerate large differences in salinity between 30 and 50 psu [*Bé and Tolderlund*, 1971; *Boltovskoy and Wright*, 1976]. Since it does not have symbionts it is not limited to the photic zone. The consequence is that it has to follow its food source through the water column.

Sea water temperatures derived from this foraminifera species do not represent surface temperatures but more likely the temperature around 50 m to 100 m [*Nürnberg et al*. 2006]. A temperature sensitivity of about 0.1 ‰ °C^{-1} in the Ca-isotope composition of *N. pachyderma sinistral* was first proposed in the study of *Zhu and Macdougall* [1998]. This temperature relation was further refined by *Hippler et al.* [2006] and found to account for 0.17 ‰ per ℃ for *N. pachyderma sinistral* in core samples from the Norwegian Current and 0.15 ‰ per °C in net catches from the Nordic Seas and the Benguela upwelling system.

3.3 Selection of sediment cores and sample locations

This study focuses on three sediment cores from the tropic/subtropical regions to high northern latitudes in the Atlantic Ocean. The cores follow the path of the Gulf Stream from the equator to the Arctic (Fig. 3.3.1, Tab. 3.2).

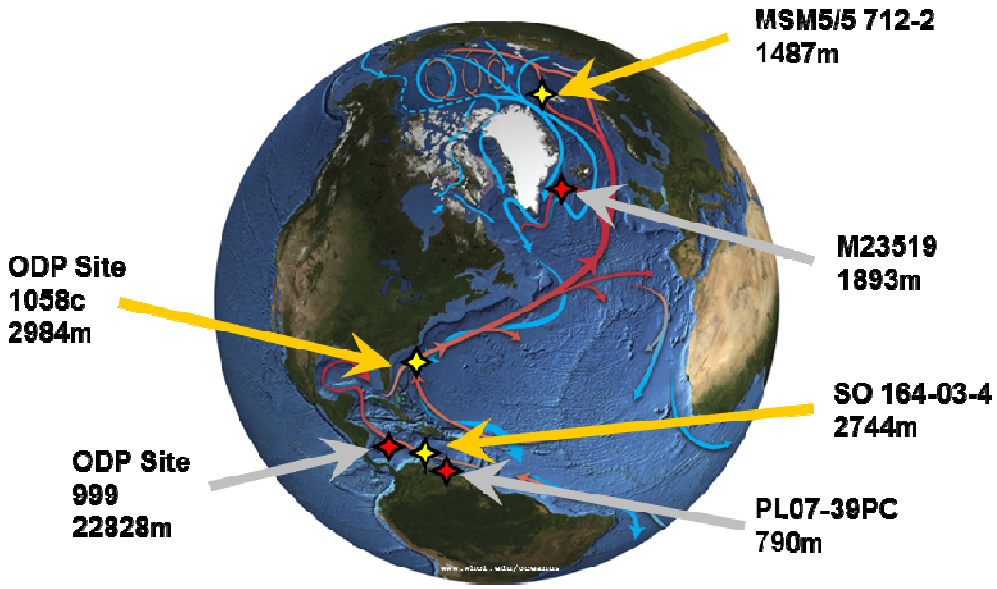

Figure 3.3.1: A schematic map of the sample locations covered in this thesis. Studied cores are presented in yellow; red for comparison data.

Table 3.2: List of sediment cores which were studied in detail within this project.

Core	Lat.	Long.	Water depth
SO 164-03-4	16°32.37'N	72°12.31'W	2744 m
ODP 1058c	31°41.38'N	75°25.80'W	2984 m
MSM5/5-712-2	78°54.94'N	06°46.04'E	1487 m

The obtained data was compared with results from different cores from the Caribbean Sea and from the North Atlantic.

Table 3.3: List of the sediment cores employed for data comparison

Core	Lat.	Long.	Water depth
ODP 999	12°44'N	78°44'W	2828 m
PL07-39PC	10°42.00'N	64°56.50'W	790 m
M23519	64°47.84'N	29°35.75'W	1893 m

3.3.1 SO 164-03-4 – Central Caribbean Sea

The gravity core SO 164-03-4 was recovered during the RV SONNE cruise 164 in 2003 in the deep Columbian Basin of the Central Caribbean Sea (*Nürnberg et al.* [2003]). The length of the core is approximately 13.2 m and the sediments consist mainly of light brown marine clays with a few patches of foraminifera-rich sands. The primary stratigraphy is based on oxygen isotope measurements on benthic foraminifera.

More detailed information, including the sedimentation rate is presented in figure 3.3.1.2; further information is found in the appendix.

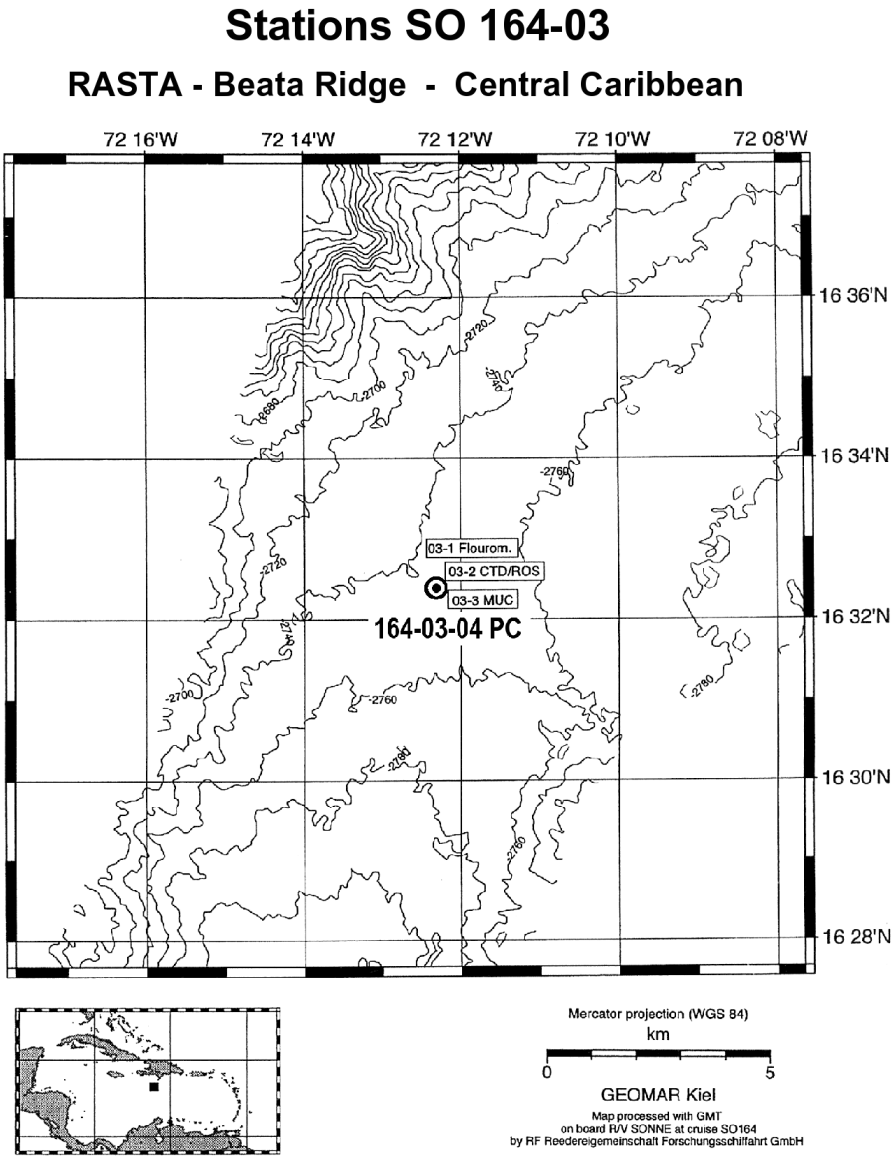

Figure 3.3.1.1: Map of the site location (*Nürnberg et al.* [2003])

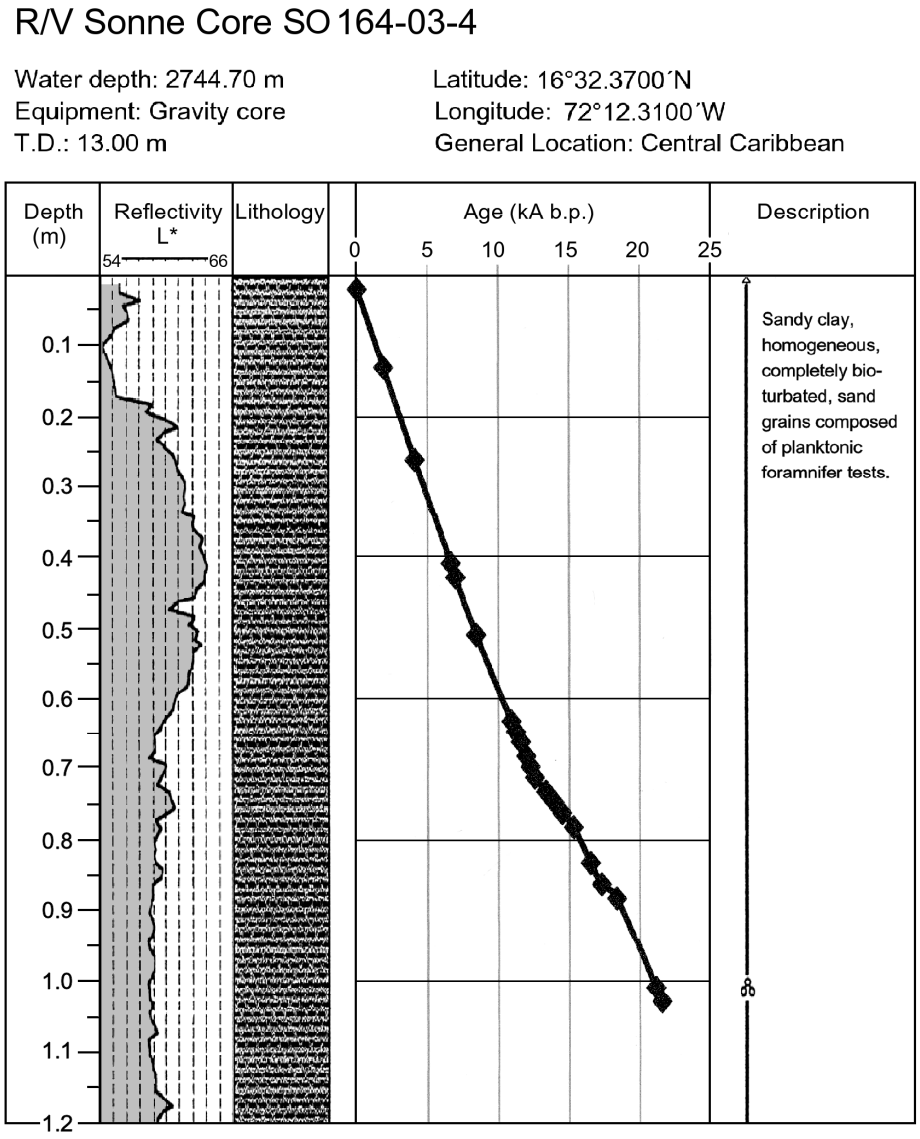

Figure 3.3.1.2: A detailed core log of the first 1.2 m covering the interval of interest including sample positions for age dating (via benthic foraminifera)

3.3.2 ODP Led 172, site 1058c – Blake Ridge

The ODP core 1058c was drilled as part of the Ocean Drilling Project Leg 172 on the Blake Ridge [*Keigwin et al.*, 1998]. The sediments in the uppermost part of the core consist of light greenish to gray nannofossil oozes with alterations of reddish brown clay. This sediment variability is caused by a high amplitude of calcium carbonate fluctuations and results in a relatively high variation of color reflectance. The sedimentation rates vary between 4 and 50 cm per 1000 years. Our focus is on the first 2 m of the core which cover the Holocene and Termination 1 and has a fairly steady sedimentation rate of about 6 to 10 cm per 1000 years. Furthermore we investigated the core section from 17 to 25 meters which covers Termination 2; the data is presented in the appendix. Sampling of the core was undertaken at the Bremen ODP Core Repository.

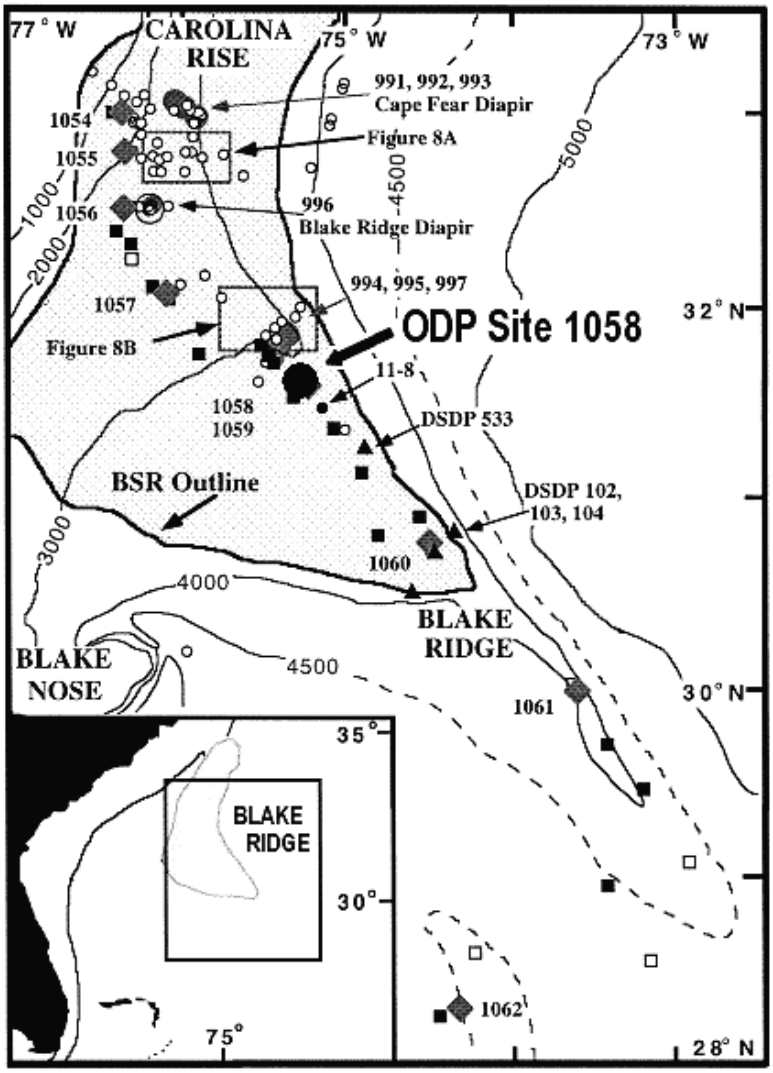

Figure 3.3.2.1: A location map for ODP core 1058c after *Keigwin et al.* [1998]

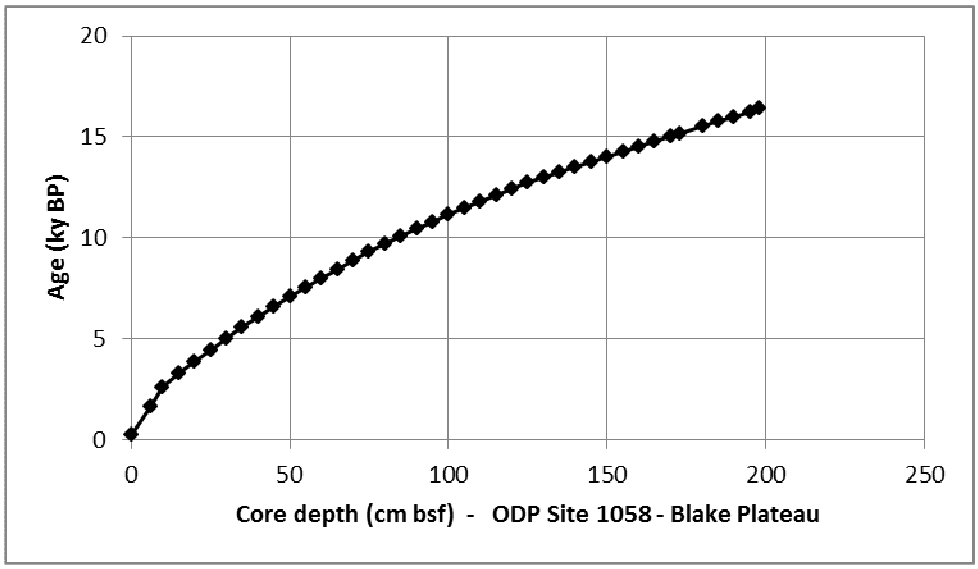

Figure 3.3.2.1: A detailed core log of the first 2 m covering the interval of interest dating after *Keigwin et al.* [1998]

3.3.3 MSM 5/5-712-2 – Arctic Sea off Svalbard

The core M/M 515-712-2 is a short gravity core taken in the Arctic Sea off the coast of the island of Spitsbergen in 2007. It is ~9.5m long and consists mainly of dark brown and black clays. A more detailed description of the core is given in figure 3.3.3.2 below.

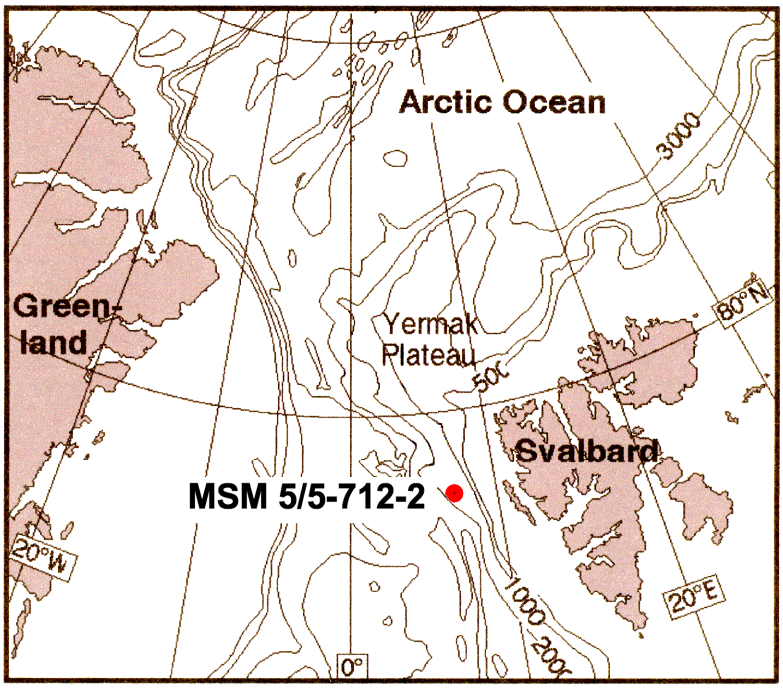

Figure 3.3.3.1: Location map for the M/M 5/5-712-2 core

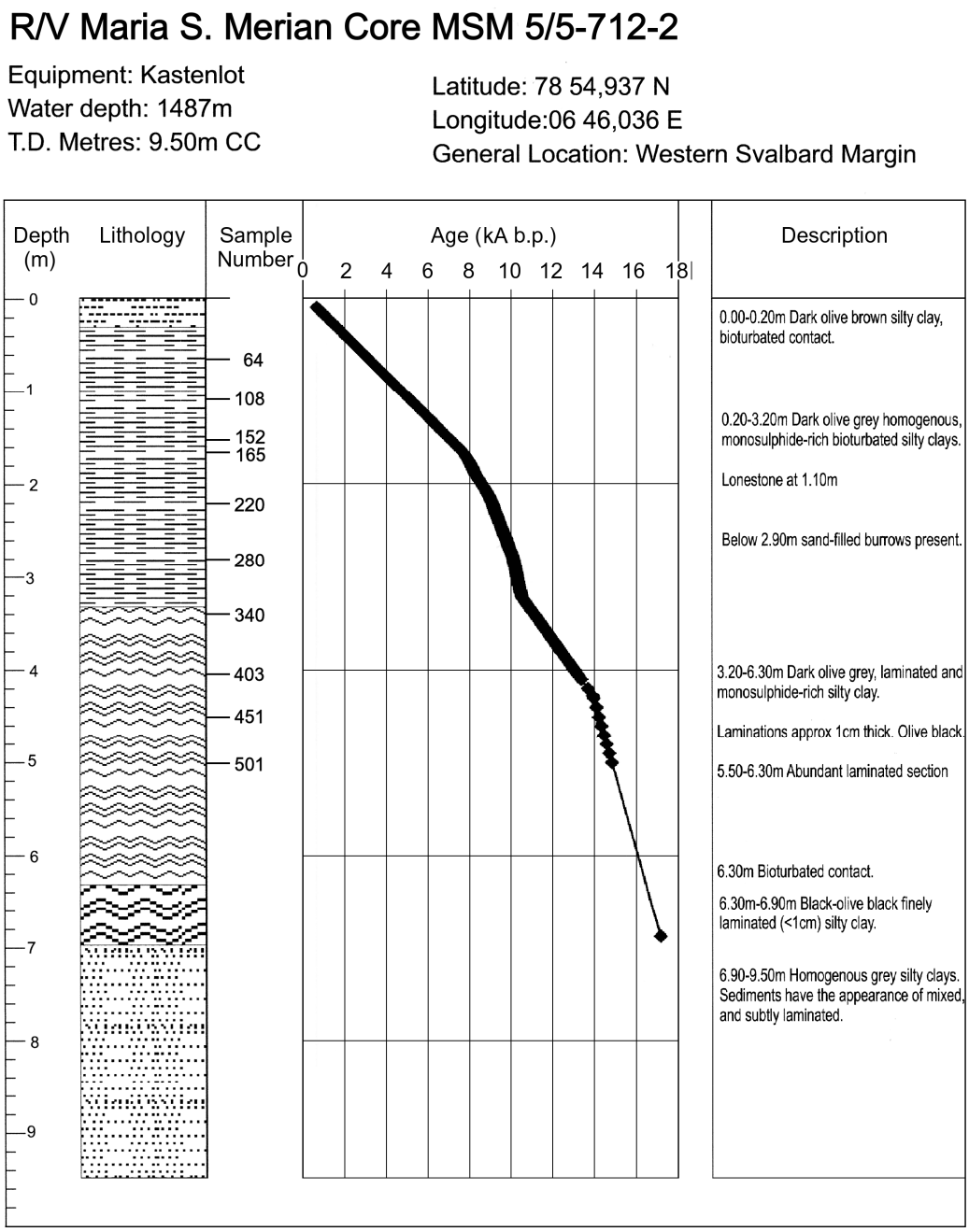

Figure 3.3.3.2: Lithological composition and age dating of the section of the M/M 5/5-712-2 core

4 METHODS and SAMPLE PREPARATION

In this study a variety of measurements of different proxies were applied on planktonic foraminifera in order to better understand their different dependencies on environmental changes during the glacial / interglacial transition and post-glacial phases. The combined measurement of the ratios of $\delta^{44/40}Ca$, $\delta^{18}O$ and Mg/Ca in the same planktonic foraminiferal species is not a widely employed approach.

4.1 Basic sample preparation

The following sample preparation method was employed for all the samples processed in this study. Only minor variations of the standard preparation techniques for the different measurements of $\delta^{18}O$, Mg/Ca and $\delta^{44/40}Ca$ were necessary and are mentioned in the corresponding sections.

The sediment cores were sampled with 10 ml plastic syringes and then the sediment samples were freeze dried. The freeze dried samples were washed and sieved (>63 µm). The resulting size fraction > 63 µm was carefully dried and then divided into six different fractions ranging from >63 µm to > 400 µm. All measured samples were chosen from the size fraction of 315-355 µm: In order to eliminate any size related influences on the measurements we only used this single size 315-355 µm fraction of foraminifera. The cleaning procedure followed the manual by *S. Barker* [2005] with slight variations.

All the samples were carefully crushed between two glass plates in order to break open the inner chambers since sometimes clay minerals were trapped inside the shells of the foraminifera. The crushed samples were washed with Milli-Q water several times and treated with ultrasound for ~30 seconds between each washing step. Then the foraminifera shell fragments were washed twice with methanol and thoroughly rinsed with water, in order to remove any remaining clay particles and traces of methanol. For the $\delta^{18}O$ and $\delta^{13}C$ measurements further cleaning was not considered necessary, however, for the $\delta^{44/40}Ca$ and Mg/Ca measurements additional cleaning steps were undertaken.

The samples were treated with a NaOH buffered H_2O_2 solution and heated to about 95℃ for 20 minutes in a water bath. After ten minu tes the sample rack was removed and each sample was shaken until all bubbles had disappeared from the vial. The $NaOH/H_2O_2$ solution was removed and the samples cleaned several times with water to remove any remaining contaminations.

4.2 Mg/Ca measurements

The Mg/Ca ratio samples were prepared employing the basic sample preparation method discussed in section 4.1. After the basic treatment was completed the samples were washed with a weak acidic HNO_3 solution in order to remove any remaining surface contaminations.

Before the Mg/Ca analysis, the samples had to be transferred to clean vials for dissolution. The cleaned samples were dissolved in nitric acid.

The measurements of the Mg/Ca ratios were carried out on an ICP-AES (Spectro Ciros CCD SOP) at the Institute of Geosciences at the University of Kiel. Each individual sample was measured five times and the calculated average mean utilized. An average precision of ±0.2 (2σ, n=5) mmol/mol for Mg/Ca is reached.

4.3 Ca double spike technique for Ca isotope measurements

Prior to the thermal ionization mass-spectrometer (TIMS) measurements, which are performed on a Finnigan Triton TI thermal ionization mass spectrometer at the IFM-GEOMAR, for Ca isotope ratios, a Ca double spike has to be added to the foraminiferal samples.

In order to measure the original Ca isotope composition of our foraminiferal samples we applied the Ca double spike technique originally introduced by *Zhu and MacDougall* [1998] and based on earlier studies of *Russel et al.* [1978]. This procedure was improved by *Nägler et al.* [2000] and *Heuser et al.* [2002] with the use of an enriched ^{43}Ca and ^{48}Ca spike instead of ^{42}Ca and ^{48}Ca, respectively. The spike is required to have a known isotope composition and must be depleted in ^{40}Ca and ^{44}Ca since this isotope ratio of the sample is of interest.

In the mixture (spike + samples) most of the ^{43}Ca and ^{48}Ca comes from the spike whereas most of the ^{40}Ca and ^{44}Ca is from the sample. From the measured $^{40}Ca/^{48}Ca$ and $^{44}Ca/^{48}Ca$ ratio and the knowledge of the $^{43}Ca/^{48}Ca$ ratio of the spike, it is possible to correct for all not naturally introduced fractionation of the Ca isotopes during the cleaning procedure and the measurement itself.

4.4 $^{44}Ca/^{40}Ca$ sample loading and measurements

After the basic sample preparation and the addition of 12 µL Kaiser Karl Ca double spike, the samples – containing about 300 ng of Calcium each – were loaded onto zone refined rhenium ribbon single filaments in combination with a Ta_2O_5-activator and the so called “sandwich-technique” following a method previously published by *Birck* [1986]. Before the sample was loaded about 0.5 µL Ta_2O_5 activator solution was first added onto the filament and heated to near dryness at a current of about 0.7A. The activator solution stabilizes the signal intensity resulting in more precise measurements of the Ca isotopic composition of the sample/spike mixture. Then 1–2 µL sample solution with concentrations of 200–400 ng Ca/µL were added on top of the activator solution and again heated close to dryness at 0.7A. Another 0.5 µL of the activator were then loaded onto the filament and heated at 0.7A to dryness. Finally the filament was heated to 1.5A and left there for about 30 seconds. The electrical current was slowly increased until a weak red glow was visible followed by an immediate shut down of the electrical current.

For data reduction we use an iterative algorithm based on the routine of *Compston and Oversby* [1969], modified for Ca isotope analysis by replacing the linear fractionation correction term by an exponential term [*Nägler et al.*, 2000; *Heuser et al.*, 2002]. This algorithm calculates the $^{44}Ca/^{40}Ca$ ratio of the sample from the measured $^{44}Ca/^{48}Ca$, $^{43}Ca/^{48}Ca$ and $^{40}Ca/^{48}Ca$ ratios. The isotopic variations are expressed as $\delta^{44/40}Ca$ values $(^{44/40}Ca_{sample}/^{44/40}Ca_{standard} - 1) * 1000$, using NIST SRM915a $CaCO_3$ reference powder as standard material following the notation as proposed in *Heuser et al.,* [2002]. The overall uncertainty of the method is ± 0.12 ‰.

4.5 $\delta^{18}O$ and $\delta^{13}C$ measurements

For the $\delta^{18}O$ measurements only the removal of the clay contaminations was considered necessary. The foraminiferal samples were crushed and washed three times with deionized water. Then methanol was added and the sample exposed to ultrasound for one minute. This was repeated once and finally the sample was again washed with water in order to remove any methanol traces. The $^{18}O/^{16}O$ and simultaneous $^{13}C/^{12}C$ measurements were routinely carried out at the IFM-GEOMAR mass-spectrometer facilities using a FINNIGAN 252 Mass Spectrometer equipped with Kiel CARBO device.

The $^{16}O/^{18}O$ and $^{13}C/^{12}C$ ratio values are expressed and presented in the usual δ-notation (see equation 1). The analytical reproducibility for this machine is ~0.07‰ for $\delta^{18}O$ and ~±0.04 ‰ for $\delta^{13}C$.

The values are reported relative to Pee Dee belemnite (PDB) based on the calibrations of the National Bureau of Standards (NBS-19).

5 RESULTS

5.1 Results of the sediment core SO 164-03-4 – Central Caribbean Sea

The sediment core SO 164-03-4 recovered in the Central Caribbean Sea during the Sonne Cruise 164 in 2002 was investigated in detail and a multi proxy temperature record combining Mg/Ca, $\delta^{18}O$ and $\delta^{44/40}Ca$ ratios was obtained on the same species of foraminifera.

5.1.1 Mg/Ca record of core SO 164-03-4

The Mg/Ca ratios of *G. ruber* were measured for the entire length of the core from the core top to about 1300 cm down-core with an average depth resolution of 10 cm/sample. This was done in order to narrow down the section of interest and to check for any signs of possible diagenesis or contamination in the core which could have occurred during storage or transport of the core.

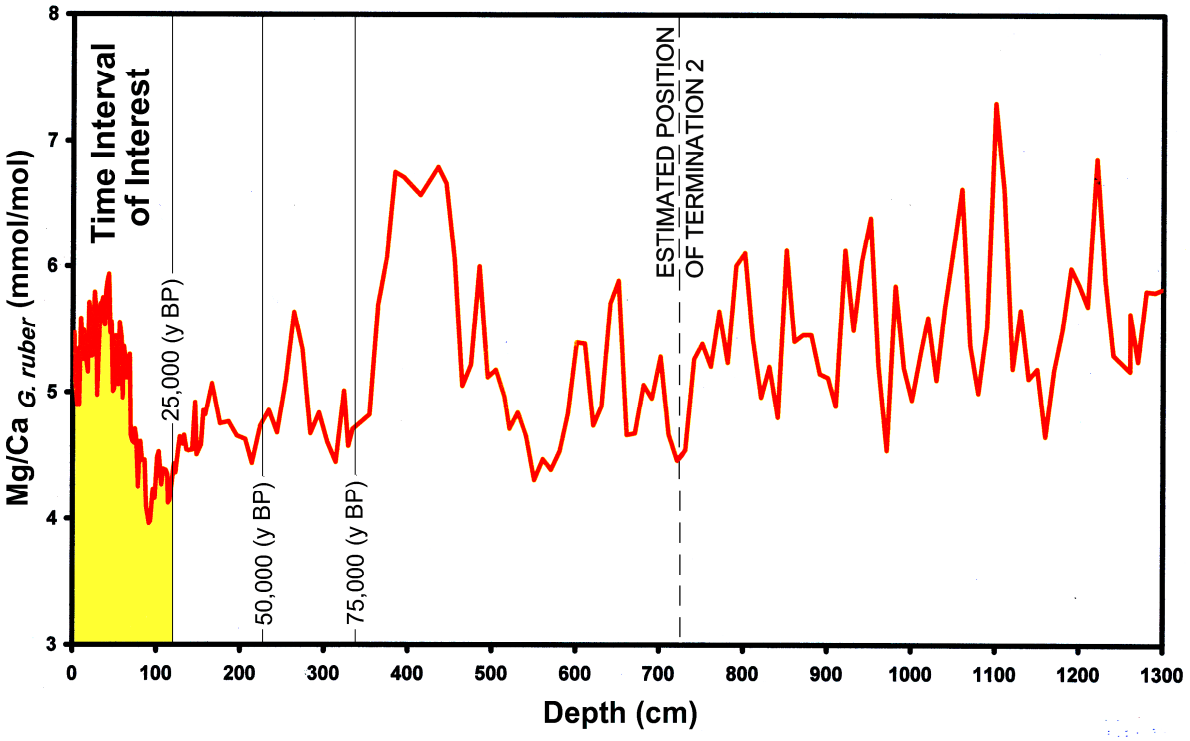

Figure 5.1: Mg/Ca ratios of *G. ruber* for core SO 164-03-4. The time interval of interest corresponds to the top 120 cm (marked in yellow), covering roughly the last 25.000 years together with the glacial/interglacial transition from MIS 2 to 1 (Termination 1).

The Mg/Ca record shows the long term variations of the Mg/Ca ratios in *G. ruber* in the water column during the sedimentation the section of core SO 164-03-4. The alternating warm and cold periods can be followed back in time for about 200 ky BP over the whole core based on an age model employing $\delta^{18}O$ measurements on the

benthic foraminifera species *C. wuellerstorfi* (see appendix). The position of MIS 5 to 6 is probably around the seven meter mark (see figure 5.2) and the zone of interest, the Transition from MIS 1 to 2 together with Termination 1 is in the upper meter of the core.

The Mg/Ca ratios can be converted into SST following the calibration by *Lea et al.* [2000]. The resulting temperatures are presented in figure 5.2 below.

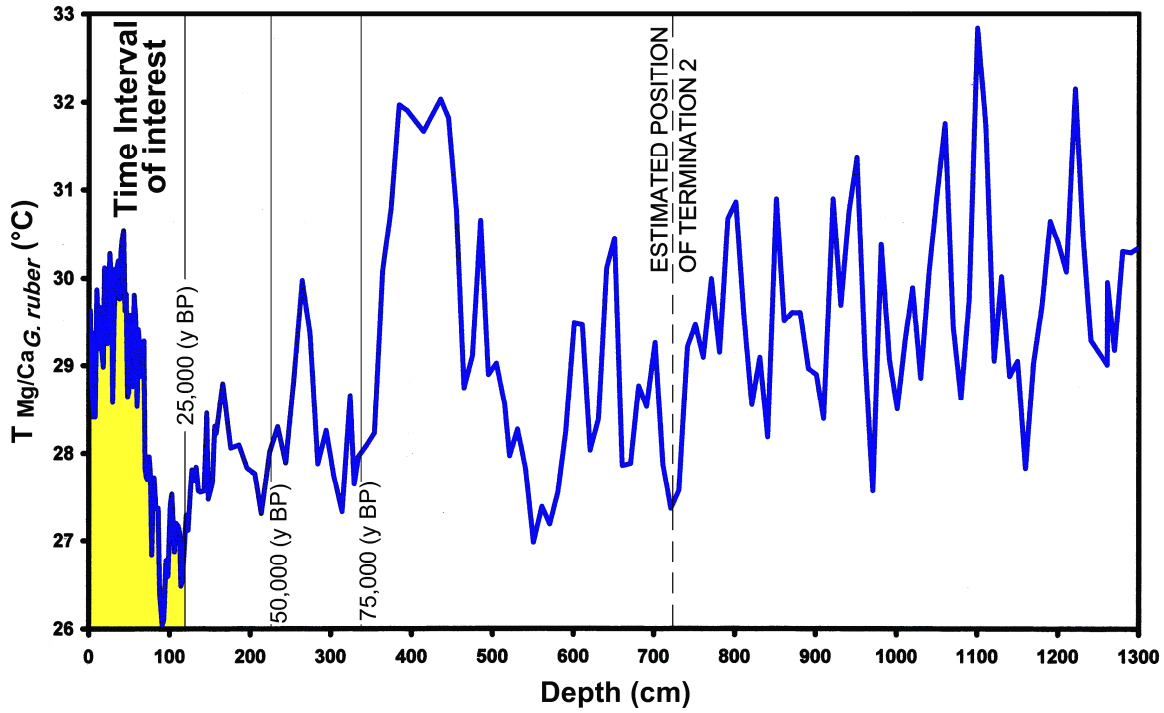

Figure 5.2: Mg/Ca ratio based SST of *G. ruber* as a function of depth in the SO 164-03-4 core.

The calculated SST varies between ~26℃ and ~33℃ f or the whole length of the core. The differences in absolute temperatures from the Holocene to the LGM are about ~5℃ which is higher than the ~1-2℃ predicte d by the CLIMAP project. The measured temperature maximum was recorded between 4 and 5 meters down-core with a temperature of about 32℃.

5.1.2 $\delta^{18}O$ record of core SO 164-03-4

Since Termination 1 is the time interval of main interest in this study, the core SO 164-03-4 was more densely sampled, every 2-3 cm, in the interval from 0 to 120 cm. On all diagrams, the absolute ages of the Bølling (B), Allerød (A) and the Younger Dryas (YD) periods during the Termination 1 are shown as yellow (warmer periods) and as blue bars (cooler periods).

In order to further examine the changes in near surface ocean waters for the time interval of interest, $\delta^{18}O$ ratios of *G. sacculifer* were measured. The obtained data are presented in figure 5.3.

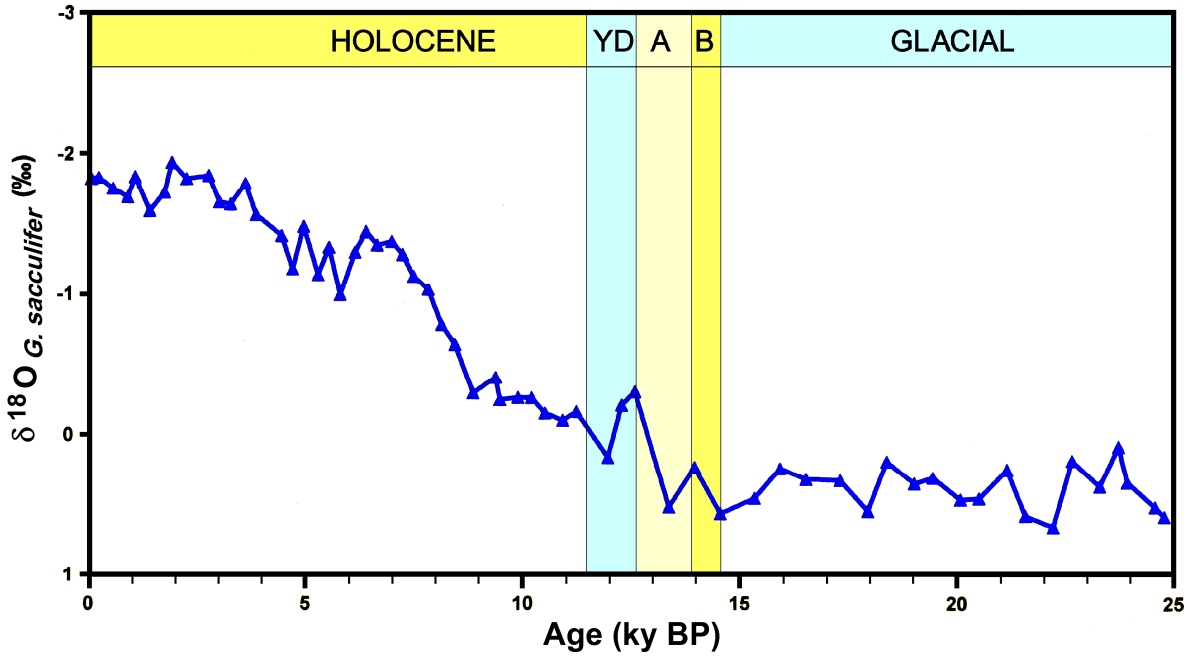

Figure 5.3: $\delta^{18}O$ values for *G. sacculifer* for the core SO164-03-4 for the past 25.000 years. (B - Bølling, A - Allerød, YD - Younger Dryas). (Note: the $\delta^{18}O$ ratios are inversely plotted).

The $\delta^{18}O$ ratios are relatively constant around a value of 0.5 ‰ during the Last Glacial period which is an indication of differential fluctuations in temperature or in salinity of the sea water. In contrast the Holocene is characterised by a constant decrease of the $\delta^{18}O$ signal from 0.5 to 0 ‰ across the Termination 1 (15.000 years BP) to -2 ‰ at the present time.

During the Holocene period the $\delta^{18}O$ ratios again show no major fluctuations despite a steady decrease of the $\delta^{18}O$ signal pattern. This leads to the conclusion that there were no drastic environmental changes in the Central Caribbean Sea. The main ocean parameters, SST and SSS, do not seem to suffer from abrupt changes in the Holocene or during the LGM as far as the $\delta^{18}O$ data suggest.

During the LGM (section between 25.000 and 20.000 years) and right into the onset of the Younger Dryas there are also no major $\delta^{18}O$ signal variations visible. This is quite surprising since a response of the proxy would have been expected because of the warming of the surface ocean waters during the Bølling / Allerød period. There is an overall drop in the $\delta^{18}O$ values of 2 ‰ over the Termination 1 from 15.000 years BP to present day values.

5.1.3 Mg/Ca ratios of *G. ruber* and *G. sacculifer* across Termination 1

Both the Mg/Ca ratio records and their corresponding temperatures of *G. ruber* and *G. sacculifer* are presented in figures 5.4 (Mg/Ca ratios) and in figure 5.5 (temperature calculations based on the Mg/Ca ratios as outlined in section 3).

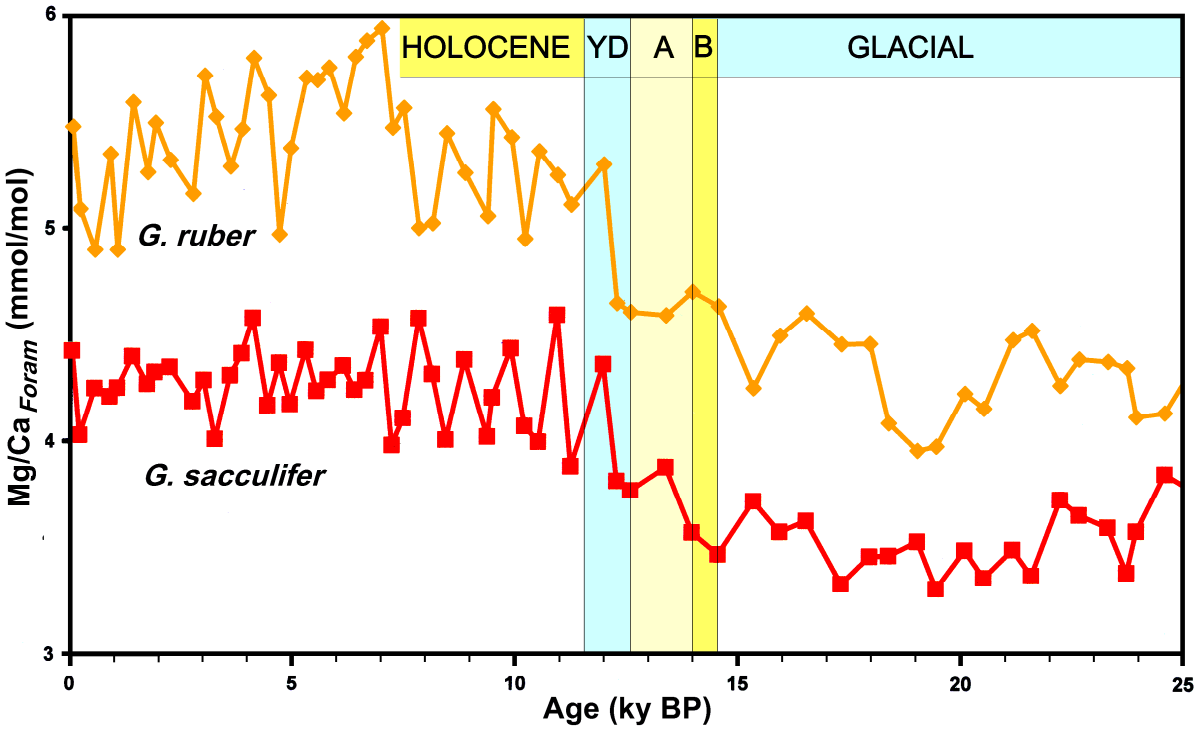

Figure 5.4: Mg/Ca ratios for both *G. ruber* and *G. sacculifer* for the core SO164-03-4 for the last 25,000 years BP.
(B - Bølling, A - Allerød, YD - Younger Dryas).

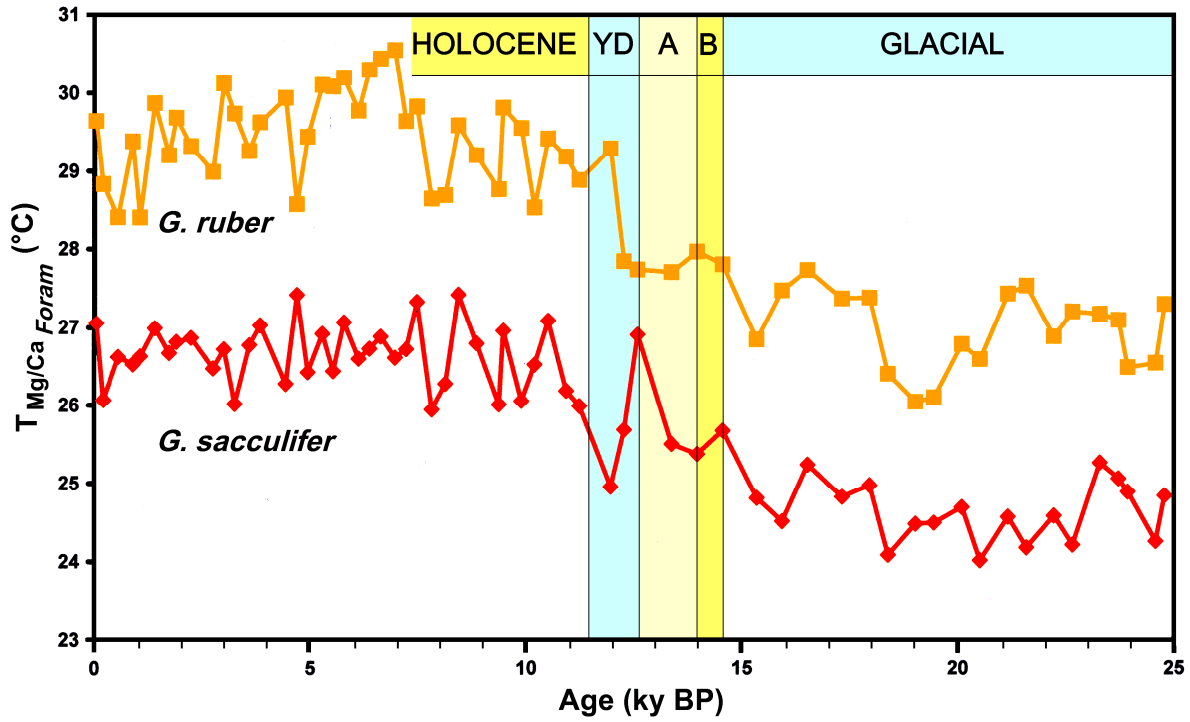

Figure 5.5: Sea surface temperature (SST) calculations based on Mg/Ca ratio measurements for *G. ruber* and *G. sacculifer* for the core SO164-03-4 for the last 25,000 years.
(B - Bølling, A - Allerød, YD - Younger Dryas).

The patterns of both, the Mg/Ca ratios as well as their corresponding SST of the two planktonic foraminifera *G. ruber* (orange) and *G. sacculifer* (red) show a similar trend. The calculated $T_{Mg/Ca}$ for *G. ruber* are generally higher by ~1.5℃ relative to *G. sacculifer*: This is expected because the habitat of *G. sacculifer* is deeper in the water column by ~20 m, whereas *G. ruber* is living in the warmer shallower part of the water column.

The $T_{Mg/Ca}$ differences between the LGM and the Holocene climate optimum are about 4℃ for *G. ruber* and about 3℃ for *G. sacculifer.*

5.1.4 Comparison of the $\delta^{18}O$ and Mg/Ca record for *G. sacculifer*

Here we compare the $\delta^{18}O$ and Mg/Ca ratio records for *G. sacculifer*. The combined $\delta^{18}O$ (blue) and Mg/Ca (red) measurements for *G. sacculifer* for the examined time interval of the last 25.000 years are presented in figure 5.6.1-1 and 5.6.1-2.

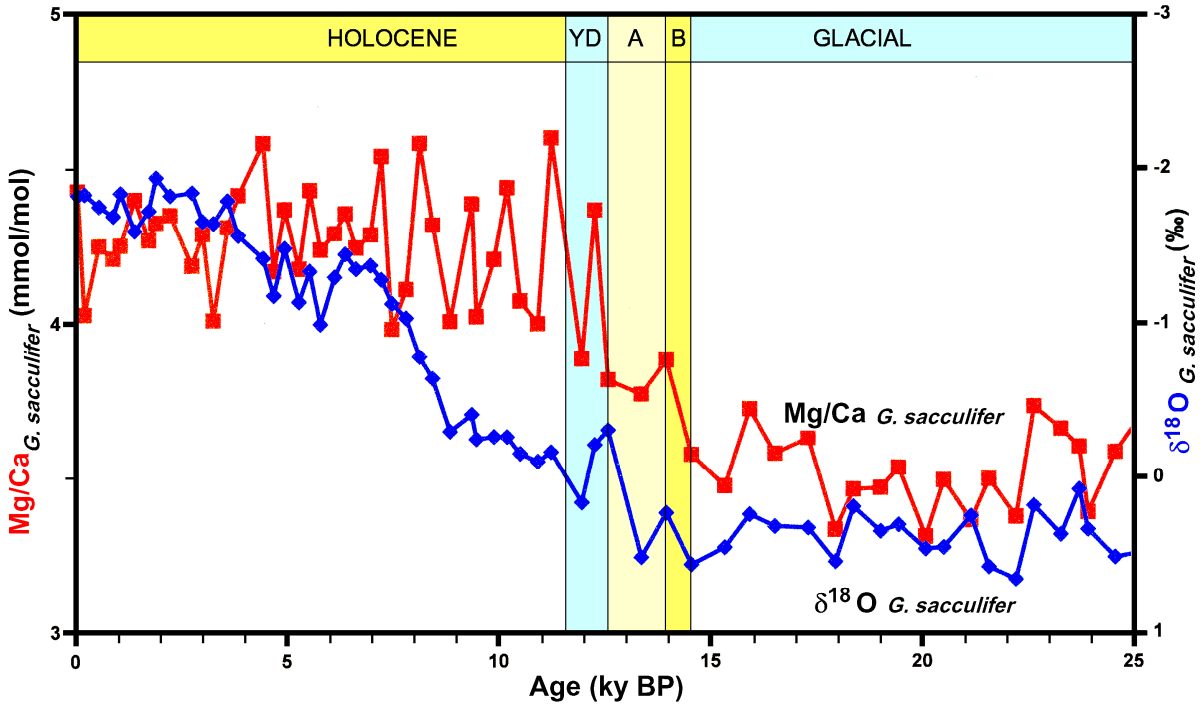

Figure 5.6.1-1: Comparison of the Mg/Ca and $\delta^{18}O$ record for the core SO164-03-4 for *G. sacculifer* across Termination 1. The position of the individual Terminations of each proxy is marked by the short dashed line. A more detailed schematic of the phase shift is presented in figure 5.6.1. Note, for convenience of comparison the $\delta^{18}O$ values are plotted inversely. (B - Bølling, A - Allerød, YD - Younger Dryas).

The pattern of Mg/Ca and $\delta^{18}O$ are in general very similar. However, at Termination 1, the pattern and phasing of the two proxies are different. It can be seen that the Termination 1 is reached earlier for the Mg/Ca record, whereas the Termination in the $\delta^{18}O$ record is reached about 4 thousand years later.

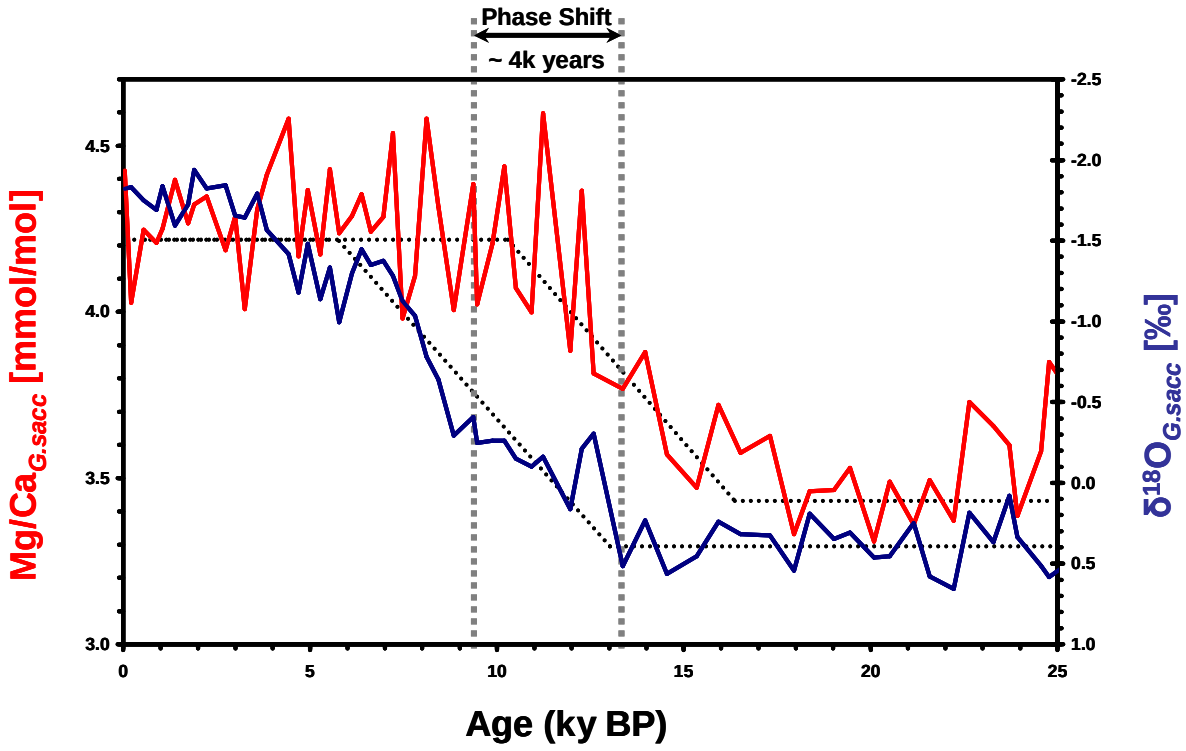

Figure 5.6.1-2: Comparison of the Mg/Ca and $\delta^{18}O$ record for the core SO164-03-4 for *G. sacculifer* across Termination 1 and the position of the phase shift. The main signal patterns and their variations are marked with the dotted black lines (added by eyeballing). The phase phift is marked by the grey bars. Note, for convenience of comparison the $\delta^{18}O$ values are plotted inversely.

This is demonstrated in more detail in figure 5.6.1-2 which gives a visualization of the phase shift. Note that the overall signal pattern is almost identical during the Holocene and prior to the onset of the warming in the Bølling Allerød. During the transition, this is not the case.

In summary, the phase shift is clearly observed at the core site SO 164-03-4.

5.1.5 Employing $\delta^{44/40}$Ca measurements to decipher the phase shift

The measured $\delta^{44/40}$Ca ratios for *G. sacculifer* are shown in figure 5.7 and 5.8 below. The $\delta^{44/40}$Ca values vary in between 0.35 and 0.75, respectively, and are thought to represent SST fluctuations. There is one pronounced core section with a peak in $\delta^{44/40}$Ca values corresponding to the warm Allerød period (14.000 years BP) which is not visible in the δ^{18}O and Mg/Ca records.

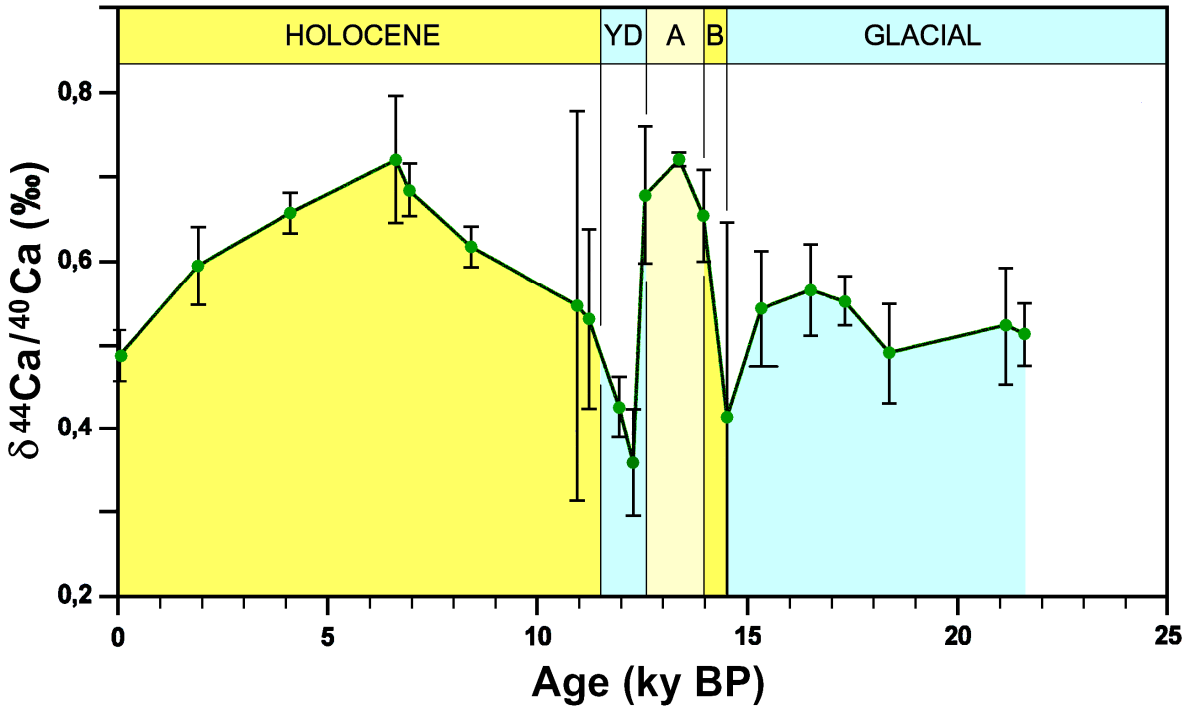

Figure 5.7: $\delta^{44}Ca/^{40}Ca$ ratios of *G. sacculifer* for the core SO164-03-4 for the last 23.000 years. The black bars represent the mean weighted errors of the internal reproducibility of each individual measurement (2σ of the mean). (B - Bølling, A - Allerød, YD - Younger Dryas).

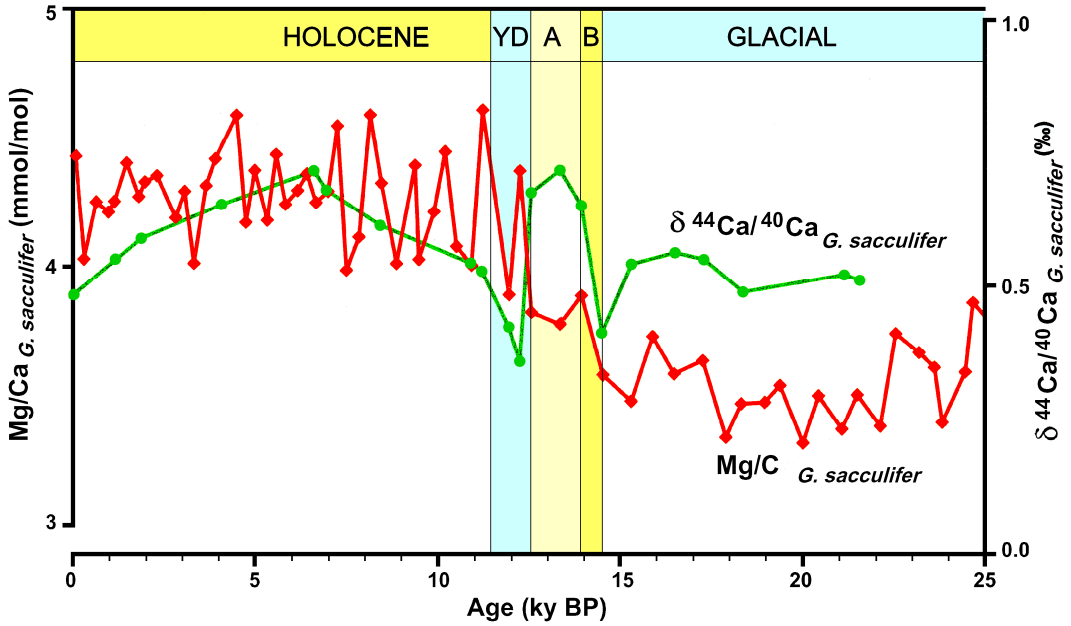

Figure 5.8: $\delta^{44}Ca/^{40}Ca$ and Mg/Ca ratios for the core SO 164-03-4 for *G. sacculifer*. Both proxies show no major signal variations during the LGM and Holocene. (B - Bølling, A - Allerød, YD - Younger Dryas).

If the $\delta^{44/40}Ca$ ratios are converted into temperature values ($T_{\delta 44/40Ca}$) using the temperature calibrations from *Hippler et al.* [2006] a difference in absolute values is visible to the corresponding $T_{Mg/Ca}$ (figure 5.9). During the LGM the two proxies show similar values but during the Holocene (after Termination 1) the $\delta^{44/40}Ca$ temperature values are offset by ~2 ℃. The exact reason for th is is still unknown.

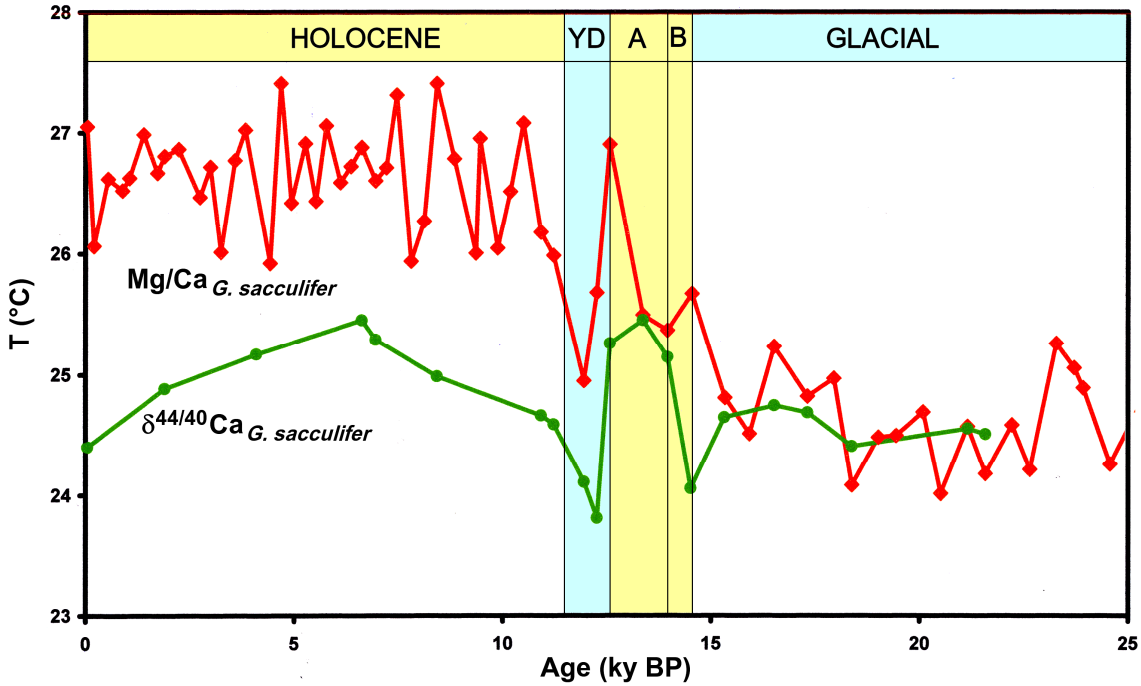

Figure 5.9: Comparison of the $T_{\delta 44/40Ca}$ and $T_{Mg/Ca}$. for the core SO 164-03-4 for *G. sacculifer*. (B - Bølling, A - Allerød, YD - Younger Dryas).

The measured $\delta^{44/40}$Ca ratios of the Sonne 164-03-4 core from the Central Caribbean Sea are compared with the Greenland ice core record GISP 2 [taken from *Lea et al.* [2003]) to further verify our results. From figure 5.10 it can be seen that the Bølling / Allerød / Younger Dryas period is clearly represented in both records.

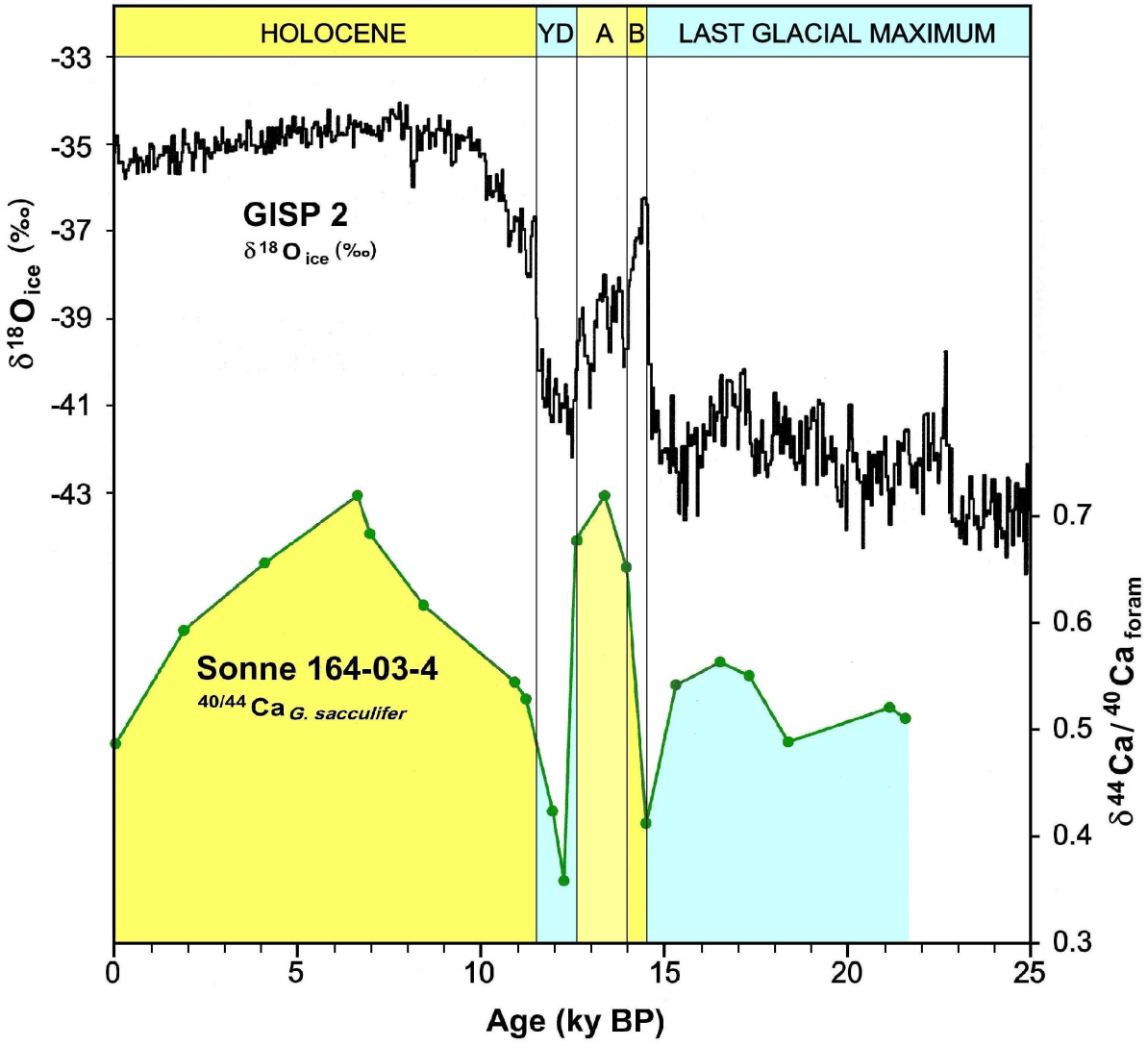

Figure 5.10: Comparison of the δ^{18}O of the Greenland ice core GISP 2 data with the δ^{44}Ca/^{40}Ca ratios of *G. sacculifer* from the SO-164-03-4 core. (B - Bølling, A - Allerød, YD - Younger Dryas).

The strength of the $\delta^{44/40}$Ca isotope system is quite obvious: it shows the warming during the Bølling / Allerød period very clearly; the generated absolute temperature values are comparable with the temperatures during the Holocene climate optimum generated with other proxy systems. The temperature increase during the Bølling / Allerød period is not observed in the δ^{18}O record of *G. sacculifer* at the SO 164-03-4 (figure 5.6). The reasons for such discrepancy will be discussed in more detail in the following chapters taking into SSS variations into consideration.

5.1.6 Estimation of the variations of the evaporation to precipitation ratios

In order to estimate the SSS variations in past seawater the paleo temperature equation by *Thunnel et al*. [1999] was employed (equation 3).

This equation can be employed to remove the temperature component from the original $\delta^{18}O_{seawater}$ signal, leaving behind only the salinity and the ice volume influence. The SST values based on the Mg/Ca or $\delta^{44/40}Ca$ ratios are used to reconstruct temperature independent seawater $\delta^{18}O$ values. In order to account for the glacial / interglacial induced SSS variations, the calculated $\delta^{18}O_{seawater}$ values from equation 3 have to be corrected for the systematic $\delta^{18}O$ difference in the global ice volume between Marine Isotope Stage 2 and Marine Isotope Stage 1 (equation 4).

After correction, the $\Delta\delta^{18}O_{ivf\text{-}seawater}$ values give an indirect estimation of the variations in SSS.

1	2	3	4	5	6	7
Depth [cm]	**Age [ka BP]**	**$T_{44/40Ca}$ (±0.5) [℃]**	**$\delta^{18}O$ *G. sacc* (±0.07) [‰]**	**RSL variation**	**$\Delta\delta^{18}O_{ivfsw}$ [‰]**	**Deviation from Holocene mean**
2	0.04	24.40	-1.822	0.0000	0.43	0.51
13	1.90	24.88	-1.940	0.0012	0.41	0.49
26	4.09	25.17	-1.919	0.0145	0.48	0.57
41	6.63	25.45	-1.350	0.0448	1.07	1.29
43	6.97	25.29	-1.375	0.0541	1.01	1.21
51	8.43	24.99	-0.640	0.1182	1.61	1.93
63	10.92	24.66	-0.262	0.3236	1.72	2.06
64.5	11.23	24.59	-0.163	0.3720	1.75	2.10
68	11.96	24.11	0.162	0.4496	1.90	2.28
69.5	12.27	23.81	-0.210	0.5018	1.41	1.70
71	12.58	25.26	-0.305	0.5409	1.58	1.90
73	13.37	25.45	0.517	0.5798	2.41	2.89
74.5	13.96	25.15	0.231	0.6764	1.96	2.35
76	14.51	24.06	0.564	0.8042	1.94	2.32
78	15.32	24.65	0.453	0.8765	1.88	2.25
83	16.52	24.74	0.317	0.9778	1.66	1.99
86	17.31	24.68	0.326	0.9992	1.63	1.96
88	18.38	24.40	0.545	1.0134	1.78	2.14
101	21.15	24.55	0.453	1.0353	1.70	2.04
103	21.58	24.50	0.249	1.0262	1.49	1.79

Table 5.1.6.1: Compilation of the calculated $\Delta\delta^{18}O_{ivfsw}$ values for SO 164-03-4 and the original data used for the calculation employing the procedure from chapter 2. The subsequent error of the calculation is σ=±0.2.

5 RSL variation correction by *Waelbroeck et al.*
6 $\Delta\delta^{18}O_{ivfsw}$ calculated with equation 3 & 4, employing the temperature values from **3**, the $\delta^{18}O$ values from **4** and the RSL correction from **5**
7 Deviation from Holocene mean is the difference from the average of the first six values from **6** which is normalized to 1

The result is presented in figure 5.11, the $\Delta\delta^{18}O_{ivf\text{-}seawater}$ values are plotted as a deviation of the mean Holocene average (calculated for this site from the measured Holocene samples, the average of the first 6 samples which are then normalized to one). Unfortunately the $\Delta\delta^{18}O_{ivf\text{-}seawater}$ values cannot easily be transferred into absolute salinity values because the salinity-$\Delta\delta^{18}O_{ivf\text{-}seawater}$ relationship is not known. However this technique makes it possible to observe qualitative inferences concerning temporal salinity fluctuations.

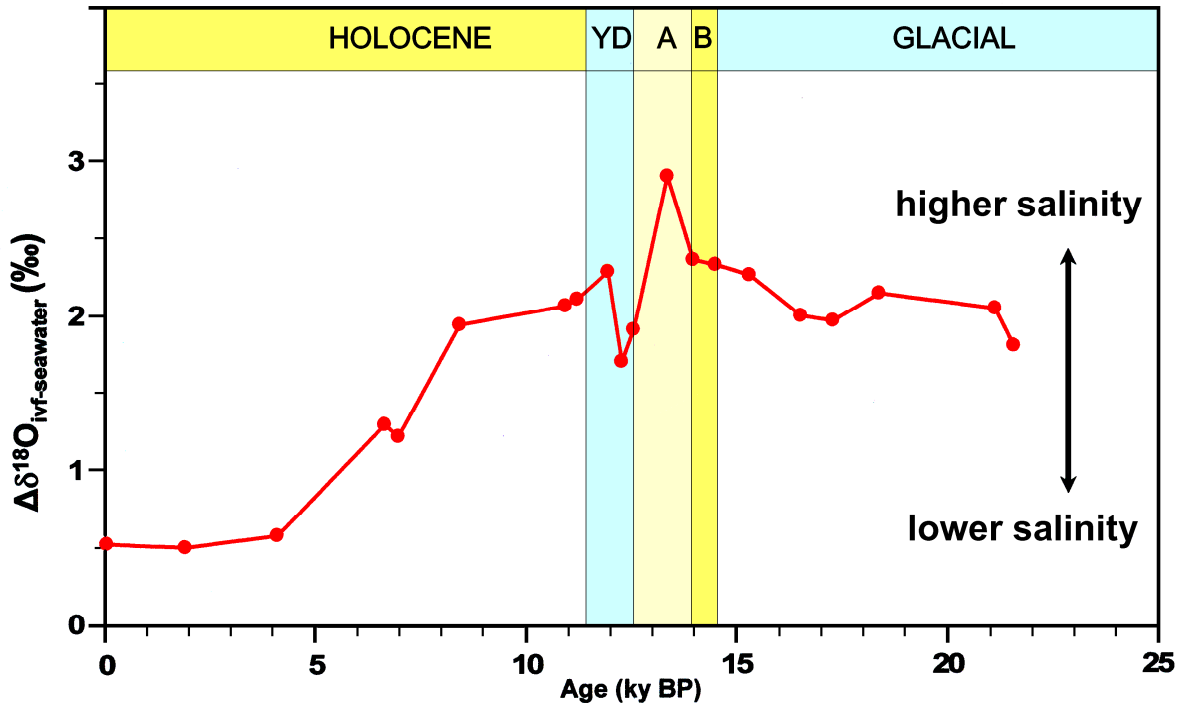

Figure 5.11: $\Delta\delta^{18}O_{ivf\text{-}seawater}$ calculated for the SO 164-03-4 core using $\delta^{44/40}Ca$ generated temperatures and corrected for the variations of the global ice volume.
(B - Bølling, A - Allerød, YD - Younger Dryas).

In this regard more positive values are interpreted to represent an evaporation environment. This leads to a higher overall salinity in the surface ocean waters at this site in the Central Caribbean Sea, due to the strong evaporation of surface water. In contrast, relatively low values indicate a more precipitation environment.

During the glacial period there are higher than present day $\Delta\delta^{18}O_{ivf\text{-}seawater}$ values. This is in agreement with the fact that large amounts of fresh water were confined in the glaciers on the Northern hemisphere which resulted in a lower sea level and a higher overall ocean salinity in the world ocean. With the onset of the Bølling-Allerød, the $\Delta\delta^{18}O_{ivf\text{-}seawater}$ values reach a certain maximum indicating highest level of salinity at that time and in this region.

With the onset of the Younger Dryas period, declining $\Delta\delta^{18}O$ values are observed indicating generally dropping regional salinity independent of the development in the global oceans. With the onset of the Holocene the $\Delta\delta^{18}O$ values rapidly decline until they reach stable values of about 0.5 ‰.

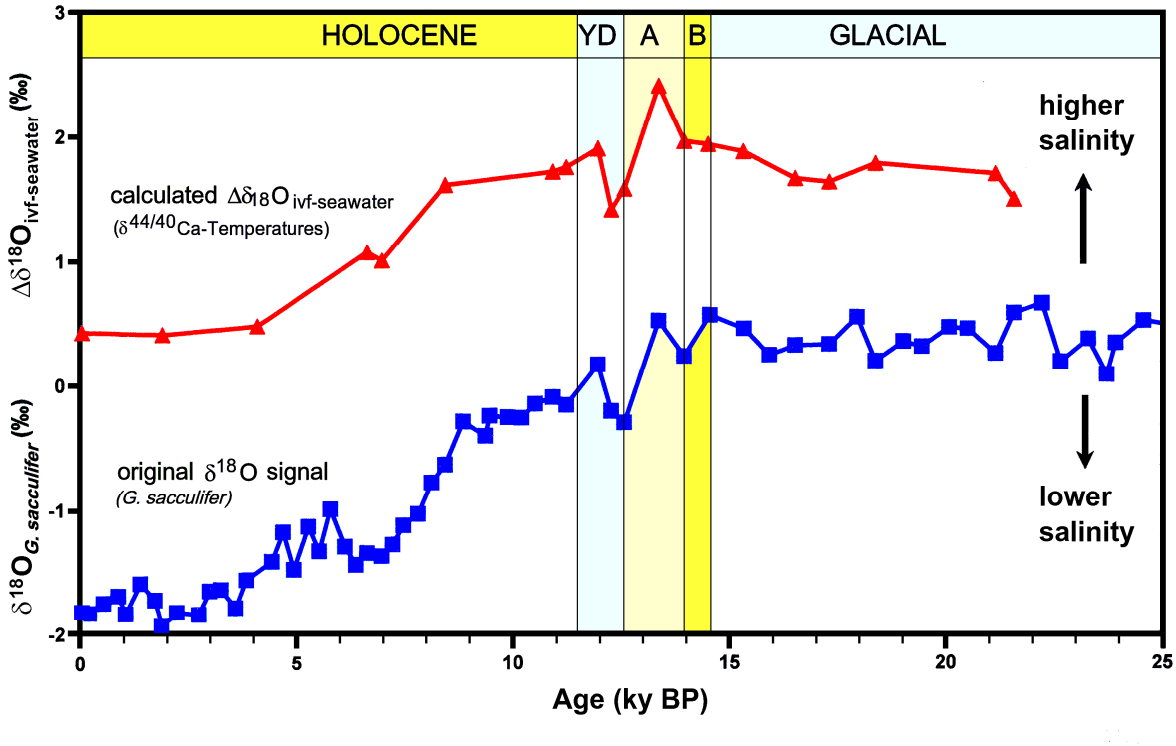

Figure 5.12: Comparison of the original $\delta^{18}O$ signal with the calculated $\Delta\ \delta^{18}O_{ivf\text{-}sw}$ values from the core SO 164-03-4. (B - Bølling, A - Allerød, YD - Younger Dryas).

Our data indicate a strong increase in regional SSS during glacial / interglacial transition. The timing of this salinity maximum coincides with the onset of the phase shift and is discussed in the conclusions. The general pattern of the regional salinity variation follows the general pattern of the $\delta^{18}O$-curve in the world ocean ((*Nürnberg and Groeneveld* [2006]).

5.2 Results ODP Leg 172, Site 1058c – Blake Ridge

The ODP core Leg 172, Site 1058c was recovered off the coast of Florida on the Blake Bahama Ridge [*Keigwin et al.*, 1998]. The core site is close to the entry of the Gulf Stream from the Caribbean Sea and the Gulf of Mexico into the Atlantic Ocean. This location was selected with the goal to check if a phase shift between Mg/Ca- and $\delta^{18}O$- ratios occurs not only in the Caribbean Sea but also at the initial path of the Gulf Stream. Such a presence would be a possible indication for varying SSS or large fluxes of the ocean parameters, like for example temperature, during the glacial and interglacial transition periods.

5.2.1 Holocene and Termination 1

In order to check for the presence of short term fluxes in salinities and temperatures, detailed analyses of the first 1.5 meters of the ODP core 1058c were undertaken; covering a time interval of the last 16000 years.

Combined $\delta^{18}O$ and Mg/Ca measurements were obtained; the results for the planktonic foraminifera *G. ruber* are presented in figure 5.2.1.

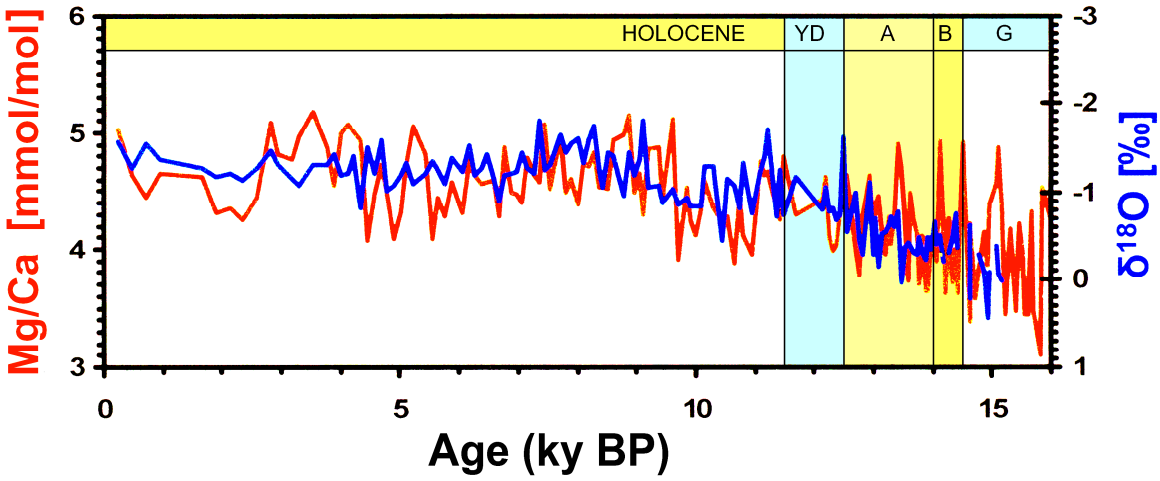

Figure 5.2.1: A comparison of the Mg/Ca and the $\delta^{18}O$ ratios of *G. ruber* for the ODP core 172-1058c. The time interval analysed are the last 16.000 years. (B - Bølling, A - Allerød, YD - Younger Dryas).

The densely measured $\delta^{18}O$ samples indicate many short term climate variations. The overall scatter is in the order of about 0.5 ‰. The long term differences between

the glacial and interglacial climate are also observed, these variations are approximately 1.5 ‰.

The Mg/Ca ratios measured on *G. ruber* of the same samples show similar variation patterns like the $\delta^{18}O$ signals. Again, smaller short term variations of some 0.5 mmol/mol are observed whereas the long term variations in the Mg/Ca ratios from the LGM to the Holocene are about 1.5 to 2 mmol/mol. This is in the order of magnitude of the signal variations from *G. ruber* observed in the Sonne core SO 163-03-4 (see figure 5.4). These variations in the $\delta^{18}O$ and Mg/Ca ratios of *G. ruber* represent the expected changes from a glacial environment to a more temperate climate.

The overall trends and signal patterns of the two proxies at first glance seem to be very similar. In order to verify this assumption a seven point running mean was calculated and is presented in figure 5.2.2 below. This should enable a more direct comparison and reveal if a possible phase shift can be identified.

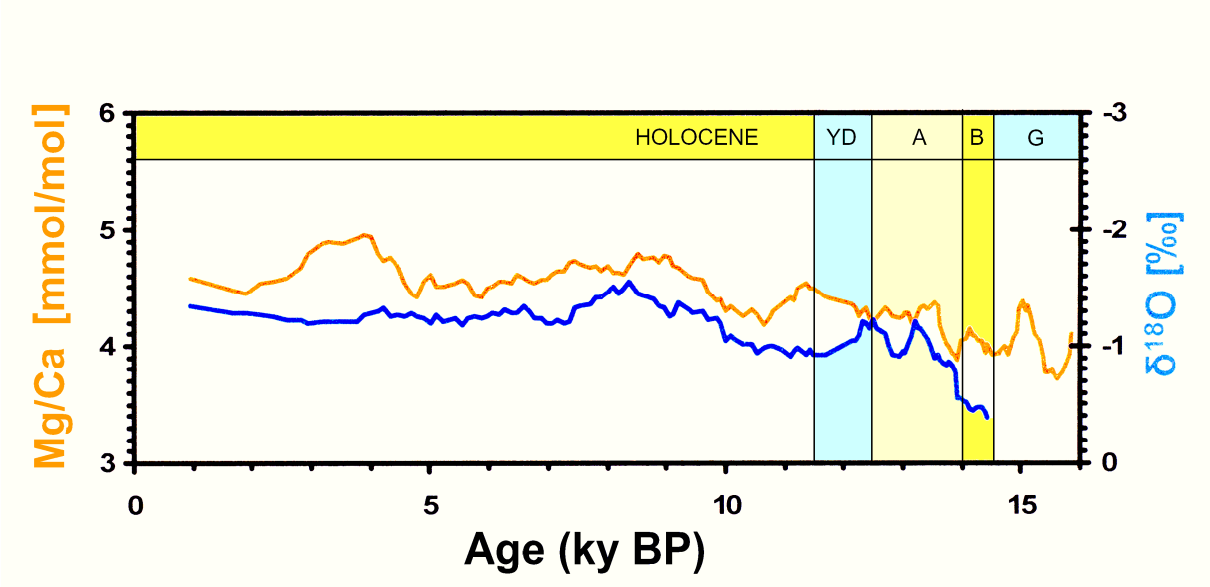

Figure 5.2.2: A seven Point running mean of the Mg/Ca and $\delta^{18}O$ ratios of *G. ruber* for the last 16k years for the ODP core 172-1058c. (B - Bølling, A - Allerød, YD - Younger Dryas).

The overall picture presented by the running mean is that there are no major signal variations in the $\delta^{18}O$ ratios during the Holocene, the signal is stable with only minor variations in the order of 0.5 ‰. The Mg/Ca ratios show a very similar behaviour with no large variations, too. The variations are approximately 0.7 ‰ for the first 10.000 years. The onset of the main climate change during, the glacial/interglacial transition between 15.000 and 11.500 years BP is not indicated by any large changes in the running means of the individual proxies. The $\delta^{18}O$ values do not change more than 1

‰, the Mg/Ca element ratios are exposed to similar changes. The overall signal patterns do not show any significant differences that would indicate the presence of a phase shift between the $\delta^{18}O$ and Mg/Ca ratios. There is no phase shift present at this core site of the coast of Florida (figure 5.2.1).

In order to verify these findings and check for the presence of any strong fluxes in SSS, $\Delta\delta^{18}O_{ivf\text{-}sw}$ values were calculated from the temperatures of the measured Mg/Ca ratios. The Mg/Ca ratios were converted into their corresponding temperature values in figure 5.2.3.

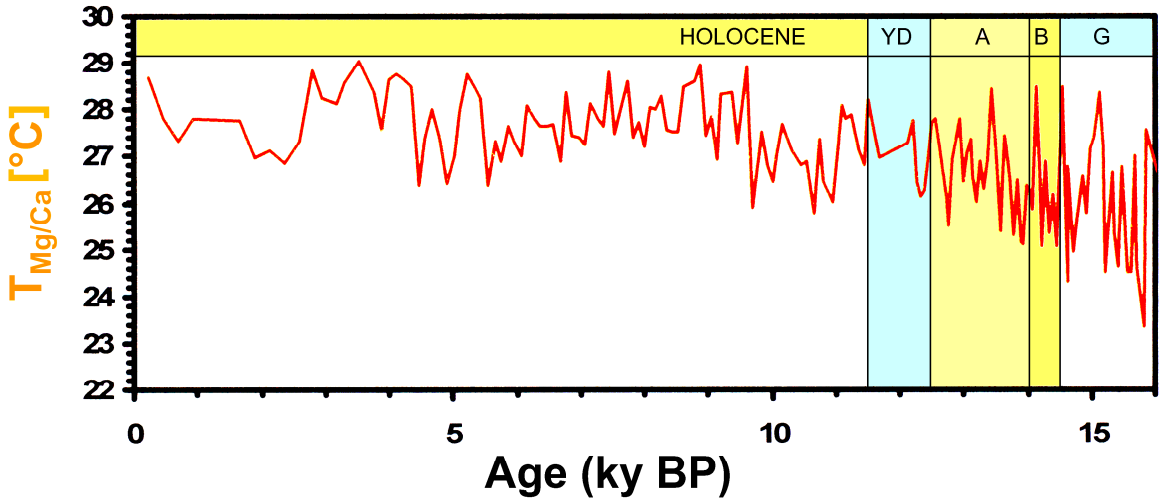

Figure 5.2.3: Mg/Ca derived temperature values of *G. ruber* for the ODP core 172-1058c. (B - Bølling, A - Allerød, YD - Younger Dryas).

The temperatures vary between 27℃ to 29℃ during t he Holocene and 23 to 25℃ during the LGM. Overall the SST of *G. ruber* present a gradual increase in temperature over the measured time interval with many short term fluctuations. These variations are strongest at the onset of the Bølling / Allerød, the fluxes are larger than 4℃. This could possibly be an indicati on for short term instable climate conditions at the core site before the onset of the Transition.

Following the procedure described in section 2, the $\Delta\delta^{18}O_{ivf\text{-}sw}$ values obtained for the Termination 1 are presented in figure 5.2.4.

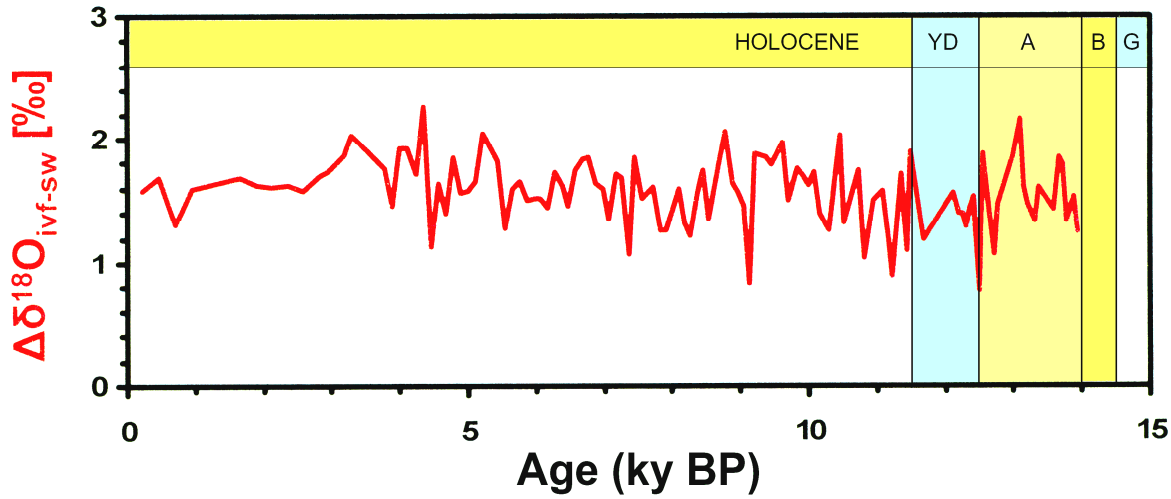

Figure 5.2.4: $\Delta\delta^{18}O_{ivf\text{-}sw}$ values calculated for *G. ruber* of the ODP core 172-1058c. (B - Bølling, A - Allerød, YD - Younger Dryas).

The $\Delta\delta^{18}O_{ivf\text{-}sw}$ values were calculated for the last 14.000 years. They can be interpreted as changes in the evaporation to precipitation ratio of the surface ocean. Many short term variations of the $\Delta\delta^{18}O_{ivf\text{-}sw}$ values are observed but the values do not give any indication to long term major changes. The overall average is about 1.5 ‰, the Holocene values are in the order of magnitude of the values during the Transition. During the Allerød a minor maximum is reached, the $\Delta\delta^{18}O_{ivf\text{-}sw}$ are 0.2 ‰ higher than average. At the onset of the cooler Younger Dryas the lowest $\Delta\delta^{18}O_{ivf\text{-}sw}$ values of about 0.9 ‰ were calculated. This could be a possible be caused by a melt water pulse.

Overall there are no indications for major changes in the evaporation to precipitation ratio during the Bølling / Allerød and Younger Dryas time span. This is a different result than in the core SO 164-03-4, where larger long variations in the order of 1 ‰ were observed. In conclusion, the overall picture points to a more stable long term surface ocean environment over the past 16.000 years on the Blake Bahama Ridge.

In order to verify this assumption of relative stable ocean conditions a more detailed look at the situation in deeper water masses with a variety of measurements of *G. truncatulinoides* was undertaken. The $\delta^{18}O$ and Mg/Ca ratios were measured for the same samples and are presented in the following figures.

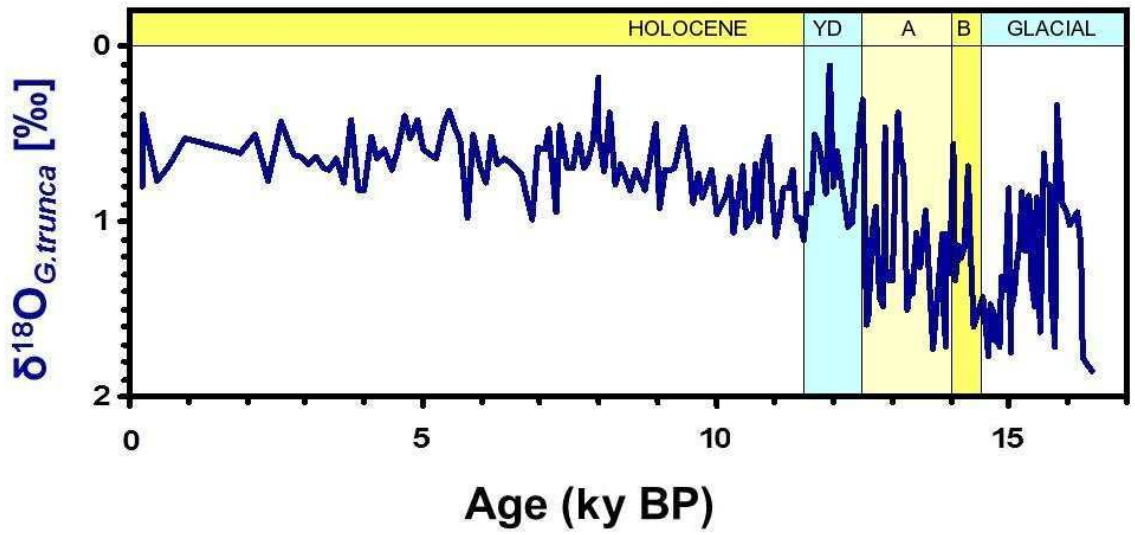

Figure 5.2.5: $\delta^{18}O$ ratios of *G. truncatulinoides* for the ODP core 172-1058c.
(B - Bølling, A - Allerød, YD - Younger Dryas).

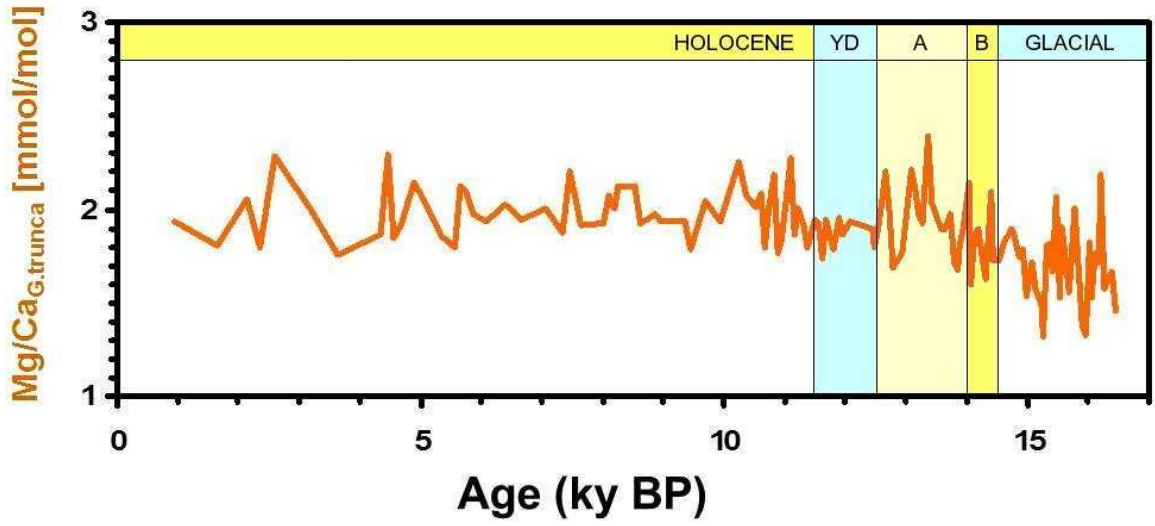

Figure 5.2.6: Mg/Ca ratios of *G. truncatulinoides* for the ODP core 172-1058c.
(B - Bølling, A - Allerød, YD - Younger Dryas).

The $\delta^{18}O$ ratios show very interesting signal variations for *G. truncatulinoides* whereas the Mg/Ca ratios are more stable at first glance. If the Mg/Ca ratios are then converted into temperature values the stable conditions are even more obvious but the transition from the Last Glacial Maximum to the Holocene can be observed more easily.

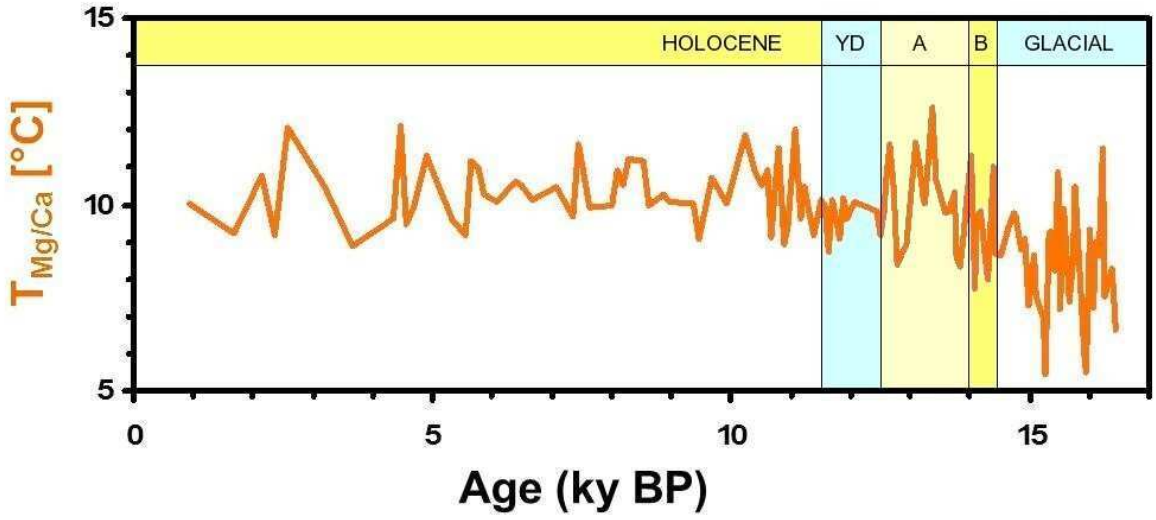

Figure 5.2.7: Mg/Ca generated temperatures of *G. truncatulinoides* for the ODP core 172-1058c. (B - Bølling, A - Allerød, YD - Younger Dryas).

The temperatures during the LGM are about 2℃ lower than the average Holocene temperatures generated from *G. truncatulinoides.* This is in the order of magnitude of previously reported temperature over the last Transition period. Our record points to large variations in sub surface ocean temperatures prior to the Bølling / Allerød. This is in agreement to the findings of *G. ruber* at this core site.

To further verify this observation, $\Delta\delta^{18}O_{ivf\text{-}sw}$ values calculated for *G. truncatulinoides* of the ODP core 172-1058c were calculated following the standard procedure from chapter 2. The results are presented in figure 5.2.8.

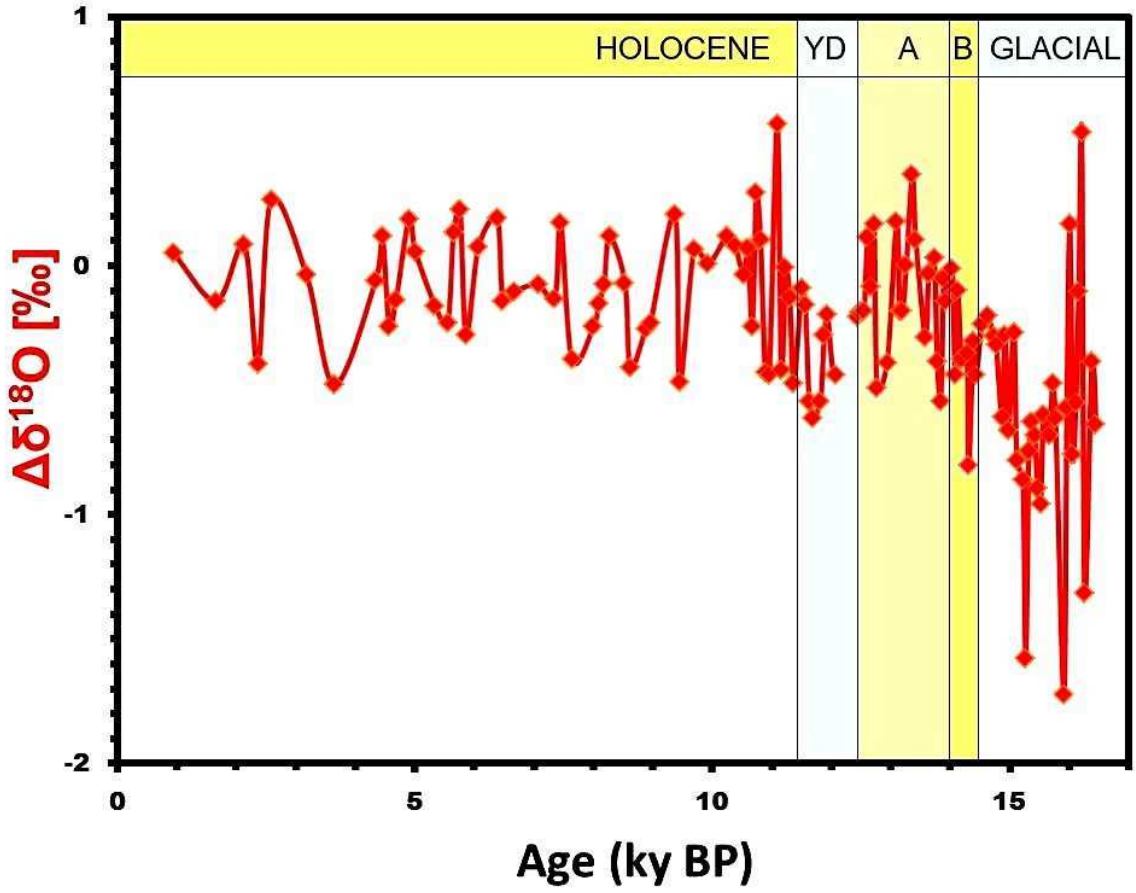

Figure 5.2.8: $\Delta\delta^{18}O_{ivf\text{-}sw}$ values calculated for *G. truncatulinoides* of the ODP core 172-1058c. (B - Bølling, A - Allerød, YD - Younger Dryas).

The results from the $\Delta\delta^{18}O_{ivf\text{-}sw}$ calculations are very interesting, even though the employed Mg/Ca ratio generated temperature values are also dependant on salinity variations. The results point to a gradual increase in sub surface salinity to present day values during the Transition period. Of further interest are the large fluctuations prior to the glacial / interglacial transition. This phenomenon has been observed for different species of foraminifera and at different habitat depths (see e.g. *Hippler et al.*, [2006]; *Lea et al*. [2003]; *Nürnberg et. al.*, [2000]).

The exact reason for this is unclear and still unknown. Further future investigations could explain if this observation is of any significance.

5.3 Searching for a High Northern Latitude phase shift

In order to verify if the phase shift, which has been observed in the tropical oceans during the last glacial/interglacial transition period, is also present in high northern latitudes a study on the area was undertaken where the warm Caribbean water masses were transported by the Gulf Stream into the Arctic. The Arctic Ocean is in so far of importance since this area has undergone dramatic changes from the last ice age when it was totally covered by sea ice until today.
Two sites were evaluated at high northern latitude, in the Denmark Strait between Iceland and Greenland and off the west coast of Spitsbergen.

5.3.1 Core M/M 51/5-712-2 off the coast of Spitsbergen

In order to verify the existence of possible phase shifts between temperature proxies in the high North Atlantic Ocean, samples from the core M/M 5/5-712-2 off the coast of Spitsbergen were reviewed. The foraminifera *N. pachyderma* is abundant in this core and thus can be used as a temperature archive. A brief comparison between the measured $\delta^{18}O$ values and the $\delta^{44/40}Ca$ ratios should reveal the presence of any fluctuations in ocean parameters or even the existence of a possible phase shift. The time window of interest is the last 10-15.000 years since the phase shift was observed in the core SO 164-03-4 in this time interval. Unfortunately, no Mg/Ca ratios measurements are available but previously mentioned results have shown the comparability of the Mg/Ca and $\delta^{44/40}Ca$ ratios [see *Hippler et al.*, 2006, Kozdon et al., 2009].
The age model for the core was done with the help of the benthic foraminifera *C. wuellerstorfi.* The measured $\delta^{18}O$ values for *N. pachyderma* are presented below in figure 5.3.1. The main setback was that during the Younger Dryas the amount of sample material, more specific the abundance of our sampled foraminifera was extremely low which did not grant enough material for multiple $\delta^{44/40}Ca$ measurements. Overall the core has a different, coarser composition during this cooler time interval.

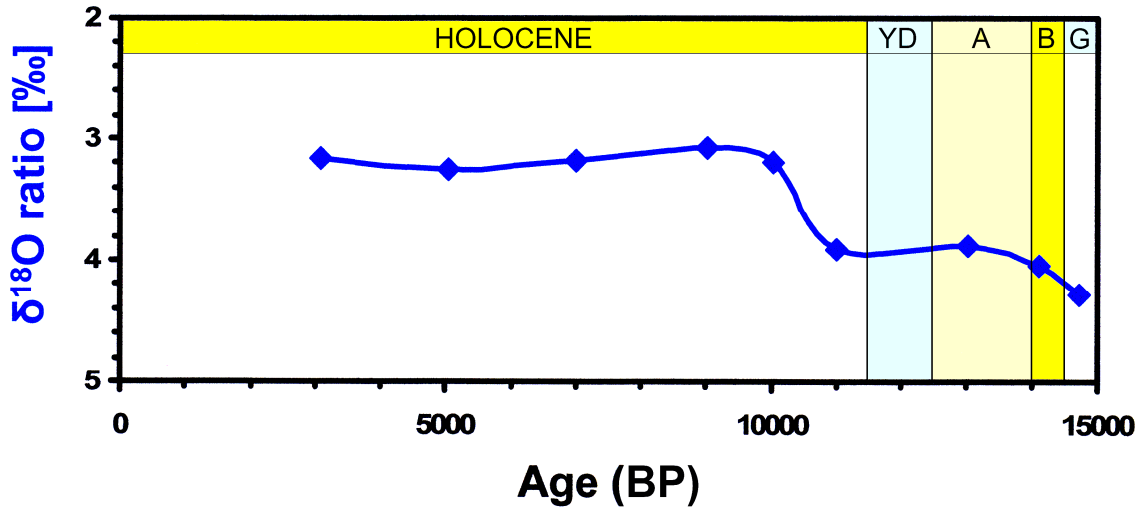

Figure 5.3.1: $\delta^{18}O$ values for *N. pachyderma* for the M/M 5/5-712-2 core. The $\delta^{18}O$ ratios are plotted inverse for the last 15.000 years (G-Glacial, B-Bølling, A-Allerød, YD-Younger Dryas)

The $\delta^{18}O$ values for *N. pachyderma* for M/M 5/5-712-2 core are more or less constant during the Holocene. The main signal increase by ~0.75 ‰ occurs at about 11.000 years BP which coincides with the end of the Y.D. It is of interest that no major signal variations are visible in our samples in the Bølling-Allerød. The $\delta^{18}O$ ratios do not show any major reactions at the onset of the Transition from a glacial to interglacial climate.

In order to check for the occurrence or absence of a phase shift, $\delta^{44/40}Ca$ ratios of the same foraminiferal samples of *N. pachyderma* were measured. The results are presented in figure 5.3.2 for the same time window, the last 15.000 years.

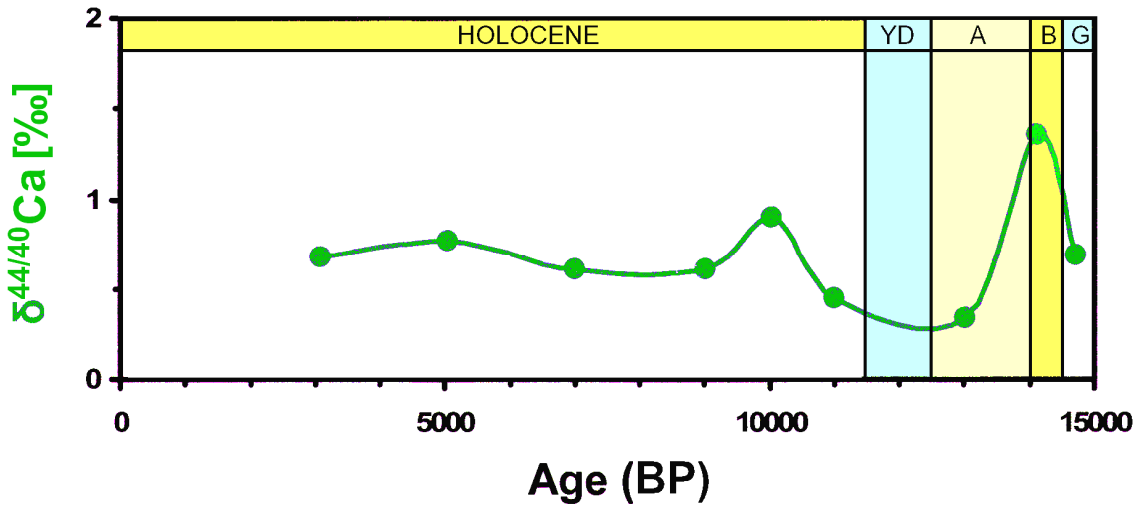

Figure 5.3.2: $\delta^{44/40}$Ca ratios for *N. pachyderma* for the M/M 5/5-712-2 core for the last 15. kyears. The signal maxima are at ~10 kyears and ~14 kyears (B-Bølling, A-Allerød, YD-Younger Dryas)

The measured $\delta^{44/40}$Ca ratios of *N. pachyderma* show very stable values during most of the Holocene with the exception of a maximum near the onset of this time period, about 10.000 years BP. A similar signal in the δ^{18}O ratios is not observed. This is close to the Holocene climate optimum.

During the Allerød and probably Younger Dryas, a distinct reduction of the values of the $\delta^{44/40}$Ca proxy is visible, but the sample density is not high enough to very this assumption. The overall uncertainty of the samples is in the order of 0.12-0.15 ‰ and a denser spacing in the samples would be desirable.

The Ca isotope ratios were converted into their corresponding temperature values ($T_{\delta 44/40Ca}$). The results are presented in figure 5.3.3.

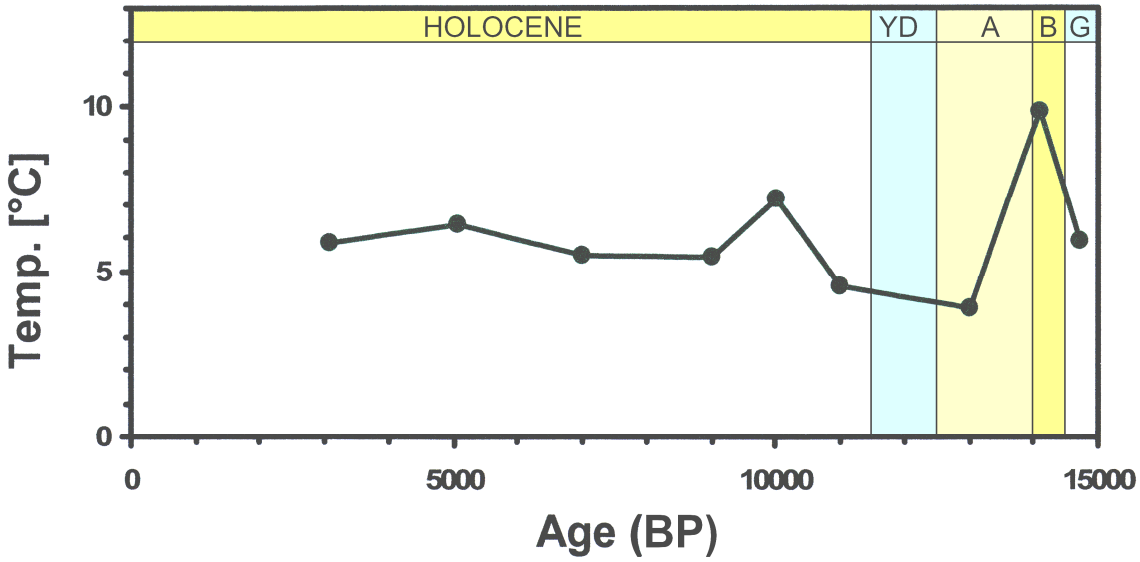

Figure 5.3.3: The Ca isotope based Temperature values ($T_{\delta 44/40Ca}$) for *N. pachyderma* from core M/M 5/5-712-2 for the last 15.000 years. The temperatures vary between 4 and 10 ℃ (B-Bølling, A-Allerød, YD-Younger Dryas)

The warmest observed $\delta^{44/40}Ca$ temperature values were recorded during the Bølling-Allerød time interval. A similar signal variation was not observed for the $\delta^{18}O$ ratios and a more direct comparison of the two proxies is shown in figure 5.3.4.

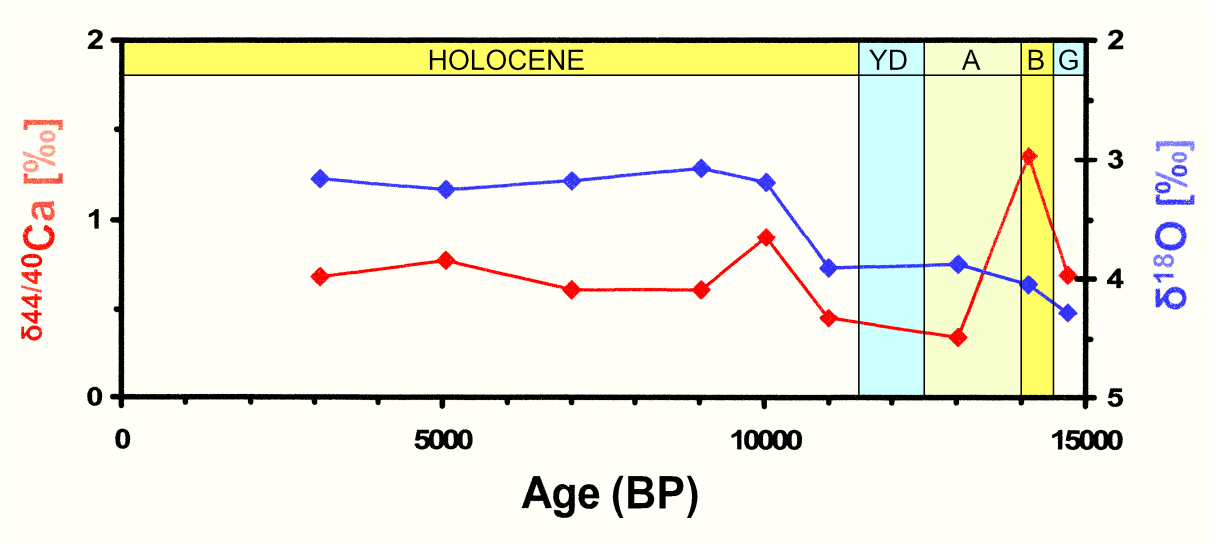

Figure 5.3.4: Comparison of the $\delta^{18}O$ and the $\delta^{44/40}Ca$ ratios for *N. pachyderma* for the M/M 5/5-712-2 core for the last 15.000 years (, B-Bølling, A-Allerød, YD-Younger Dryas)

The overall signal patterns for the onset of the Holocene and the Younger Dryas are almost identical and furthermore both proxies show very stable values during the Holocene. The most striking difference is seen during the Bølling-Allerød were the $\delta^{44/40}Ca$ ratios react strongly to the ocean warming. A phase shift between the $\delta^{44/40}Ca$ and $\delta^{18}O$ ratios, however, is not observable; the overall signal pattern is identical until the Holocene climate optimum is reached. The $\delta^{18}O$ ratios do not drop like the corresponding Calcium isotope ratios. This is most likely influenced by variations in SSS, possibly even melt water influxes. The $\delta^{18}O$ proxy, as previously shown in chapter 2, is prone to variations in salinity and temperature.

In order to check for variations in the evaporation to precipitation ratio, $\Delta\delta^{18}O_{ivf\text{-}sw}$ values were calculated following the procedure detailed in section 2. The results are presented in figure 5.3.5.

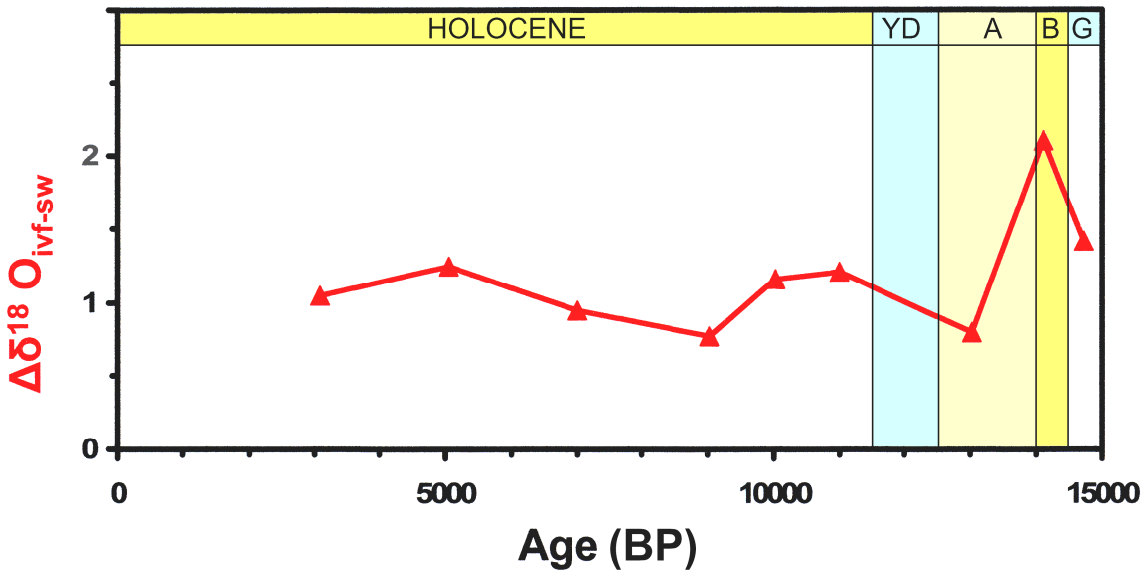

Figure 5.3.5: Calculated $\Delta\delta^{18}O_{ivf\text{-}sw}$ values for *N. pachyderma* for the M/M 5/5-712-2 core for the last 15.000 years (B-Bølling, A-Allerød, YD-Younger Dryas)

The calculated $\Delta\delta^{18}O_{ivf\text{-}sw}$ values point to a relative constant regional salinity during the Holocene. The main features are the higher than present day values during the Bølling-Allerød which point to very large variation in the ocean parameters, like SSS and SST, during the onset of the deglaciation.

In order to check if the results from the core M/M 5/5-712-2 show regional variations the results are compared with data from the core M23519 taken at a position further southward in the North Atlantic.

5.3.2 Core M23519 in the Denmark Strait

The core M23519 is located in the Denmark Strait between Greenland and Iceland (see section 3). The data have kindly been provided by *R.Kozdon* [personal communication] (Fig. 5.3.6).

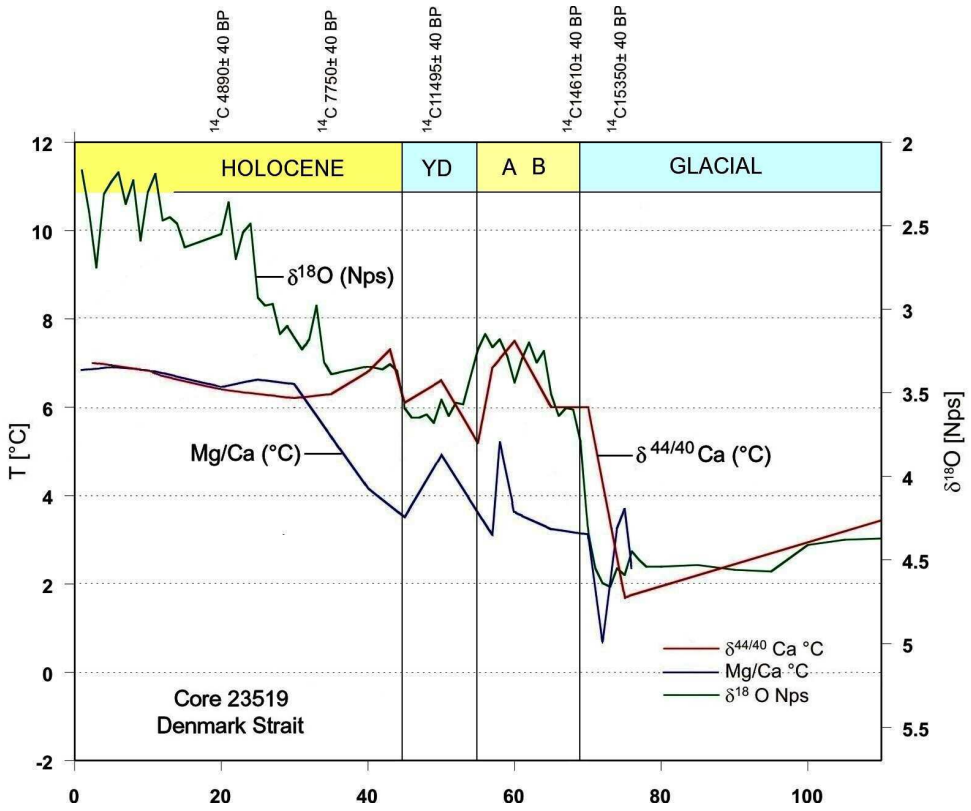

Figure 5.3.6: This figure shows $T_{Mg/Ca}$ and $T_{\delta 44/40Ca}$ together with $\delta^{18}O$ as a function of depth (cm) in core 23519 from the Denmark Strait. The stratigraphic correlation is tentative since no detailed time scale was available (B-Bølling, A-Allerød, YD-Younger Dryas).

There is no phase shift between the Mg/Ca and the $\delta^{18}O$ ratios as observed in core SO164 from the Caribbean Sea. The overall signal patterns of the three proxies are very similar. When compared to the results obtained from the M/M 515-712-2 core it is noticeable that the $\delta^{44/40}Ca$ and $\delta^{18}O$ ratios show synchronous signal variations, especially during the warm period of the Bølling-Allerød. This is not observed in the $\delta^{44/40}Ca$ ratios of the M/M 515-712-2 core.

Remarkable at this core site is the observation that the individual temperature proxies run closely synchronous in the LGM and the early Holocene: The Mg/Ca and $\delta^{44/40}Ca$ generated temperatures are identical within the statistical uncertainty. This was not case in the Caribbean core SO 164-03-4 (for more detail refer to section 5.1).

In conclusion, the collected data from the high North Atlantic Ocean do not point to a phase shift between the $\delta^{18}O$ and Mg/Ca or $\delta^{44/40}Ca$ proxy systems as observed in tropical oceans.

6 Comparing the Results with other core sites from the Caribbean region

In order to achieve a better understanding of the phase shift and the proposed movement of the ITCZ, the obtained results and employed methods of calculating $\Delta\delta^{18}O_{ivfsw}$ values were compared with other previously published data from the Caribbean Region.

It was hoped to find more evidence for rapid changes in SSS which could be linked to a possible movement of the ITCZ. A selection of cores from the overall area of the Caribbean Sea was made and compared to our results.

6.1 PL07-39c

One of the most detailed cores available comes from the Carriaco Basin near the Orinoco delta, core PL07-39c. The core itself shows unique bands of different reflectivity which provide an extremely detailed time log. It is possible to link this data to variations to other previously measured climate archives, like a CO_2 ice core record. This has been done in detail by *Lea et al*. [2003] and is not part of this thesis. The data obtained from the core PL07-39c, e.g. the Mg/Ca record of *G. ruber*, can be compared with the collected Calcium isotope record from the Sonne core SO 164-03-4. The remarkable results are presented in figure 6.1.1.

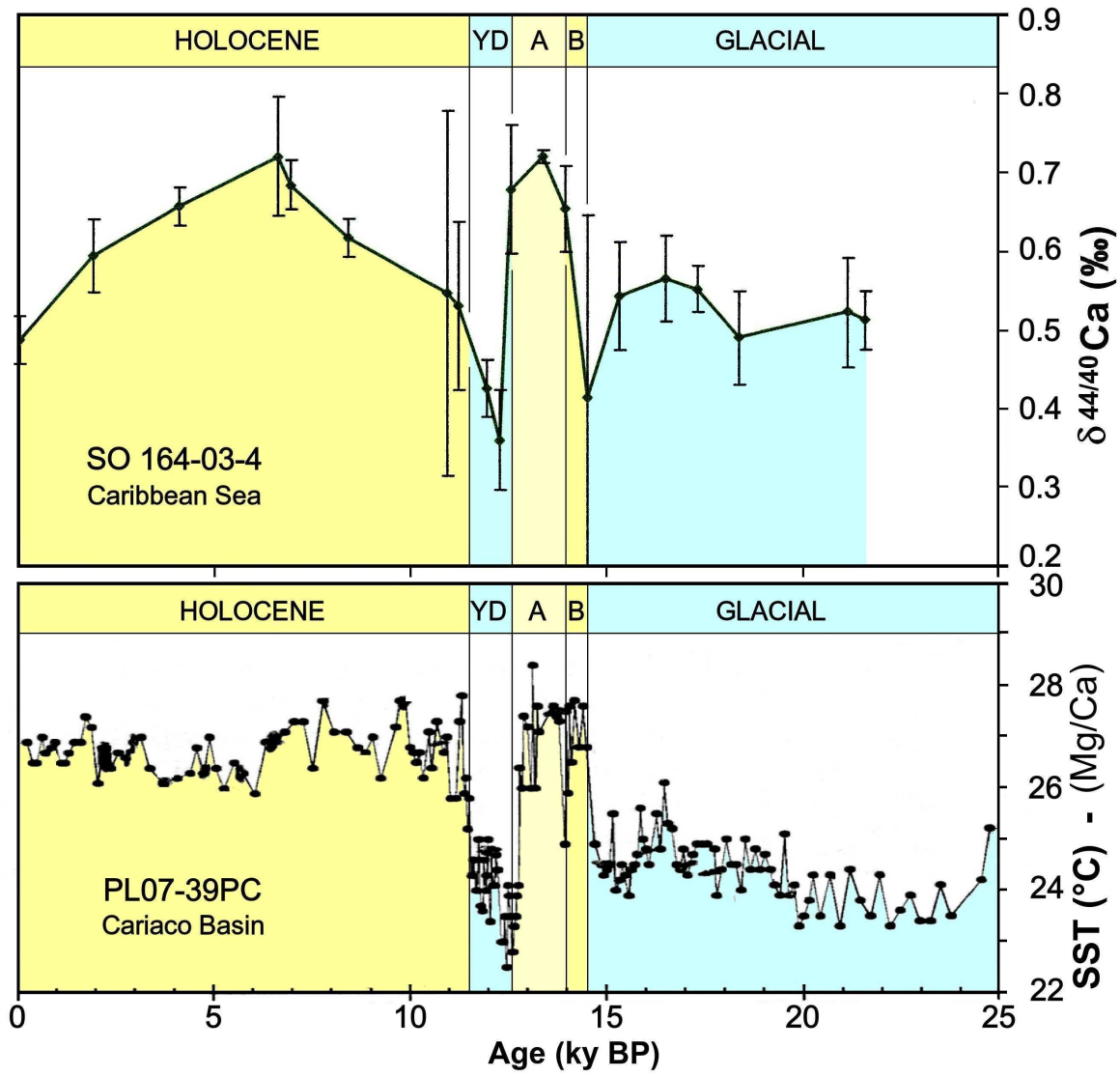

Figure 6.1.1: Comparison of the Mg/Ca SST (see *Lea et al.,* 2003) of core PL07-39c and the Calcium isotope record from the Sonne core SO 164-03-4. (B - Bølling, A - Allerød, YD - Younger Dryas).

The two proxies show very similar signal patterns, with the exception of the Holocene maxima which the Calcium isotope values seem to contain.

A selection of $\Delta\delta^{18}O_{ivf\text{-}sw}$ values have been generated for this core site employing the technique described in section 2. Since no $\delta^{44/40}Ca$ temperature values exist for this site several of the above shown Mg/Ca ratios for *G. ruber* were converted into their corresponding temperature values. With these generated temperatures and the $\delta^{18}O$ values a set of $\delta^{18}O_{sw}$ was generated. After the correction for the changes in the global ice volume the $\Delta\delta^{18}O_{ivfsw}$ were obtained. A short but incomplete overview for the last 20.000 years is presented in figure 6.1.2.

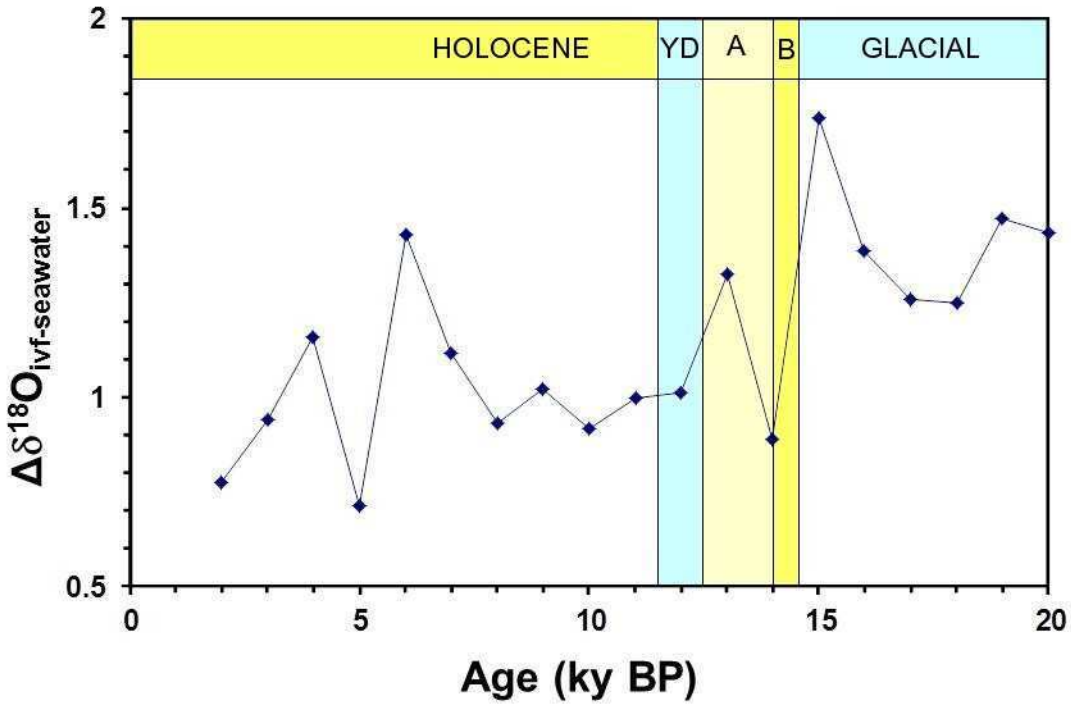

Figure 6.1.2:$\Delta\delta^{18}O_{ivf\text{-}sw}$ calculated from data available from the core PL07-39c.
(B - Bølling, A - Allerød, YD - Younger Dryas).

The above figure shows the variations of the $\Delta\delta^{18}O_{ivfsw}$ values in the Carriaco Basin for a few samples. There are major variations visible. Our focus will be the time frame of the glacial to interglacial Transition. The data material for the Holocene time period is not dense enough to allow for significant conclusions.

The variations during the Transition are an indication for changes in the evaporation to precipitation ratio, thus resulting SSS shifts. The maximum of the signal is reached at about 15.000 years BP during the onset of the B.A.. This is in agreement with the results from the core SO 164-03-4 (see section 5.1 for more detail) which show a major increase in the $\Delta\delta^{18}O_{ivfsw}$ values with the onset of the B.A.. The timing of this increase is the same in both of these cores. This is an indication for the fact, that similar environmental conditions were present at the two sites. The conclusion is that a possible shift of the ITCZ occurred in the Carricao Basin at the onset of the B.A., too. It could even be possible that the ITCZ was exactly positioned between these two locations thus the similarities in the signals even though there are great differences in the geographical locations.

6.2 Comparison with ODP 999

The ODP core 999 was taken in the southern part of the Caribbean Basin near the coast of Panama (see *Gusonne et al*., [2004]). It comes from a very similar climatic environment as the Sonne core 163-03-4 which was covered in chapter 5. The major difference is that this core is not positioned in the direct path of the Gulf Stream and today lies closer to the ITCZ than the Sonne core.

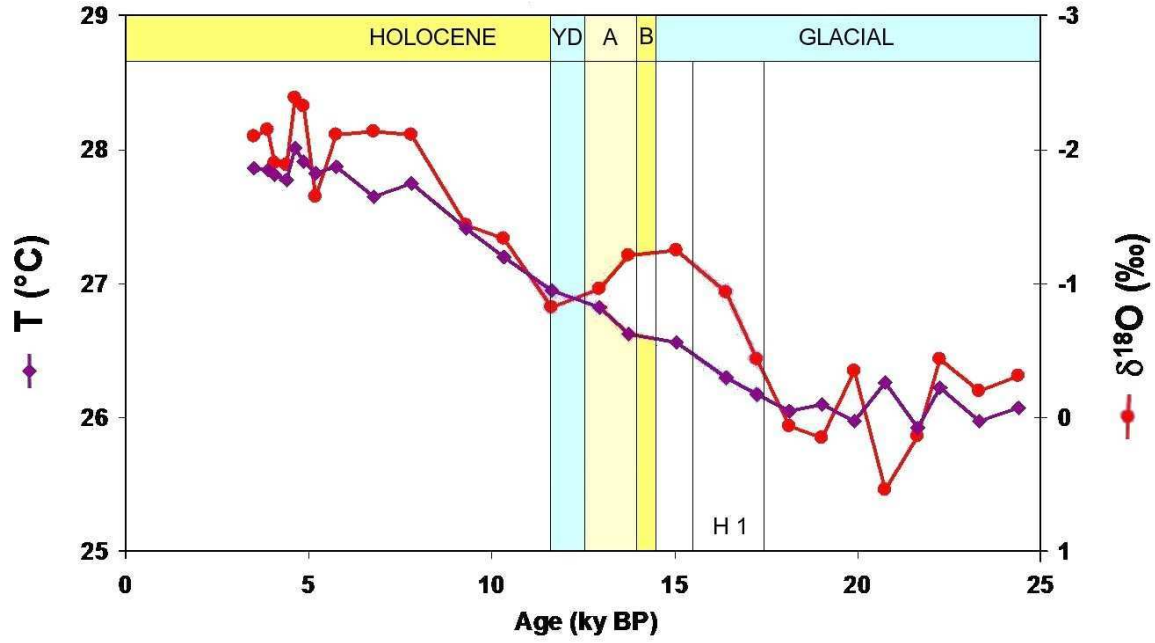

Figure 6.2.1: Mg/Ca generated temperatures (red) from *G. ruber* and their corresponding $\delta^{18}O$ values (purple) for the ODP core 999. The time window covered is the last 25.000 years, the glacial to interglacial Transition. (B - Bølling, A - Allerød, YD - Younger Dryas).

The most interesting fact about the results from the ODP 999 core for the last 25.000 years is that the $\delta^{18}O$ ratios continuously decrease from the LGM to the Holocene. On the other hand the Mg/Ca ratios show a different pattern with two areas of major increases in generated temperatures at about 15.000 and 8.000 years. The $\delta^{18}O$ ratios do not show the same signal pattern at these specific points in time.

Employing the method presented in section 2 a set of $\Delta\delta^{18}O_{ivf\text{-}sw}$ values were calculated. Since no $\delta^{44/40}Ca$ ratios were available the Mg/Ca generated temperatures were employed as the basis of the calculation in order to provide a simple estimation of the variations in the evaporation to precipitation ratio. The $\Delta\delta^{18}O_{ivf\text{-}sw}$ values are of interest because the result can be compared to the results generated from the Sonne core SO 164-03-4 from the Central Caribbean Sea. This

will enable to check for any major variations and fluxes in ocean parameters in the southern Caribbean Sea since this would most likely effect both cores equally.

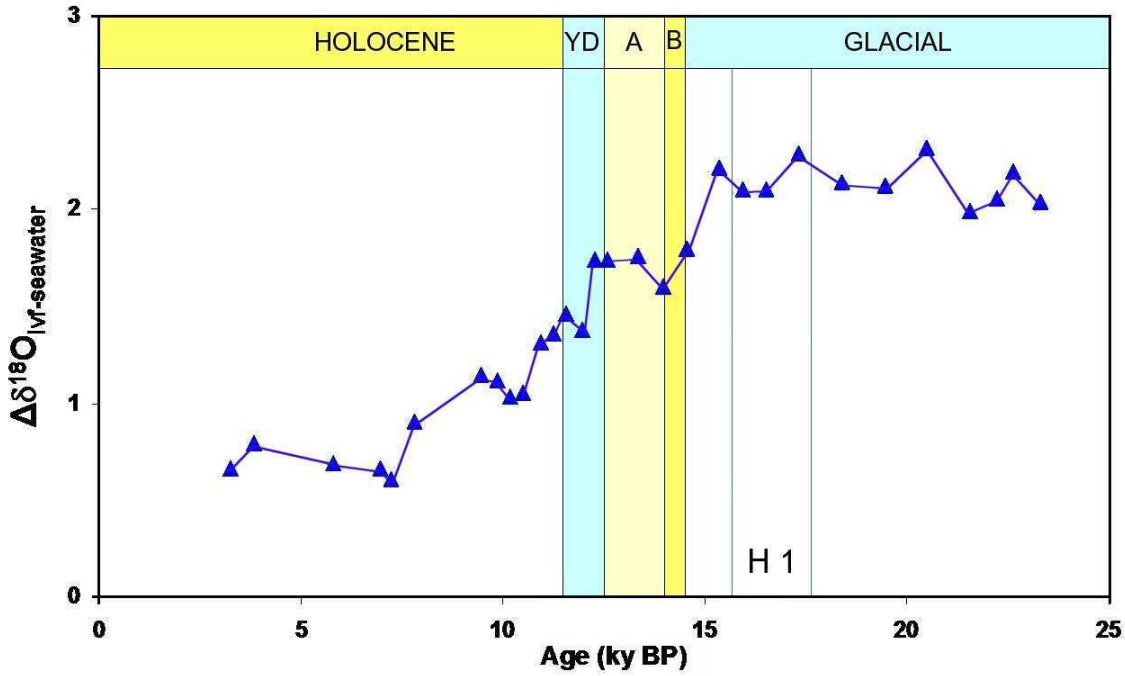

Figure 6.2.2: $\Delta\delta^{18}O_{ivf\text{-}sw}$ values employed with Mg/Ca generated temperatures and their corresponding $\delta^{18}O$ values from *G. ruber* for the ODP core 999.. The time window covered is the last 25.000 years, the glacial to interglacial transition. (B - Bølling, A - Allerød, YD - Younger Dryas).

The most obvious result from $\Delta\delta^{18}O_{ivf\text{-}sw}$ calculations is the fact that there are no short term changes in the evaporation to precipitation ratio. There is a gradual decrease of the ratios during the 15.000 to 9.000 year BP mark. The data is different to the $\delta^{44/40}Ca$ generated $\Delta\delta^{18}O_{ivf\text{-}sw}$ from the SO 164-03-4 core. This is mainly due to the fact, that during the transition from the LGM to the Holocene the Ca isotope ratios react differently to the Mg/Ca ratios. In order to compensate for this; the $\Delta\delta^{18}O_{ivf\text{-}sw}$ for the Sonne core were also calculated employing the Mg/Ca generated temperatures. The results are presented in figure 6.2.3.

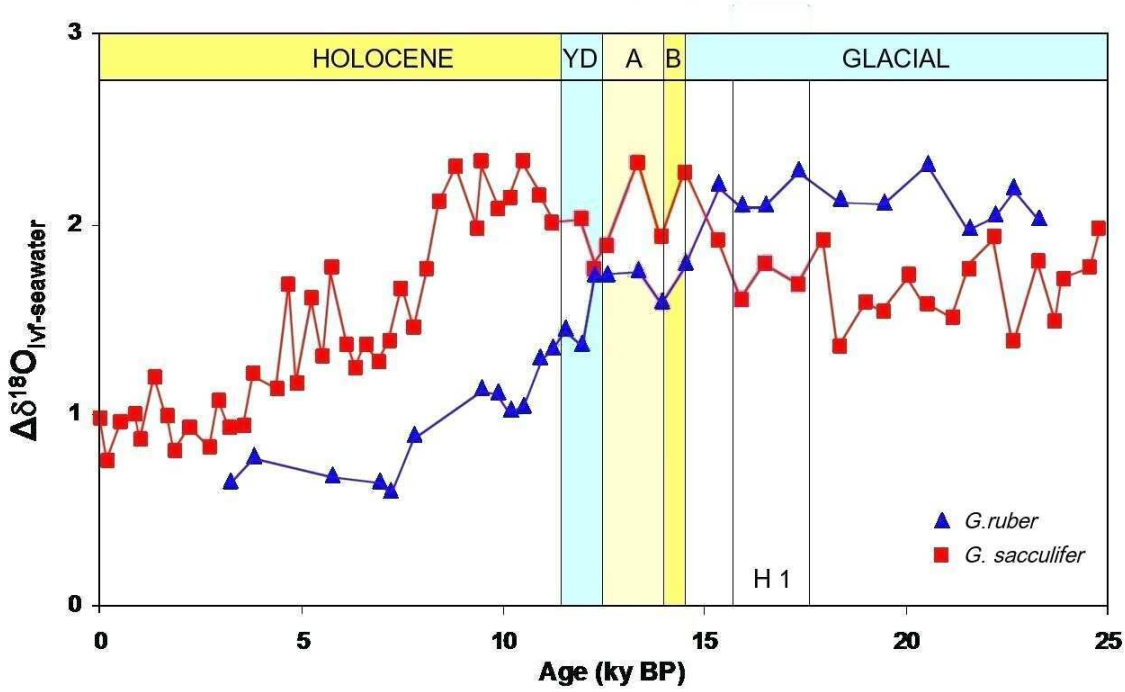

Figure 6.2.3: $\Delta\delta^{18}O_{ivf\text{-}sw}$ values employed with Mg/Ca generated temperatures and their corresponding $\delta^{18}O$ values from *G.ruber* (blue) for ODP core 999 and from *G.sacculifer* (red) from Sonne core SO 164-03-4. The time window covered is the last 25.000 years, the glacial to interglacial transition. (B - Bølling, A - Allerød, YD - Younger Dryas).

The obvious differences between these two differently generated sets of values are in the onset of the main signal variations. The Central Caribbean Sea seems to follow a very different variation in the changes of the evaporation to precipitation changes. This is even obvious if the Calcium isotope generated $\Delta\delta^{18}O_{ivf\text{-}sw}$ values are considered which are not known to be influenced by changes in SSS.

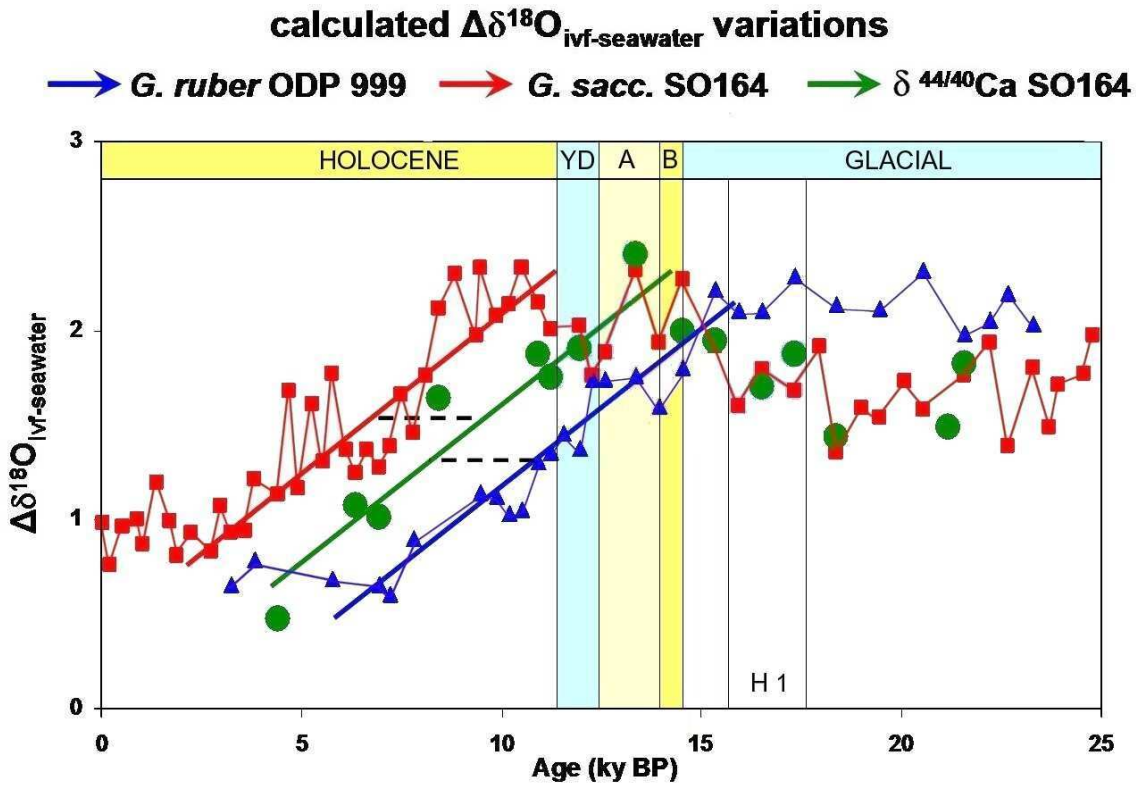

Figure 6.2.4: $\Delta\delta^{18}O_{ivf\text{-}sw}$ values employed with Mg/Ca generated temperatures and their corresponding $\delta^{18}O$ values from *G.ruber* (blue) for ODP core 999 and from *G.sacculifer* (red) from Sonne core SO 164-03-4. In green the values for *G.sacculifer* from Sonne core SO 164-03-4 were calculated with the Calcium isotope data from section 5.1. The time window covered is the last 25.000 years, the glacial to interglacial transition and the main signal variations are presented with the coloured lines. (B - Bølling, A - Allerød, YD - Younger Dryas).

The most significant result is the fact that the timing of the main signal variation not only depends on the core location but also on the type of proxy measured. If the Mg/Ca generated temperature values are employed as the basis of the calculations the overall signal pattern is different from the Calcium isotope results (see chapter 5.1 for more detail). No major increase in the $\Delta\delta^{18}O_{ivf\text{-}sw}$ values during the Bølling / Allerød is observed with this proxy. Especially at core site 999 an event like this is not observed.

The Mg/Ca generated $\Delta\delta^{18}O_{ivf\text{-}sw}$ values for site SO 164-03-4 show an increase during the transition phase and a decrease in the Younger Dryas but on the other hand a further maximum during the onset of the Holocene. An exact reason for this behaviour is not known and it is still under discussion why the different proxies show time differentiated Terminations in their signal variations. The most likely explanation

for this discrepancy is the influence of the ocean salinity on the Mg/Ca ratio in the examined foraminifera. This context is still not fully understood for most species of foraminifera and the results from the comparison of the different proxies underlines the sensitivity of SSS variations on planktonic foraminifera.

7 Conclusions

The main goal of this thesis was to confirm the existence of a phase shift in tropical oceans, like the Caribbean Sea where it had previously not been observed, between the Mg/Ca and $\delta^{18}O$ ratios at the transition from the last glacial to interglacial and to check for the extent of this phenomenon in other regions further distant from the equator. This is of importance since it will enable a more detailed assumption of the origin of the phase shift between the Termination points of the individual Mg/Ca and $\delta^{18}O$ ratios of a single species of planktonic foraminifera and help answer the question as to why this phenomenon has not been observed elsewhere.

The main area of interest of our study was the Central Caribbean Sea. A direct comparison of the $\delta^{18}O$ values and the Mg/Ca ratios from the core location SO 164-03-4 show that they run very stable during the time window from 25k to 18k BP during the LGM, no major signal fluctuations are observed. There do not seem to be major environmental changes, like jumps in SST or SSS prior to the Transition.
During the Holocene the $\delta^{18}O$ values and the Mg/Ca ratios again show similar signal patterns. This is again an indication for stable conditions in the Central Caribbean Sea during this time frame.
On the other hand, we note that the two proxies do not run in phase during the Transition from the glacial to interglacial. In this period of time the spatial difference in onset the main signal variations between the $\delta^{18}O$ values and the Mg/Ca ratios is about 3.500 years. This variation is the previously discussed phase shift; which is also present at our core site in the tropical Central Caribbean Sea. The absence of the phase shift at other non-equatorial sites, like ODP 1058c on the Blake Ridge (see section 5.3), is an indication that the unique conditions at low latitudes are responsible for the formation of a phase shift.
In order to decipher this effect, we measured a number of $\delta^{44/40}Ca$ ratios over the Transition period at core site SO 164-03-4 in the Central Caribbean Sea. A strong correlation between the Mg/Ca ratios and the $\delta^{44/40}Ca$ ratios during the LGM is evident. The three proxies show very similar signal patterns. On the other hand after the Bølling / Allerød period the $\delta^{44/40}Ca$ ratios seem to follow more the signal pattern of the $\delta^{18}O$ values. The exact reason for this and the fact that the absolute temperatures between the Mg/Ca ratios and $\delta^{44/40}Ca$ ratios differ in the Holocene is

unclear. This is probably an influence of varying SSS. In order to underline this hypothesis a variety of $\Delta\delta^{18}O_{ivf\text{-}seawater}$ values were calculated which can be directly interpreted as variations in the evaporation to precipitation ratio at the core site. During the LGM we have stable higher than present day $\Delta\delta^{18}O_{ivf\text{-}seawater}$ values. This is expected since a large amount of fresh water was stored in the continental ice sheets. The overall ocean salinity was thus higher at that time than today.
With the onset of the Bølling / Allerød our foraminifera records indicate that the environmental conditions drastically changed. Furthermore, our calculations of $\Delta\delta^{18}O_{ivf\text{-}seawater}$ values, employing the $\delta^{44/40}Ca$ generated temperatures, indicate an additional increase in the SSS during the transition. This is most likely caused by a large increase in SST at the core site.
With the onset of the interglacial the overall SSS gradually sinks, deduced from the declining $\Delta\delta^{18}O$ values. This is of course caused by continental melt water input into the world oceans and variations in SST. These variations in ocean parameters influence the $\delta^{18}O$ signal in foraminifera. The temperature component slowly gains the upper hand again as the declining salinity loses its dominant position and the $\Delta\delta^{18}O$ values rapidly decline until they reach stable values during the mid Holocene. Our conclusion is that the phase shift between the $\delta^{18}O$ values and the Mg/Ca ratios in planktonic foraminifera is caused by rapid variations of the SSS.
The question that remains to be answered is the origin of these short term salinity variations in tropical ocean environments. The main weather phenomenon in this region is the presence of the ITCZ. Its position relative to the core site has a major influence on the evaporation to precipitation ratio in this region. The further away the ITCZ is positioned the smaller the $\Delta\delta^{18}O_{ivf\text{-}seawater}$ values should be due to the diminishing evaporation of the sea water. With this in mind it should be possible to track movement of the ITCZ with the help of the $\Delta\delta^{18}O_{ivf\text{-}seawater}$ values.

Following this approach the spike in the $\Delta\delta^{18}O_{ivf\text{-}seawater}$ values at around 14.000 years BP could have been caused by the ITCZ which may have been positioned further north or south than it is today. It may even have even been positioned very close to or even directly above the site of the core site SO 164-03-4 in summer, thus causing this strong increase in the $\Delta\delta^{18}O_{ivf\text{-}seawater}$ values. A different explanation could be, that the size of the ITCZ system, meaning the expansion between the north and south borders, as a whole was much larger than today. Movments of the ITCZ in

past are a know occurance and have been reported in the past (e.g. *Haug et al.* 2001).
This is a possible explanation for the results found in this study. Our conclusion is that the phase shift between the Mg/Ca ratios and the $\delta^{18}O$ values during the Termination 1 is actually caused by a strong local variation in the SSS. This increased salinity is responsible for compensating the temperature and ice volume effects on the $\delta^{18}O$ signals, thus keeping the signal stable for a longer period of time and creating the phase shift relative to other proxies, like Mg/Ca.
We see no evidence that the tropical ocean is a trigger for global climate changes. Our observations do not challenge the role of the North Atlantic as the pacemaker of glacial/interglacial transitions. The warming of the Caribbean coincides with the warming in the North Atlantic and thus there is no indication of a regional rise in temperature.

The results for the ODP core 1058c on the Blake Ridge do not indicate the presence of a phase shift between the $\delta^{18}O$ and Mg/Ca ratios at this latitude. This underlines our hypothesis that the phase shift is limited to the tropics and the presence of the ITCZ. The ITCZ does not venture this far north and no abrupt climate changes are indicated by our results. The measured proxies show very gradual long term changes in ocean parameters at this location. The most interesting observations are the large fluctuations in both the Mg/Ca and $\delta^{18}O$ ratios prior to the onset of the Transition from the glacial to interglacial climate. These short term variations are a possible indication for an instable climate at the end of the LGM. Further detailed investigations are necessary to verify this assumption.

The measured results from high Northern latitudes (core MSM 5/5-712-2 – Arctic Sea) are also of interest. First of all, the absence of the phase shift between the $\delta^{18}O$ and Mg/Ca ratios is obvious. There are no major variations in the SSS observed which do not coincide with similar shifts in SST. The main problem is that the applied proxy, *N. pachyderma,* does not record strong decreases in SSS since this species of foraminifera will leave the surface ocean region and migrate to deeper more saline water masses. This behaviour has previously been recorded by *R.Kozdon et al.* [2009] and our findings underline this. The large inputs of melt water which has a

lower density and salinity than normal ocean water in the North Atlantic float on top of the original top water masses which then of course do not reflect SSS or SST anymore. As these two water bodies slowly intermix the foraminifera begin to travel to deeper more saline water in order to survive. The $\delta^{18}O$ signals indicate a decrease of 1.5 to 2 ‰ but the influx of a large amount of fresh water would most likely represent a drop of 4 to 5 ‰, maybe even more in the vicinity of large land based glaciers. Our proxy archive simply cannot reflect these drastic changes in SSS because *N. pachyderma* is unable to survive in such an environment. In order to observe the true extent of melt water influxes to the surface ocean a different proxy is necessary.

A multi proxy approach can help decipher the reactions of individual proxies to changes in ocean parameters and thus enable a better interpretation of the obtained data.

The main conclusion of this thesis are that the phase shift between the Termination points of Mg/Ca and $\delta^{18}O$ ratios in planktonic foraminifera in tropical ocean environments is caused by coinciding variations in ocean salinity and temperature at the core site. This phenomenon is restricted to areas close to the ITCZ and is most likely influenced by variations in its position. Future investigations in the tropics of various paleo climate proxies could help to decipher this interesting phenomenon and broaden our understanding of the transition from a glacial to interglacial period.

References

Anand P., Elderfield H., and M.H. Conte (2003)
Calibration of Mg/Ca thermometry in planktonic foraminifera from a sediment trap time series.
Paleoceanography **18**(2), 1050, doi:10.1029/2002PA000846.

Barry R. G.; Chorley R. J. (1992).
Atmosphere, weather, and climate.
London: *Routledge*. ISBN 9780415077606. OCLC 249331900

Bé A.W.H. (1977)
An ecological, zoogeographic and taxonomic review of recent planktonic foraminifera. *Oceanic Micropaleontology*, vol. **1**,edited by A.T.S. Ramsay, pp. 1–100, Elsevier, New York

Birck, J. L. (1986)
Precision K-Rb-Sr isotopic analysis: Application to Rb-Sr chronology.
Chem. Geol. **56**, 73–83

Bijma J., Hemleben C., Wellnitz K. (1994)
Population dynamics of the planktic foraminifer Globigerinoides sacculifer (Brady) from the central Red Sea.
Deep Sea Res., Part **I**, 41(3), 485–510

Black D. E., Peterson L. C, Overpeck J. T., Kaplan A., Evans M. N., Kashgarian M. (1999)
Eight Centuries of North Atlantic Ocean atmosphere variability
Science **286**, 1709-1713

Blanz T., Emeis K.-C., and Siegel H. (2005)
Controls on alkenone unsaturation ratios along the salinity gradient between the open ocean and the Baltic Sea.
Geochimica et Cosmochimica Acta **69**(14): 3589-3600.

Broecker W. and Henderson G. (1998)
The sequence of events surrounding Termination II and their implications for the cause of glacial-interglacial CO2 changes.
Paleoceanography **13**(4), 352-364.

Brown S. J., and Elderfield H. (1996)
Variations in Mg/Ca and Sr/Ca ratios of planktonic foraminifera caused by postdepositional dissolution: Evidence of shallow Mg-dependent dissolution.
Paleoceanography **11**, 543–551

Craig, H. & Gordon, L. I. (1965)
Deuterium and oxygen 18 variations in the ocean and the marine atmosphere.
Stable Isotopes in Oceanographic Studies and Paleotemperatures (ed. E. Tongiorgi), 9–130, Laboratorio di Geologia Nucleare, Pisa, Italy.

Conte M. H., Sicre A., Rühlemann C., Weber J.C. Schulte S., Schulz-Bull D. and Blanz T. (2006)
Global temperature calibration of the alkenone unsaturation index (UK´37) in surface waters and comparison with surface sediments.
Geochemistry, Geophysics, Geosystems **7**(2), doi:10.1029/2005GC001054: 1-22.

Dekens P.S., Lea D.W., Pak D.K. and Spero H.J. (2002)
Core top calibration of Mg/Ca in tropical foraminifera: Refining paleotemperature estimation.
Geochemistry, Geophysics, Geosystems **3**(4), 10.1029/2001GC000200.

deMenocal P., Ortiz J., Guilderson T., and Sarnthein M. (2000)
Coherent High- and Low-Latitude Climate Variability During the Holocene Warm Period.
Science **288**, 2198-2202.

Deuser W.G. (1987)
Seasonal variations in isotopic composition and deep-water fluxes of the tests of perennially abundant planktonic foraminifera of the Sargasso Sea: Results from sediment trap collections and their paleoceanographic significance.
J. Foraminiferal Res. **17**, 14–27

Elderfield H., and Ganssen G. (2000)
Past temperature and ^{18}O of surface ocean waters inferred from foraminiferal Mg/Ca ratios.
Nature ***405***, 442-445.

Epstein S., Buchsbaum R., Lowenstamm H.A., and Urey H.C. (1953)
Revised carbonate-water isotopic temperature scale.
Geol. Soc. Am. Bull. **64**, 1315-1325.

Erez J. (2003)
The source of ions for biomineralization in foraminifera and their implications for paleoceanographic proxies.
Reviews in Mineralogy and Geochemistry **54**, 115-149.

Fairbanks R.G., Sverdlove M., Free R., Wiebe P.H. and Bé A.W.H. (1982)
Vertical distribution and isotopic fractionation of living planktonic foraminifera from the Panama Basin.
Nature **298**, 841–844.

Gussone N., Eisenhauer A., Heuser A., Dietzel M., Bock B., Böhm F., Spero H., Lea D. W., Bijma J., and Nägler T. F. (2003)
Model for Kinetic Effects on Calcium Isotope Fractionation ($\delta^{44}Ca$) in Inorganic Aragonite and Cultured Planktonic Foraminifera.
Geochim Cosmochim Acta **67**(7), 1375-1382.

Gussone N., Eisenhauer A., Tiedemann R., Haug G.H., Heuser A., Bock, B., Nägler, Th.F. and Müller A. (2004)
$\delta^{44}Ca$, $\delta^{18}O$ and Mg/Ca Reveal Caribbean Sea Surface Temperature and Salinity Fluctuations During the Pliocene Closure of the Central-American Gateway.
Earth and Planetary Science Letters **227**, 201-214.

Haug G. H., Hughen K. A., Sigman D. M., Peterson L. C. & Röhl U. (2001)
Southward migration of the Intertropical convergence Zone through the Holocene.
Science **293**, 1304-1308

Hastings D.W, Russell A.D., and
Emerson S.R. (1998)
Foraminiferal magnesium in *Globigerinoides sacculifer* as a paleotemperature proxy.
Paleoceanography **13**(2), 161-169.

Heuser A., Eisenhauer A., Gussone N., Bock B., Hansen B. T., and Nägler T. F. (2002)
Measurement of Calcium Isotopes ($\delta^{44}Ca$) Using a Multicollector TIMS Technique.
International Journal of Mass Spectrometry **220**, 385-397.

Heuser A., Eisenhauer A., Böhm F., Wallmann K., Gussone N., Pearson P., Nägler T. F. and Dullo W-C. (2005)
Calcium isotope ($\delta^{44/40}Ca$) variations of Neogene planktonic foraminifera
Paleoceanography **20**, 2013, doi:10.1029/2004PA001048.

Hippler D., Gussone N., Darling K., Eisenhauer A., and Nägler T. (2002)
$\delta^{44}Ca$ in *N. pachyderma* (left): a new SST-proxy in polar regions.
Geochim. Cosmochim. Acta Spec. Suppl. **66** (15A), A331.

Hippler D., Schmitt A.-D., Gussone N., Heuser A., Stille P., Eisenhauer A., Nägler Th.F., (2003)
Ca isotopic composition of various standards and seawater.
Geostandards Newsletter **27**, 13–19.

Hippler D., Eisenhauer A. and Nägler Th. F. (2006)
Tropical Atlantic SST history inferred from Ca isotope thermometry over the last 140 ka
Geochim Cosmochim Acta, **70**, 90-100.

Hughen K. A., Peterson L. C, Overpeck J. T., Trumbore S. E. (1996)
Rapid climate changes in the tropical Atlantic region during the last deglaciation.
Nature **380**, 51-54

Jones G. A., and Keigwin L. D. (1988)
Evidence from Fram Strait (78°) for early deglaciat ion.
Nature **336**, 56-59.

Keigwin L. (1998)
Glacial-age hydrography of the far northwest Pacific.
Paleoceanography **13** (4), 323-339.

Kiefer T., Sarnthein M., Erlenkeuser H., Grootes P. M., and Roberts A. P. (2001)
North Pacific response to millennial-scale changes in ocean circulation over the last 60 kyr.
Paleoceanography **16**(2), 179-189.

Kısakürek B., Eisenhauer A., Böhm F, Garbe-Schönberg D, Erez J. (2008)
Controls on shell Mg/Ca and Sr/Ca in cultured planktonic foraminiferan, Globigerinoides ruber (white).
Earth and Planetary Science Letters, **273**, 260–269

Kroon D., and Darling K. (1995)
Size and upwelling control of the stable isotope composition of Neogloboquadrina dutertrei (d'Orbigny), Globigerinoides ruber (d'Orbigny), and Globigerina bulloides (d'Orbigny): Examples from the Panama Basin and the Arabian Sea.
J. Foraminiferal Res. **25**, 39–52

Kozdon R., Eisenhauer A., Weinelt M., Hippler D., Meland M. (2006)
Paired Mg/Ca & $^{44/40}$Ca temperature estimates of N. pachyderma (sin.) in the Nordic Seas
Geophysical Research Abstracts, Vol. **8**, 08816, 2006

Kozdon R., Eisenhauer A., Weinelt M., Meland M.Y. and Nürnberg D. (2009)
Reassessing Mg/Ca temperature calibrations of *Neogloboquarina pacyderma* (sinistral) using paired $\delta^{44/40}$Ca and Mg/Ca measurements.
Geochem. Geophys. Geosys. **10** (2009) 10.1029/2008GC002169

Lea D. W., Mashiotta T. A., and Spero H. J. (1999)
Controls on magnesium and strontium uptake in planktonic foraminifera determined by live culturing.
Geochim. Cosmochim. Acta, 63, 2369-2379.

Lea D. W., Pak D. K., and Spero H. J. (2000)
Climate Impact of Late Quatternary Equatorial Pacific Sea Surface Temperature Variations.
Science **289**, 1719-1724.

Lea D. W., Pak D. K., Peterson L. C., Hughen K. A. (2003)
Synchroneity of Tropical and High-Latitude Atlantic Temperatures over the Last Glacial Termination
Science **301**, Number 5638, pp.1361-1364, 5

Lin H.-L., Peterson L. C, Overpeck J. T., Trumbore S. E. & Murray D. W. (1997)
Late Quaternary climate change from δ18O records of multiple species of planktonic foraminifera: High-resolution records from the anoxic Cariaco Basin, Venezuela.
Paleoceanography **12**, 415-427

Majoube M. (1971)
Fractionnement en oxygene 18 et en deuterium entre l'eau et sa vapeur.
J. Chim. Phys. **68**, 1423-1436

Mashiotta T.A., Lea D.W., and Spero H.J. (1999)
Glacial-interglacial changes in Subantarctic sea surface temperature and $\delta^{18}O$-water using foraminiferal Mg.
Earth Planet. Sci. Letters **170**, 417-432.

McCrea J.M. (1950)
On the isotopic chemistry of carbonates and a paleotemperature scale.
Jour. Chem. Phys., **18,** 849-857

Macdonald R.W., Paton D.W. and Carmack E.C. (1995)
The freshwater budget and underice spreading of Mackenzie River water in the Canadian Beaufort Sea based on salinity and $^{18}O/^{16}O$ measurements in water and ice.
JGR, **100**, 895919

McKenna V. S., and Prell W.L. (2004)
Calibration of the Mg/Ca of *Globorotalia truncatulinoides* (R) for the reconstruction of marine temperature gradients.
Paleoceanography **19**, PA2006, doi:10.1029/2000PA000604.

Müller P.J., Kirst G., Ruhland G., Storch I.V. and Rosell-Melé, A. (1998)
Calibration of the alkenone paleotemperature index UK′37 based on core-tops from the eastern South Atlantic and the global ocean (60°N-60°S).
Geochim. Cosmochim. Acta **62**, 1757-1772.

Nägler T., Eisenhauer A., Müller A., Hemleben C., and Kramers J. (2000)
The $\delta^{44}Ca$-isotopes: New Powerful Tool for Reconstruction of Past Sea Surface Temperatures.
Geochemistry, Geophysics, Geosystems **1**(2000GC000091).

Nürnberg D. (1995)
Magnesium in tests of *Neogloboquadrina pachyderma* sinistral from high northern and southern latitudes.
J. Foram. Res. **25/4**, 350-368.

Nürnberg D., Bijma J. & Hemleben C. (1996)
Assessing the reliability of magnesium in foraminiferal calcite as a proxy for water mass temperatures.
Geochim. Cosmochim. Acta **60/5**, 803-814.

Nürnberg D., Bijma J. & Hemleben C. (1996)
Erratum to "Assessing the reliability of magnesium in foraminiferal calcite as a proxy for water mass temperatures".
Geochim. Cosmochim. Acta **60/13**, 2483-2484.

Nürnberg D. (2000)
Taking the temperature of past ocean surfaces.
Science **289**, 1698-1699.

Nürnberg D., Müller, A. & Schneider R. (2000)
Paleo-sea surface temperature calculations in the equatorial east Atlantic from Mg/Ca ratios in planktic foraminifera – A comparison to sea surface temperature estimates from UK' 37, oxygen isotopes, and foraminiferal transfer function.
Paleoceanography **15** (1), 124-134.

Nürnberg D., Schönfeld J., Dullo W.-Chr., Rühlemann C. (2003)
RASTA Rapid climate changes in the western tropical Atlantic - Assessment of the biogenous and sedimentary record. R/V SONNE cruise report SO164
GEOMAR Report Bd. **109**, Kiel.

Nürnberg D., Groeneveld G. (2006)
Pleistocene variability of the Subtropical Convergence at East Tasman Plateau: Evidence from planktonic foraminiferal Mg/Ca (OPD Site 1172A).
Geochemistry, Geophysics, Geosystems **7** (4), doi:10.1029/2005GC000984.

Peterson L. C., Haug G.H. (2006).
Variability in the mean latitude of the Atlantic Intertropical Convergence Zone as recorded by riverine input of sediments to the Cariaco Basin (Venezuela).
Palaeogeography Palaeoclimatology Palaeoecology **234**(1):97-113

Petit J. R., Jouzel J., Raynaud D., Barkov N. I., Barnola J.-M., Basile I., Bender M., Chappellaz J., Davis M., Delaygue G., Delmotte M., Kotlyakov V. M., Legrand M., Lipenkov V. Y., Lorius C., Pépin L., Ritz C., Saltzman E., and Stievenard M. (1999)
Climate and atmospheric history of the past 420,000 years from the Vostok ice core, Antarctica.
Nature **399**, 429-436.

Prahl F.G. and Wakeham S.G. (1987)
Calibration of unsaturation patterns in long-chain ketone compositions for paleotemperature assessment.
Nature **330**, 367-369.

Prahl F.G., Muehlhausen L.A., and Zahnle D.I. (1988)
Further evaluation of long-chain alkenones as indicators of paleoceanographic conditions.
Geochim. Cosmochim. Acta **52**, 2303-2310.

Regenberg M., Nürnberg D., et al. (2006)
Assessing the effect of dissolution on planktonic foraminiferal Mg/Ca ratios: Evidence from Caribbean core tops.
Geochemistry, Geophysics, Geosystems **7** (7), doi:10.1029/2005GC001019.

Regenberg M., Steph S., Nürnberg D., Tiedemann R., Garbe-Schönberg D., (2009)
Calibrating Mg/Ca ratios of multiple planktonic foraminiferal species with $\delta^{18}O$-calcification temperatures: Paleothermometry for the upper water column.
Earth and Planetary Science Letters, **278**(3-4), 324-336

Rosenthal Y., Lohmann G.P., Lohmann K.C., and Sherrell R.M. (2000)
Incorporation and preservation of Mg in Globigerinoides sacculifer: Implications for reconstructing the temperature and $^{18}O/^{16}O$ of seawater.
Paleoceanography **15**(1), 135-145.

Rosenthal Y., and Lohmann G.P. (2002)
Accurate estimation of sea surface temperatures using dissolutioncorrected calibrations for Mg/Ca paleothermometry.
Paleoceanography, **17**(3), 1044, doi:10.1029/2001PA000749.

Rosell-Melé A., Weinelt M. S., Sarnthein M., Koc N., and Jansen E. (1998)
Variability of the Arctic front during the last climatic cycle: application of a novel molecular proxy.
Terra Nova **10** (2), 86-89.

Rosell-Melé A., Bard E., Emeis K.C., Schneider R., and Blanz T. (2001)
Precision of the current methods to measure the alkenone proxy UK'37 and absolute alkenone abundance in sediments: Results of an interlaboratory comparison study.
Geochemistry, Geophysics, Geosystems **2**, 2000 GC000141.

Russell W. A., Papanastassiou D.A., Tombrello T.A. (1978)
Ca isotope fractionation on the Earth and other solar materials.
Geochim Cosmochim Acta **42:** 1075-1090

Sarnthein M., Stattegger K., Dreger D., Erlenkeuser H., Grootes P., Haupt B. J., Jung S., Kiefer T., Kuhnt W., Pflaumann U., Schäfer-Neth C., Schulz H., Schulz M., Seidov D., Simstich J., Kreveld S. v., Vogelsang E., Völker A., and Weinelt M. (2000)
Fundamental Modes and Abrupt Changes in North Atlantic Circulation and Climate over the last 60 ky - Concepts, Reconstruction and Numerical Modeling. In *The Northern North Atlantic: A Changing Environment* (ed. P. Schäfer, W. Ritzrau, M. Schlüter, and J. Thiede), pp. 365-410. *Springer*

Sarnthein M. and Tiedemann R. (1990)
Younger Dryas-style cooling events at glacial Terminations I-VI: associated benthic $\delta^{13}C$ anomalies at ODP Site 658 constrain meltwater hypothesis.
Paleoceanography **5**, 1041-1055.

Schmidt G.A. (1999)
Forward modeling of carbonate proxy data from planktonic foraminifera using oxygen isotope tracers in a global ocean model.
Paleoceanography **14**(4), 482, 10.1029/1999PA900025.

Schmidt G.A., Shindell D.T., Harder S., (2004)
A note on the relationship between ice core methane concentrations and insolation.
Geophys. Res. Lett., **31**, L23206, doi:10.1029/2004GL021083

Schmuker, B., and Schiebel, R. (2002)
Planktic foraminifers and hydrography of the eastern and northern Caribbean Sea. Mar.
Micropaleontol. **428**, 387–403

Shackleton N.J. (1974)
Attainment of isotopic equilibrium between ocean water and the benthonic foraminifer genus Uvigerina: isotopic changes in the ocean during the last glacial.
In *Les methodes quantitative d'etude des variations du climate au cours du Pleistocene*, edited by L. Labeyrie, Cent. Nat. de la Rech. Sci. Colloq Int., **219**, 203-210.

Shackleton N. J., Hall, Michael A., Vincent E., (2000)
Phase relationships between millennial-scale events 64,000-24,000 years ago.
Paleoceanography, **15(6)**, 565-569, doi:10.1029/2000PA000513

Spero H. J.; Schmidt M. W.; Lea D. W.; Lavagnino L. (2009)
Evidence for a Southern Pattern of Deglacial Surface Warming in the Eastern Equatorial Pacific
American Geophysical Union, Fall Meeting **2009**, abstract #PP14C-06

Stidd C. K. (1967)
The use of eigenvektors for climatic estimates.
J. Appl. Meteor., **6**, 255-264

Stuiver M., Braziunas T. F., and Grootes P. M. (1997)
Is There Evidence for Solar Forcing of Climate in the GISP2 Oxygen Isotope Record?
Quaternary Research **48**, 259-266.

Thunell R. C., Tappa E., Pride C., Kincaid E. (1999)
Sea-surface temperature anomalies associated with the 1997– 1998 El
Nino recorded in the oxygen isotope composition of planktonic foraminifera
Geology **27**, 843– 846

Visser K., Thunell R., and Stott L. (2003)
Magnitude and timing of temperature change in the Indo-Pacific warm pool during Deglaciation.
Nature **421**, 152–155.

Voelker A. H. L., Sarnthein M., Grootes P. M., Erlenkeuser H., Laj C., Mazaud A., Nadeau M.-J., and Schleicher M. (1998)
Correlation of marine 14C ages from the Nordic Seas with the GISP2 isotope record: Implications for 14C calibration beyond 25 ka b.p. *Radiocarbon* **40**(1), 517-534.

Vogelsang E. (1990)
Paläo- Ozeanographie des Europäischen Nordmeeres an Hand stabiler Kohlenstoff- und Sauerstoffisotope.
Ber. SFB 313 Univ. Kiel **23**, 136 pp.

Waelbroeck C., Labeyrie L., Michel E., Duplessy J.C., McManus J.F., Lambeck K., Balbon E., and Labracherie M. (2002)
Sea-level and deep water temperature changes derived from benthic foraminifer isotopic records.
Quat. Sci. Rev. **21**, 295-305

Waniek J., Schulz-Bull D., Blanz T., Prien, R., Oschlies A., Müller T.J. (2005)
Interannual variability of deep water particle flux in relation to production and lateral sources in the northeast Atlantic.
Deep Sea Research I **52**, 33-50.

Zeebe R. E. and Wolf-Gladrow (2001)
CO_2 in Seawater: Equilibrium, Kinetics, Isotopes
ISBN-10 0444509461

Zhu P. and MacDougall J.D. (1998)
Calcium isotopes in the marine environment and the oceanic calcium cycle.
Geochim. Cosmochim. Acta, **62** (10), 1691-1698.

Appendix:

Section 1 SO 164-03-4 – Central Caribbean Sea

- $\delta^{18}0$ and $\delta^{13}C$ *C. wuellersdorfi*
- Data compilation for *G. ruber*
- Data compilation for *G. sacculifer*
- Ca isotope ratios and calculations

Section 2 ODP 1058c – Blake Ridge

- A brief look at the Alkenone UK´37 system
- Alkenone measurements
- Termination 2
- $\delta^{18}0$ and $\delta^{13}C$ *C. wuellersdorfi*
- Data compilation for *G. ruber*
- Data compilation for *G. truncatulinoides*
- Uk37 Data

Section 3 M/M 515-712-2 core – off the coast of Spitsbergen

- Data compilation

Section 4 Model & Results

- Data compilation of the modelled Mg/Ca and $\delta^{18}0$ ratios for chapter 2

Section 1 - SO 164-03-4 – Central Carribean Basin

Table 1.1:

A compilation of the $\delta^{18}O$ and $\delta^{13}C$ measurements of *C. wuellerstorfi* for the core SO164-03-4. The last column contains the percentage of the coarse fraction (>63µm, in weight%).

Table 1.2:

A compilation of the Mg/Ca and Sr/Ca measurements for *G. ruber*. Table 1.2a further contains the measurements of the trace elements and calculated temperatures from the Mg/Ca ratios following the calibration by *Lea et al.* [2000].

Table 1.3:

A compilation of the $\delta^{18}O$ and Mg/Ca measurements for *G.sacculifer.* The mperatures were calculated with the calibration by *Nürnberg et al.* [2000].

Table 1.4:

Contains the calculated $\Delta\delta^{18}O_{ivfsw}$ for *G. sacculifer* following the procedure descibed in chapter 2 (equation 3) using the Mg/Ca based temperatures and the $\delta^{18}O$ values as starting points. The sealevel variations were taken into accord employing the RSL variations by *Waelbroeck et al.* (equation 3+4).

$$\boldsymbol{\delta^{18}O_{seawater}}\,[‰] = \frac{\left[\mathbf{T_{Mg/Ca}}\,(°\mathbf{C}) - \mathbf{14.9}\right]}{\mathbf{4.8}} + (\boldsymbol{\delta^{18}O_{foram}}\,[‰] + \mathbf{0.27})$$

$$\boldsymbol{\Delta\delta^{18}O_{ivf-seawater}}\,[‰] = \boldsymbol{\delta^{18}O_{seawater}}\,[‰] - \boldsymbol{\delta^{18}O_{ice-volume}}\,[‰]$$

Table 1.5:

The measured $\delta^{44/40}Ca$ values and the $\delta^{44/40}Ca$ based temperatures, employing the calibration by Hipler et al., for *G. sacculifer* are presented. The wghted errors of each individual measurent are included aswell.

Table 1.6:

Contains the calculated $\Delta\delta^{18}O_{ivfsw}$ for *G. sacculifer* using the Ca isotope based temperatures following the same procedure as in Table 1.4.

Table 1.1: A compilation of $\delta^{18}O$ and $\delta^{13}C$ of *C. wuellerstorfi* (C.w.) for the core SO164-03-4

Depth [cm]	$\delta^{18}O_{korr}$ C.w. [‰]	Age [ka BP]	$\delta^{13}C_{korr}$ C.w. [‰]	>63µm [w.%]
2	2.390	0.04	1.013	41.239
3	2.319	0.21	0.779	
5	2.386	0.55	0.832	37.756
7	2.516	0.89	1.069	36.634
8	2.244	1.05	1.128	
10	2.399	1.39	1.018	39.073
12	2.339	1.73	0.777	42.396
13	2.453	1.90	1.080	
15	2.292	2.24	1.116	41.451
18	2.334	2.74	1.025	
19.5	2.224	3.00	1.060	36.901
21	2.384	3.25	1.001	38.630
23	2.353	3.59	1.101	
24.5	2.432	3.84	0.638	35.272
26	2.473	4.09	0.986	36.599
28	2.303	4.43	0.876	
29.5	2.412	4.69	0.881	33.576
31	2.501	4.94	1.107	29.221
33	2.405	5.28	1.103	
34.5	2.557	5.53	1.114	29.928
36	2.581	5.78	1.036	33.026
38	2.303	6.12	1.003	
39.5	2.602	6.37	1.020	31.810
41	2.714	6.63	0.981	36.337
43	2.581	6.97	1.012	
44.5	2.457	7.22	0.921	29.639
46	2.647	7.47	0.966	32.612
48	2.410	7.81	1.036	
49.5	2.582	8.12	0.978	25.452
51	2.535	8.43	0.930	40.672
53	3.161	8.85	0.980	
54.5		9.37		30.051
56	3.235	9.47	1.096	34.887
58	3.055	9.88	1.042	
59.5	3.420	10.20	1.032	27.312
61	3.107	10.51	0.837	27.500
63	3.092	10.92	0.721	
64.5	3.032	11.23	0.754	23.094
66	3.129	11.54	0.808	22.190
68	3.303	11.96	0.669	
69.5		12.27		15.628
71	2.972	12.58	0.628	20.044
73	2.967	13.37	0.849	
74.5	3.819	13.96	1.200	15.844
76	3.927	14.55	1.180	17.749
78		15.34		
79.5		15.93		14.622
81	3.604	16.52	1.024	19.121
83	4.127	17.31	1.260	
86	4.091	17.95	1.336	22.237
88	4.065	18.38	1.345	
91	3.922	19.02	1.322	18.745
93	4.125	19.44	1.274	
96	3.910	20.08	1.311	19.812
98	3.941	20.51	1.256	
101	3.844	21.15	1.366	19.244
103		21.58		
106		22.22		17.606

Depth [cm]	$\delta^{18}O_{korr}$ C.w. [‰]	Age [ka BP]	$\delta^{13}C_{korr}$ C.w. [‰]	>63µm [w.%]
108		22.65		
111		23.29		17.099
113		23.71		
114		23.93		22.035
116	3.682	24.57	1.310	16.601
118	3.773	24.78	1.282	
121	3.452	25.42	1.218	23.551
123	3.645	25.77	1.197	
126	3.630	26.29	1.220	19.009
128	3.733	26.63	1.367	
131	3.579	27.15	1.412	20.866
133	3.594	27.50	1.237	
136	3.609	28.02	1.133	25.626
138	3.705	28.36	1.280	
143	3.645	29.23	1.296	
146	3.744	29.75	1.348	24.181
148	3.622	30.09	1.283	
153	3.662	30.96	1.327	
156	3.760	31.48	1.352	32.242
158	3.729	31.83	1.334	
166	3.415	33.21	1.230	28.065
176	3.673	35.81	1.107	18.229
186	3.603	38.40	1.296	20.396
196	3.513	41.00	1.311	22.309
206	3.569	44.35	1.166	30.173
214	3.594	47.04	1.319	23.713
224	3.379	50.39	1.218	28.049
234	3.556	52.28	1.262	69.158

Depth [cm]	$\delta^{18}O_{korr}$ C.w. [‰]	Age [ka BP]	$\delta^{13}C_{korr}$ C.w. [‰]	>63µm [w.%]
244	3.318	54.16	1.171	26.233
254	3.275	56.05	0.676	22.870
264	3.406	59.11	1.067	22.878
274		62.16		10.885
284	3.689	65.22	1.153	13.294
294		67.22		10.858
304		69.23		7.401
314		71.23		14.673
324	3.038	73.24	1.048	11.454
329	2.955	74.24	1.070	9.168
334	3.242	75.24	1.064	10.308
344	3.013	77.25	1.019	29.779
354	2.949	79.25	1.146	18.001
364	2.939	80.32	0.718	19.856
374	2.489	81.40	0.831	42.096
384	3.040	82.47	1.006	46.517
394	2.861	83.55	0.606	45.297
404	2.739	84.62	0.636	44.406
414	3.197	85.70	1.187	45.622
435	3.191	87.95	1.002	47.968
445	3.314	89.03	0.876	45.332
455	3.592	90.10	1.114	43.954
465		90.63		61.389
475	2.746	91.17	0.843	8.956
485	3.190	91.70	0.880	35.749
495	3.842	92.23	1.064	20.263
505		92.76		16.870
515	3.320	93.30	0.879	16.878

Table 1.2a: A compilation of Mg/Ca measurements for *G. ruber* for the core SO 164-03-4

Depth [cm]	Age [ka BP]	Meas. Ca [mg/L]	Mg/Ca (±0.04) [mmol/mol]	$T_{Mg/Ca}$ [℃]	Sr/Ca (±0.04) [mmol/mol]	Fe/Ca [mmol/mol]	Al/Ca [mmol/mol]	Mn/Ca [mmol/mol]	Fe/Mg [mmol/mol]
2	0.04	20.3	5.47	29.64	1.47	0.284	0.399	0.071	0.051
3	0.21	11.1	5.09	28.83	1.37	0.122	0.098	0.015	0.022
5	0.55	34.3	4.90	28.41	1.51	0.047	0.135	0.011	0.009
7	0.89	21.5	5.34	29.37	1.47	0.051	0.004	0.001	0.009
8	1.05	30.1	4.90	28.41	1.49	0.015	0.105	0.008	0.003
10	1.39	46.3	5.59	29.87	1.56	0.009	0.075	0.015	0.002
12	1.73	46.6	5.26	29.20	1.56	0.053	0.238	0.022	0.010
13	1.90	40.3	5.49	29.68	1.52	0.226	0.168	0.018	0.041
15	2.24	27.3	5.32	29.32	1.52	0.334	0.125	0.023	0.062
18	2.74	35.9	5.16	28.98	1.49	0.169	0.204	0.095	0.032
19.5	3.00	26.4	5.71	30.12	1.52	0.049	0.221	0.040	0.009
21	3.25	29.5	5.52	29.73	1.54	0.185	0.743	0.085	0.033
23	3.59	21.4	5.29	29.25	1.47	0.217	0.097	0.002	0.041
24.5	3.84	15.9	5.46	29.62	1.43	0.160	0.125	0.068	0.029
26	4.09	30.2	5.80	30.28	1.50	0.015	0.015	0.010	0.003
28	4.43	13.4	5.62	29.93	1.40	0.011	0.094	0.044	0.002
29.5	4.69	38.3	4.97	28.57	1.54	0.243	0.092	0.083	0.048
31	4.94	35.9	5.37	29.44	1.52	0.040	0.143	0.558	0.007
33	5.28	23.3	5.70	30.10	1.49	0.080	0.129	0.097	0.014
34.5	5.53	32.8	5.69	30.08	1.54	0.011	0.027	0.026	0.002
36	5.78	27.3	5.75	30.19	1.54	0.029	0.177	0.105	0.005
38	6.12	23.9	5.54	29.77	1.50	0.210	0.072	0.026	0.038
39.5	6.37	21.1	5.80	30.29	1.50	0.003	0.138	0.031	0.000
41	6.63	38.5	5.88	30.43	1.57	0.523	0.499	0.077	0.095
43	6.97	41.7	5.94	30.54	1.56	0.125	0.768	0.105	0.021
44.5	7.22	34.8	5.47	29.63	1.55	0.002	0.071	0.223	0.000
46	7.47	57.3	5.56	29.82	1.57	0.059	0.045	0.022	0.010
48	7.81	59.5	5.00	28.64	1.54	0.028	0.036	0.238	0.006

Depth [cm]	Age [ka BP]	Meas. Ca [mg/L]	Mg/Ca (±0.04) [mmol/mol]	$T_{Mg/Ca}$ [℃]	Sr/Ca (±0.04) [mmol/mol]	Fe/Ca [mmol/mol]	Al/Ca [mmol/mol]	Mn/Ca [mmol/mol]	Fe/Mg [mmol/mol]
49.5	8.12	33.6	5.03	28.69	1.53	0.024	0.047	0.042	0.005
51	8.43	32.7	5.44	29.58	1.51	0.094	0.144	0.126	0.017
53	8.85	42.2	5.26	29.20	1.49	0.005	0.012	0.120	0.001
54.5	9.37	33.1	5.06	28.76	1.51	0.030	0.047	0.073	0.006
56	9.47	66.9	5.56	29.81	1.53	0.079	0.102	0.095	0.014
58	9.88	40.6	5.43	29.54	1.48	0.094	0.103	0.122	0.017
59.5	10.20	16.6	4.95	28.53	1.39	0.075	0.258	0.189	0.014
61	10.51	44.3	5.36	29.41	1.49	0.101	0.148	0.215	0.019
63	10.92	31.8	5.25	29.18	1.48	0.054	0.043	1.188	0.010
64.5	11.23	27.9	5.11	28.88	1.48	0.152	0.171	0.466	0.029
68	11.96	15.6	5.30	29.28	1.42	0.025	0.109	0.116	0.005
69.5	12.27	17.8	4.65	27.84	1.44	0.048	0.037	0.255	0.010
71	12.58	28.4	4.61	27.73	1.49	0.013	0.118	0.037	0.003
73	13.37	37.2	4.60	27.70	1.48	0.012	0.046	0.059	0.002
74.5	13.96	53.9	4.71	27.96	1.52	0.143	0.204	0.073	0.030
76	14.55	53.6	4.64	27.80	1.52	0.146	0.246	0.054	0.031
78	15.34	16.5	4.25	26.84	1.40	0.061	0.218	0.073	0.015
79.5	15.93	37	4.50	27.46	1.47	0.349	0.935	0.159	0.077
81	16.52	40.3	4.61	27.72	1.50	0.046	0.063	0.085	0.010
83	17.31	31	4.46	27.36	1.47	0.047	0.064	0.082	0.010
86	17.95	21.7	4.46	27.37	1.43	0.082	0.184	0.090	0.018
88	18.38	8.3	4.09	26.40	1.21	0.177	0.149	0.061	0.051
91	19.02	11.2	3.96	26.04	1.35	0.034	0.067	0.061	0.009
93	19.44	21.6	3.98	26.10	1.44	0.164	0.186	0.081	0.041
96	20.08	20.1	4.23	26.77	1.43	0.044	0.184	0.119	0.010
98	20.51	23	4.16	26.59	1.51	0.045	0.084	0.113	0.011
101	21.15	19.4	4.48	27.42	1.43	0.094	0.357	0.152	0.021
103	21.58	18.4	4.53	27.53	1.39	0.018	0.053	0.096	0.004
106	22.22	21.2	4.27	26.87	1.45	1.632	0.196	0.119	0.379
108	22.65	23.2	4.39	27.19	1.43	0.068	0.104	0.103	0.015

Depth [cm]	Age [ka BP]	Meas. Ca [mg/L]	Mg/Ca (±0.04) [mmol/mol]	$T_{Mg/Ca}$ [℃]	Sr/Ca (±0.04) [mmol/mol]	Fe/Ca [mmol/mol]	Al/Ca [mmol/mol]	Mn/Ca [mmol/mol]	Fe/Mg [mmol/mol]
111	23.29	30.3	4.38	27.16	1.45	0.021	0.120	0.105	0.005
113	23.71	32.7	4.35	27.09	1.47	0.034	0.027	0.110	0.008
114	23.93	26	4.12	26.48	1.47	0.027	0.052	0.095	0.006
116	24.57	28.2	4.14	26.53	1.45	0.019	0.050	0.108	0.004
121	25.42	37.9	4.43	27.29	1.49	0.080	0.157	0.148	0.018
123	25.77	23.8	4.36	27.12	1.44	0.081	0.149	0.132	0.018
126	26.29	22.3	4.54	27.57	1.43	0.047	0.110	0.208	0.010
128	26.63	18.9	4.64	27.81	1.43	0.901	0.084	0.125	0.192

Table 1.2b: 2nd part of the compilation of Mg/Ca measurements for *G. ruber* for the core SO 164-03-4

Depth [cm]	Age [ka BP]	Mg/Ca (±0.04) [mmol/mol]	$T_{Mg/Ca}$ [℃]	Sr/Ca (±0.04) [mmol/mol]	Depth [cm]	Age [ka BP]	Mg/Ca (±0.04) [mmol/mol]	$T_{Mg/Ca}$ [℃]	Sr/Ca (±0.04) [mmol/mol]
131	27.15	4.59	27.68	1.39	224	50.39	4.73	28.01	1.39
133	27.50	4.66	27.84	1.38	234	52.28	4.85	28.30	1.39
136	28.02	4.54	27.57	1.41	244	54.16	4.68	27.89	1.40
138	28.36	4.54	27.55	1.38	254	56.05	5.09	28.83	1.37
143	29.23	4.54	27.57	1.38	264	59.11	5.64	29.97	1.38
146	29.75	4.92	28.45	1.42	274	62.16	5.34	29.36	1.39
148	30.09	4.50	27.47	1.38	284	65.22	4.67	27.88	1.41
153	30.96	4.58	27.66	1.37	294	67.22	4.83	28.26	1.44
156	31.48	4.85	28.30	1.36	304	69.23	4.61	27.73	1.48
158	31.83	4.82	28.22	1.37	314	71.23	4.45	27.33	1.40
166	33.21	5.07	28.79	1.41	324	73.24	5.01	28.66	1.37
176	35.81	4.75	28.06	1.38	329	74.24	4.57	27.64	1.39
186	38.40	4.76	28.10	1.36	334	75.24	4.71	27.96	1.38
196	41.00	4.65	27.83	1.36	344	77.25	4.76	28.09	1.39
206	44.35	4.62	27.76	1.36	354	79.25	4.82	28.23	1.40
214	47.04	4.44	27.31	1.41	364	80.32	5.70	30.09	1.36

Depth [cm]	Age [ka BP]	Mg/Ca (±0.04) [mmol/mol]	$T_{Mg/Ca}$ [℃]	Sr/Ca (±0.04) [mmol/mol]	Depth [cm]	Age [ka BP]	Mg/Ca (±0.04) [mmol/mol]	$T_{Mg/Ca}$ [℃]	Sr/Ca (±0.04) [mmol/mol]
374	81.40	6.07	30.79	1.33	465	90.63	5.05	28.74	1.40
384	82.47	6.75	31.97	1.32	475	91.17	5.22	29.11	1.45
394	83.55	6.71	31.90	1.34	485	91.70	6.00	30.66	1.36
414	85.70	6.57	31.67	1.36	495	92.23	5.12	28.90	1.36
435	87.95	6.79	32.03	1.31	505	92.76	5.18	29.03	1.34
445	89.03	6.66	31.82	1.35	515	93.30	4.97	28.56	1.39
455	90.10	6.06	30.77	1.37					

Table 1.2c: 3rd part of the compilation of Mg/Ca measurements for *G. ruber* for the core SO 164-03-4

Depth [cm]	Mg/Ca (±0.04) [mmol/mol]	$T_{Mg/Ca}$ [℃]	Sr/Ca (±0.04) [mmol/mol]	Depth [cm]	Mg/Ca (±0.04) [mmol/mol]	$T_{Mg/Ca}$ [℃]	Sr/Ca (±0.04) [mmol/mol]	Depth [cm]	Mg/Ca (±0.04) [mmol/mol]	$T_{Mg/Ca}$ [℃]	Sr/Ca (±0.04) [mmol/mol]
521	4.71	27.97	1.39	691	4.95	28.52	1.37	861	5.41	29.51	1.44
531	4.84	28.27	1.41	701	5.29	29.26	1.38	871	5.46	29.61	1.36
541	4.65	27.83	1.39	711	4.67	27.87	1.40	881	5.46	29.61	1.36
551	4.31	26.98	1.40	721	4.46	27.37	1.40	891	5.15	28.96	1.41
561	4.47	27.39	1.41	731	4.55	27.57	1.39	901	5.12	28.90	1.37
571	4.39	27.19	1.41	741	5.27	29.22	1.39	910	4.89	28.39	1.40
581	4.53	27.54	1.42	751	5.39	29.47	1.41	921	6.13	30.90	1.34
591	4.83	28.25	1.40	761	5.21	29.09	1.43	931	5.50	29.69	1.38
601	5.40	29.49	1.38	771	5.65	29.99	1.38	941	6.05	30.75	1.34
611	5.39	29.47	1.36	781	5.24	29.15	1.41	951	6.39	31.36	1.32
621	4.74	28.03	1.38	791	6.01	30.68	1.40	961	5.22	29.11	1.34
631	4.89	28.39	1.41	801	6.11	30.86	1.41	971	4.54	27.57	1.40
641	5.71	30.11	1.36	811	5.43	29.55	1.38	981	5.85	30.38	1.39
651	5.89	30.45	1.42	821	4.96	28.55	1.41	991	5.20	29.07	1.37
661	4.66	27.86	1.34	831	5.21	29.09	1.41	1001	4.94	28.50	1.38
671	4.67	27.88	1.37	841	4.80	28.18	1.42	1011	5.31	29.30	1.40
681	5.06	28.77	1.35	851	6.13	30.90	1.44	1020	5.60	29.89	1.36

Depth [cm]	Mg/Ca (±0.04) [mmol/mol]	$T_{Mg/Ca}$ [℃]	Sr/Ca (±0.04) [mmol/mol]	Depth [cm]	Mg/Ca (±0.04) [mmol/mol]	$T_{Mg/Ca}$ [℃]	Sr/Ca (±0.04) [mmol/mol]	Depth [cm]	Mg/Ca (±0.04) [mmol/mol]	$T_{Mg/Ca}$ [℃]	Sr/Ca (±0.04) [mmol/mol]
1030	5.10	28.85	1.38	1150	5.19	29.05	1.38	1270	5.25	29.18	1.42
1040	5.68	30.05	1.36	1160	4.65	27.83	1.43	1280	5.81	30.30	1.38
1050	6.15	30.93	1.35	1170	5.18	29.03	1.38	1290	5.80	30.28	1.38
1060	6.62	31.75	1.37	1180	5.50	29.69	1.37	1300	5.83	30.34	1.40
1070	5.38	29.45	1.35	1190	5.99	30.64	1.33				
1080	5.00	28.63	1.39	1200	5.86	30.40	1.35				
1090	5.53	29.75	1.35	1210	5.69	30.07	1.33				
1100	7.30	32.84	1.27	1221	6.86	32.15	1.36				
1110	6.61	31.74	1.32	1231	5.89	30.45	1.38				
1121	5.19	29.05	1.37	1241	5.30	29.28	1.37				
1130	5.66	30.01	1.34	1261	5.17	29.01	1.35				
1140	5.11	28.88	1.36	1261	5.63	29.95	1.36				

Table 1.3: A compilation of measurements for *G. sacculifer* (*G. sacc*) for the core SO 164-03-4

Depth [cm]	Age [ka BP]	$\delta^{18}O_{korr.}$ *G.sacc.* (±0.07) [‰]	Mg/Ca (±0.04) [mmol/mol]	$T_{Mg/Ca}$ (±0.4) [℃]	Depth [cm]	Age [ka BP]	$\delta^{18}O_{korr.}$ *G.sacc.* (±0.07) [‰]	Mg/Ca (±0.04) [mmol/mol]	$T_{Mg/Ca}$ (±0.4) [℃]
2	0.04	-1.822	4.425	27.05	49.5	8.12	-0.781	4.581	26.27
3	0.21	-1.831	4.028	26.06	51	8.43	-0.640	4.316	27.41
5	0.55	-1.751	4.247	26.62	53	8.85	-0.294	4.006	26.79
7	0.89	-1.691	4.208	26.52	54.5	9.37	-0.407	4.385	26.01
8	1.05	-1.837	4.25	26.63	56	9.47	-0.247	4.022	26.95
10	1.39	-1.594	4.398	26.99	58	9.88	-0.261	4.206	26.05
12	1.73	-1.725	4.267	26.67	59.5	10.20	-0.262	4.438	26.52
13	1.90	-1.940	4.324	26.81	61	10.51	-0.152	4.072	27.08
15	2.24	-1.824	4.348	26.87	63	10.92	-0.101	3.998	26.18
18	2.74	-1.844	4.186	26.47	64.5	11.23	-0.163	4.598	25.99
19.5	3.00	-1.655	4.287	26.72	68	11.96	0.162	3.883	24.95
21	3.25	-1.642	4.009	26.01	69.5	12.27	-0.210	4.364	25.68
23	3.59	-1.791	4.309	26.77	71	12.58	-0.305	3.815	26.90
24.5	3.84	-1.565	4.413	27.02	73	13.37	0.517	3.769	25.50
28	4.43	-1.417	4.581	26.27	74.5	13.96	0.231	3.88	25.37
29.5	4.69	-1.179	4.167	27.41	76	14.55	0.564	3.572	25.67
31	4.94	-1.482	4.367	26.42	78	15.34	0.453	3.471	24.81
33	5.28	-1.137	4.174	26.91	79.5	15.93	0.239	3.72	24.51
34.5	5.53	-1.334	4.429	26.44	81	16.52	0.317	3.576	25.23
36	5.78	-0.994	4.236	27.06	83	17.31	0.326	3.627	24.82
38	6.12	-1.298	4.289	26.59	86	17.95	0.545	3.331	24.97
39.5	6.37	-1.446	4.354	26.72	88	18.38	0.191	3.46	24.08
41	6.63	-1.350	4.242	26.88	91	19.02	0.347	3.465	24.48
43	6.97	-1.375	4.286	26.61	93	19.44	0.307	3.531	24.49
44.5	7.22	-1.281	4.539	26.71	96	20.08	0.463	3.309	24.69
46	7.47	-1.127	3.981	27.32	98	20.51	0.453	3.49	24.01
48	7.81	-1.034	4.109	25.94	101	21.15	0.249	3.361	24.57

Depth [cm]	Age [ka BP]	$\delta^{18}O_{korr.}$ *G.sacc.* (±0.07) [‰]	Mg/Ca (±0.04) [mmol/mol]	$T_{Mg/Ca}$ (±0.4) [℃]
111	23.29	0.367	3.657	25.26
113	23.71	0.080	3.599	25.05
114	23.93	0.336	3.386	24.89
116	24.57	0.513	3.581	24.25
118	24.78	0.584	3.849	24.83
121	25.42	0.475	3.746	25.59

Depth [cm]	Age [ka BP]	$\delta^{18}O_{korr.}$ *G.sacc.* (±0.07) [‰]
123	25.77	0.173
126	26.29	0.187
128	26.63	-0.007
131	27.15	-0.018
133	27.50	0.176
136	28.02	0.376
138	28.36	0.087
143	29.23	0.084
146	29.75	-0.014
148	30.09	0.276
153	30.96	0.135
156	31.48	0.016
158	31.83	-0.257
166	33.21	-0.093
176	35.81	0.340
186	38.40	0.270
196	41.00	0.029
206	44.35	0.369

Depth [cm]	Age [ka BP]	$\delta^{18}O_{korr.}$ *G.sacc.* (±0.07) [‰]
214	47.04	-0.259
224	50.39	0.106
234	52.28	-0.211
244	54.16	-0.012
254	56.05	-0.102
264	59.11	-0.488
274	62.16	0.086
284	65.22	0.145
294	67.22	-0.298
304	69.23	-0.207
314	71.23	-0.537
324	73.24	-0.535
329	74.24	-0.460
334	75.24	-0.734
344	77.25	-0.701
354	79.25	-0.595
364	80.32	-0.656
374	81.40	-0.411

Depth [cm]	Age [ka BP]	$\delta^{18}O_{korr.}$ *G.sacc.* (±0.07) [‰]
384	82.47	-0.188
394	83.55	-0.016
404	84.62	-0.206
414	85.70	-0.149
435	87.95	-0.381
445	89.03	-0.132
455	90.10	-0.435
465	90.63	0.035
475	91.17	0.028
485	91.70	0.099
495	92.23	-0.188
505	92.76	0.065
515	93.30	0.128

Table 1.4: Calculated $\Delta\delta^{18}O_{ivfsw}$ for *G. sacculifer* (*G. sacc*) using the Mg/Ca based temperatures

Depth [cm]	Age [ka BP]	$\delta^{18}O_{korr.}$ *G.sacc.* (±0.07) [‰]	$T_{Mg/Ca}$ (±0.4) [℃]	RSL variation	$\Delta\delta^{18}O_{ivfsw}$ [‰]	Depth [cm]	Age [ka BP]	$\delta^{18}O_{korr.}$ *G.sacc.* (±0.07) [‰]	$T_{Mg/Ca}$ (±0.4) [℃]	RSL variation	$\Delta\delta^{18}O_{ivfsw}$ [‰]
2	0.04	-1.822	27.05	0.0000	0.98	51	8.43	-0.640	27.41	0.0925	2.14
3	0.21	-1.831	26.06	0.0000	0.76	53	8.85	-0.294	26.79	0.1182	2.33
5	0.55	-1.751	26.62	0.0000	0.96	54.5	9.37	-0.407	26.01	0.1524	2.02
7	0.89	-1.691	26.52	0.0003	1.00	56	9.47	-0.247	26.95	0.1951	2.34
8	1.05	-1.837	26.63	0.0005	0.88	58	9.88	-0.261	26.05	0.2037	2.13
10	1.39	-1.594	26.99	0.0007	1.19	59.5	10.20	-0.262	26.52	0.2510	2.18
12	1.73	-1.725	26.67	0.0010	1.00	61	10.51	-0.152	27.08	0.2873	2.37
13	1.90	-1.940	26.81	0.0012	0.81	63	10.92	-0.101	26.18	0.3236	2.20
15	2.24	-1.824	26.87	0.0026	0.94	64.5	11.23	-0.163	25.99	0.3720	2.04
18	2.74	-1.844	26.47	0.0056	0.83	68	11.96	0.162	24.95	0.4496	2.08
19.5	3.00	-1.655	26.72	0.0071	1.07	69.5	12.27	-0.210	25.68	0.5018	1.80
21	3.25	-1.642	26.01	0.0085	0.93	71	12.58	-0.305	26.90	0.5409	1.93
23	3.59	-1.791	26.77	0.0107	0.94	73	13.37	0.517	25.50	0.5798	2.41
24.5	3.84	-1.565	27.02	0.0126	1.22	74.5	13.96	0.231	25.37	0.6764	2.01
28	4.43	-1.417	26.27	0.0145	1.21	76	14.55	0.564	25.67	0.7488	2.33
29.5	4.69	-1.179	27.41	0.0170	1.68	78	15.34	0.453	24.81	0.8042	1.98
31	4.94	-1.482	26.42	0.0189	1.17	79.5	15.93	0.239	24.51	0.8765	1.63
33	5.28	-1.137	26.91	0.0208	1.61	81	16.52	0.317	25.23	0.9131	1.83
34.5	5.53	-1.334	26.44	0.0249	1.31	83	17.31	0.326	24.82	0.9432	1.72
36	5.78	-0.994	27.06	0.0283	1.78	86	17.95	0.545	24.97	0.9778	1.93
38	6.12	-1.298	26.59	0.0317	1.38	88	18.38	0.191	24.08	0.9992	1.37
39.5	6.37	-1.446	26.72	0.0362	1.25	91	19.02	0.347	24.48	1.0134	1.60
41	6.63	-1.350	26.88	0.0396	1.38	93	19.44	0.307	24.49	1.0261	1.55
43	6.97	-1.375	26.61	0.0448	1.29	96	20.08	0.463	24.69	1.0332	1.74
44.5	7.22	-1.281	26.71	0.0541	1.40	98	20.51	0.453	24.01	1.0413	1.58
46	7.47	-1.127	27.32	0.0610	1.67	101	21.15	0.249	24.57	1.0353	1.50
48	7.81	-1.034	25.94	0.0680	1.47	103	21.58	0.578	24.17	1.0262	1.75
49.5	8.12	-0.781	26.27	0.0773	1.78	106	22.22	0.656	24.58	1.0200	1.92

Depth [cm]	Age [ka bp]	$\delta^{18}O_{korr.}$ *G.sacc.* (±0.07) [‰]	$T_{Mg/Ca}$ (±0.4) [℃]	RSL variation	$\Delta\delta^{18}O_{ivfsw}$ [‰]
108	22.65	0.183	24.21	1.0099	1.38
111	23.29	0.367	25.26	1.0031	1.79
113	23.71	0.080	25.05	0.9899	1.48
114	23.93	0.336	24.89	0.9785	1.71
116	24.57	0.513	24.25	0.9728	1.76
118	24.78	0.584	24.83	0.9550	1.97
121	25.42	0.475	25.59	0.9468	2.03

Table 1.5: Measured $\delta^{44/40}$Ca values and the $\delta^{44/40}$Ca based temperatures for *G. sacculifer* (*G. sacc*)

Depth [cm]	Age [ka BP]	$\delta^{44/40}$Ca *G.sacc.* (±0.12) [‰]	Weighted Error	$T_{44/40Ca}$ (±0.5) [℃]
2	0.04	0.49	0.03	24.40
13	1.90	0.59	0.05	24.88
26	4.09	0.66	0.02	25.17
41	6.63	0.72	0.08	25.45
43	6.97	0.68	0.03	25.29
51	8.43	0.62	0.02	24.99
63	10.92	0.54	0.23	24.66
64.5	11.23	0.53	0.11	24.59
68	11.96	0.42	0.04	24.11
69.5	12.27	0.36	0.06	23.81
71	12.58	0.68	0.08	25.26
73	13.37	0.72	0.01	25.45
74.5	13.96	0.65	0.05	25.15
76	14.51	0.41	0.23	24.06
78	15.32	0.54	0.07	24.65
83	16.52	0.56	0.05	24.74
86	17.31	0.55	0.03	24.68
88	18.38	0.49	0.06	24.40
101	21.15	0.52	0.07	24.55
103	21.58	0.51	0.04	24.50

Table 1.6: Calculated $\Delta\delta^{18}O_{ivfsw}$ for *G. sacculifer* (*G.*) using the Ca isotope based temperatures

Depth [cm]	Age [ka BP]	$T_{44/40Ca}$ (±0.5) [℃]	$\delta^{18}O$ *G.sacc* (±0.07) [‰]	RSL variation	$\Delta\delta^{18}O_{ivfsw}$ [‰]	Deviation from Holocene mean
2	0.04	24.40	-1.822	0.0000	0.43	0.51
13	1.90	24.88	-1.940	0.0012	0.41	0.49
26	4.09	25.17	-1.919	0.0145	0.48	0.57
41	6.63	25.45	-1.350	0.0448	1.07	1.29
43	6.97	25.29	-1.375	0.0541	1.01	1.21
51	8.43	24.99	-0.640	0.1182	1.61	1.93
63	10.92	24.66	-0.262	0.3236	1.72	2.06
64.5	11.23	24.59	-0.163	0.3720	1.75	2.10
68	11.96	24.11	0.162	0.4496	1.90	2.28
69.5	12.27	23.81	-0.210	0.5018	1.41	1.70
71	12.58	25.26	-0.305	0.5409	1.58	1.90
73	13.37	25.45	0.517	0.5798	2.41	2.89
74.5	13.96	25.15	0.231	0.6764	1.96	2.35
76	14.51	24.06	0.564	0.8042	1.94	2.32
78	15.32	24.65	0.453	0.8765	1.88	2.25
83	16.52	24.74	0.317	0.9778	1.66	1.99
86	17.31	24.68	0.326	0.9992	1.63	1.96
88	18.38	24.40	0.545	1.0134	1.78	2.14
101	21.15	24.55	0.453	1.0353	1.70	2.04
103	21.58	24.50	0.249	1.0262	1.49	1.79

Section 2 – ODP 1058c – Blake Ridge

Contents of ODP 1058c evaluation (Alkenone and Tables 2.1-2.4):

A brief look at the Alkenone $U^{K'}_{37}$ system

Alkenone measurements

Termination 2

Table 2.1a+b:

A compilation of the $\delta^{18}O$ and $\delta^{13}C$ measurments of *C. wuellerstorfi* for the ODP core 1058c. Table 2.1a contains the first 2m downcore, whereas table 2.1b contains the section between 17 and 25m.

For all following tables in this section part ´a´ allways covers the first 2m and part ´b´ the 8m section covering Termination 2.

Table 2.2a+b:

Contains a compilation of $\delta^{18}O$ and $\delta^{13}C$ of *G.ruber* for the core ODP 1058c.

Table 2.3a+b:

Contains the compilation of Mg/Ca and Sr/Ca measurements for *G. ruber* for the core ODP 1058c.

Table 2.4a+b:

Contains the compilation of $\delta^{18}O$ and $\delta^{13}C$ measurements for *G. truncatulinoides* for the core ODP 1058c.

Table 2.5a+b:

1st part of the compilation of Mg/Ca and Sr/Ca measurements for *G. truncatulinoides* for the core ODP 1058c. The temperatures were calculated using the calibration by *McKenna und Prell*.

Table 2.6:

Compilation of the Uk´37 measurements for the core ODP 1058c

A brief look at the Alkenone $U^{K'}_{37}$ system

The $U^{K'}_{37}$ proxy is derived from the interpretation of long chain organic compounds that are preserved in sediment samples [*Rosell-Melé et al.,* 2001; *Blanz et al*., 2005]. The temperature sensitivity is based on the relative abundance of temperature-sensitive, long-chain, di- and tri-unsaturated carbon bonds (methyl and ethyl ketones) [e.g., *Prahl and Wakeham*, 1987; *Prahl et al*., 1988; *Müller et al*., 1998; *Rosell-Melé et al*., 1998]. These compounds are mainly formed by planctic organisms. Thus they represent the water temperatures of the habitat of the producers.

The main problem with the $U^{K'}_{37}$ proxy is the preservation of the long chain organic compounds; in particular in carbonate rich cores the alkaline environment is not suitable for their preservation. For more detailed information on alkenones and the UK´37 proxy sample preparation refer to section 4 and *Blanz et al*. [2005], *Waniek et al*. [2005], *Conte et al*. [2006].

Alkenone measurements

For the measurement of long chain alkenones (e.g. Uk´37) a different cleaning and sample preparation procedure was necessary. First of all the alkenones had to be extracted from portions of freeze-dried and homogenized sediment (1 to 3 g) after the addition of 0.5 µg of cholestane and 0.5 µg of hexatriacontane as internal standards. An accelerated solvent extractor (Dionex ASE 200), which accelerates the extraction process by using solvent at elevated temperatures and pressures, was used. Each sample was extracted twice for 10 min using 25 mL dichloromethane at a temperature of 75℃ and pressure of 80 bar (nitroge n). After heating, the extract was flushed from the sample cell into a standard collection vial and cooled down in a freezer (-20℃). The resulting extracts were concen trated to 50 µL with a rotary evaporator. The residual was transferred into glass vials and dried over nitrogen. After drying, the residues were taken up in 100 µL hexane.

The multidimensional gas chromatography was carried out with two Agilent 6890 gas chromatographs equipped with two independent ovens and two flame ionization detectors (MDGC-FID): MDGC combines the separation efficiency of two capillary columns with different polarities, each in a separate temperature-controlled oven, arranged in series and the sensitivity of two FID for organic biomarker. The two

columns were serially coupled through a dean switching system and the transfer line, which was maintained at 330℃ throughout the experi mentation.

The eluate of the first column passed either through the monitor detector or through the second column and the main detector. In the latter mode, a preselected small fraction was cut from the eluate of the first column and transferred to the second column. This can be achieved efficiently, quantitatively and reproducibly. The usual FID chromatogram was recorded by the monitor detector, only interrupted during the cut time. The chromatogram recorded by the main FID shows only a few peaks depending on the components included in that cut. The main detector has a much higher sensitivity than the monitor detector, because of the reduced memory effect and reduced level of contamination, as it receives small selected fractions from the first column through the heart cut.

Quantification of C37 alkenones was archived with the internal standard. The analytical precision based on multiple extractions of sediment samples was better than 0.3℃ for the UK'37 Index. We calculated the s ea surface temperatures from the UK'37 according to *Müller et al*. [1998].

Termination 2

In order to further verify the above observations during Termination 1, a detailed study of the Termination 2 - Marine Isotope Stage 5-6 - was undertaken in this core. Data from several different proxies were collected over the area of interest. The section sampled was between 17 and 26m below the sea floor and dates back to about 150 ky BP.

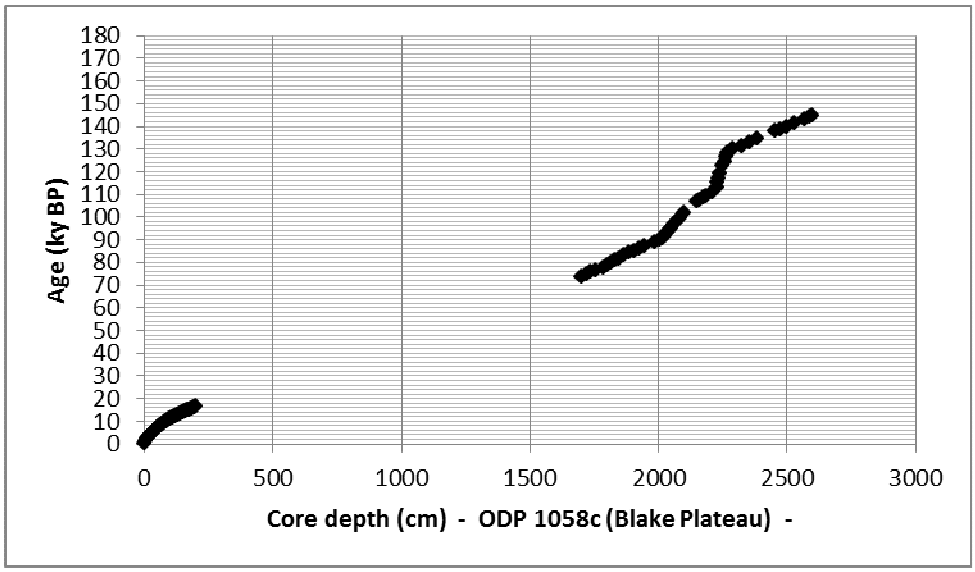

The dataset for Termination 2 unfortunately has a few less denser sampled areas and even some gaps due to changes in the population of the sampled foraminifera. The position of the Termination 2 is between the 130k and 138k year mark in the figures Ap.1 and Ap.2.

Combined $\delta^{18}O$ and Mg/Ca ratio measurements were not only undertaken for *G. ruber* but also for the intermediate species of *G. truncacolidoides* which lives at about 300m below sea level.

The measured data for *G. ruber* for the time window of 70ky to 150ky BP is presented in figure Ap. 1. and figure Ap. 2.

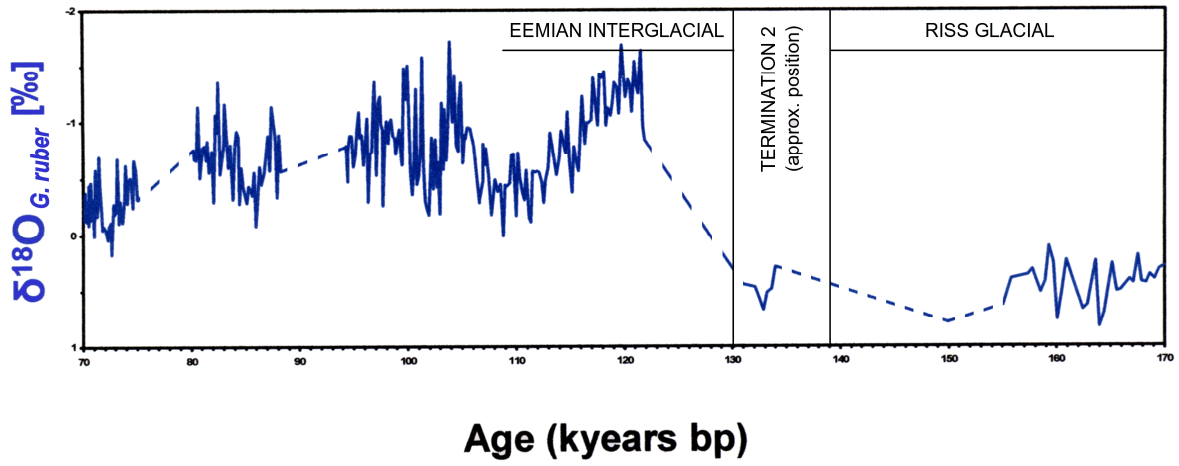

Figure Ap.1: $\delta^{18}O$ ratio of *G. ruber* for the ODP core 172-1058c for the time frame of 70.000 to 170.000 years covering the Termination 2.

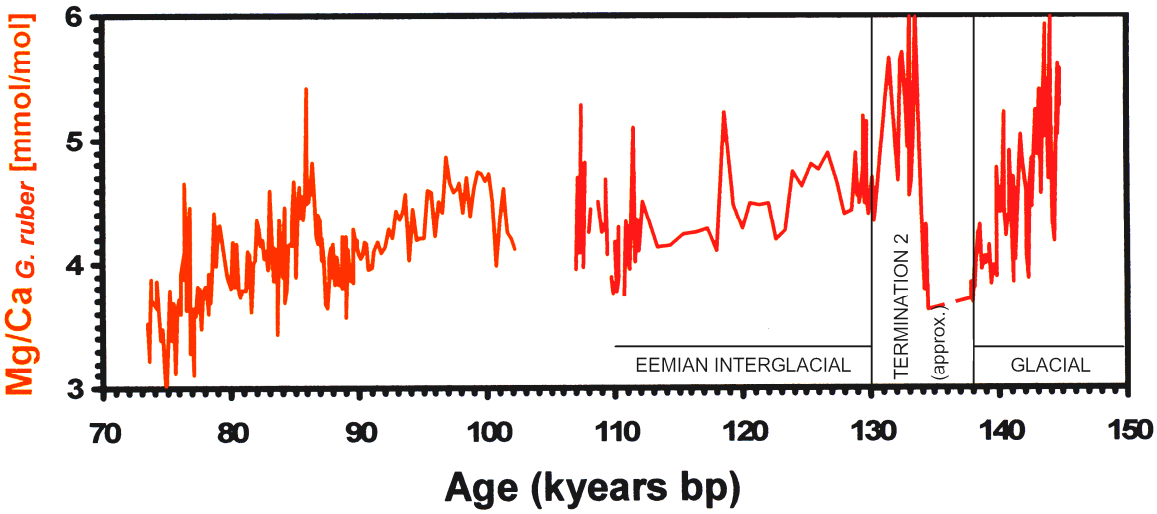

Figure Ap.2: Mg/Ca ratio of *G. ruber* for the ODP core 172-1058c for the time frame of 70.000 to 150.000 years covering the Termination 2.

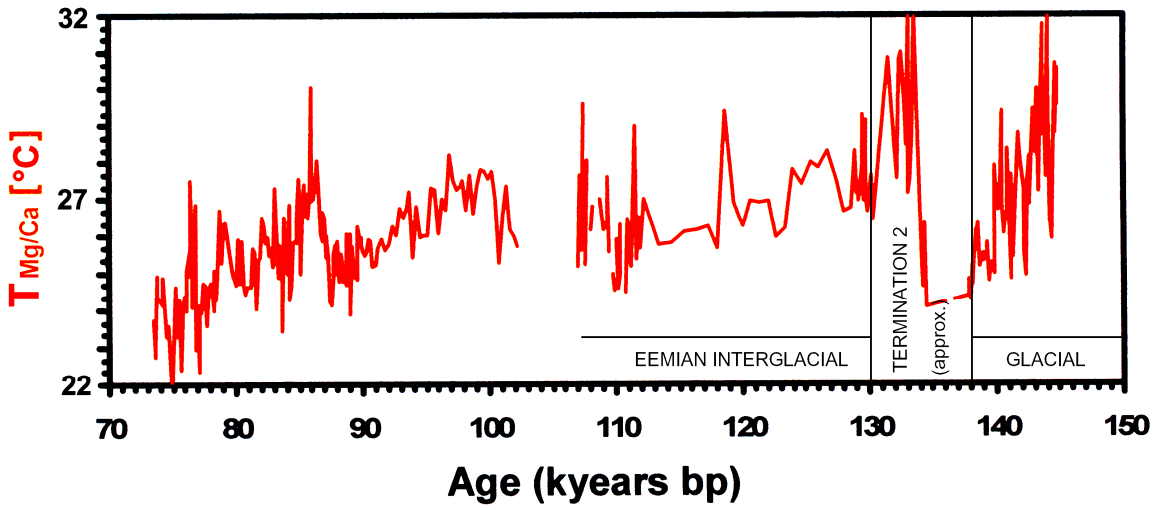

Figure Ap.3: Mg/Ca generated temperatures of *G. ruber* for the ODP core 172-1058c for the time frame of 70.000 to 150.000 years covering the Termination 2.

The overall picture thus far is that no visible phase shift is present at Termination 2. In order to verify this observation, several UK´37 proxies were gathered over the Termination 2 to provide an independent temperature proxy for further comparison purposes. The results are presented in figure Ap.4.

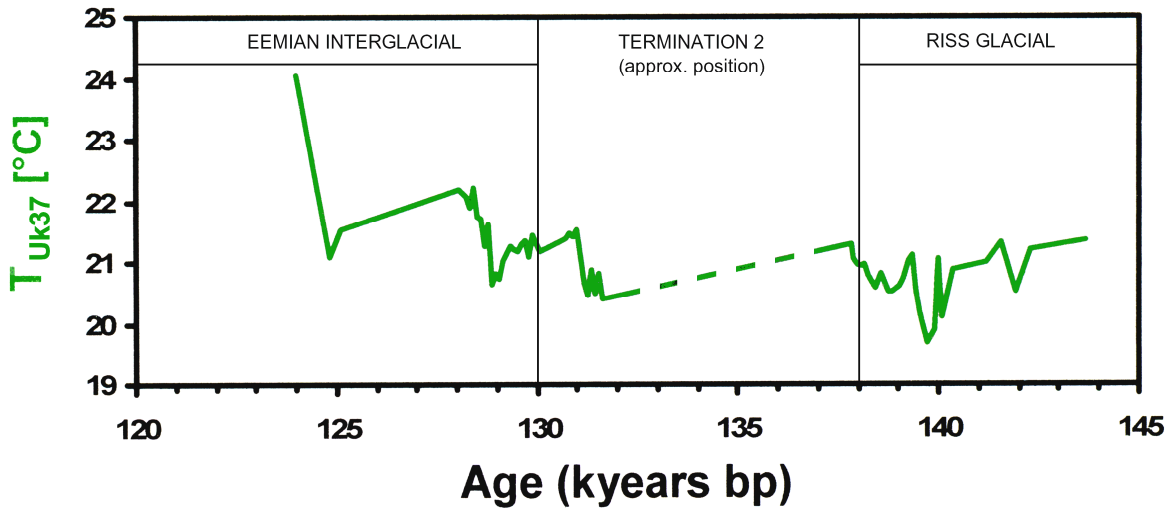

Figure Ap.4: A compilation of the temperatures derived from the UK´37 proxy for the time interval of MIS 5-6 for ODP core 172-1058C.

The UK´37 time series is less dense but the main variations are still very clearly visible. Termination 2, the transition from MIS 5 to 6, is easily recognized at about 130.000 years before present.

Of further interest was the development and change of the ocean parameters below the sea surface, in intermediate water masses of more than 100m depth. For this a series of measurements *G. truncatulinoides,* who´s habitat is about 300m below sea level were performed. Both $\delta^{18}O$ and Mg/Ca ratios were measured in order receive a complete picture of the environmental conditions at this water depth.

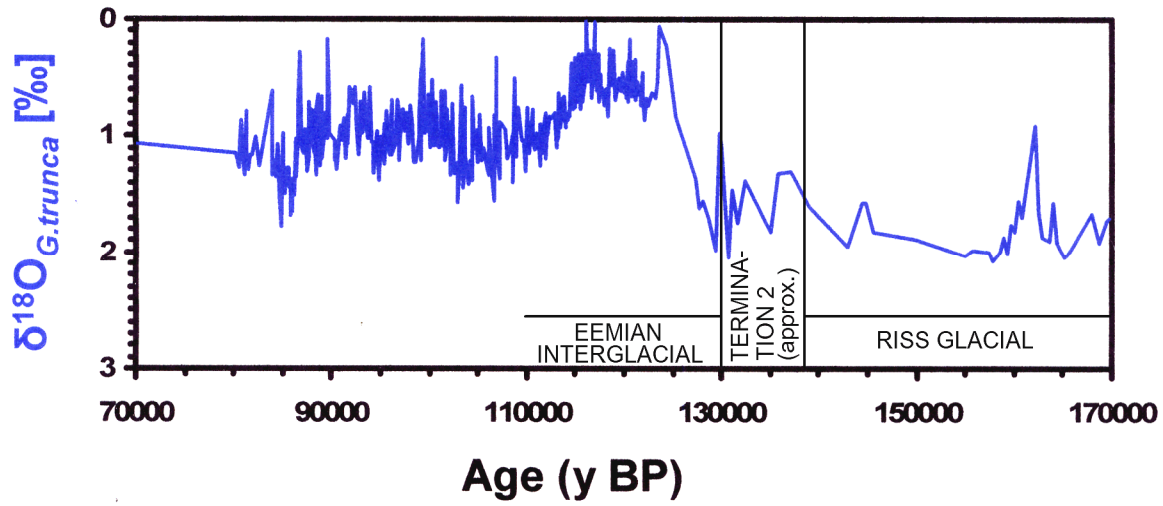

Figure Ap.5: $\delta^{18}O$ ratio of *G. truncatulinoides* for the ODP core 172-1058c.

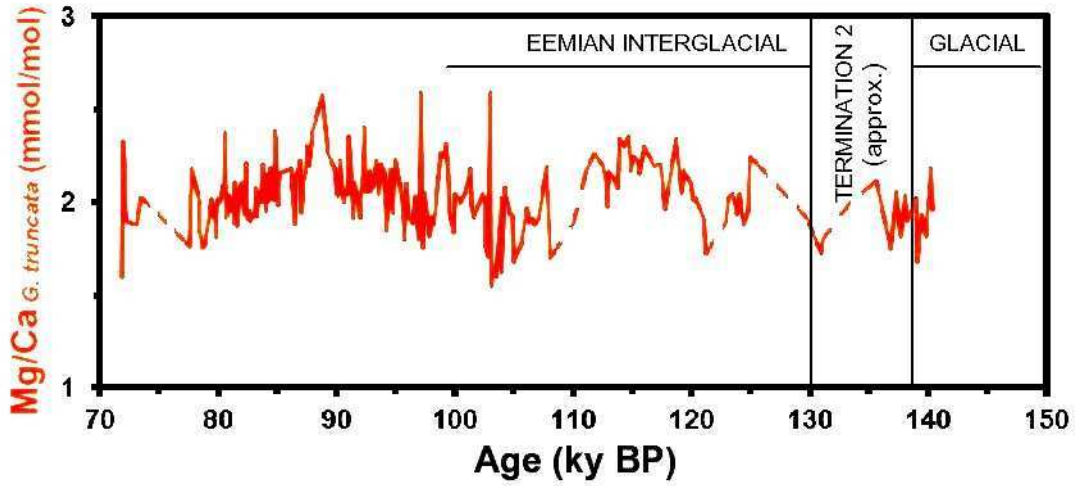

Figure Ap.6: Mg/Ca ratio of *G. truncatulinoides* for the ODP core 172-1058c.

The datasets for *G. truncatulinoides* are realtively complete and present us a detailed overview of the climatic changes in intermediate waters.

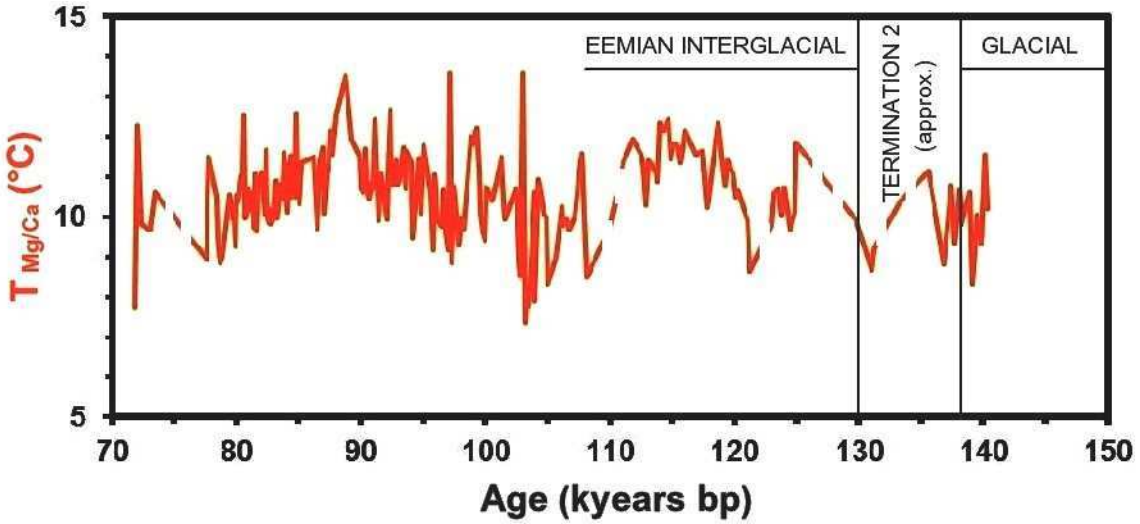

Figure Ap.7: Mg/Ca generated temperatures of *G. truncatulinoides* for the ODP core 172-1058c.

The overall picture presented for the time window from 70 to 140 ky BP by the foraminifera *G. truncatulinoides* is that there are many short term fluxes but overall this region does not seem to be exposed to large shifts in temperature or variations in sea salinity.

The changes during Termination 2 are very interesting because they are large differences between the individual water masses, both in the water column and the time series.

The most striking effect is the strong increase in temperatures over a short period of time in the surface region(figure Ap. 1-3) whereas the intermediate water masses do not seem to follow the same trend (figure Ap. 5-7). This jump is achieved in only a few thousand years and a considerable warm period follows this increase, especially at Termination 2. There the signal variation for *G.ruber* is more than 2 ‰ which corresponds to a temperature increase of more than 5 ℃.

In conclusion, the samples of the ODP 1058c site unfortunately could not be analysed close enough and consequently detailed statements about a possible phase shift between Mg/Ca and $\delta^{18}O$ ratios observed for Termination 2 were not possible.

Table 2.1a: A compilation of $\delta^{18}O$ and $\delta^{13}C$ of *C. wuellerstorfi* (*C. w.*) for the core ODP 1058c

Depth [cm]	$\delta^{18}O_{korr}$ C.w. (±0.07) [‰]	Age [ka BP]	$\delta^{13}C_{korr}$ C.w. (±0.04) [‰]	Depth [cm]	$\delta^{18}O_{korr}$ C.w. (±0.07) [‰]	Age [ka BP]	$\delta^{13}C_{korr}$ C.w. (±0.04) [‰]
0	2.720	0.236	1.151	39	2.725	5.970	1.053
1	2.471	0.472	1.195	43	2.363	6.378	-0.370
2	2.403	0.708	0.794	46	2.714	6.676	0.923
3	2.715	0.944	1.294	47	2.583	6.774	-0.149
6	2.748	1.652	1.284	47	2.967		1.033
7	2.679	1.888	1.045	48	2.670	6.872	0.927
8	2.705	2.124	1.082	50	2.584	7.066	1.322
9	2.768	2.360	0.602	51	2.633	7.162	0.831
10	2.479	2.524	0.004	52	2.548	7.258	1.029
10	2.815		0.801	53	2.666	7.354	1.243
11	2.830	2.688	0.662	55	2.818	7.542	1.302
12	2.677	2.852	0.493	56	2.576	7.634	1.203
13	2.575	3.016	1.265	57	2.719	7.726	1.249
14	2.819	3.180	0.929	62	2.607	8.180	1.219
15	2.660	3.298	0.289	64	2.700	8.360	1.195
15	2.869		0.910	81	2.671	9.766	1.138
16	2.451	3.416	1.289	82	2.526	9.844	1.118
18	2.638	3.652	0.757	90	2.964	10.452	1.030
19	2.697	3.770	0.872	92	2.804	10.596	1.030
20	2.628	3.884	1.206	94	2.732	10.740	1.047
21	2.947	3.998	0.864	100	2.826	11.158	1.225
24	2.967	4.340	1.339	101	2.787	11.226	1.105
25	2.703	4.452	-0.251	102	2.750	11.294	1.010
27	2.757	4.676	0.227	103	2.955	11.362	1.024
29	2.886	4.900	1.128	104	2.933	11.430	1.120
31	2.800	5.116	-0.673	105	2.790	11.494	0.957
36	2.716	5.652	1.325	106	2.828	11.558	1.034

Depth [cm]	$\delta^{18}O_{korr}$ C.w. (±0.07) [‰]	Age [ka BP]	$\delta^{13}C_{korr}$ C.w. (±0.04) [‰]
107	2.759	11.628	1.061
108	2.628	11.692	0.906
109	2.737	11.757	0.990
110	2.870	11.821	1.009
112	2.966	11.946	1.071
114	2.956	12.070	0.990
116	2.815	12.192	0.811
117	2.929	12.252	0.830
118	3.298	12.312	1.036
119	2.839	12.371	1.049
120	2.834	12.430	1.016
121	2.870	12.488	0.865
122	2.671	12.546	0.945
123	3.622	12.603	0.952
124	3.346	12.660	0.968
125	3.368	12.717	0.324
125	3.381		0.377
126	3.330	12.773	0.978
127	2.869	12.829	0.711
128	2.873	12.885	0.413
128	3.018		0.913
129	3.722	12.941	0.787
130	3.586	12.992	0.628
131	3.358	13.044	0.514
131	3.607		1.104
132	3.352	13.099	0.649
133	3.670	13.152	0.930
134	3.314	13.204	0.648
135	3.591	13.257	0.953
136	3.017	13.308	0.898

Depth [cm]	$\delta^{18}O_{korr}$ C.w. (±0.07) [‰]	Age [ka BP]	$\delta^{13}C_{korr}$ C.w. (±0.04) [‰]
137	3.266	13.363	0.956
138	3.274	13.417	0.972
139	3.378	13.472	0.393
139	3.654		1.121
140	2.890	13.526	0.952
142	2.721	13.628	0.780
143	3.090	13.682	0.418
143	3.657		1.065
144	3.527	13.733	0.821
145	3.730	13.784	0.918
146	3.772	13.836	0.969
147	3.662	13.885	1.010
149	3.445	13.934	0.796
150	3.553	14.030	0.876
151	3.519	14.080	0.923
152	3.409	14.130	0.691
153	3.684	14.180	0.923
154	3.224	14.230	0.432
154	3.679		0.886
155	3.101	14.272	0.903
156	3.497	14.314	0.821
157	3.620	14.356	0.949
159	3.501	14.440	0.742
160	3.498	14.498	0.777
162	3.415	14.614	0.555
163	3.661	14.672	0.724
164	3.654	14.730	0.812
165	3.735	14.778	0.754
166	3.406	14.826	0.695
167	3.582	14.874	0.572

Depth [cm]	$\delta^{18}O_{korr}$ C.w. (±0.07) [‰]	Age [ka BP]	$\delta^{13}C_{korr}$ C.w. (±0.04) [‰]
168	3.703	14.922	0.744
169	3.710	14.970	-0.657
169	3.570		0.477
170	3.609	15.020	-0.761
171	3.712	15.070	0.662
172	3.373	15.120	0.751
173	3.703	15.170	0.612
177	3.490	15.370	0.865
179	3.572	15.470	0.932
180	3.480	15.520	0.849
185	3.355	15.768	0.670
187	2.939	15.864	1.042
193	2.996	16.160	0.928
194	3.507	16.210	0.857

Table 2.1b: A compilation of $\delta^{18}O$ and $\delta^{13}C$ of *C. wuellerstorfi* (*C. w.*) for the core ODP 1058c

Depth [cm]	$\delta^{18}O_{korr}$ C.w. (±0.07) [‰]	Age [ka BP]	$\delta^{13}C_{korr}$ C.w. (±0.04) [‰]	Depth [cm]	$\delta^{18}O_{korr}$ C.w. (±0.07) [‰]	Age [ka BP]	$\delta^{13}C_{korr}$ C.w. (±0.04) [‰]
1790	3.963	71.912	0.521	2016	3.405	84.990	0.964
1796	4.110	72.308	0.652	2066	3.543	88.486	0.803
1807	4.124	73.096	-0.050	2072	3.470	88.948	1.017
1808	3.891	73.168	0.281	2076	3.728	89.256	0.465
1814	3.904	73.610	0.926	2084	3.760	89.880	0.371
1818	3.950	73.890	0.439	2106	3.332	91.576	0.959
1820	3.838	74.032	0.657	2116	3.430	92.346	0.534
1826	3.841	74.464	0.909	2120	3.334	92.658	0.999
1828	3.800	74.608	0.576	2124	3.364	92.970	0.933
1830	3.775	74.772	0.720	2132	3.180	93.588	0.994
1832	3.522	74.956	0.431	2146	3.006	94.666	0.253
1834	3.879	75.140	0.497	2172	3.285	96.678	0.714
1838	3.812	75.588	0.774	2194	3.240	98.380	0.921
1854	3.623	77.200	1.107	2214	3.477	99.920	0.767
1860	4.067	77.440	1.077	2222	3.244	100.544	0.325
1876	3.620	78.090	1.123	2228	3.197	101.004	0.631
1886	3.592	78.506	0.027	2230	3.375	101.156	0.414
1888	3.417	78.602	0.674	2232	3.012	101.308	0.602
1956	3.381	81.990	0.566	2246	3.619	102.392	0.202
1962	3.180	82.290	0.580	2266	3.692	103.940	0.678
1970	3.299	82.690	0.674	2266	3.511	103.940	0.762
1972	3.338	82.790	0.356	2276	3.595	104.712	0.572
1974	3.311	82.890	0.983	2282	3.341	105.176	0.486
1976	3.135	82.990	0.998	2284	3.266	105.330	0.662
1978	3.220	83.090	0.186	2286	3.479	105.484	0.879
1988	3.258	83.590	0.963	2288	3.130	105.639	0.323
2006	3.127	84.490	0.861	2290	3.251	105.793	0.515
2012	3.051	84.790	0.080	2294	3.353	106.102	0.394
2014	3.139	84.890	0.793	2304	3.983	106.874	0.879

Keine leeren Seiten!

Depth [cm]	$\delta^{18}O_{korr}$ C.w. (±0.07) [‰]	Age [ka BP]	$\delta^{13}C_{korr}$ C.w. (±0.04) [‰]
2314	3.608	107.650	0.514
2318	3.696	107.954	0.400
2320	3.658	108.108	0.507
2324	3.615	108.420	0.798
2326	3.353	108.584	0.507
2330	3.515	108.920	0.057
2332	3.475	109.100	0.929
2336	3.542	109.460	-0.180
2358	3.002	111.440	0.980
2368	3.420	112.350	0.547
2376	2.837	113.070	0.775
2380	2.958	113.432	0.480
2414	2.504	116.510	0.190
2418	2.448	116.878	0.802
2420	2.426	117.060	0.688
2422	2.404	117.240	0.616
2424	2.539	117.420	0.642
2428	2.503	117.780	0.481
2430	2.472	117.960	0.506
2434	2.591	118.320	0.758
2436	2.639	118.500	0.360
2438	2.646	118.680	0.760
2442	2.559	119.040	0.750
2446	2.571	119.400	0.760
2450	2.455	119.760	0.485
2454	2.583	120.120	0.370
2456	2.470	120.300	0.114
2458	2.542	120.480	0.374
2460	2.300	120.660	0.300
2462	2.632	120.840	0.815

Depth [cm]	$\delta^{18}O_{korr}$ C.w. (±0.07) [‰]	Age [ka BP]	$\delta^{13}C_{korr}$ C.w. (±0.04) [‰]
2464	2.537	121.020	0.472
2468	2.525	121.372	0.736
2470	2.618	121.550	0.438
2472	2.504	121.730	0.653
2474	2.598	121.910	0.758
2476	2.594	122.086	0.509
2478	2.418	122.262	0.581
2480	2.359	122.438	0.638
2482	2.725	122.614	0.078
2484	2.573	122.790	0.668
2488	2.898	123.142	-0.167
2490	3.027	123.318	0.083
2492	3.086	123.494	0.039
2494	4.008	123.670	0.412
2496	3.082	123.846	-0.019
2498	3.241	124.022	-0.187
2499	3.250	124.110	-0.239
2501	3.072	124.286	-0.068
2503	3.360	124.462	0.028
2513	3.872	125.346	0.482
2519	4.293	125.880	0.556
2521	4.218	126.056	0.219
2523	4.710	126.232	0.554
2525	4.281	126.408	0.143
2527	4.563	126.584	0.420
2529	4.551	126.760	0.241
2531	4.517	126.936	0.508
2533	4.345	127.112	0.136
2543	4.648	128.000	0.179
2547	4.660	128.354	0.201

Depth [cm]	$\delta^{18}O_{korr}$ C.w. (±0.07) [‰]	Age [ka BP]	$\delta^{13}C_{korr}$ C.w. (±0.04) [‰]
2549	4.349	128.530	0.137
2551	4.467	128.706	0.446
2553	4.582	128.882	0.264
2555	4.518	129.058	0.445
2561	4.610	129.586	0.240
2563	4.670	129.762	0.184
2567	4.589	130.120	0.264
2569	4.429	130.300	0.190
2573	4.661	130.652	0.217
2641	4.247	136.656	0.241
2647	4.309	137.184	-0.318
2649	3.877	137.360	-0.022
2651	4.190	137.536	-0.118
2691	3.840	137.712	0.781
2695	4.098	137.888	-0.372
2697	4.216	138.064	0.226
2701	4.210	138.240	0.238
2703	4.268	138.416	-0.062
2705	4.193	138.592	-0.354

Table 2.2a: A compilation of $\delta^{18}O$ and $\delta^{13}C$ of *G. ruber* (*G. r.*) for the core ODP 1058c

Depth [cm]	$\delta^{18}O_{korr}$ *G.r.* (±0.07) [‰]	Age [ka BP]	$\delta^{13}C_{korr}$ *G.r.* (±0.04) [‰]	Depth [cm]	$\delta^{18}O_{korr}$ *G.r.* (±0.07) [‰]	Age [ka BP]	$\delta^{13}C_{korr}$ *G.r.* (±0.04) [‰]
0	-1.557	0.23	0.608	31	-1.320	5.12	1.105
1	-1.274	0.47	1.546	32	-1.084	5.23	1.586
2	-1.542	0.70	0.727	33	-1.403	5.34	1.528
3	-1.365	0.94	1.077	34	-1.211	5.44	1.008
6	-1.267	1.66	1.419	35	-1.351	5.55	0.783
7	-1.166	1.89	1.022	36	-1.243	5.65	0.907
8	-1.204	2.13	1.397	37	-1.089	5.76	1.164
9	-1.133	2.36	0.840	38	-1.396	5.86	1.239
10	-1.271	2.59	0.800	39	-1.317	5.97	1.124
11	-1.465	2.81	1.198	40	-1.235	6.07	1.203
12	-1.304	2.94	1.347	41	-1.536	6.17	0.819
13	-0.996	3.06	1.290	42	-1.192	6.28	1.149
14	-1.151	3.18	1.327	43	-1.266	6.38	1.050
15	-1.072	3.30	1.486	44	-1.424	6.48	1.283
16	-1.194	3.42	0.952	45	-1.150	6.58	1.188
17	-1.315	3.53	1.383	46	-0.898	6.68	1.323
18	-1.434	3.65	0.985	47	-1.188	6.77	1.121
19	-1.309	3.77	1.249	48	-1.202	6.87	1.083
20	-1.433	3.89	1.393	49	-1.232	6.97	0.959
21	-1.188	4.00	1.058	50	-1.439	7.07	0.605
22	-1.218	4.12	0.763	51	-1.262	7.16	0.900
23	-1.410	4.23	0.608	52	-1.214	7.26	1.009
24	-0.819	4.34	1.095	53	-1.800	7.35	0.755
25	-1.510	4.46	1.194	54	-1.252	7.45	1.014
26	-1.215	4.57	1.395	55	-1.317	7.54	0.952
27	-1.585	4.68	1.139	56	-1.643	7.64	0.996
28	-1.006	4.79	1.052	57	-1.438	7.73	0.606
29	-1.078	4.90	0.850	58	-1.539	7.82	1.043
30	-1.198	5.01	0.943	59	-1.609	7.91	1.302

Depth [cm]	$\delta^{18}O_{korr}$ *G.r.* (±0.07) [‰]	Age [ka BP]	$\delta^{13}C_{korr}$ *G.r.* (±0.04) [‰]	Depth [cm]	$\delta^{18}O_{korr}$ *G.r.* (±0.07) [‰]	Age [ka BP]	$\delta^{13}C_{korr}$ *G.r.* (±0.04) [‰]
61	-1.335	8.09	0.916	91	-1.152	10.53	0.479
62	-1.586	8.18	1.310	92	-1.063	10.60	0.848
63	-1.748	8.27	0.897	94	-0.818	10.74	0.971
64	-1.248	8.36	1.352	95	-1.327	10.81	0.809
65	-1.059	8.45	1.372	96	-0.957	10.89	1.151
66	-1.442	8.53	1.197	97	-0.761	10.96	1.027
67	-1.406	8.62	1.464	98	-1.258	11.03	1.174
69	-0.948	8.79	0.510	99	-1.099	11.09	0.775
70	-1.447	8.88	1.147	100	-1.386	11.16	0.858
71	-1.192	8.96	1.312	101	-1.710	11.23	0.602
72	-1.374	9.04	1.200	102	-1.167	11.30	1.057
73	-1.803	9.13	0.735	103	-0.710	11.37	0.628
74	-1.042	9.21	1.285	104	-1.253	11.43	0.991
75	-1.188	9.29	0.486	105	-0.732	11.50	0.876
76	-1.067	9.37	0.712	106	-0.814	11.56	1.013
77	-0.865	9.45	0.674	107	-0.580	11.63	0.877
78	-1.318	9.53	1.201	108	-1.176	11.69	1.065
79	-1.026	9.61	0.844	109	-1.075	11.75	1.638
80	-0.854	9.69	0.848	110	-1.072	11.82	0.795
81	-1.306	9.77	0.911	111	-1.142	11.88	1.040
82	-0.933	9.85	1.144	112	-1.232	11.94	0.945
83	-0.838	9.93	0.878	113	-1.300	12.00	0.643
84	-0.825	10.00	1.015	114	-1.475	12.07	1.153
85	-0.828	10.08	1.167	115	-0.787	12.13	0.711
86	-1.283	10.16	1.384	116	-1.040	12.19	0.864
87	-1.022	10.24	0.833	117	-0.774	12.25	0.508
88	-1.284	10.31	1.215	118	-0.808	12.31	1.101
89	-0.701	10.38	0.961	119	-0.663	12.37	1.019
90	-0.437	10.45	0.787	120	-0.723	12.43	0.884

Depth [cm]	$\delta^{18}O_{korr}$ *G.r.* (±0.07) [‰]	Age [ka BP]	$\delta^{13}C_{korr}$ *G.r.* (±0.04) [‰]
120	-0.723	12.43	0.884
121	-1.635	12.49	1.225
122	-0.539	12.55	0.865
123	-0.780	12.61	1.260
124	-0.726	12.66	0.835
125	-0.990	12.72	0.988
126	-0.462	12.77	0.979
127	-0.264	12.83	0.547
128	-1.104	12.89	0.874
130	-0.268	12.99	0.803
130	-0.856	12.99	1.331
131	-0.688	13.05	0.891
132	-0.131	13.10	0.794
133	-0.507	13.15	0.901
134	-0.533	13.20	0.907
135	-0.615	13.26	0.832
136	-0.718	13.31	0.869
137	-0.586	13.36	0.685
138	-0.775	13.42	0.910
139	0.053	13.47	0.758
140	-0.358	13.53	1.038
141	-0.422	13.58	0.974
142	-0.373	13.64	0.795
143	-0.293	13.68	0.874
144	-0.276	13.73	0.808
145	-0.471	13.78	0.941
146	-0.296	13.84	0.657
147	-0.211	13.89	1.166
148	-0.464	13.93	1.066
149	-0.340	13.98	0.596
150	-0.643	14.03	0.751
151	-0.385	14.08	0.971
152	-0.495	14.13	0.619
153	-0.191	14.18	0.635
155	-0.286	14.28	0.746
156	-0.383	14.31	0.829
157	-0.453	14.34	0.996
158	-0.759	14.39	0.758
159	-0.353	14.44	0.722
161	0.215	14.63	0.650
163	-0.604	14.68	0.751
165	-0.271	14.77	0.701
167	-0.077	14.87	0.939
168	0.433	14.92	0.344
169	-0.069	14.97	0.678
171	-0.371	15.07	0.860
172	-0.057	15.12	0.987
173	0.021	15.17	0.467
177	-0.011	15.37	0.901
179	-0.270	15.47	0.915
181	-0.238	15.57	0.616
183	-0.104	15.67	0.746
185	0.030	15.77	0.628
193	-0.371	16.16	0.588

Table 2.2b: A compilation of $\delta^{18}O$ and $\delta^{13}C$ of *G. ruber* for the core ODP 1058c

Depth [cm]	$\delta^{18}O_{korr}$ *G.r.* (±0.07) [‰]	Age [ka BP]	$\delta^{13}C_{korr}$ *G.r.* (±0.04) [‰]	Depth [cm]	$\delta^{18}O_{korr}$ *G.r.* (±0.07) [‰]	Age [ka BP]	$\delta^{13}C_{korr}$ *G.r.* (±0.04) [‰]
1790	-0.127	70.08	0.648	1848	-0.111	72.54	0.915
1791	-0.321	70.11	0.790	1850	0.173	72.67	0.932
1792	-0.377	70.14	1.224	1852	-0.274	72.80	0.277
1794	-0.206	70.21	1.037	1854	-0.188	72.92	0.604
1796	-0.298	70.28	1.046	1856	-0.220	73.05	1.046
1798	-0.117	70.35	0.879	1858	-0.679	73.18	0.870
1800	-0.248	70.41	1.120	1860	-0.107	73.30	0.381
1802	-0.084	70.48	0.710	1862	-0.301	73.43	0.866
1804	-0.437	70.55	0.547	1864	-0.151	73.56	1.212
1807	-0.140	70.65	0.784	1866	-0.115	73.69	0.719
1808	-0.463	70.68	1.029	1868	-0.335	73.81	0.456
1810	-0.202	70.75	1.080	1870	-0.621	73.94	0.343
1814	-0.316	70.89	0.350	1872	-0.283	74.07	1.361
1816	-0.182	70.95	1.086	1874	-0.483	74.19	0.671
1818	0.009	71.02	0.715	1876	-0.507	74.32	0.787
1820	-0.575	71.09	0.321	1878	-0.470	74.45	0.728
1822	-0.276	71.16	1.426	1880	-0.244	74.58	1.280
1824	-0.399	71.22	0.676	1882	-0.657	74.70	0.276
1826	-0.170	71.29	0.987	1884	-0.589	74.83	0.635
1828	-0.284	71.36	0.674	1886	-0.316	74.98	1.007
1830	-0.695	71.43	0.969	1888	-0.316	75.13	0.893
1832	-0.427	71.52	0.908	1956	-0.754	80.16	0.925
1834	-0.319	71.65	0.394	1958	-0.664	80.31	0.452
1836	-0.043	71.78	1.097	1960	-0.661	80.46	0.693
1838	-0.082	71.91	0.988	1962	-1.141	80.61	0.309
1840	-0.055	72.03	0.516	1964	-0.504	80.75	0.293
1844	0.047	72.29	0.953	1966	-0.601	80.90	0.758
1846	-0.078	72.41	0.916	1968	-0.774	81.05	0.323

Depth [cm]	$\delta^{18}O_{korr}$ *G.r.* (±±0.07) [‰]	Age [ka BP]	$\delta^{13}C_{korr}$ *G.r.* (±0.04) [‰]	Depth [cm]	$\delta^{18}O_{korr}$ *G.r.* (±0.07) [‰]	Age [ka BP]	$\delta^{13}C_{korr}$ *G.r.* (±0.04) [‰]
1970	-0.789	81.20	0.306	2038	-0.446	86.45	0.855
1972	-0.658	81.34	1.113	2042	-0.551	86.78	0.344
1974	-0.827	81.49	0.965	2046	-0.879	87.11	0.557
1976	-0.555	81.64	0.640	2048	-0.569	87.27	0.301
1978	-0.641	81.79	0.485	2050	-1.140	87.43	1.458
1980	-0.744	81.93	1.177	2054	-0.868	87.76	1.465
1982	-0.294	82.08	0.552	2056	-0.333	87.93	0.730
1984	-1.064	82.23	0.565	2058	-0.892	88.09	0.539
1986	-0.916	82.38	0.864	2060	-0.561	88.25	0.750
1988	-1.362	82.52	0.110	2134	-0.782	94.32	0.320
1990	-0.540	82.67	0.205	2134	-0.787	94.32	0.578
1994	-0.796	82.96	0.988	2136	-0.474	94.49	1.146
1996	-1.168	83.11	1.213	2136	-0.761	94.49	0.635
2000	-0.596	83.41	0.886	2138	-0.882	94.65	0.646
2002	-0.801	83.55	1.131	2140	-0.882	94.82	0.943
2006	-0.312	83.85	0.828	2142	-0.606	94.98	-0.143
2008	-0.782	84.00	0.799	2144	-0.701	95.14	0.666
2010	-0.924	84.15	0.775	2146	-0.939	95.31	0.558
2012	-0.870	84.32	0.734	2148	-1.092	95.47	0.949
2014	-0.274	84.48	0.898	2150	-0.861	95.62	0.067
2016	-0.591	84.64	0.860	2152	-0.891	95.77	0.848
2018	-0.424	84.81	0.795	2154	-0.616	95.92	0.718
2020	-0.360	84.97	1.000	2156	-0.804	96.07	0.907
2022	-0.282	85.14	1.108	2158	-1.039	96.22	0.388
2024	-0.429	85.30	0.949	2160	-0.288	96.37	0.481
2026	-0.398	85.46	1.084	2162	-0.711	96.52	0.284
2028	-0.345	85.63	0.869	2164	-0.738	96.67	0.211
2030	-0.552	85.79	1.302	2166	-1.213	96.82	0.547
2032	-0.080	85.96	0.634	2168	-1.360	96.97	0.454
2036	-0.601	86.28	0.298	2170	-0.525	97.12	0.797

Depth [cm]	$\delta^{18}O_{korr}$ *G.r.* (±0.07) [‰]	Age [ka BP]	$\delta^{13}C_{korr}$ *G.r.* (±0.04) [‰]
2172	-1.164	97.27	-0.034
2174	-1.233	97.42	1.097
2176	-0.983	97.57	0.123
2178	-0.926	97.72	0.692
2178	-0.257	97.72	0.517
2180	-0.766	97.87	0.429
2182	-1.007	98.02	0.658
2184	-0.812	98.17	-0.669
2186	-0.991	98.32	0.064
2188	-1.025	98.47	-0.166
2190	-0.883	98.62	0.681
2192	-0.859	98.77	0.497
2194	-0.716	98.92	0.308
2196	-0.839	99.07	0.611
2198	-0.935	99.22	0.613
2200	-0.687	99.37	0.893
2202	-0.621	99.52	0.521
2204	-1.487	99.67	0.956
2206	-1.206	99.82	0.699
2208	-1.513	99.97	0.136
2212	-0.563	100.27	-0.851
2214	-0.356	100.42	0.040
2216	-0.669	100.57	-0.155
2218	-1.297	100.72	0.235
2220	-0.446	100.87	0.065
2222	-0.523	101.02	0.130
2224	-0.766	101.17	0.376
2226	-1.587	101.32	0.622
2228	-0.668	101.47	0.364
2230	-0.303	101.62	0.268
2232	-0.227	101.77	0.222
2234	-0.175	101.92	0.337
2236	-0.574	102.07	-0.064
2238	-0.866	102.23	0.116
2240	-0.407	102.38	0.487
2242	-0.848	102.53	0.583
2244	-0.420	102.68	0.348
2246	-0.646	102.83	0.410
2248	-0.187	102.98	0.486
2250	-1.174	103.13	0.830
2252	-0.574	103.28	0.252
2254	-1.119	103.43	0.839
2256	-0.659	103.58	0.324
2258	-0.989	103.73	0.122
2260	-1.722	103.88	-0.119
2262	-1.150	104.03	0.188
2264	-1.005	104.18	0.422
2266	-1.410	104.33	1.179
2266	-1.341	104.33	0.691
2268	-0.789	104.48	0.352
2270	-0.742	104.63	0.458
2272	-1.157	104.78	-0.271
2274	-1.352	104.93	1.269
2276	-0.635	105.08	0.548
2278	-0.891	105.23	0.392
2280	-0.855	105.38	0.215
2282	-0.954	105.53	0.304
2284	-0.948	105.81	0.499
2286	-0.780	106.09	0.733
2288	-0.529	106.36	0.495

Depth [cm]	$\delta^{18}O_{korr}$ *G.r.* (±0.07) [‰]	Age [ka BP]	$\delta^{13}C_{korr}$ *G.r.* (±0.04) [‰]
2290	-0.285	106.64	0.336
2290	-0.311	106.64	0.354
2292	-0.476	106.92	0.751
2292	-0.804	106.92	0.544
2294	-0.615	107.20	0.968
2294	-0.762	107.20	0.352
2296	-0.538	107.48	0.502
2298	-0.178	107.76	0.301
2300	-0.485	108.03	0.239
2302	-0.378	108.31	0.812
2304	-0.447	108.59	0.481
2306	0.010	108.79	0.572
2308	-0.437	108.99	0.282
2310	-0.428	109.19	0.701
2312	-0.457	109.39	0.608
2314	-0.706	109.59	0.580
2316	-0.717	109.79	0.590
2318	-0.171	109.98	0.842
2320	-0.721	110.18	0.480
2322	-0.510	110.38	0.875
2324	-0.364	110.58	0.704
2326	-0.306	110.78	0.572
2328	-0.573	110.98	0.787
2330	-0.155	111.18	0.349
2332	-0.111	111.38	0.389
2334	-0.558	111.58	0.205
2336	-0.556	111.78	0.127
2338	-0.560	111.98	0.359
2340	-0.552	112.18	0.491
2342	-0.466	112.37	0.536
2344	-0.285	112.57	0.398
2346	-0.478	112.77	0.381
2348	-0.593	112.97	0.602
2350	-0.901	113.17	0.721
2356	-0.525	113.77	0.852
2358	-0.677	113.97	0.387
2360	-0.917	114.17	0.813
2364	-0.725	114.57	0.264
2366	-1.095	114.77	0.086
2368	-0.669	114.96	0.407
2370	-0.377	115.16	0.435
2372	-0.783	115.36	0.231
2374	-0.677	115.56	0.479
2376	-0.564	115.76	0.472
2378	-0.898	115.96	0.519
2380	-1.229	116.16	0.401
2382	-0.809	116.36	0.324
2384	-0.998	116.56	0.074
2386	-0.991	116.76	0.300
2388	-1.023	116.96	0.186
2390	-1.399	117.16	0.542
2392	-1.215	117.35	0.152
2394	-0.974	117.55	0.448
2396	-1.424	117.75	0.007
2398	-1.396	117.95	0.892
2400	-1.452	118.15	0.129
2402	-0.970	118.35	0.429
2404	-1.128	118.55	0.219
2406	-1.063	118.75	0.506
2408	-1.173	118.95	-0.043

Depth [cm]	$\delta^{18}O_{korr}$ *G.r.* (±0.07) [‰]	Age [ka BP]	$\delta^{13}C_{korr}$ *G.r.* (±0.04) [‰]
2410	-1.356	119.15	0.249
2412	-1.303	119.35	-0.449
2414	-1.080	119.55	0.228
2416	-1.693	119.75	0.342
2420	-1.223	120.14	-0.578
2422	-1.378	120.34	-0.591
2424	-1.331	120.54	-0.861
2426	-1.092	120.74	-0.317
2428	-1.546	120.94	-0.107
2430	-1.329	121.14	-0.221
2432	-1.259	121.34	0.391
2434	-1.637	121.54	-0.057
2436	-0.970	121.74	-0.070
2438	-0.836	121.94	-0.090
2505	0.441	131.00	0.765
2511	0.469	132.12	0.355
2515	0.671	132.86	0.171
2517	0.515	133.23	0.031
2519	0.482	133.60	0.706
2521	0.289	133.98	0.533
2523	0.297	134.35	0.591
2603	0.787	149.93	0.976
2629	0.630	155.01	0.526
2633	0.397	155.79	0.606
2641	0.359	157.35	1.134
2643	0.313	157.75	0.559
2647	0.519	158.53	0.656
2649	0.422	158.92	0.531
2651	0.113	159.31	0.341
2653	0.253	159.70	0.400

Depth [cm]	$\delta^{18}O_{korr}$ *G.r.* (±0.07) [‰]	Age [ka BP]	$\delta^{13}C_{korr}$ *G.r.* (±0.04) [‰]
2655	0.766	160.09	0.934
2657	0.519	160.48	0.639
2659	0.231	160.87	0.270
2667	0.673	162.43	0.571
2669	0.631	162.82	0.118
2673	0.240	163.60	-0.026
2675	0.828	164.00	0.145
2677	0.706	164.39	0.156
2681	0.264	165.17	0.748
2683	0.513	165.56	0.914
2685	0.504	165.95	0.181
2689	0.404	166.73	0.413
2691	0.438	167.12	0.466
2693	0.190	167.51	0.538
2695	0.431	167.90	0.408
2697	0.440	168.29	0.477
2699	0.361	168.68	0.650
2701	0.400	169.07	0.332
2703	0.313	169.46	0.411
2707	0.275	170.24	0.138
2709	0.639	170.64	0.118
2711	0.225	171.03	0.890
2713	0.678	171.42	0.340
2715	0.562	171.81	0.353
2717	0.453	172.20	0.024
2719	0.400	172.59	-0.031
2721	0.836	172.98	0.227

Table 2.3a: 1st part of the compilation of Mg/Ca measurements for *G. ruber* for the core ODP 1058c

Depth [cm]	Age [ka BP]	Mg/Ca (±0.04) [mmol/mol]	$T_{Mg/Ca}$ [°C]	Sr/Ca (±0.04) [mmol/mol]	Depth [cm]	Age [ka BP]	Mg/Ca (±0.04) [mmol/mol]	$T_{Mg/Ca}$ [°C]	Sr/Ca (±0.04) [mmol/mol]
0	0.23	5.03	28.70	1.38	31	5.12	4.73	28.02	1.35
1	0.47	4.65	27.82	1.38	32	5.23	5.06	28.76	1.33
2	0.70	4.45	27.33	1.35	34	5.44	4.83	28.24	1.29
3	0.94	4.65	27.83	1.36	35	5.55	4.08	26.38	1.33
6	1.66	4.62	27.76	1.36	36	5.65	4.45	27.34	1.33
7	1.89	4.31	26.98	1.36	37	5.76	4.28	26.90	1.35
8	2.13	4.36	27.12	1.36	38	5.86	4.58	27.66	1.38
9	2.36	4.26	26.85	1.28	39	5.97	4.45	27.35	1.33
10	2.59	4.45	27.33	1.30	40	6.07	4.32	27.00	1.30
11	2.81	5.09	28.84	1.34	41	6.17	4.76	28.08	1.35
12	2.94	4.83	28.24	1.36	42	6.28	4.64	27.81	1.34
14	3.18	4.78	28.12	1.35	43	6.38	4.57	27.64	1.36
15	3.30	4.97	28.57	1.36	44	6.48	4.58	27.65	1.37
17	3.53	5.18	29.03	1.39	45	6.58	4.59	27.69	1.36
19	3.77	4.88	28.37	1.36	46	6.68	4.28	26.90	1.38
20	3.89	4.55	27.59	1.40	47	6.77	4.88	28.37	1.33
21	4.00	5.00	28.64	1.40	48	6.87	4.50	27.45	1.39
22	4.12	5.07	28.78	1.37	49	6.97	4.48	27.41	1.34
23	4.23	5.01	28.65	1.36	50	7.07	4.41	27.24	1.37
24	4.34	4.94	28.49	1.39	51	7.16	4.78	28.14	1.35
25	4.46	4.08	26.38	1.29	52	7.26	4.65	27.82	1.33
26	4.57	4.47	27.39	1.31	53	7.35	4.58	27.65	1.37
27	4.68	4.73	28.01	1.36	54	7.45	5.08	28.81	1.28
28	4.79	4.49	27.43	1.33	55	7.54	4.52	27.51	1.30
29	4.90	4.09	26.41	1.34	57	7.73	4.98	28.60	1.26
30	5.01	4.32	27.02	1.35	58	7.82	4.49	27.43	1.34

Depth [cm]	Age [ka BP]	Mg/Ca (±0.04) [mmol/mol]	$T_{Mg/Ca}$ [℃]	Sr/Ca (±0.04) [mmol/mol]
59	7.91	4.62	27.74	1.30
60	8.00	4.40	27.20	1.42
61	8.09	4.74	28.05	1.37
62	8.18	4.72	27.99	1.36
63	8.27	4.84	28.27	1.19
64	8.36	4.54	27.56	1.39
65	8.45	4.53	27.54	1.37
66	8.53	4.53	27.53	1.35
67	8.62	4.94	28.51	1.37
69	8.79	4.99	28.62	1.37
70	8.88	5.15	28.97	1.32
71	8.96	4.49	27.44	1.38
72	9.04	4.65	27.84	1.36
73	9.13	4.30	26.95	1.39
74	9.21	4.87	28.34	1.34
76	9.37	4.88	28.36	1.38
77	9.45	4.43	27.29	1.28
79	9.61	5.12	28.91	1.29
80	9.69	3.91	25.90	1.26
82	9.85	4.53	27.54	1.27
83	9.93	4.25	26.82	1.38
84	10.00	4.11	26.46	1.36
85	10.08	4.34	27.07	1.34
86	10.16	4.59	27.69	1.37
88	10.31	4.36	27.12	1.35
90	10.45	4.24	26.81	1.30
91	10.53	4.28	26.90	1.37

Depth [cm]	Age [ka BP]	Mg/Ca (±0.04) [mmol/mol]	$T_{Mg/Ca}$ [℃]	Sr/Ca (±0.04) [mmol/mol]
93	10.67	3.87	25.80	1.30
94	10.74	4.47	27.38	1.38
95	10.81	4.11	26.47	1.36
97	10.96	3.95	26.02	1.28
99	11.09	4.76	28.08	1.25
100	11.16	4.64	27.79	1.28
101	11.23	4.67	27.89	1.36
103	11.37	4.36	27.12	1.28
104	11.43	4.25	26.82	1.39
105	11.50	4.81	28.19	1.29
108	11.69	4.30	26.96	1.36
115	12.13	4.43	27.28	1.28
116	12.19	4.63	27.77	1.30
117	12.25	4.11	26.46	1.23
118	12.31	3.99	26.13	1.31
119	12.37	4.03	26.24	1.34
120	12.43	4.30	26.95	1.36
121	12.49	4.62	27.75	1.34
122	12.55	4.65	27.82	1.32
125	12.72	3.99	26.12	1.32
126	12.77	3.77	25.49	1.35
127	12.83	4.29	26.92	1.43
129	12.94	4.64	27.81	1.42
130	12.99	4.11	26.47	1.36
131	13.05	4.36	27.11	1.44
132	13.10	4.46	27.37	1.34
133	13.15	4.15	26.57	1.34

Depth [cm]	Age [ka BP]	Mg/Ca (±0.04) [mmol/mol]	$T_{Mg/Ca}$ [℃]	Sr/Ca (±0.04) [mmol/mol]
134	13.20	3.95	26.02	1.33
135	13.26	4.28	26.91	1.41
136	13.31	4.05	26.28	1.32
137	13.36	4.30	26.95	1.33
138	13.42	4.92	28.44	1.44
139	13.47	4.69	27.92	1.44
140	13.53	4.24	26.80	1.40
141	13.58	3.73	25.37	1.28
142	13.64	4.49	27.44	1.36
143	13.68	4.26	26.84	1.34
144	13.73	4.13	26.51	1.33
145	13.78	3.71	25.30	1.26
146	13.84	4.13	26.50	1.38
147	13.89	3.65	25.13	1.24
148	13.93	3.64	25.10	1.32
149	13.98	4.08	26.37	1.41
150	14.03	4.02	26.21	1.36
151	14.08	3.90	25.88	1.38
152	14.13	4.94	28.50	1.41
153	14.18	4.18	26.64	1.37
154	14.23	3.63	25.06	1.43
155	14.28	4.27	26.88	1.42
156	14.34	3.71	25.33	1.34
158	14.39	4.01	26.17	1.40
159	14.44	3.62	25.05	1.37
160	14.53	4.93	28.47	1.41
161	14.63	3.39	24.31	1.38
162	14.63	4.23	26.76	1.41

Depth [cm]	Age [ka BP]	Mg/Ca (±0.04) [mmol/mol]	$T_{Mg/Ca}$ [℃]	Sr/Ca (±0.04) [mmol/mol]
164	14.73	3.59	24.94	1.38
165	14.77	3.83	25.66	1.33
167	14.87	4.15	26.56	1.41
168	14.92	3.87	25.78	1.37
169	14.97	4.39	27.19	1.34
170	15.02	4.48	27.41	1.42
171	15.07	4.59	27.68	1.37
172	15.12	4.88	28.35	1.36
173	15.17	4.39	27.20	1.38
174	15.22	3.45	24.51	1.41
176	15.32	4.18	26.65	1.44
177	15.37	3.71	25.32	1.37
178	15.42	3.48	24.61	1.41
179	15.47	4.23	26.77	1.36
180	15.52	3.96	26.04	1.41
181	15.57	3.45	24.50	1.40
182	15.62	3.45	24.53	1.40
183	15.67	4.33	27.03	1.38
184	15.72	3.48	24.61	1.42
186	15.81	3.11	23.35	1.39
188	15.86	4.54	27.57	1.38
190	16.11	4.03	26.23	1.34
192	16.16	4.53	27.54	1.44
196	16.31	4.69	27.93	1.43

Table 2.3b: 2nd part of the compilation of Mg/Ca measurements for *G. ruber* for the core ODP 1058c

Depth [cm]	Age [ka BP]	Mg/Ca (±0.04) [mmol/mol]	$T_{Mg/Ca}$ [℃]	Sr/Ca (±0.04) [mmol/mol]	Depth [cm]	Age [ka BP]	Mg/Ca (±0.04) [mmol/mol]	$T_{Mg/Ca}$ [℃]	Sr/Ca (±0.04) [mmol/mol]
1700	73.54	3.52	24.75	1.39	1766	76.92	0.139	24.89	1.32
1701	73.59	3.22	23.75	1.37	1768	76.98	0.099	24.98	1.35
1702	73.64	3.35	24.19	1.38	1770	77.04	0.197	23.31	1.37
1704	73.74	3.89	25.84	1.38	1772	77.10	0.241	24.46	1.37
1706	73.84	3.71	25.32	1.39	1774	77.16	0.186	25.13	1.36
1712	74.14	3.64	25.10	1.37	1776	77.27	0.089	24.95	1.35
1714	74.24	3.86	25.76	1.36	1778	77.38	0.064	25.66	1.39
1718	74.44	3.39	24.30	1.34	1780	77.51	0.091	25.62	1.37
1720	74.56	3.40	24.35	1.37	1782	77.64	0.168	24.61	1.34
1722	74.70	3.48	24.61	1.38	1784	77.78	0.144	25.54	1.36
1726	75.00	2.91	22.63	1.35	1786	77.92	0.158	25.65	1.37
1728	75.15	3.79	25.55	1.35	1788	78.05	0.164	25.49	1.35
1730	75.30	3.39	24.32	1.34	1790	78.19	0.122	24.97	1.38
1732	75.45	3.69	25.26	1.39	1792	78.33	0.198	25.96	1.39
1734	75.61	3.12	23.40	1.38	1794	78.46	0.129	25.25	1.35
1736	75.76	3.63	25.09	1.35	1796	78.60	0.239	26.17	1.37
1738	75.91	3.71	25.33	1.35	1798	78.73	0.193	27.27	1.39
1740	76.04	3.60	24.98	1.38	1800	78.87	0.159	26.12	1.39
1742	76.15	3.92	25.93	1.39	1802	79.01	0.206	26.96	1.40
1746	76.32	4.10	26.42	1.40	1804	79.14	0.091	26.99	1.38
1748	76.38	3.89	25.83	1.35	1812	79.69	0.125	25.85	1.38
1750	76.44	4.65	27.83	1.34	1816	79.96	0.089	25.59	1.40
1752	76.50	3.97	26.07	1.36	1818	80.10	0.067	26.66	1.41
1754	76.56	3.63	25.06	1.36	1820	80.23	0.105	25.66	1.39
1756	76.62	4.19	26.68	1.39	1824	80.51	0.061	26.59	1.38
1760	76.74	4.46	27.36	1.41	1826	80.64	0.193	25.62	1.39
1764	76.86	3.29	23.98	1.36	1828	80.78	0.066	25.37	1.39

Depth [cm]	Age [ka BP]	Mg/Ca (±0.04) [mmol/mol]	$T_{Mg/Ca}$ [℃]	Sr/Ca (±0.04) [mmol/mol]
1830	80.92	3.80	25.57	1.39
1834	81.19	3.79	25.57	1.38
1836	81.32	4.10	26.42	1.38
1838	81.46	4.08	26.36	1.40
1840	81.60	3.62	25.03	1.39
1842	81.73	4.00	26.15	1.40
1844	81.87	4.03	26.23	1.38
1846	82.01	4.36	27.11	1.41
1848	82.14	4.29	26.92	1.39
1850	82.28	4.15	26.57	1.41
1852	82.41	4.20	26.69	1.38
1854	82.55	4.05	26.28	1.40
1856	82.69	4.11	26.46	1.41
1860	82.95	3.95	26.02	1.40
1862	83.06	4.59	27.69	1.41
1864	83.17	4.18	26.65	1.41
1866	83.27	3.87	25.79	1.33
1868	83.36	4.14	26.54	1.32
1870	83.46	4.13	26.50	1.31
1872	83.56	3.98	26.10	1.31
1874	83.66	3.44	24.47	1.31
1876	83.75	4.36	27.12	1.32
1878	83.85	3.99	26.12	1.25
1880	83.95	4.21	26.71	1.30
1882	84.04	3.90	25.87	1.29
1884	84.14	4.46	27.37	1.32
1886	84.24	3.68	25.24	1.27
1888	84.34	3.78	25.54	1.23
1892	84.53	4.15	26.57	1.36

Depth [cm]	Age [ka BP]	Mg/Ca (±0.04) [mmol/mol]	$T_{Mg/Ca}$ [℃]	Sr/Ca (±0.04) [mmol/mol]
1894	84.63	4.16	26.59	1.34
1896	84.72	4.15	26.56	1.40
1898	84.82	4.36	27.12	1.35
1900	84.92	4.68	27.89	1.41
1902	85.02	4.25	26.82	1.39
1904	85.11	3.89	25.84	1.37
1906	85.21	4.38	27.15	1.37
1908	85.31	4.63	27.78	1.38
1910	85.40	4.37	27.13	1.40
1912	85.50	4.56	27.60	1.40
1914	85.60	4.50	27.46	1.40
1916	85.70	4.36	27.11	1.35
1918	85.79	4.54	27.56	1.39
1920	85.89	5.42	29.53	1.40
1922	85.99	4.50	27.46	1.39
1924	86.09	4.51	27.49	1.38
1926	86.18	4.69	27.93	1.39
1928	86.28	4.57	27.63	1.40
1930	86.38	4.82	28.23	1.39
1932	86.47	4.56	27.60	1.38
1934	86.57	4.56	27.62	1.38
1936	86.67	4.22	26.75	1.37
1938	86.77	4.17	26.61	1.35
1940	86.86	4.40	27.21	1.40
1942	86.96	4.36	27.10	1.37
1944	87.06	4.03	26.24	1.37
1946	87.15	4.21	26.72	1.35
1948	87.25	4.05	26.28	1.33
1952	87.45	3.68	25.21	1.35

Depth [cm]	Age [ka BP]	Mg/Ca (±0.04) [mmol/mol]	$T_{Mg/Ca}$ [℃]	Sr/Ca (±0.04) [mmol/mol]
1954	87.54	3.64	25.10	1.36
1956	87.64	3.89	25.84	1.33
1958	87.74	4.06	26.32	1.37
1960	87.84	4.13	26.50	1.37
1962	87.94	3.90	25.87	1.36
1964	88.04	4.17	26.61	1.36
1966	88.14	3.83	25.68	1.36
1968	88.24	4.06	26.33	1.36
1970	88.33	3.93	25.95	1.39
1972	88.43	3.83	25.68	1.35
1974	88.53	3.85	25.74	1.37
1976	88.63	3.81	25.60	1.35
1978	88.73	4.22	26.76	1.37
1980	88.83	3.93	25.96	1.35
1982	88.93	4.22	26.74	1.36
1984	89.03	3.57	24.89	1.36
1986	89.12	4.12	26.48	1.38
1988	89.22	3.88	25.81	1.36
1994	89.52	3.85	25.72	1.37
1996	89.62	4.28	26.90	1.37
1998	89.72	4.19	26.68	1.36
2000	89.82	4.20	26.69	1.38
2002	89.92	4.13	26.51	1.37
2004	90.03	4.08	26.36	1.37
2006	90.17	4.05	26.28	1.37
2008	90.31	4.07	26.35	1.38
2010	90.46	4.17	26.62	1.37
2012	90.60	4.16	26.59	1.37
2014	90.74	3.96	26.03	1.36

Depth [cm]	Age [ka BP]	Mg/Ca (±0.04) [mmol/mol]	$T_{Mg/Ca}$ [℃]	Sr/Ca (±0.04) [mmol/mol]
2018	91.03	3.97	26.08	1.35
2020	91.22	4.11	26.44	1.37
2022	91.47	4.18	26.64	1.38
2024	91.72	4.09	26.41	1.37
2026	92.00	4.14	26.53	1.37
2028	92.28	4.29	26.93	1.38
2030	92.57	4.21	26.71	1.39
2032	92.85	4.43	27.30	1.38
2034	93.13	4.35	27.10	1.37
2036	93.41	4.45	27.34	1.39
2038	93.69	4.57	27.63	1.38
2040	93.97	4.03	26.24	1.36
2042	94.25	4.45	27.33	1.36
2044	94.53	4.19	26.67	1.38
2046	94.81	4.21	26.72	1.37
2048	95.09	4.21	26.73	1.39
2050	95.37	4.60	27.70	1.39
2052	95.65	4.59	27.68	1.38
2054	95.93	4.22	26.74	1.36
2056	96.21	4.51	27.48	1.37
2058	96.49	4.42	27.25	1.40
2060	96.77	4.86	28.31	1.40
2062	97.06	4.65	27.83	1.42
2064	97.34	4.58	27.66	1.40
2066	97.62	4.60	27.72	1.40
2068	97.90	4.65	27.84	1.38
2070	98.18	4.41	27.24	1.36
2072	98.46	4.70	27.94	1.37
2074	98.74	4.39	27.18	1.37

Depth [cm]	Age [ka BP]	Mg/Ca (±0.04) [mmol/mol]	$T_{Mg/Ca}$ [℃]	Sr/Ca (±0.04) [mmol/mol]
2076	99.02	4.61	27.74	1.37
2078	99.30	4.75	28.07	1.37
2080	99.58	4.72	28.00	1.38
2082	99.86	4.67	27.86	1.35
2084	100.14	4.73	28.01	1.38
2086	100.42	4.51	27.48	1.39
2088	100.70	3.99	26.12	1.36
2090	100.98	4.36	27.11	1.39
2092	101.26	4.61	27.72	1.37
2094	101.55	4.25	26.84	1.35
2096	101.83	4.22	26.74	1.37
2098	102.11	4.11	26.46	1.35
2106		4.16	26.58	1.39
2108		4.63	27.79	1.42
2110		4.46	27.36	1.41
2112		3.94	25.97	1.37
2114		4.20	26.69	1.42
2120		4.36	27.11	1.40
2122		4.09	26.39	1.40
2124		4.38	27.15	1.43
2128		4.43	27.30	1.40
2130		4.46	27.36	1.40
2132		3.78	25.53	1.37
2136		4.26	26.85	1.41
2138		4.58	27.67	1.38
2148		5.19	29.05	1.37
2150	106.92	3.95	26.02	1.34
2152	107.08	4.70	27.95	1.40
2154	107.24	4.09	26.39	1.36

Depth [cm]	Age [ka BP]	Mg/Ca (±0.04) [mmol/mol]	$T_{Mg/Ca}$ [℃]	Sr/Ca (±0.04) [mmol/mol]
2156	107.38	5.28	29.24	1.45
2156		4.28	26.90	1.40
2158	107.52	3.97	26.07	1.36
2160	107.65	4.82	28.22	1.37
2160		4.65	27.84	1.38
2162	107.78	4.26	26.86	1.37
2162		4.40	27.21	1.41
2164	107.91	4.26	26.85	1.38
2166	108.09	4.45	27.33	1.38
2166		3.95	26.01	1.38
2168	108.28	3.90	25.87	1.37
2168		4.10	26.42	1.38
2170	108.47	4.44	27.32	1.39
2170		4.96	28.56	1.39
2172	108.66	4.50	27.47	1.40
2174	108.85	4.37	27.13	1.38
2176	108.97	4.25	26.83	1.39
2178	109.10	4.31	26.98	1.39
2178		4.80	28.17	1.38
2180	109.22	4.27	26.87	1.39
2182	109.35	4.69	27.92	1.37
2184	109.47	4.08	26.38	1.40
2184		4.15	26.57	1.36
2186	109.60	4.71	27.96	1.39
2186		4.63	27.79	1.39
2188	109.72	3.90	25.88	1.38
2190	109.85	3.76	25.47	1.38
2190		3.59	24.96	1.35
2192	109.97	4.18	26.65	1.39

Depth [cm]	Age [ka BP]	Mg/Ca (±0.04) [mmol/mol]	$T_{Mg/Ca}$ [℃]	Sr/Ca (±0.04) [mmol/mol]
2194	110.10	3.78	25.52	1.38
2196	110.22	3.89	25.84	1.39
2198	110.35	4.30	26.97	1.39
2198		4.84	28.28	1.36
2200	110.47	4.15	26.56	1.39
2200		3.82	25.63	1.38
2202		4.28	26.91	1.39
2204	110.72	3.74	25.42	1.39
2206	110.85	4.34	27.07	1.37
2208	110.98	4.08	26.38	1.37
2210	111.10	3.96	26.04	1.39
2216	111.48	5.10	28.85	1.42
2218	111.60	4.01	26.19	1.39
2220	111.76	4.36	27.11	1.40
2222	111.95	4.11	26.44	1.40
2224	112.14	4.50	27.47	1.40
2226	113.26	4.13	26.50	1.38
2228	114.39	4.15	26.56	1.40
2230	115.41	4.23	26.78	1.38
2232	116.32	4.26	26.85	1.38
2234	117.23	4.28	26.91	1.42
2236	117.91	4.10	26.43	1.38
2238	118.58	5.22	29.11	1.42
2240	119.26	4.48	27.41	1.39
2242	119.93	4.28	26.90	1.41
2244	120.61	4.50	27.45	1.40
2246	121.28	4.48	27.42	1.40
2248	121.96	4.49	27.43	1.41
2250	122.63	4.19	26.67	1.39

Depth [cm]	Age [ka BP]	Mg/Ca (±0.04) [mmol/mol]	$T_{Mg/Ca}$ [℃]	Sr/Ca (±0.04) [mmol/mol]
2252	123.31	4.27	26.89	1.40
2254	123.99	4.74	28.04	1.39
2256	124.66	4.62	27.75	1.39
2258	125.34	4.80	28.19	1.40
2260	126.01	4.75	28.07	1.41
2262	126.69	4.89	28.39	1.41
2264	127.36	4.66	27.86	1.40
2266	127.95	4.41	27.23	1.39
2268	128.53	4.43	27.30	1.39
2270	128.87	4.89	28.38	1.40
2272	128.97	4.55	27.59	1.39
2274	129.07	4.56	27.61	1.39
2276	129.17	4.49	27.43	1.41
2278	129.27	4.61	27.72	1.36
2280	129.36	4.77	28.11	1.40
2282	129.46	5.19	29.05	1.38
2284	129.56	4.49	27.45	1.37
2286	129.66	5.15	28.97	1.40
2288	129.76	4.53	27.54	1.38
2290	129.90	4.41	27.24	1.40
2292	130.10	4.71	27.96	1.40
2294	130.30	4.34	27.05	1.37
2322	131.43	5.66	30.00	1.42
2338	132.21	4.68	27.89	1.41
2340	132.31	5.64	29.97	1.44
2344	132.51	5.71	30.10	1.42
2350	132.80	5.30	29.29	1.42
2352	132.90	4.94	28.49	1.40
2354	133.00	6.20	31.03	1.41

Depth [cm]	Age [ka BP]	Mg/Ca (±0.04) [mmol/mol]	$T_{Mg/Ca}$ [℃]	Sr/Ca (±0.04) [mmol/mol]
2356	133.10	4.55	27.60	1.41
2359	133.24	4.66	27.84	1.42
2361	133.34	4.98	28.59	1.42
2363	133.44	6.03	30.72	1.38
2379	134.23	3.79	25.54	1.36
2381	134.32	4.31	26.98	1.24
2383	134.42	3.62	25.05	1.31
2451	137.83	3.71	25.32	1.39
2453	137.88	3.85	25.73	1.40
2455	137.96	3.69	25.27	1.41
2457	138.06	3.97	26.07	1.39
2459	138.15	3.81	25.61	1.40
2461	138.25	4.06	26.33	1.38
2463	138.35	4.25	26.84	1.37
2465	138.45	4.16	26.59	1.41
2467	138.55	4.31	26.99	1.42
2469	138.64	3.96	26.04	1.38
2473	138.84	4.02	26.20	1.39
2475	138.94	4.05	26.30	1.41
2477	139.04	3.99	26.14	1.42
2479	139.14	4.01	26.18	1.39
2481	139.23	4.04	26.28	1.42
2483	139.33	4.14	26.55	1.42
2485	139.43	3.84	25.69	1.39
2487	139.53	3.99	26.12	1.38
2491	139.72	3.93	25.96	1.42
2493	139.81	3.90	25.86	1.37
2495	139.90	4.77	28.11	1.43

Depth [cm]	Age [ka BP]	Mg/Ca (±0.04) [mmol/mol]	$T_{Mg/Ca}$ [℃]	Sr/Ca (±0.04) [mmol/mol]
2497	140.00	4.52	27.52	1.41
2499	140.09	4.41	27.24	1.42
2501	140.18	4.61	27.74	1.37
2503	140.27	4.45	27.35	1.32
2505	140.36	5.23	29.13	1.40
2507	140.45	4.48	27.42	1.36
2509	140.55	4.26	26.85	1.34
2511	140.64	4.23	26.76	1.31
2513	140.73	4.39	27.20	1.30
2515	140.82	4.38	27.16	1.27
2517	140.91	4.91	28.43	1.34
2521	141.10	3.85	25.73	1.41
2523	141.19	4.71	27.96	1.40
2525	141.28	4.32	27.02	1.41
2527	141.37	4.03	26.24	1.36
2535	141.74	5.05	28.75	1.28
2539	141.92	4.83	28.25	1.42
2543	142.11	4.58	27.67	1.36
2545	142.20	4.07	26.35	1.32
2549	142.38	3.88	25.82	1.35
2551	142.47	4.67	27.86	1.30
2553	142.56	4.86	28.31	1.33
2555	142.66	4.47	27.38	1.32
2557	142.75	4.85	28.30	1.35
2561	142.93	5.24	29.15	1.39
2563	143.02	5.01	28.65	1.37
2565	143.11	4.88	28.35	1.35
2567	143.21	5.41	29.51	1.31

Depth [cm]	Age [ka BP]	Mg/Ca (±0.04) [mmol/mol]	$T_{Mg/Ca}$ [℃]	Sr/Ca (±0.04) [mmol/mol]
2571	143.39	4.57	27.63	1.26
2575	143.57	5.92	30.51	1.39
2577	143.66	5.03	28.70	1.37
2579	143.76	5.48	29.65	1.38
2581	143.85	4.69	27.93	1.40
2583	143.94	4.77	28.11	1.40
2585	144.03	6.21	31.05	1.45
2587	144.12	5.67	30.03	1.41
2589	144.22	4.34	27.06	1.39
2591	144.40	4.18	26.65	1.39
2593	144.58	5.62	29.93	1.39
2595	144.70	5.05	28.74	1.40
2597	144.74	5.57	29.84	1.40
2599	144.79	5.27	29.21	1.38

Table 2.4a: A compilation of $\delta^{18}O$ and $\delta^{13}C$ of *G. trunca.* (*G. t.*) for the core ODP 1058c

Depth [cm]	$\delta^{18}O_{korr}$ *G.t.* (±0.07) [‰]	Age [ka BP]	$\delta^{13}C_{korr}$ *G.t.* (±0.04) [‰]	Depth [cm]	$\delta^{18}O_{korr}$ *G.t.* (±0.07) [‰]	Age [ka BP]	$\delta^{13}C_{korr}$ *G.t.* (±0.04) [‰]
0	0.795	0.23	1.091	27	0.404	4.68	0.704
0	0.389	0.23	0.873	28	0.522	4.79	0.933
1	0.768	0.47	0.735	29	0.425	4.90	1.129
2	0.669	0.70	0.752	30	0.588	5.01	0.973
3	0.530	0.94	0.600	32	0.638	5.23	1.157
6	0.585	1.66	0.937	33	0.457	5.34	1.055
7	0.613	1.89	1.013	34	0.372	5.44	0.855
8	0.509	2.13	0.685	35	0.460	5.55	1.059
9	0.773	2.36	1.324	36	0.534	5.65	0.992
10	0.430	2.59	0.212	37	0.975	5.76	1.097
11	0.617	2.81	0.979	38	0.502	5.86	0.536
12	0.630	2.94	0.828	39	0.695	5.97	1.036
13	0.673	3.06	0.956	40	0.777	6.07	1.032
14	0.629	3.18	0.966	41	0.512	6.17	0.916
15	0.692	3.30	1.162	42	0.671	6.28	0.942
16	0.705	3.42	1.021	43	0.641	6.38	1.111
17	0.646	3.53	1.086	44	0.662	6.48	0.992
18	0.781	3.65	1.153	46	0.725	6.68	1.423
19	0.423	3.77	0.583	48	0.992	6.87	1.187
20	0.822	3.89	1.309	49	0.578	6.97	0.771
21	0.826	4.00	1.255	50	0.585	7.07	1.066
22	0.517	4.12	0.792	51	0.475	7.16	0.723
23	0.640	4.23	1.146	52	0.943	7.26	1.184
24	0.588	4.34	0.934	53	0.455	7.35	0.946
25	0.704	4.46	0.835	54	0.697	7.45	0.799
26	0.604	4.57	1.057	55	0.691	7.54	0.875

Depth [cm]	$\delta^{18}O_{korr}$ *G.t.* (±0.07) [‰]	Age [ka BP]	$\delta^{13}C_{korr}$ *G.t.* (±0.04) [‰]	Depth [cm]	$\delta^{18}O_{korr}$ *G.t.* (±0.07) [‰]	Age [ka BP]	$\delta^{13}C_{korr}$ *G.t.* (±0.04) [‰]
56	0.507	7.64	1.310	86	0.856	10.16	0.820
57	0.696	7.73	1.079	87	0.749	10.24	0.621
58	0.661	7.82	0.591	88	1.066	10.31	0.744
59	0.535	7.91	0.975	89	0.843	10.38	0.750
60	0.178	8.00	0.385	90	0.686	10.45	0.546
60	0.465	8.00	0.716	91	1.027	10.53	1.060
60	0.504	8.00	-0.072	92	0.980	10.60	0.857
61	0.713	8.09	1.224	93	0.671	10.67	0.477
62	0.375	8.18	0.753	94	0.995	10.74	1.052
63	0.790	8.27	1.094	95	0.639	10.81	0.542
64	0.670	8.36	1.002	96	0.513	10.89	0.144
66	0.825	8.53	1.030	97	0.875	10.96	0.893
67	0.701	8.62	0.776	98	1.088	11.03	0.866
69	0.819	8.79	0.820	99	0.978	11.09	0.739
71	0.437	8.96	0.717	100	0.807	11.16	1.213
72	0.922	9.04	1.333	101	0.813	11.23	1.214
73	0.705	9.13	1.005	102	0.708	11.30	0.808
74	0.700	9.21	0.862	103	0.989	11.37	0.772
75	0.695	9.29	0.928	104	0.978	11.43	0.818
77	0.468	9.45	0.931	105	1.110	11.50	0.823
78	0.659	9.53	0.696	106	0.841	11.56	0.833
79	0.894	9.61	0.962	107	0.898	11.63	0.853
80	0.725	9.69	0.539	108	0.502	11.69	0.001
81	0.865	9.77	0.759	109	0.558	11.75	0.789
83	0.702	9.93	0.746	110	0.670	11.82	0.828
84	0.954	10.00	0.989	111	0.842	11.88	0.930
85	0.911	10.08	0.958	112	0.092	11.94	-0.388

Depth [cm]	$\delta^{18}O_{korr}$ *G.t.* (±0.07) [‰]	Age [ka BP]	$\delta^{13}C_{korr}$ *G.t.* (±0.04) [‰]
113	0.799	12.00	0.679
114	0.603	12.07	0.346
117	1.034	12.25	0.618
118	1.015	12.31	0.392
120	0.477	12.43	-0.165
121	0.307	12.49	-0.353
122	1.587	12.55	0.830
123	1.537	12.61	0.941
124	1.063	12.66	0.308
125	0.913	12.72	-0.126
126	1.434	12.77	0.629
127	1.479	12.83	0.683
128	0.462	12.89	-0.252
128	1.252	12.89	0.355
129	1.339	12.94	0.627
130	1.341	12.99	0.531
131	0.612	13.05	0.176
132	0.378	13.10	-0.730
133	0.664	13.15	-0.251
134	0.671	13.20	-0.456
135	1.505	13.26	1.026
136	1.311	13.31	0.714
137	1.407	13.36	0.680
138	1.066	13.42	0.810
139	1.266	13.47	0.436
141	0.937	13.58	-0.522
143	1.728	13.68	0.927
145	1.343	13.78	0.913
146	1.073	13.84	-0.365
147	1.558	13.89	0.461
148	1.711	13.93	0.951
148	1.073	13.93	0.283
149	1.293	13.98	0.376
150	0.559	14.03	0.147
151	1.332	14.08	0.160
152	1.137	14.13	-0.097
153	1.214	14.18	0.748
154	1.145	14.23	-0.008
155	0.682	14.28	0.027
156	1.069	14.31	-0.259
158	1.599	14.39	0.915
160	1.431	14.53	0.307
162	1.764	14.63	0.700
163	1.478	14.68	0.682
164	1.530	14.73	0.315
165	1.680	14.77	0.872
166	1.570	14.82	0.676
166	1.717	14.82	0.978
167	1.318	14.87	0.355
168	1.386	14.92	0.412
169	0.808	14.97	-0.039
170	1.751	15.02	0.630
170	1.507	15.02	0.631
171	1.414	15.07	0.425

Depth [cm]	$\delta^{18}O_{korr}$ *G.t.* (±0.07) [‰]	Age [ka BP]	$\delta^{13}C_{korr}$ *G.t.* (±0.04) [‰]
172	1.273	15.12	0.408
173	1.118	15.17	0.260
174	0.829	15.22	0.272
175	1.170	15.27	0.875
176	0.857	15.32	-0.197
177	1.315	15.37	0.100
178	1.486	15.42	0.857
179	0.868	15.47	-0.093
180	1.636	15.52	1.217
181	0.615	15.57	0.640
182	0.789	15.62	0.179
183	0.793	15.67	-0.512
184	1.429	15.72	0.734
185	1.719	15.77	0.653
186	0.333	15.81	-0.190
188	0.903	15.91	0.018
189	0.934	15.96	0.509
190	1.023	16.01	-0.127
193	0.952	16.16	0.826
194	1.140	16.21	0.097
195	1.784	16.26	1.443
198	1.852	16.41	0.911

Table 2.4b: A compilation of $\delta^{18}O$ and $\delta^{13}C$ of *G. trunca.* (*G. t.*) for the core ODP 1058c

Depth [cm]	$\delta^{18}O_{korr}$ *G.t.* (±0.07) [‰]	Age [ka BP]	$\delta^{13}C_{korr}$ *G.t.* (±0.04) [‰]	Depth [cm]	$\delta^{18}O_{korr}$ *G.t.* (±0.07) [‰]	Age [ka BP]	$\delta^{13}C_{korr}$ *G.t.* (±0.04) [‰]
1790	-0.119	70.08	-0.815	1848	1.475	72.54	0.472
1791	0.211	70.11	-0.384	1848	1.584	75.87	0.720
1792	1.128	70.14	0.738	1850	1.541	72.67	0.605
1794	1.481	70.21	0.903	1850	1.542	76.02	0.835
1796	1.246	70.28	0.383	1852	1.276	72.80	0.015
1798	0.971	70.35	0.523	1852	1.594	76.17	0.666
1800	0.344	70.41	-0.697	1854	1.476	76.32	1.287
1802	0.105	70.48	-0.486	1860	0.321	73.30	0.016
1804	0.070	70.55	-1.046	1862	0.494	73.43	0.651
1807	0.651	70.65	0.197	1862	0.962	76.91	-0.541
1808	0.963	70.68	0.011	1864	0.543	73.56	0.495
1812	0.545	73.43	0.123	1864	1.294	73.56	0.861
1816	1.343	73.69	1.153	1866	0.509	73.56	0.479
1818	1.665	73.81	1.193	1866	1.330	77.21	0.751
1820	1.281	73.94	0.973	1868	0.551	73.81	0.244
1822	1.317	74.07	1.377	1868	1.836	77.36	1.553
1826	1.140	74.32	1.225	1870	1.332	77.50	1.200
1828	1.223	74.45	1.275	1874	1.120	77.80	0.622
1832	1.863	74.70	1.093	1878	1.143	74.45	1.105
1834	1.102	74.83	0.113	1880	1.552	78.25	1.541
1838	1.401	75.13	0.199	1882	1.306	78.40	0.892
1842	1.446	72.16	0.592	1884	1.520	78.54	1.180
1842	1.473	75.42	0.552	1886	0.494	78.69	-0.099
1844	1.847	72.29	0.590	1956	1.152	80.16	0.773
1844	1.507	75.57	0.757	1958	1.197	80.31	0.928
1846	1.622	72.41	0.612	1960	1.282	80.46	0.964
1846	1.502	75.72	0.729	1962	1.213	80.61	0.610

Depth [cm]	$\delta^{18}O_{korr}$ *G.t.* (±0.07) [‰]	Age [ka BP]	$\delta^{13}C_{korr}$ *G.t.* (±0.04) [‰]	Depth [cm]	$\delta^{18}O_{korr}$ *G.t.* (±0.07) [‰]	Age [ka BP]	$\delta^{13}C_{korr}$ *G.t.* (±0.04) [‰]
1964	0.873	80.75	0.280	2030	1.463	85.79	0.863
1966	1.178	80.90	1.146	2030	1.685	85.79	0.974
1968	1.347	81.05	1.161	2030	1.563	85.79	0.980
1970	0.795	81.20	0.408	2032	1.664	85.96	1.129
1972	1.188	81.34	0.740	2032	1.374	85.96	0.788
1974	1.287	81.49	1.035	2034	1.522	86.12	1.024
1976	1.162	81.64	1.118	2036	1.023	86.28	0.211
1978	1.173	81.79	0.711	2036	1.350	86.28	0.455
1984	1.011	82.23	0.719	2038	1.014	86.45	0.987
1988	1.266	82.52	1.040	2040	0.754	86.61	0.337
2006	0.614	83.85	0.212	2042	0.286	86.78	-0.008
2008	1.341	84.00	0.870	2044	1.099	86.94	0.753
2010	1.210	84.15	0.929	2046	1.146	87.11	0.605
2012	1.357	84.32	1.019	2048	0.941	87.27	0.303
2014	1.070	84.48	0.489	2050	1.307	87.43	1.028
2016	1.531	84.64	0.993	2052	1.189	87.60	0.848
2018	1.790	84.81	0.862	2052	0.715	87.60	0.569
2020	0.978	84.97	0.610	2054	0.881	87.76	0.694
2020	1.389	84.97	0.985	2054	0.812	87.76	0.297
2022	1.376	85.14	0.961	2056	0.776	87.93	0.477
2022	1.279	85.14	0.712	2058	0.794	88.09	0.568
2024	1.498	85.30	0.902	2058	1.078	88.09	0.599
2024	1.401	85.30	0.916	2060	1.152	88.25	1.089
2026	1.334	85.46	0.976	2060	1.014	88.25	0.658
2026	1.278	85.46	0.740	2062	1.349	88.42	0.944
2028	1.275	85.63	0.834	2062	0.775	88.42	0.387
2028	1.434	85.63	0.666	2064	0.649	88.58	-0.310

Depth [cm]	$\delta^{18}O_{korr}$ *G.t.* (±0.07) [‰]	Age [ka BP]	$\delta^{13}C_{korr}$ *G.t.* (±0.04) [‰]	Depth [cm]	$\delta^{18}O_{korr}$ *G.t.* (±0.07) [‰]	Age [ka BP]	$\delta^{13}C_{korr}$ *G.t.* (±0.04) [‰]
2064	0.794	88.58	0.706	2112	0.960	92.52	0.563
2064	1.151	88.58	1.286	2114	1.167	92.68	0.836
2066	1.261	88.75	1.101	2116	0.880	92.85	0.426
2068	1.042	88.91	0.970	2118	0.714	93.01	0.238
2068	0.671	88.91	0.745	2120	0.985	93.18	0.569
2070	1.206	89.07	1.147	2122	0.636	93.34	0.351
2072	1.045	89.24	0.932	2124	0.918	93.50	0.795
2074	0.803	89.40	0.139	2126	1.019	93.67	0.484
2076	1.028	89.57	0.984	2128	0.581	93.83	-0.128
2076	0.170	89.57	-0.092	2130	1.056	94.00	0.631
2078	0.718	89.73	0.644	2132	1.065	94.16	0.485
2078	0.972	89.73	1.173	2134	1.325	94.32	1.257
2084	1.043	90.22	0.592	2136	1.159	94.49	1.033
2084	1.218	90.22	1.209	2138	0.971	94.65	0.727
2086	1.088	90.39	0.449	2140	1.389	94.82	0.656
2088	1.298	90.55	0.880	2142	1.004	94.98	0.448
2090	1.113	90.71	0.816	2144	1.216	95.14	0.566
2092	0.917	90.88	0.424	2146	0.900	95.31	0.219
2094	1.040	91.04	1.003	2148	1.241	95.47	1.043
2096	0.856	91.21	0.592	2150	0.788	95.62	0.308
2098	1.200	91.37	0.468	2152	1.113	95.77	0.984
2100	0.824	91.53	0.756	2154	1.162	95.92	0.572
2102	1.080	91.70	0.575	2156	0.691	96.07	-0.266
2104	0.584	91.86	0.129	2158	1.164	96.22	1.076
2106	0.621	92.03	0.066	2160	1.123	96.37	0.843
2108	0.727	92.19	-0.069	2162	1.073	96.52	1.049
2110	0.592	92.35	0.005	2164	0.699	96.67	0.443

Depth [cm]	$\delta^{18}O_{korr}$ *G.t.* (±0.07) [‰]	Age [ka BP]	$\delta^{13}C_{korr}$ *G.t.* (±0.04) [‰]	Depth [cm]	$\delta^{18}O_{korr}$ *G.t.* (±0.07) [‰]	Age [ka BP]	$\delta^{13}C_{korr}$ *G.t.* (±0.04) [‰]
2166	0.805	96.82	0.064	2216	1.013	100.57	0.469
2168	1.219	96.97	1.129	2218	1.036	100.72	0.131
2170	0.849	97.12	0.333	2218	0.710	100.72	0.190
2172	0.770	97.27	0.317	2220	1.083	100.87	0.472
2174	0.971	97.42	0.795	2222	1.109	101.02	0.717
2176	0.864	97.57	0.228	2224	0.928	101.17	0.688
2178	0.813	97.72	0.263	2224	0.612	101.17	-0.632
2180	1.079	97.87	0.557	2226	1.095	101.32	0.753
2182	0.742	98.02	0.351	2228	0.835	101.47	0.009
2184	0.891	98.17	0.347	2228	0.860	101.47	0.228
2186	1.233	98.32	0.843	2230	0.610	101.62	-0.136
2190	1.238	98.62	0.876	2230	1.219	101.62	0.938
2192	1.131	98.77	0.756	2232	1.082	101.77	0.633
2194	1.014	98.92	0.468	2232	0.771	101.77	0.183
2194	0.781	98.92	0.414	2234	1.078	101.92	0.344
2196	0.431	99.07	-0.880	2236	0.880	102.07	0.219
2196	1.059	99.07	0.541	2236	1.338	102.07	0.995
2198	1.209	99.22	0.380	2238	1.118	102.23	0.870
2198	0.696	99.22	-0.175	2238	0.983	102.23	0.125
2200	0.173	99.37	-0.269	2240	1.258	102.38	0.683
2202	0.986	99.52	0.261	2240	0.733	102.38	-0.401
2204	0.950	99.67	0.450	2242	1.328	102.53	0.924
2206	0.963	99.82	0.628	2244	1.331	102.68	0.859
2208	0.645	99.97	-0.302	2244	1.290	102.68	0.707
2210	1.111	100.12	0.758	2246	1.231	102.83	0.603
2212	0.522	100.27	-0.352	2246	1.326	102.83	0.580
2214	1.091	100.42	0.838	2248	1.231	102.98	0.566

Depth [cm]	$\delta^{18}O_{korr}$ *G.t.* (±0.07) [‰]	Age [ka BP]	$\delta^{13}C_{korr}$ *G.t.* (±0.04) [‰]	Depth [cm]	$\delta^{18}O_{korr}$ *G.t.* (±0.07) [‰]	Age [ka BP]	$\delta^{13}C_{korr}$ *G.t.* (±0.04) [‰]
2248	1.583	102.98	0.650	2292	0.984	106.92	0.167
2250	1.251	103.13	0.452	2292	0.339	106.92	-0.771
2252	0.563	103.28	-1.136	2292	1.081	106.92	0.546
2254	1.457	103.43	0.811	2294	1.367	107.20	0.613
2256	0.756	103.58	-0.416	2294	1.220	107.20	0.761
2258	1.166	103.73	0.235	2294	0.887	107.20	-0.044
2262	1.426	104.03	0.642	2296	0.899	107.48	0.259
2264	1.213	104.18	0.384	2298	0.951	107.76	0.029
2266	1.385	104.33	0.593	2300	1.206	108.03	0.894
2268	1.144	104.48	0.407	2302	1.089	108.31	0.683
2268	0.667	104.48	-0.493	2304	1.002	108.59	0.151
2270	1.088	104.63	0.642	2304	1.404	108.59	0.943
2272	1.128	104.78	0.191	2306	0.504	108.79	-0.443
2272	1.028	104.78	0.304	2308	1.187	108.99	0.497
2274	1.237	104.93	0.629	2308	0.958	108.99	0.556
2274	0.955	104.93	-0.185	2310	0.914	109.19	0.486
2276	0.957	105.08	-0.321	2310	0.756	109.19	0.202
2278	0.826	105.23	-0.257	2312	1.048	109.39	0.641
2280	1.208	105.38	0.466	2314	1.054	109.59	0.446
2282	1.101	105.53	0.192	2314	1.044	109.59	0.530
2284	1.184	105.81	0.409	2316	1.306	109.79	0.716
2284	1.203	105.81	0.218	2318	0.757	109.98	0.047
2286	1.348	106.09	0.695	2318	0.859	109.98	0.289
2286	0.935	106.09	0.108	2320	1.160	110.18	0.813
2288	1.224	106.36	0.723	2322	0.880	110.38	0.404
2290	1.556	106.64	0.680	2322	1.010	110.38	0.583
2290	0.821	106.64	-0.399	2324	0.778	110.58	-0.112

Depth [cm]	$\delta^{18}O_{korr}$ *G.t.* (±0.07) [‰]	Age [ka BP]	$\delta^{13}C_{korr}$ *G.t.* (±0.04) [‰]	Depth [cm]	$\delta^{18}O_{korr}$ *G.t.* (±0.07) [‰]	Age [ka BP]	$\delta^{13}C_{korr}$ *G.t.* (±0.04) [‰]
2324	1.032	110.58	0.459	2360	0.875	114.17	0.506
2326	1.117	110.78	0.565	2360	0.828	114.17	0.383
2326	1.091	110.78	0.165	2362	0.844	114.37	0.508
2328	0.979	110.98	0.394	2362	0.815	114.37	0.340
2330	1.028	111.18	0.107	2364	0.381	114.57	0.135
2332	1.263	111.38	0.770	2364	0.456	114.57	0.198
2332	0.901	111.38	0.615	2366	0.776	114.77	0.618
2334	1.153	111.58	0.747	2366	0.430	114.77	-0.005
2336	0.926	111.78	0.295	2368	0.765	114.96	0.783
2338	0.804	111.98	-0.182	2368	0.334	114.96	0.019
2338	1.205	111.98	0.713	2370	0.513	115.16	0.279
2340	0.859	112.18	0.784	2372	0.307	115.36	-0.031
2340	0.987	112.18	0.787	2372	0.714	115.36	0.429
2342	0.834	112.37	0.289	2374	0.640	115.56	0.574
2344	0.847	112.57	0.151	2374	0.777	115.56	0.480
2346	0.805	112.77	0.149	2376	0.303	115.76	-0.028
2346	0.820	112.77	0.485	2376	0.709	115.76	0.545
2348	1.098	112.97	0.761	2378	0.467	115.96	0.197
2348	1.059	112.97	0.578	2378	-0.032	115.96	0.570
2350	1.004	113.17	0.771	2380	0.439	116.16	0.322
2350	0.637	113.17	0.407	2380	0.542	116.16	0.363
2352	0.936	113.37	0.534	2382	0.266	116.36	-0.203
2354	0.684	113.57	0.278	2384	0.358	116.56	-0.176
2356	0.866	113.77	0.380	2384	0.679	116.56	0.616
2356	0.665	113.77	0.562	2386	0.451	116.76	0.143
2358	0.936	113.97	0.675	2388	0.015	116.96	-0.529

Depth [cm]	$\delta^{18}O_{korr}$ *G.t.* (±0.07) [‰]	Age [ka BP]	$\delta^{13}C_{korr}$ *G.t.* (±0.04) [‰]
2358	0.807	113.97	0.199
2360	0.875	114.17	0.506
2360	0.828	114.17	0.383
2362	0.844	114.37	0.508
2362	0.815	114.37	0.340
2364	0.381	114.57	0.135
2364	0.456	114.57	0.198
2366	0.776	114.77	0.618
2366	0.430	114.77	-0.005
2368	0.765	114.96	0.783
2368	0.334	114.96	0.019
2370	0.513	115.16	0.279
2372	0.307	115.36	-0.031
2372	0.714	115.36	0.429
2374	0.640	115.56	0.574
2374	0.777	115.56	0.480
2376	0.303	115.76	-0.028
2376	0.709	115.76	0.545
2378	0.467	115.96	0.197
2378	-0.032	115.96	0.570
2380	0.439	116.16	0.322
2380	0.542	116.16	0.363
2382	0.266	116.36	-0.203
2384	0.358	116.56	-0.176
2384	0.679	116.56	0.616
2386	0.451	116.76	0.143
2388	0.015	116.96	-0.529
2388	0.369	116.96	0.224
2390	0.608	117.16	0.429
2390	0.491	117.16	0.311
2392	0.293	117.35	0.121
2392	0.715	117.35	0.695
2394	0.469	117.55	0.558
2394	0.570	117.55	0.551
2396	0.597	117.75	0.445
2398	0.735	117.95	0.667
2400	0.597	118.15	0.341
2402	0.844	118.35	0.923
2404	0.245	118.55	0.018
2406	0.299	118.75	0.172
2406	0.563	118.75	0.556
2408	0.425	118.95	0.214
2408	0.262	118.95	0.025
2410	0.687	119.15	0.689
2412	0.498	119.35	0.173
2414	0.609	119.55	0.479
2416	0.450	119.75	0.353
2418	0.625	119.94	0.830
2420	0.520	120.14	0.172
2420	0.675	120.14	0.558
2422	0.364	120.34	0.026
2422	0.718	120.34	0.737

Depth [cm]	$\delta^{18}O_{korr}$ *G.t.* (±0.07) [‰]	Age [ka BP]	$\delta^{13}C_{korr}$ *G.t.* (±0.04) [‰]
2424	0.175	120.54	-0.295
2424	0.528	120.54	0.446
2426	0.420	120.74	0.317
2426	0.661	120.74	0.537
2428	0.369	120.94	0.294
2428	0.622	120.94	0.617
2430	0.352	121.14	-0.109
2430	0.696	121.14	0.725
2432	0.530	121.34	0.313
2432	0.615	121.34	0.327
2434	0.568	121.54	0.323
2434	0.651	121.54	0.453
2436	0.581	121.74	0.275
2436	0.744	121.74	0.676
2438	0.453	121.94	0.234
2438	0.663	121.94	0.596
2440	0.862	122.14	0.896
2442	0.677	122.33	0.217
2444	0.741	122.53	0.451
2446	0.625	122.73	0.724
2448	0.652	122.93	0.297
2450	0.674	123.13	0.580
2452	0.531	123.33	0.191
2454	0.058	123.53	-0.658
2462	0.237	124.33	-0.158
2472	0.843	125.32	-0.025
2486	1.376	127.39	0.234
2488	1.633	127.78	0.497
2490	1.565	128.18	0.319
2492	1.703	128.57	0.450
2496	1.985	129.33	0.583
2498	0.973	129.70	0.045
2499	1.087	129.89	0.403
2503	2.058	130.63	0.464
2505	1.474	131.00	0.375
2509	1.759	131.75	0.269
2513	1.393	132.49	0.125
2527	1.824	135.09	0.487
2531	1.332	135.87	1.104
2537	1.307	137.04	0.129
2547	1.614	139.00	-0.026
2567	1.955	142.90	1.057
2575	1.576	144.46	0.044
2577	1.584	144.86	0.402
2581	1.836	145.64	0.079
2603	1.901	149.93	0.400
2629	2.031	155.01	0.345
2633	1.986	155.79	0.619
2641	1.999	157.35	0.631
2643	2.084	157.75	0.830
2647	2.001	158.53	0.646
2649	1.875	158.92	0.303
2651	2.024	159.31	0.471
2653	1.761	159.70	0.310

Depth [cm]	$\delta^{18}O_{korr}$ *G.t.* (±0.07) [‰]	Age [ka BP]	$\delta^{13}C_{korr}$ *G.t.* (±0.04) [‰]
2655	1.827	160.09	0.505
2657	1.570	160.48	0.087
2659	1.700	160.87	0.310
2665	0.914	162.04	0.333
2667	1.660	162.43	0.470
2669	1.881	162.82	0.433
2673	1.917	163.60	0.522
2675	1.575	164.00	0.352
2677	1.932	164.39	0.714
2681	2.053	165.17	0.511
2683	2.026	165.56	0.690
2685	1.980	165.95	0.125
2695	1.680	167.90	0.191
2699	1.929	168.68	0.965
2703	1.738	169.46	0.109
2705	1.706	169.85	0.219

Table 2.5a: 1st part of the compilation of Mg/Ca measurements for *G. trunca.* for the core ODP 1058c

Depth [cm]	Age [ka BP]	Mg/Ca (±0.04) [mmol/mol]	$T_{Mg/Ca}$ [℃]	Depth [cm]	Age [ka BP]	Mg/Ca (±0.04) [mmol/mol]	$T_{Mg/Ca}$ [℃]	Depth [cm]	Age [ka BP]	Mg/Ca (±0.04) [mmol/mol]	$T_{Mg/Ca}$ [℃]
3	0.94	1.93	10.03	61	8.09	2.08	10.91	107	11.63	1.73	8.72
6	1.66	1.81	9.24	62	8.18	2.01	10.51	108	11.69	1.95	10.13
8	2.13	2.06	10.79	63	8.27	2.13	11.20	110	11.82	1.78	9.07
9	2.36	1.80	9.16	66	8.53	2.12	11.18	111	11.88	1.96	10.20
10	2.59	2.29	12.06	67	8.62	1.92	9.97	112	11.94	1.87	9.62
14	3.18	2.00	10.48	70	8.88	1.97	10.28	114	12.07	1.94	10.08
18	3.65	1.76	8.88	71	8.96	1.94	10.06	118	12.31	3.51	17.24
24	4.34	1.87	9.62	76	9.37	1.93	10.04	120	12.43	1.90	9.80
25	4.45	2.30	12.12	77	9.45	1.78	9.07	121	12.49	1.80	9.16
26	4.57	1.85	9.50	80	9.69	2.04	10.71	122	12.55	1.90	9.81
27	4.68	1.92	9.94	83	9.93	1.93	10.04	123	12.61	2.04	10.68
29	4.90	2.15	11.31	87	10.24	2.25	11.88	124	12.66	2.20	11.61
30	5.01	2.08	10.90	89	10.38	2.08	10.91	125	12.72	2.01	10.50
33	5.34	1.86	9.55	91	10.53	2.01	10.52	126	12.77	1.69	8.40
35	5.55	1.80	9.16	92	10.60	2.08	10.93	129	12.94	1.77	8.95
36	5.65	2.13	11.19	93	10.67	1.79	9.12	132	13.10	2.22	11.69
37	5.76	2.09	10.99	94	10.74	2.00	10.43	133	13.15	2.11	11.09
38	5.86	1.97	10.29	95	10.81	2.19	11.52	134	13.20	1.96	10.23
40	6.07	1.94	10.09	96	10.89	1.76	8.93	135	13.26	1.93	10.01
43	6.38	2.03	10.61	97	10.96	1.84	9.43	137	13.36	2.39	12.61
44	6.48	2.01	10.51	99	11.09	2.28	12.02	138	13.42	2.04	10.69
46	6.68	1.94	10.11	100	11.16	1.87	9.63	141	13.58	1.89	9.79
50	7.07	2.01	10.49	101	11.23	2.00	10.47	142	13.64	1.90	9.81
53	7.35	1.87	9.66	102	11.30	1.92	9.93	144	13.73	1.98	10.31
54	7.45	2.20	11.60	103	11.37	1.80	9.18	145	13.78	1.72	8.60
56	7.64	1.92	9.94	105	11.50	1.94	10.11	146	13.84	1.68	8.36
60	8.00	1.93	10.00	106	11.56	1.92	9.99	147	13.89	1.81	9.22

Depth [cm]	Age [ka BP]	Mg/Ca (±0.04) [mmol/mol]	$T_{Mg/Ca}$ [℃]
148	13.93	1.91	9.87
150	14.03	2.15	11.31
151	14.08	1.60	7.73
152	14.13	1.87	9.62
153	14.18	1.90	9.82
155	14.28	1.68	8.39
156	14.31	1.63	7.97
158	14.39	2.10	11.02
159	14.44	1.73	8.68
160	14.53	1.72	8.65
161	14.63	1.83	9.36
164	14.73	1.89	9.80
165	14.77	1.87	9.67
167	14.87	1.74	8.79
168	14.92	1.78	9.07
169	14.97	1.54	7.31
171	15.07	1.72	8.61
172	15.12	1.57	7.54
174	15.22	1.49	6.94
175	15.27	1.32	5.44
176	15.32	1.80	9.21
177	15.37	1.82	9.30
178	15.42	1.66	8.23
179	15.47	2.07	10.85
180	15.52	1.52	7.17
181	15.57	1.90	9.86
183	15.67	1.55	7.41

Depth [cm]	Age [ka BP]	Mg/Ca (±0.04) [mmol/mol]	$T_{Mg/Ca}$ [℃]
148	13.93	1.91	9.87
150	14.03	2.15	11.31
151	14.08	1.60	7.73
152	14.13	1.87	9.62
153	14.18	1.90	9.82
155	14.28	1.68	8.39
156	14.31	1.63	7.97
158	14.39	2.10	11.02
159	14.44	1.73	8.68
160	14.53	1.72	8.65
161	14.63	1.83	9.36
164	14.73	1.89	9.80
165	14.77	1.87	9.67
167	14.87	1.74	8.79
168	14.92	1.78	9.07
169	14.97	1.54	7.31
171	15.07	1.72	8.61
172	15.12	1.57	7.54
174	15.22	1.49	6.94
175	15.27	1.32	5.44
176	15.32	1.80	9.21
177	15.37	1.82	9.30
178	15.42	1.66	8.23
179	15.47	2.07	10.85
180	15.52	1.52	7.17
181	15.57	1.90	9.86
183	15.67	1.55	7.41

Table 2.5b: 2nd part of the compilation of Mg/Ca measurements for *G. trunca.* for the core ODP 1058c

Depth [cm]	Age [ka BP]	Mg/Ca (±0.04) [mmol/mol]	$T_{Mg/Ca}$ [°C]	Depth [cm]	Age [ka BP]	Mg/Ca (±0.04) [mmol/mol]	$T_{Mg/Ca}$ [°C]	Depth [cm]	Age [ka BP]	Mg/Ca (±0.04) [mmol/mol]	$T_{Mg/Ca}$ [°C]
1790	71.88	1.59	7.71	1938	81.09	2.00	10.47	2014	84.88	2.34	12.34
1792	72.02	2.33	12.30	1942	81.29	2.02	10.60	2016	84.98	2.04	10.71
1796	72.31	1.90	9.81	1944	81.39	1.89	9.74	2018	85.08	1.98	10.32
1807	73.10	1.87	9.67	1946	81.49	2.11	11.10	2022	85.28	2.16	11.36
1812	73.46	2.03	10.62	1948	81.59	1.87	9.64	2036	86.17	2.18	11.51
1864	77.60	1.76	8.93	1950	81.69	2.05	10.74	2038	86.32	2.08	10.92
1866	77.68	2.00	10.45	1956	81.99	2.11	11.10	2040	86.48	1.88	9.71
1868	77.76	2.18	11.49	1962	82.29	1.93	10.04	2042	86.63	2.14	11.26
1884	78.41	2.01	10.49	1964	82.39	2.21	11.67	2046	86.94	2.22	11.73
1886	78.49	1.84	9.46	1966	82.49	1.92	9.98	2048	87.09	1.94	10.08
1890	78.69	1.75	8.84	1968	82.59	1.90	9.86	2050	87.25	2.10	11.06
1894	78.89	1.78	9.02	1970	82.69	1.96	10.21	2052	87.40	2.16	11.37
1906	79.49	2.02	10.54	1972	82.79	1.90	9.82	2054	87.56	2.30	12.15
1908	79.59	1.96	10.22	1978	83.09	1.94	10.11	2056	87.71	2.19	11.55
1910	79.69	1.91	9.92	1980	83.19	2.08	10.92	2060	88.02	2.38	12.52
1912	79.79	1.93	10.02	1982	83.29	1.92	9.97	2070	88.79	2.59	13.55
1914	79.89	1.81	9.26	1986	83.49	2.06	10.81	2076	89.26	2.27	11.95
1916	79.99	2.02	10.56	1990	83.69	2.00	10.45	2084	89.88	2.18	11.51
1918	80.09	1.99	10.38	1992	83.79	2.21	11.63	2086	90.03	2.04	10.70
1920	80.19	2.02	10.55	1998	84.09	1.94	10.11	2088	90.18	2.03	10.61
1924	80.39	2.10	11.01	2000	84.19	2.15	11.33	2090	90.34	2.22	11.72
1926	80.49	2.06	10.84	2002	84.29	2.00	10.47	2092	90.50	2.04	10.72
1928	80.59	2.38	12.53	2004	84.39	2.19	11.53	2094	90.65	2.00	10.44
1930	80.69	1.92	9.96	2006	84.49	2.02	10.56	2096	90.80	2.07	10.86
1932	80.79	1.93	10.03	2008	84.59	2.10	11.06	2098	90.96	2.04	10.72
1934	80.89	2.04	10.69	2010	84.69	2.01	10.51	2100	91.12	2.36	12.46
1936	80.99	1.95	10.17	2012	84.79	2.39	12.60	2104	91.43	1.91	9.91

Depth [cm]	Age [ka BP]	Mg/Ca (±0.04) [mmol/mol]	$T_{Mg/Ca}$ [℃]
2106	91.58	2.11	11.10
2110	91.89	1.99	10.38
2112	92.04	1.92	9.93
2114	92.20	2.12	11.14
2116	92.35	2.41	12.68
2118	92.50	2.06	10.80
2120	92.66	2.06	10.81
2122	92.81	2.17	11.42
2124	92.97	2.06	10.79
2126	93.12	2.09	10.97
2130	93.43	2.23	11.74
2132	93.58	2.04	10.71
2134	93.74	2.21	11.64
2138	94.05	2.16	11.36
2140	94.20	1.84	9.47
2146	94.67	2.17	11.46
2148	94.82	1.94	10.07
2150	94.98	2.23	11.79
2158	95.60	2.02	10.59
2160	95.75	1.80	9.18
2162	95.90	2.10	11.06
2164	96.06	1.97	10.30
2166	96.21	1.91	9.87
2170	96.52	1.89	9.75
2172	96.67	2.04	10.66
2174	96.83	1.86	9.59
2176	96.99	1.80	9.18
2178	97.14	2.59	13.58
2180	97.30	1.75	8.85
2182	97.45	2.05	10.76
2184	97.60	2.00	10.44
2188	97.91	1.81	9.28
2190	98.07	1.92	9.97
2192	98.22	1.88	9.69
2200	98.84	2.27	11.99
2202	98.99	2.24	11.84
2206	99.30	2.32	12.22
2208	99.46	2.12	11.13
2210	99.61	1.94	10.08
2212	99.77	1.87	9.62
2214	99.92	1.83	9.40
2216	100.08	2.05	10.73
2220	100.38	2.02	10.57
2222	100.54	1.99	10.41
2226	100.85	2.05	10.78
2232	101.31	2.18	11.49
2234	101.46	1.98	10.35
2236	101.62	1.92	9.93
2246	102.39	2.04	10.72
2248	102.55	2.02	10.60
2250	102.70	1.76	8.90
2252	102.86	1.70	8.53
2254	103.01	2.59	13.58
2256	103.16	1.54	7.33
2258	103.32	1.65	8.13
2260	103.47	1.60	7.76
2266	103.94	2.02	10.60
2266	103.94	1.62	7.91
2270	104.25	2.08	10.94
2276	104.71	1.94	10.06
2278	104.87	1.93	10.00
2280	105.02	1.68	8.33
2288	105.64	1.77	9.00
2294	106.10	1.97	10.25
2296	106.26	1.89	9.79
2300	106.56	1.92	9.93
2302	106.72	1.87	9.67
2308	107.18	1.93	9.99
2312	107.49	2.08	10.93
2316	107.80	2.20	11.58
2320	108.11	1.70	8.49
2342	110.00	1.89	9.75
2352	110.90	2.10	11.04
2354	111.08	2.16	11.38
2362	111.81	2.26	11.93
2370	112.53	2.20	11.57
2372	112.71	2.13	11.20
2374	112.89	1.97	10.29
2376	113.07	2.17	11.42
2382	113.62	2.12	11.14
2384	113.80	2.07	10.89
2386	113.98	2.34	12.37
2390	114.34	2.30	12.15
2394	114.70	2.36	12.44

Depth [cm]	Age [ka BP]	Mg/Ca (±0.04) [mmol/mol]	$T_{Mg/Ca}$ [℃]
2396	114.88	2.17	11.44
2398	115.06	2.24	11.84
2400	115.25	2.24	11.83
2402	115.43	2.23	11.74
2404	115.61	2.15	11.34
2408	115.97	2.30	12.16
2418	116.87	2.19	11.56
2424	117.42	2.21	11.64
2428	117.78	1.96	10.23
2438	118.68	2.34	12.34
2442	119.04	2.15	11.30
2444	119.22	2.05	10.76
2446	119.40	2.17	11.42
2452	119.94	2.10	11.06
2454	120.12	2.01	10.51
2456	120.30	2.03	10.64
2464	121.02	1.91	9.91
2466	121.20	1.72	8.65
2486	122.97	1.89	9.79
2488	123.14	2.02	10.59
2492	123.50	2.04	10.71
2496	123.85	1.93	10.04
2498	124.02	2.05	10.74
2503	124.46	1.88	9.67
2507	124.82	1.95	10.15
2509	124.99	2.25	11.86
2563	129.77	1.91	9.92
2577	131.00	1.73	8.67
2579	131.18	1.80	9.19
2603	133.30	1.99	10.39
2629	135.60	2.12	11.15
2643	136.83	1.74	8.81
2649	137.36	2.06	10.78
2653	137.71	1.82	9.30
2657	138.07	2.04	10.68
2659	138.25	1.90	9.82
2667	138.95	2.03	10.60
2669	139.13	1.67	8.30
2673	139.48	1.94	10.07
2677	139.84	1.82	9.31
2681	140.19	2.19	11.55
2683	140.36	1.96	10.20

Table 2.6: Compilation of the Uk´37 measurements for the core ODP 1058c

Depth [cm]	Age [ka bp]	Uk´37	$T_{Mg/Ca}$ [℃]	Depth [cm]	Age [ka bp]	Uk´37	$T_{Mg/Ca}$ [℃]
2358	124.02	0.837	24.03	2429	130.05	0.743	21.18
2367	124.82	0.74	21.09	2432	130.72	0.75	21.39
2373	125.10	0.755	21.55	2433	130.82	0.753	21.48
2385	128.03	0.776	22.18	2435	130.91	0.751	21.42
2387	128.12	0.774	22.12	2437	131.00	0.755	21.55
2389	128.21	0.772	22.06	2439	131.18	0.726	20.67
2391	128.30	0.767	21.91	2441	131.27	0.719	20.45
2393	128.39	0.777	22.21	2443	131.36	0.733	20.88
2395	128.48	0.762	21.76	2445	131.46	0.72	20.48
2397	128.58	0.761	21.73	2447	131.55	0.731	20.82
2399	128.67	0.746	21.27	2449	131.64	0.717	20.39
2401	128.76	0.758	21.64	2451	137.83	0.747	21.3
2403	128.85	0.725	20.64	2453	137.88	0.739	21.06
2405	128.94	0.731	20.82	2455	137.96	0.736	20.97
2407	129.04	0.728	20.73	2457	138.06	0.735	20.94
2409	129.13	0.738	21.03	2459	138.15	0.736	20.97
2411	129.22	0.742	21.15	2461	138.25	0.73	20.79
2413	129.31	0.746	21.27	2465	138.45	0.723	20.58
2415	129.40	0.744	21.21	2467	138.55	0.731	20.82
2417	129.49	0.743	21.18	2469	138.64	0.726	20.67
2419	129.59	0.747	21.3	2471	138.74	0.721	20.52
2421	129.68	0.749	21.36	2473	138.84	0.721	20.52
2423	129.77	0.74	21.09	2477	139.04	0.724	20.61
2425	129.86	0.752	21.45	2479	139.14	0.728	20.73

Depth [cm]	Age [ka bp]	Uk´37	$T_{Mg/Ca}$ [℃]
2481	139.23	0.738	21.03
2483	139.33	0.741	21.12
2485	139.43	0.721	20.52
2487	139.53	0.709	20.15
2491	139.72	0.694	19.7
2495	139.90	0.701	19.91
2497	140.00	0.739	21.06
2499	140.09	0.707	20.09
2505	140.36	0.733	20.88
2523	141.19	0.737	21
2531	141.56	0.748	21.33
2539	141.92	0.721	20.52
2547	142.29	0.744	21.21
2577	143.66	0.749	21.36

Section 3 – M/M 515-712-2 – off the coast of Spitsbergen

Table 3.1:

Compilation of the complete data for *N. pachyderma* for the core M/M 515-712-2. This table contains all available $\delta^{18}O$, $\delta^{13}C$, and $\Delta\delta^{18}O_{ivfsw}$ values. The weighted errors are indicated for the $\delta^{44/40}Ca$ isotope ratios. The $\Delta\delta^{18}O_{ivfsw}$ were calculated employing the $T_{44/40Ca}$ measurements and the procedure presented in chapter 2.

Table 3.1: Compilation of the complete data for *N. pachyderma* for the core M/M 515-712-2

Depth [cm]	Age [years bp]	$\delta^{18}O$ *N.pachyderma* (±0.07) [‰]	$\delta^{13}C$ *N.pachyderma* (±0.07) [‰]	$\delta^{44/40}Ca$ *N.pachy* (±0.12) [‰]	weighted error for $\delta^{44/40}Ca$	$T_{\delta 44/40Ca}$ [℃]	RSL variation	$\Delta\delta^{18}O_{ivfsw}$
64	3082	3.16	0.854	0.67	0.035	5.84	0.0071	1.53
108	5053	3.25	0.470	0.77	0.079	6.41	0.0189	1.73
152	7002	3.18	0.574	0.61	0.139	5.46	0.0448	1.44
220	9023	3.08	0.267	0.60	0.022	5.43	0.1182	1.26
280	10026	3.19	-0.095	0.90	0.297	7.17	0.2037	1.64
340	10999	3.91	0.195	0.45	0.125	4.53	0.3236	1.70
403	13016	3.89	0.134	0.34	0.111	3.87	0.5698	1.29
451	14110	4.04	0.032	1.36	0.214	9.86	0.6764	2.59
501	14725	4.28	0.066	0.68	0.005	5.90	0.7688	1.91

Section 4 Model

The following equations were employed in the model of the different types of phase shift. Equation Ap. 1, from *Shakleton* [1974], was simply combined with the salinity variation, equation Ap. 2, by *Schmidt et al.* [1999] to form equation A.

App. Equation 1:

$$\delta^{18}O_{temperature} = [\sqrt{(4.38^2 - 0.4 * 16.9 - (T + \Delta T))}) - 4.38]/0.2$$

T = salinity starting temperature value (25℃)
ΔT = modelled temperature variation

App. Equation 2:

$$\delta^{18}O_{salinity} = 0.13 * [(S + \Delta S) + 0.27] - 4$$

S = salinity starting value (33)
ΔS = modelled salinity variation

Equation A:

$$\delta^{18}O = \delta^{18}O_{salinity} + \delta^{18}O_{temperature}$$